TOWARDS NEW NANOCOMPOSITES WITH IMPROVED PROPERTIES: ELABORATION, CHARACTERIZATION, PROPERTIES AND DURABILITY OF PP/LDH NANOCOMPOSITES

A THESIS SUBMITTED TO THE

UNIVERSITY OF PUNE

FOR THE DEGREE OF

DOCTOR OF PHILOSOPHY (Ph.D)

IN

CHEMISTRY

BY

SUNIL P. LONKAR

RESEARCH SUPERVISOR

DR. R.P. SINGH

POLYMER SCIENCE AND ENGINEERING DIVISION
NATIONAL CHEMICAL LABORATORY
PUNE 411 008 (INDIA)

MAY 2010

राष्ट्रीय रासायनिक प्रयोगशाला
(वैज्ञानिक तथा औद्योगिक अनुसंधान परिषद)
डॉ. होमी भाभा मार्ग पुणे - 411 008. भारत
NATIONAL CHEMICAL LABORATORY
(Council of Scientific & Industrial Research)
Dr. Homi Bhabha Road, Pune - 411 008. India.

Date: May 3, 2010

CERTIFICATE

This is to certify that the work presented in the thesis entitled **"Towards New Nanocomposites with Improved Properties: Elaboration, Characterization, Properties and Durability of PP/LDH Nanocomposites"** submitted by **Mr. Sunil P. Lonkar** was carried out by the candidate at **National Chemical Laboratory**, Pune, under my supervision. Such materials as obtained from other sources have been duly acknowledged in the thesis.

Dr. R. P. Singh [F.R.S.C]
Research Supervisor,
Scientist- F & Deputy Director,
Polymer Science and Engineering Division,
National Chemical Laboratory,
Pune 411 008, INDIA.
rp.singh@ncl.res.in

DECLARATION BY RESEARCH SCHOLAR

I, **Mr. Sunil P. Lonkar**, hereby declare that the thesis entitled **"Towards New Nanocomposites with Improved Properties: Elaboration, Characterization, Properties and Durability of PP/LDH Nanoconposites"** submitted for the degree of Doctor of Philosophy to the University of Pune, has been carried out by me at Polymer Science and Engineering Division, National Chemical Laboratory, Pune 411 008, India under the supervision of **Dr. R.P. Singh**.

The work is original and has not been submitted to in part or full by me for any other degree or diploma to this or any other university.

Lonkar

SUNIL P.LONKAR

(Research Scholar)

though we love the destination but we have to love the path more……..

Acknowledgements

First and foremost, I would like to express a sincere gratitude to my research supervisor Dr. R.P. Singh for his excellent research insight, invaluable guidance and constant encouragement. His tireless enthusiasm was always a source of motivation and inspiration throughout the duration of my work. His constant support was invaluable and went a long way towards the completion of this thesis. I also express my sincere gratitude to Mrs. Durgesh Singh for her moral support.

I am very grateful to Prof. Jean-Luc Gardette and Dr. Sandrine Therias, Laboratoire de Photochimie Moléculaire et Macromoléculaire (LPMM) and Prof. Fabrice Leroux (LMI), University of Blaise Pascal, France for exposing me towards this exciting field of research, for fruitful discussions and also being kind to provide the encouragement throughout. I will never forget their help and kindness and still our collaboration is continuing.

I also express my indebtedness to Mr.K.G.Raut without his support, advice and encouragement this could not have come true.

My sincere thanks also goes to Dr.P.K.Khanna (C-MET, Pune) under whose guidance I spend my initial days of research and where I dreamed of this highest degree in education.

I am grateful to Dr. Sivaram, the Director, NCL, Pune, for providing the infrastructure and facilities for my research work. I am very much grateful to Dr. M. G. Kulkarni, Head, PSE division, for providing me access to the facilities in the division. I am also very thankful to other scientists in the division namely, Dr. B .B. Idage, Dr. P. P. Wadgaonkar, Dr. C. V. Avadhani, Mr. S. K. Menon, Dr.A. S. Patil, Dr. B.M. Sarvade, Dr(Mrs). D. A. Dhoble, Dr(Mrs). S. B. Idage, Dr.R .A. Kulkarni, Dr. N. N. Chavan, Dr.A.S.Jadhav, Dr. C. Ramesh, Dr(Mrs). B. Garnaik, Dr. A.K. Lele, Dr. Neelima, Dr. Sangeeta, Mrs.Anuya, Mrs. Nilakshi, Mrs. Poorvi and Mr.Saroj for their timely help and support.

I am forever indebted to all my teachers for guiding me to embrace the good in everything I see.

I deeply acknowledge CSIR, New Delhi for financial assistance for my research work and granting Senior Research Fellowship. I am also thankful to French Embassy in India for the award of Sandwich Ph.D Fellowship and for giving me an opportunity to explore myself to the French research culture.

I sincerely thank my seniors and lab colleagues for their support, co-operation and maintaining cheerful atmosphere in the laboratory. So I extend my gratitude to my earlier and present lab-mates Pratheep (Genius fellow), Mukesh, Dilip, Sravendra, Omkar, Narshimha, Rupali, Sangeeta, and Vijay.

I also express my sincere thanks to my past and present divisional colleagues and other friends Shrikant, Sanket, Shailesh, Vivek, Prakash, Santosh, Jegan, Marie, Rajeshwari, Yogesh, Nilesh, Panjab, Jyotsna, Siddhendra, Siddharth, Yashodhan, Chetan, Ravindra, Arvind, Arun, Malli, Mohanraj, Ramesh, Ajay, Rahul, Sachin, Elahi, Shekar, Rakesh, Dr.Parashuram, Dr.Narendra Singh, Marimutthu, all TLEP (2009) group and all others for support, love and encouragement. I also thank all my friends from France for making my stay memorable.

All my other friends; you are all worthy of a big acknowledgement for your support!!

I also thank divisional office staff Mr. Mahesh, Mr. Vikrant, Mr. Zine and divisional bearers Mr. Silas S. Kakade, Mr. Shelar, Mr. More for their assistance. Special thanks are due to Student academic office, Bill section, Accounts, Stores and Purchase, Engineering services, Glass Blowing, Library and Mr. K.D. Deshpande of DIRC for their timely help.

I am also thankful to Mr. A.B. Gaikwad, Mr. Gholap (CMC) for SEM and TEM facilities. Thanks to Dr. Harshavardhan Pol, Dr.Deendayal, Mr.Naveen and Mr. Nandakishor for polymer processing and Ms.Kalyani for mechanical testing.

The words are not enough to express all my love and heartfelt gratitude to my Parents, dear brother Sachin and Deepa vahini for their encouragement, understanding and support that enabled me to overcome the obstacles I faced during my study. I am also happy to acknowledge my sweet nephew Aditya for giving joyful moments.

I am fortunate to have Ms. Poonam as my life-partner, who is my-everything now and then, and I am in immense pleasure to express my gratitude for her love, encouragement and support.

And of course again all this was possible only due to best wishes of my Parents and support of my dear Brother. I owe everything to them.

-SUNIL P. LONKAR

TABLE of CONTENTS

CHAPTER 3: EXPERIMENTAL AND CHARACTERIZATION TECHNIQUES

CHAPTER 4: SYNTHESIS AND CHARACTERIZATION

CHAPTER 5: THERMAL, MECHANICAL AND RHEOLOGICAL CHARACTERIZATION

CHAPTER 6: CRYSTALLIZATION BEHAVIOR AND KINETIC STUDY

Abstract

Title of the Thesis

"Towards New Nanocomposites with Improved Properties: Elaboration, Characterization, Properties and Durability of PP/LDH Nanocomposite"

In order to make much stiffer, light weight and high performance material products, polymer nanocomposites play an emerging role in the material innovation. Unlike other thermoplastics, polymer nanocomposites are fabricated by introducing a small amount of solid nano-scale fillers such as nanoclay, carbon nanotubes or nanofibres. Recently, the addition of such nanoscopic fillers of high anisotropy instead of conventional reinforcing agents renders the polymer/nanoclay nanocomposites to exhibit interesting structure-property relationships and promising application perspectives. In thermoplastics, polypropylene is an outstanding material with respect to its attractive combination of low cost and extraordinary versatility in terms of properties and applications. However, the increasing demand of polypropylene for various applications requires greatly improved physical and mechanical properties. Hence, polypropylene (PP)/clay nanocomposites have quite a high potential to form such innovative materials and replace the conventional plastics in many automotive and packaging applications. With an industrial motivation to commercialize PP/clay nanocomposites products, development of new nanocomposites based on PP with improved properties is still a great scientific thrust.

In the present contribution, the attention is focused on fabrication of PP nanocomposites using layered double hydroxides (LDHs) as a nano-filler and to investigate whether this results in significant improvements in the properties of the final composites. A longer term aim will be to extend the studies towards crystallization behavior and UV-durability of such hybrid materials in comparison with their smectite-type counterparts. ***Chapter 1*** *gives the brief background of polymer/clay nanocomposites, main motivation and research objective for the present study.* ***Chapter 2*** *reviews the literature background and a thorough literature survey was carried out on PP based nano structured materials, methods of synthesis, material*

processing methods and their property evaluations. ***Chapter 3*** *describes the experimental methods and characterization techniques used in the preparation and characterization of PP-LDH nanocomposites.* ***Chapter 4*** *focuses on synthesis and characterization part. Initially, a series of organomodified LDHs comprising different metal cation have been prepared and successfully characterized. In next step, PP/LDH hybrid nanocomposites were fabricated using PP-g-MAH as a compatibilizing agent by melt extrusion. The PP-g-MAH/LDH interactions result in a higher adhesion between the PP matrix and LDH nanolayers. The resultant nanocomposites give direct evidence for formation of intercalated/exfoliated structures of PP/LDH nanocomposites.*

In ***Chapter 5****, the effect of LDH nano reinforcement on different characteristic properties of PP is discussed. Presence of LDH causes distinct changes in the thermal decomposition behavior in PP and a significant improvement in the thermal stability of PP is observed. The addition of LDH also contribute to the reinforcement effect by increasing the elastic modulus E'. A remarkable mechanical response i.e both the tensile strength and the modulus increases with LDH content, similar trend is also observed in flexural properties of PP/LDH nanocomposites. Rheological analysis depicts a strong influence of LDH particles on the flow behavior of the PP/LDH melt. This also gives indirect evidence that polymer chains are interlocked on the LDH particle surface or within clusters. The incorporation LDH also resulted in improved oxygen barrier properties of PP and exhibits fairly better barrier performance than PP/ OMMt nanocomposites. The flammability studies also showed improved flame retardancy in PP/LDH nanocomposites. For different LDHs, LOI increases in the following order* Zn_2*Al-LDH > ZnMgAl-LDH >* Mg_2*Al-LDH, indicate that the LDH can act as effective flame retardant for polypropylene.*

The crystallization studies discussed in ***Chapter 6*** *reveal enhanced crystallization rates for non-isothermal as well as isothermal crystallization for nanocomposites with LDH as nanofillers. Also, LDH at nanometer level found to act as effective nucleating agent. The Avrami exponent 'n' varies from 1.9 to 2.9 for suggesting spherulitic crystal growth with heterogeneous nucleation at the low cooling rates. The melting behavior of PP is also slightly altered by addition of LDH. The addition of LDH does not change the overall crystalline structure of PP matrix. The*

crystallization studies can lead to the development of a fine grain micron-sized structure for the PP/LDH composites. ***Chapter 7*** *is devoted to understanding the performance of PP/LDH nanocomposites under photo-oxidative environment. It is observed that the PP/LDH nanocomposites are more durable in comparison with PP/OMMt nanocomposites under accelerated weathering conditions. The rates of oxidation are influenced by the divalent cations of the LDH layers. The LDH phases containing* Mg^{2+} *have a prodegradant effect on the nanocomposite material, whereas LDH with only* Zn^{2+} *has no influence on the rate of oxidation of the polymer matrix. The influence of stabilizing additives on the photooxidation of PP/LDH nanocomposites exposed to UV light shows that additive retains their activity in presence of LDH in contrast to the OMMt type nanoclay. The* Zn_2Al*-DDS is found to be better LDH nanofiller for stabilization in presence in phenolic antioxidants. Finally,* ***Chapter 8*** *summarizes the results and describes the salient conclusions of the study. Future perspectives for further research are also expressed.*

We envision that this new hybrid material, which combines the advantages of various physico-mechanical properties and better performance towards weathering, could play a significant role in the development of new nanocomposites for automotive, construction and packaging applications.

LIST OF SYMBOLS

A^o	Angstrom
θ	Contact Angle
λ	Wavelength
nm	Nanometer
cm^{-1}	Wavenumber
ω	Angular frequency
R	Universal gas constant
T_g	Glass Transition Temperature
T_c	Crystalline Temperature
T_m	Melting Temperature
$T_{0.1}$ and $T_{0.5}$	Temperature at 10.0 and 50.0 % weight loss respectively
E'	Elastic storage modulus
E"	Elastic loss modulus
G'	Shear storage modulus
G"	Shear loss modulus
tan δ	Loss tangent
η*	Complex Viscosity
T_o	Onset temperature of crystallization
T_∞	End temperature of crystallization
T_p	Crystallization peak temperature
X_c	Percent crystallinity
X_t	Relative degree of crystallinity
α	Cooling rate
t	Crystallization time
$t_{1/2}$	Crystallization half time
ΔH_c	Enthalpy of crystallization
n	Avrami exponent
m	Ozawa exponent
Z_t	Rate constant (modified Avrami equation)
F(T)	Value of cooling rate chosen at unit crystallization time
ΔE	Effective activation energy
Φ	Nucleating Activity

G	Growth rate constant
K_g	Nucleation constant
U^*	Activation energy (Growth rate equation)

NOMENCLATURE

LDH	Layered Double Hydroxide
Mg_2Al–LDH	Magnesium and Aluminum based LDH
Zn_2Al–LDH	Zinc and Aluminum based LDH
ZnMgAl–LDH	Zinc, Magnesium and Aluminum based LDH
DDS	Dodecylsulfate
MMT	Montmorillonite
PP	Polypropylene
PP-g-MAH	Maleic Anhydride Functionalized PP
FTIR	Fourier Transform Infra-red
DSC	Differential Scanning Calorimetry
TGA	Thermo gravimetric analysis
DTG	Derivative Thermogravimetry
SEM	Scanning Electron Microscopy
TEM	Transmission Electron Microscopy
UV	Ultraviolet
WAXD	Wide Angle X-Ray Diffraction
POLM	Polarized Optical Light Microscopy
UTM	Universal testing machine
LOI	Limited Oxygen Index
DMTA	Dynamic Mechanical Thermal Analysis
OTR	Oxygen Transmission Rate

LIST OF TABLES

CHAPTER 6: CRYSTALLIZATION BEHAVIOR AND KINETIC STUDY

LIST OF FIGURES

CHAPTER 1: INTRODUCTION

CHAPTER 2: LITERATURE REVIEW

CHAPTER 3: EXPERIMENTAL AND CHARACTERIZATION TECHNIQUES

CHAPTER 4: SYNTHESIS AND CHARACTERIZATION

CHAPTER 5: THERMAL, MECHANICAL AND RHEOLOGICAL CHARACTERIZATION

CHAPTER 6: CRYSTALLIZATION BEHAVIOR AND KINETIC STUDY

CHAPTER 7: PHOTO-OXIDATION BEHAVIOR AND PHOTOSTABILIZATION STUDIES

Chapter 1

INTRODUCTION

"The process of scientific discovery is, in effect, a continual flight from wonder"

~Albert Einstein

This thesis is concerned with fabrication of new nanocomposites with improved properties and structure-processing-property linkages in a new class of hybrid materials known as polymer anionic nanoclay composites. We begin the thesis with a brief introduction to polymer nanoclay composites and necessary background relevant to the contents of the thesis. The purpose of this chapter is to describe the context of the work, the overall objectives of the study and the structure of the thesis.

1.1 Motivation

Since the discovery of synthetic polymers during the early 1900's, compounding of polymers with inorganic fillers and fibers was developed as a versatile route leading to novel polymeric materials with improved thermal and mechanical properties with attractive cost/performance ratio. The field of materials science has lately begun to focus on the quest for composite materials that exhibit the positive characteristics of their initial components. Worldwide, there has been a new and intense desire to tailor the structure and composition of materials on the nanometer scale. Thus, we are seeing the introduction of a new and improved class of composites, the nanocomposites. It is in this context that the work presented here has been undertaken to investigate new nanocomposites with improved properties based on isotactic polypropylene and relatively new types of nanofiller namely layered double hydroxides. In this chapter the necessary background relevant to the contents of this thesis is provided. We also discuss the overall objectives of this work and the structure of this thesis.

1.2 Polymer Nanocomposites

Materials are key components of our civilization. We ascribe the major historical landmarks of our society to materials with epithets, such as, the stone age, bronze age, iron age, steel age (the industrial revolution), polymer age, silicon age, etc. This reflects the importance of materials in the evolution of our society. As the 21st century unfolds, it is becoming even more apparent that the next technological frontiers will unfold through a better understanding of structure-property relationship in materials and their functions. The emerging importance of nanoscale and the associated excitement surrounding nanoscience and technology affords unique opportunities to create novel materials with unique and useful materials. These new materials promise new applications by exploiting the unique synergisms between constituents that only occur when the length scale of the morphology and the critical length associated with the fundamental physics of a given property coincide. In recent years, the advances in synthesis techniques and the ability to characterize materials on atomic scale has lead to a growing interest in nanometer-size materials. Nanocomposites were first referenced as early as 1950, synthetic polymer clay nanocomposites were reported as early as 1961, when Blumstein *et. al* demonstrated polymerization of vinyl monomer intercalated into montmorillonite clay [1] and polyamide nanocomposite were reported by Fujiwara *et. al.* as early as 1976 [2].

Polymer nanocomposites (PNC) are novel class of composites that are particle-filled polymers in which; at least, one dimension of the dispersed particles is in the nanometer range. However, it was not until researchers from Toyota Central Research and Development Laboratories (TCRDL) in Japan in the late 1980s began a detailed examination of polymer/layered silicate clay mineral composites that nanocomposites became more widely studied in both academic and industrial laboratories. Accordingly, since the pioneering work of Toyota research group [2- 3], polymer nanocomposites (PNC) have shed a light on the replacement of conventional fiber-reinforced composites by using a small proportion of nanofillers, composed of inorganic layered nanofillers. Since then construction of nanostructured polymers with specific mechanical and functional properties became an important facet of contemporary materials science and engineering. PNCs represent an alternative to conventional filled polymers or polymer blends– a staple of the modern plastics industry. In contrast to conventional composites,

where the reinforcement is on the order of microns, PNCs are exemplified by discrete constituents in the order of a few nanometers.

One can distinguish three types of nanocomposites depending on how many dimensions of the dispersed particles are in the nanometer range. When the three dimensions of particulates are in the order of nanometers, they are referred as equi-axed (isodimensional) nanoparticles or nanogranules or nanocrystals such as spherical silica nanoparticles obtained by in-situ sol gel methods [4]. When two dimensions are in the nanometer scale and the third is larger, forming an elongated structure, we speak about nanotubes or whiskers as, for example, carbon nanotubes [5] or cellulose whiskers [6-7]. The third type of nanocomposites is characterized by only one dimension in the nanometer range. In this case the filler is present in the form of sheets of one to a few nanometer thick to hundreds to thousands nanometers long. This family of composites can be gathered under the name of polymer-layered crystal nanocomposites. These are the nanofillers extensively studied as reinforcing agents yielding materials with exceptional properties. Hence, within this context, in recent years, there has been a rapidly growing trend for the incorporation of inorganic fillers into the polymer matrix to enhance one or several physical properties.

Amongst the entire potential nanocomposite precursors, those based on clay and layered silicates have been more widely investigated probably because of the starting clay materials are easily available and their intercalation chemistry has been studied for a long time [8-9]. The important characteristics pertinent to application of clay minerals in polymer nanocomposites are their rich intercalation chemistry, high strength and stiffness and higher aspect ratio of individual platelets, abundance in nature and low cost. First, their unique layered structure and high intercalation capabilities allow them to be chemically modified to be compatible with polymers, which make them particularly attractive in the development of clay-based polymer nanocomposites. When well dispersed into neat polymers, these nanofillers can dramatically enhance their mechanical, thermal, barrier and flame retardant properties [10-16]. Another interesting class of layered structure is anionic clay i.e layered double hydroxides (LDHs). The basic reason for choosing LDH as a nanofiller is their typical metal hydroxide-like chemistry and conventional clay-like layered crystalline structure. The former is helpful in the

direct participation in the flame inhibition through endothermic decomposition and stable char formation. On the other hand, the later makes LDH suitable for polymer nanocomposite preparation. LDH is organically modified using anionic surfactants in order to enlarge the interlayer distance to render it more organophilic. These all properties make LDH as potential nano filler for different polymer systems. As a result, the composites made by mixing layered nanoclays in polymer matrices are attracting increasing attention commercially.

1.2.1 Current Perspective and Future Prospects: An Overview

Today, more than 70 companies, government agencies and academic institutions have been identified as having research and development (R&D) activities in the field nanocomposites. The extraordinary efforts are being put in research activities based on polymer nanocomposites and reviewed by several authors [17-22]. Polymer nanocomposite markets that have been slow in development till date, seem ready to take off with increasing application in the automotive and packaging sector. As commercial interest has moved beyond pilot programs and niche applications, it appears that nanocomposites are finally ready for a breakthrough in these markets. By 2011, nanocomposite demand will reach 150,000 tpa in USA as per Freedonia [23]. Growth will be fueled by declining prices of nanomaterials and composites, as production levels increase and technical issues concerning the dispersion of nano-additives in the compounds are overcome. By 2025, it is expected that nanocomposites will be a US$9 billion market, with volumes nearing 5 million tons. While thermoplastics currently comprise virtually all demand for nanocomposites, compounds based on thermoset resins will eventually become a substantial part of the market, constituting 20% of demand in 2025. Looking forward, however, nanocomposites based on commodity plastics, such as polypropylene, polyethylene and PVC will dominate the market. Among thermosets, nanocomposites will make the strongest impact as enhancements for reinforced polyester and epoxy compounds. Packaging and motor vehicles, two key early markets for nanocomposites, will account for nearly 50% of total demand in 2011 and 40% of demand in 2020. However, by 2025, electrical and electronics applications will gain in prominence, as nanotube-based composites will penetrate a sizable portion of the market

as a substitute for other conductive materials. Construction will emerge as a significant market as nanocomposites begin to replace fiber-reinforced plastics in a number of applications. Nanocomposites are expected to penetrate a number of key packaging applications, including soft drinks, beer, food, pharmaceuticals and electronics, driven by the improved barrier, strength and conductive properties that they offer. In motor vehicles, automotive manufacturers are increasingly turning to nanocomposites in an effort to replace higher-priced materials, increase production speed of parts and reduce motor vehicle weight in a number of exterior, interior and underhood applications.

In 2006, nearly all nanomaterial demand consisted of carbon black in conductive composites. However, as material and production costs of clay-based nanocomposites fall, clays will rise to account for over half of all nanomaterials demand by volume in 2025. Similarly, a decline in price will enable the rapid commercialization of carbon nanotubes, which will eventually gain over 60% of the nanocomposite materials market in value terms.

Table 1.1: United States volume and value for polymer nanocomposites by 2005-2020 (in million pounds) [23].

US NANOCOMPOSITES DEMAND (million pounds)				
Year	2005	2010	2020	% Annual Growth 2005-2020
Nanocomposites Demand	154	344	7030	29
Thermoplastic	152	329	5600	27
Thermoset	2	15	1430	55

According to a report by Global Industry Analysts Inc, global nanocomposites market will reach 989 million lbs by 2010. Nanocomposites play a significant role in one of the most promising technologies known as nanotechnology. Worldwide demand for nanocomposites is increasing rapidly in packaging, automotive, electrical, and other applications due to their superior thermal, electrical conductive and other properties. Development of industry related nanocomposites with enhanced features and expanding research activities in development of new nanocomposites are some of the factors that

would drive nanocomposites market in the coming years. United States and Europe dominate the global nanocomposites market, with a collective share of over 80% of the volume sales by 2008. The market is also projected to witness rapid growth, driven by enhanced volume consumption of nanocomposites in various applications. Research institutions and companies are engaged in the exploration of efficient methods for developing nanocomposites in large volumes and at lower cost. Applications of nanocomposite plastics are diversified, with automotive and packaging accounting for a majority of the consumption. Increased R&D activities and advent of innovative materials is expected to widen the application areas for nanocomposites. Packaging segment represents the largest end-use market for nanocomposites in the world, with consumption estimated at 284 million pounds for 2008. Automotive segment is projected to generate the fastest demand for nanocomposites during the period 2001-2010. Rise in demand and easy accessibility of nanocomposites would lead to their extensive usage in a wide range of applications.

Nanocomposite research is wide spread and is conducted by companies and universities across the globe. Several global plastic suppliers have already commercialized products based on nanocomposite materials, with majority of the efforts focused on either nylons or polyolefins. Other industries are also optimistic about the future role of these novel materials, attributed to the growing volume of research studies being conducted across the world. The development of innovative nanocomposite polyolefins and an array of other resin matrixes and nanofillers are also expected to bolster the market scenario. Technological advancements would reduce manufacturing costs, enabling the development of low-cost nanocomposites. Major players profiled in the report include 3M ESPE, Arkema Group, BASF AG, Cabot Corporation, Cyclics Corporation, DSM Somos, Du Pont (E.I) De Nemours & Company, Elementis Specialties Inc, eSpin Technologies Inc., Evonik Degussa GmbH, Foster Corporation, Hybrid Plastics, Industrial Nanotech Inc, Inframat Corporation, InMat Inc, Nanocor Incorporated, Nanodynamics Inc, Nanoledge SA, Nanophase Technologies Corporation, Nanova LLC, Powdermet Inc, Showa Denko K.K., Rockwood Additives Ltd, TNO and Unitika Ltd.

Continuous demand from different end-use sectors, development of advanced and superior nanocomposites would stimulate their growth. Need for new and a better nanocomposite by end users is one of the major reasons expected to drive the development of new array of nanocomposites. Identifying potential markets, intensifying research activities and government funding for R&D operations constitute major factors in the commercialization of nanocomposites. A few nanocomposites have already reached the marketplace, while a few others are on the verge, and many continue to remain in the laboratories of various research institutions and companies. The development of PNC primarily concentrates on thermoplastics as the polymer matrix with a view to their wide range of applications and environmental friendliness as depicted in **Figure 1.1**.

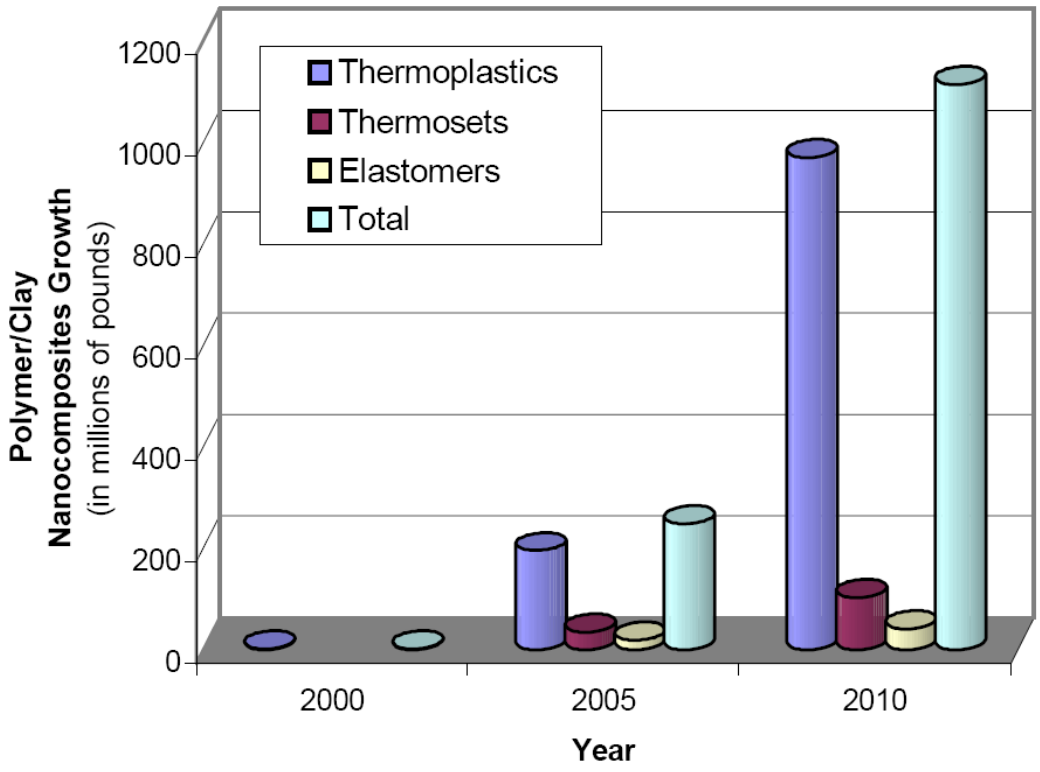

Figure 1.1: Trend of using nanocomposites from 2000 to 2010 *(Data are adapted from Principia Partners (Exton, PA))* [24]

thermoplastics predominantly demonstrate the increase of potential material usage up to five folds in manufacturing polymer/clay nanocomposites from 2005 to 2010. Furthermore, the global volume and value of PNC are going to grow more rapidly due to a huge demand in the commercial market.

Amongst the existing thermoplastics, scientific and technological interest for tailoring and modifying the polypropylene properties has been driving a very vivid research on nanostructured materials. In recent years, PP based nanocomposites have been recognized as one of the most promising research fields in material chemistry and nano-particulate fillers have been shown to significantly increase the properties of polymers. PP has simulated intensive research in order to produce polypropylene nanocomposites with improved properties. In this regard, most emphasis has been given to silicate layer nano-composites, which after intercalation and exfoliation within the polymer structure can yield large increases in various physico-chemical properties. Hence, the polymer chosen for the present work is polypropylene (PP), which offers probably the best price/performance characteristics among all thermoplastics. So far, the majority of the research work has been focused on cationic clays, like the naturally occurring smectite type, montmorillonite systems, while the other potential layered nano-fillers like layered double hydroxide (LDH) systems have been much less reported in the literature.

Thus, the understanding of the links between the microstructure and physicochemical properties is critical to the successful development of new polymer nanoclay composite products. The overall objective of this work is to try to quantify the structure-processing-property linkages in PP/LDH nanocomposites.

1.3 Problem Background

One of the most important aspects in the materials development of reinforced thermoplastics is to achieve a good combination of properties and processibility at moderate cost. In the development of reinforced thermoplastics as far as mechanical properties is concerned, the main target is to strike a balance of stiffness, strength, flammability and weatherability. There are a few approaches that have been identified as potential routes to achieving this goal: i) Reinforcement of thermoplastics with different type of nano-fillers to form nanocomposites. ii) The inclusion of fillers or fiber reinforcement into thermoplastic matrices to form thermoplastics composites. However, these approaches have their own potential and limitation. Generally, choice of ideal nanofillers is a major concern towards this issue. Hence, there is an intensive need to assess the feasibility of new types of nanofillers in structure-property improvement in polymer matrix. With this driving force, we decided to employ relatively new nano-filler called layered double hydroxide as a potential reinforcement. The strategy behind this approach is to develop a new nanocomposites with improved properties based on blending thermoplastic (PP) with the incorporation of nanofillers (organo modified LDHs) in the presence of compatibilizer (PP-g-MAH). However, an extensive study on structure property evaluation of PP in presence of LDHs as nanofiller has not yet been explored. Therefore, it is interesting to study at the system where thermoplastic (PP) combined with LDHs type nanofillers as a reinforcing agent.

1.4 Research Objective

With an industrial motivation to commercialize PP/clay nanocomposites products, development of new nanocomposites based on PP with improved properties is still a great scientific thrust. In the present contribution, the attention is focused on fabrication and property evaluation of PP nanocomposites using layered double hydroxides as a nano-filler and on their comparison with smectite-type counterparts. The work comprises herein, is preparation, characterization of different organomodified LDHs and PP/LDH nanocomposites. Furthermore, work also involves investigation of various physico-chemical properties such as thermal, mechanical and rheological of polypropylene / LDH nanocomposites. The properties like crystallization and photo-oxidative behavior of PP/LDH nanocomposites, comprising partially intercalated/exfoliated LDH platelets and tactoids have also been addressed. The outline of current research approach is illustrated step by step in **Figure 1.2.**

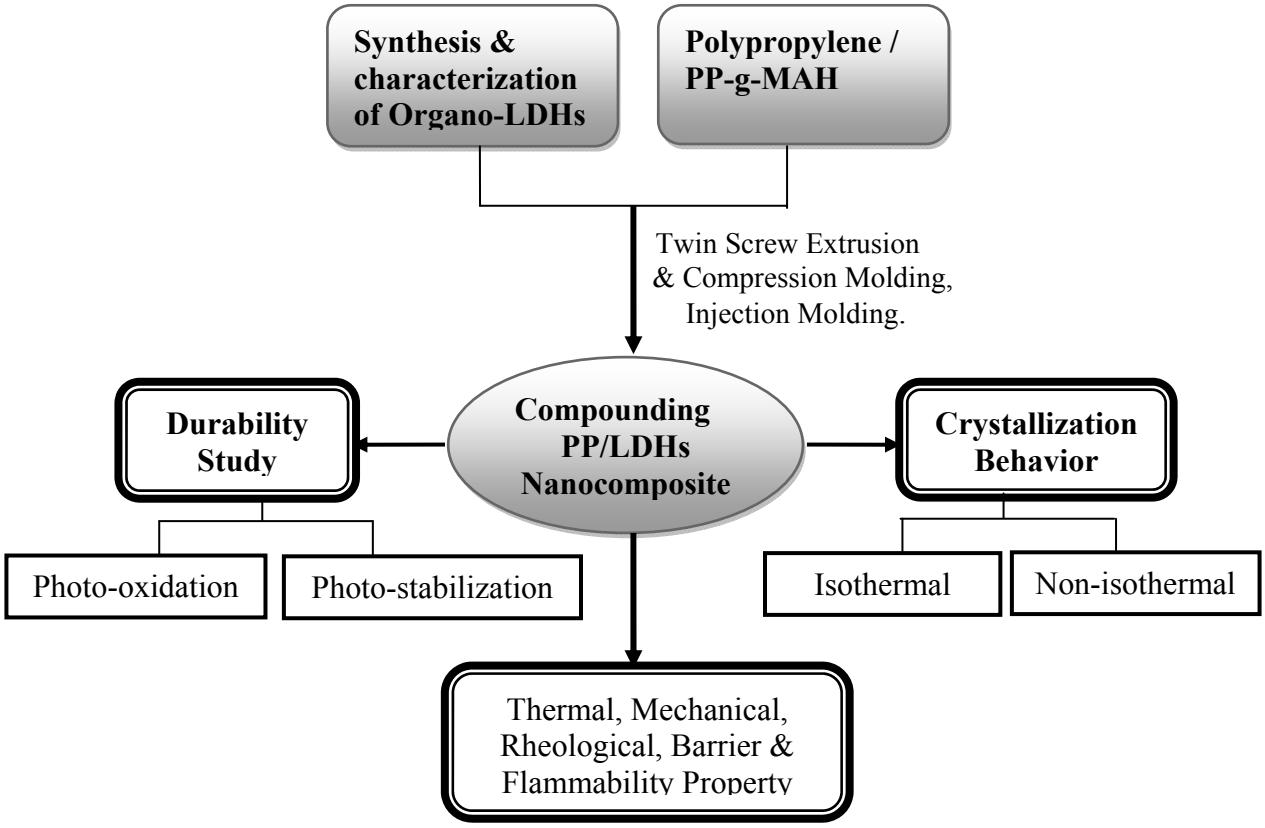

Figure 1.2: Outline of the research approach in this study

1.5 Thesis Outline

In order to better understand the overview of this research work, a thesis outline is presented including the following chapters:

- **Chapter 1** contains the brief background of polymer/clay nanocomposites and research objective.
- **Chapter 2** reviews the history and current state of knowledge in PP nanocomposites and its importance in various applications. A review of fundamental and technical information as well as the different nano-reinforcement in PP and properties obtained thereof also presented. A thorough literature survey was carried out on PP based nano structured materials, methods of synthesis, material processing methods and their property evaluations.
- **Chapter 3** elaborates on the experimental techniques employed in LDHs synthesis and fabrication of PP/LDHs nanocomposites. Also, experimental characterization results on the LDH dispersion, morphological and crystalline structures of organo-LDHs and PP/clay nanocomposites using X-ray diffraction (XRD), scanning electron microscopy (SEM) and transmission electron microscopy (TEM) etc. are discussed.
- **Chapter 4** comprises detailed synthesis of organomodified LDHs comprising different metal cations. The successful organomodification is revealed by Infra-Red spectroscopy (FT-IR), X-ray diffraction (XRD), Morphological study (SEM) and by thermal analysis (TGA). In second section, detailed investigation on preparation and characterization of PP/LDH nanocomposites using PP-g-MAH is summarized. The nanocomposite structure was revealed by XRD and TEM analysis.
- **Chapter 5** discusses the influence of nano LDH reinforcement on different characteristic properties in detail such as thermal, mechanical, rheological, gas barrier and flammability of polypropylene. These properties are evaluated by mechanical testing, differential scanning calorimetry (DSC), thermogravimetric analysis (TGA), dynamic mechanical thermal analysis (DMTA), stress/strain controlled rheometer, and cone calorimeter.

- **Chapter 6** consists of intensive study on both iso and non-isothermal crystallization behavior of PP/LDH nanocomposites. The crystallization kinetics and subsequent melting behavior of PP/LDH hybrids were studied by confronting different kinetic models. The effect of LDH type nanofillers on effective parameters like nucleation, crystal growth and crystal structure of PP is also investigated.
- **Chapter 7** is devoted to understanding the performance of PP/LDH nanocomposites under photo-oxidative environment in comparison with PP/OMMt nanocomposites using accelerated weathering conditions. The effect LDHs on efficiency of stabilizing additives towards photo-oxidation of PP has also been discussed.
- **Chapter 8** concludes the thesis by summarizing the salient points of the work described and presenting avenues for future investigations.

References

1) A. Blumstein. Etude des polymerisations en couche adsorbee .1. *Bulletin de la Societe Chimique de France*, **5** (1961), p.899-905.
2) S. Fujiwara, T. Sakomoto. *Japanese Patent Application No. 109998* (1976) (assigned to Unichika K.K., Japan).).
3) A. Okada, M. Kawasumi, A. Usuki, Y. Kojima, T. Kurauchi and O. Kamigaito, "Synthesis and properties of nylon-6/clay hybrids", in: Polymer based molecular composites, edited by D. W. Schaefer, J. E. Mark, MRS Symposium Proceedings, Pittsburgh, **171** (1990), p.45-50.
4) H. Zou, S. Wu and J. Shen. Polymer/Silica Nanocomposites: Preparation, Characterization, Properties, and Applications, *Chemical Review,* **108** (2008), p.3893–3957.
5) P. Calvert. Potential applications of nanotubes, in: Ebbesen T.W. (Ed.), *Carbon Nanotube*s, CRC Press, Boca Raton, FL, **1997**, p. 277.
6) V. Favier, G. R. Canova, S.C. Shrivastava, Mechanical percolation in cellulose whisker nanocomposites, *Polymer Engineering and Science*, **37** (1997), p.1732-1739.
7) N. Ljungberg, C. Bonini, F. Bortolussi, C. Boisson, L. Heux, and J.Y. Cavaillé. New Nanocomposite Materials Reinforced with Cellulose Whiskers in Atactic Polypropylene: Effect of Surface and Dispersion Characteristics, *Biomacromolecules*, **6** (2005), p.2732–2739.
8) B. K. G. Theng. *Formation and Properties of Clay-Polymer Complexes*, Elsevier Scientific Publishing Co., Amsterdam, The Netherlands, **1979**.
9) M. Ogawa, K. Kuroda. Preparation of inorganic-organic nanocomposites through intercalation of organoammonium ions into layered silicates, *Bulletin of the Chemical Society of Japan*, **70** (1997), p.2593-2618.
10) A. Okada, M. Kawasumi, A. Usuki, Y. Kojima, T. Kurauchi and O. Kamigaito. Synthesis and properties of nylon-6/clay hybrids", in: Polymer based molecular composites, edited by D. W. Schaefer, J. E. Mark, MRS Symposium Proceedings, Pittsburgh, **171** (1990), p.45-50.
11) E. P. Giannelis. Polymer layered silicate nanocomposites. *Advanced Materials,* **8** (1996), p.29-35.

12) R. A. Vaia, G. Price, P. N. Ruth, H. T. Nguyen and J. Lichtenhan. Polymer/layered silicate nanocomposites as high performance ablative materials. *Applied Clay Science,* **15** (1999), p.67-92.

13) E. P. Giannelis. Polymer-layered silicate nanocomposites: synthesis, properties and applications, *Applied Organometallic Chemistry,* **12** (1998), p.675-680.

14) P. B. Messersmith and E. P. Giannelis. Synthesis and barrier properties of poly(ε-caprolactone)-layered silicate nanocomposites. *Journal of Polymer Science. Part A,* **33** (1995), p.1047-1057.

15) A.Kojima, M. Usuki, A. Kawasumi, Y. Okada, T.Fukushima, Kurauchi and O. Kamigaito. Mechanical properties of nylon 6-clay hybrid. *Jornal of Material Research,* **8** (1993), p.1185-1189.

16) J. W. Gilman. Flammability and thermal stability studies of polymer-layered silicate (clay) nanocomposites, *Applied Clay Science,* **15** (1999), p.31-49.

17) S.S. Ray and M. Okamoto. Polymer/layered silicate nanocomposites: a review from preparation to processing. *Progress in Polymer Science*, **28** (2003), p.1539-1641.

18) M. Alexandre and P. Dubois. Polymer-layered silicate nanocomposites: preparation, properties and uses of new class of materials. *Materials Science and Engineering*, **28** (2000), p.1-63.

19) L. Xu, H. Nakajima, E. Manias and R. Krishnamoorti. Tailored Nanocomposites of Polypropylene with Layered Silicates. *Macromolecules*, **42** (2009), p. 3795–3803.

20) L. A. Utracki1, M. Sepehr and E. Boccaleri. Synthetic, layered nanoparticles for polymeric nanocomposites (PNCs). *Polymers for Advanced Technologies,* **18** (2007), p.1–37,

21) L. A. Goettler, K. Y. Lee, H. Thakkar. Layered Silicate Reinforced Polymer Nanocomposites: Development and Applications. *Polymer Reviews*, **47** (2007), p.291–317.

22) FR. Costa, M. Saphiannikova, U. Wangenknechat, G. Henrich. Layered Double Hydroxide Based Polymer Nanocomposites, *Advances in Polymer Science*, **270** (2007), 101-168.

23) Polymer Nanocomposite market to grow well globally. (http://www.plastemart.com/upload/Literature/Polymer-Nanocomposites-grow-globally-in-USA.asp?LiteratureID=1262).

24) A. Wood. A Big Market Potential. *Chemical week,* **164** (2002), p.17-21.

Chapter 2

LITERATURE REVIEW

"Scientific knowledge is in perpetual evolution; it finds itself changed from one day to the next"

~Jean Piaget

2.1 Polypropylene

Polypropylene (PP) is one of the thermoplastic materials with a number of desirable properties that makes it a versatile material and became one of the most important commercial thermoplastics; its consumption is still increasing more rapidly than the total for all thermoplastics. This situation is likely to continue into the future for the following reasons [1]:

i. The relatively low cost of the product is due to the low monomer cost and established polymerization technology, compared to other thermoplastics.
ii. The polymer can be modified for a variety of applications. Through copolymerization, orientation and other techniques the physical properties of the product can be varied to meet a wide range of thermal and mechanical requirements.
iii. Polypropylene has an excellent combination of low density, high stiffness and toughness and heat distortion temperature above 100°C which provides it with an extraordinary versatility of properties and applications.
iv. The ease in processing these polymers allows their use in most commercial fabrication techniques. The versatility of this product, coupled with its low cost, encourages its production into newly developing applications. As a result, new applications of PP will use forms that are significantly different from those available today.

Polyolefins are responsible for the production of approximately 84 billion kilograms of thermoplastic per year or about 50% of the total worldwide polymer industry production. Polypropylene (PP) accounts for approximately 20% of polyolefin production or 34 billion kilograms per year production. Polypropylene is used in several applications such as automotive components, laboratory equipment, plastic parts, food packaging, textiles, and reusable containers. PP has good tensile strength, a superior working temperature but lower impact strength compared to other low or high density thermoplastics. Polypropylene possesses excellent resistance to organic solvents, degreasing agents and electrolytic attack. It is light in weight, resistant to staining and has a low moisture absorption rate. PP is a tough, heat-resistant and semi-rigid material, ideal for the transfer of hot liquids or gases. PP is, therefore, used in vacuum systems where higher heats and pressures are encountered. It also has excellent acid and alkali resistance. Polypropylene can be easily fabricated using hot gas welded, spin welded, fusion & butt welded. PP can also be machined with wood or metal working tools, vacuum formed or ultra-sonic sealed.

2.1.1 Properties of Polypropylene

PP is a linear hydrocarbon polymer containing little or no unsaturation. It was found that PP and PE have many similarities in their properties, particularly in their swelling, electrical properties and solution behavior. In spite of the many similarities, the presence of a methyl group attached to alternate carbon atoms on the chain backbone can alter the properties of the polymer in number of ways [2]. The most significant influence of the methyl group is that it can lead to products of different tacticity, ranging from completely isotactic and syndiotactic structures to atactic molecules. The isotactic form is the most regular since the methyl groups are all disposed on one side of the molecule. Within the range of commercial polymers, the greater the amount of isotactic material, the greater the crystallinity and hence the greater the softening point, stiffness, tensile strength, modulus and hardness, all other structural features being equal. In the syndiotactic form they alternate the sides of the main chain, while atactic chains do not have any consistent placements of methyl groups. **Figure 2.1** show the structure of PP

and a schematic representation of isotactic, syndiotactic and atactic PP chains, respectively.

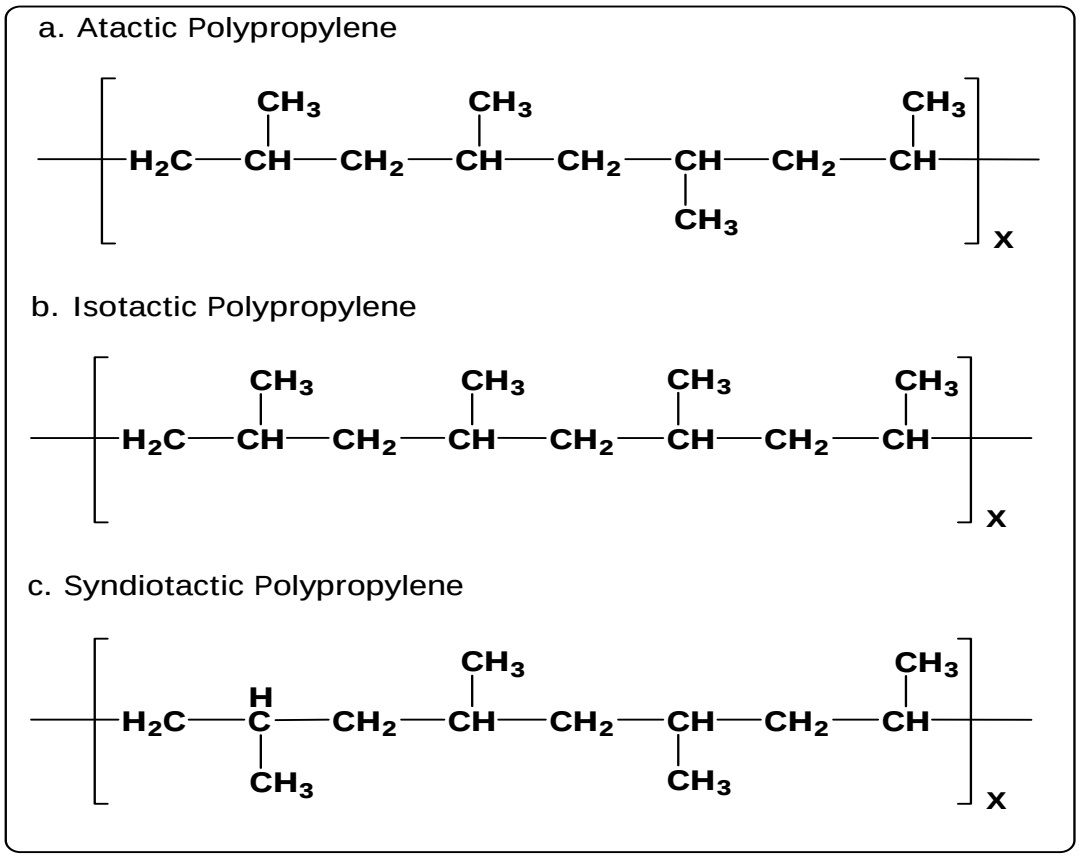

Figure 2.1: Types of different Polypropylenes

The influence of molecular weight on the bulk properties of PP is often opposite to that experienced with most other well-known polymers. Although an increase in molecular weight leads to an increase in melt viscosity and impact strength, in accordance with most other polymers, it also leads to a lower yield strength, lower hardness, lower stiffness and softening point. This effect is believed to be due to the fact that high molecular weight polymers do not crystallize so easily as a lower molecular weight material one and it is the differences in the degree of crystallization which affect the bulk properties [3]. It may also be mentioned that an increase in molecular weight leads to a reduction in the brittle point. Products of improved strength and lower brittle points may be obtained by block copolymerization of propylene with small amounts (4 -

15%) of ethylene copolymers and are often preferred to the homopolymer in injection molding and bottle blowing applications [2]. Test methods and typical properties of homopolymer PP are shown in **Table 2.1.**

Table 2.1: Physical and chemical properties of polypropylene

Property	**ASTM**	**Extrusion, Sheet Profiles**		**General Purpose, Injection Molding**		**Injection Molding, Thin Complex Parts**
Melt flow g/10 min	1238 L	0.4	0.8	4	12	35
Density g/cm^3	D792-2	0.902	0.903	0.903	0.903	0.902
Tensile strength MPa	D638	37	35	35	34.8	33.2
Elongation %	D638	13.5	13	12	11	12
Notched Izod Impact At 23 ºC, J/m	D256A	161	133	1724	1793	1470
Flexural modulus, 1% secant, MPa	D790B	1655	1666	42.7	37.3	32

2.2 Types of Nanofillers

Nanocomposites are defined as constituents in which nanofillers with at least one dimension smaller than 100 nm are well dispersed into the polymer matrix. "*Nano*" originates from a Greek word meaning midget, namely a very tiny object. Three different types of nanofillers in geometry are demonstrated in **Figure. 2.2** with 1-D platelet-like, 2-D fibre-like and 3-D sphere-like structures. In general, montmorillonite (MMT) silicates or smectite clay and layered double hydroxide (LDHs) belong to the first type with the lateral dimension in the range of several hundred nanometers to microns while the thickness is within a few nanometers. Such platelet-like structures lead to a large particle aspect ratio between 100-1000 with the superior biaxial reinforcement effect. On the other hand, when nanofillers have two dimensions at a nanoscale level and the third one is much larger in the size of microns, a unidirectional continuous fiber-like reinforcement takes place. Single-wall or multi-wall carbon nanotubes and nanofibres are good representatives of the second type with a greatly elongated structure. Finally, the third type of nanofillers such as nanoporous silica possesses all three dimensions at the nanoscale level.

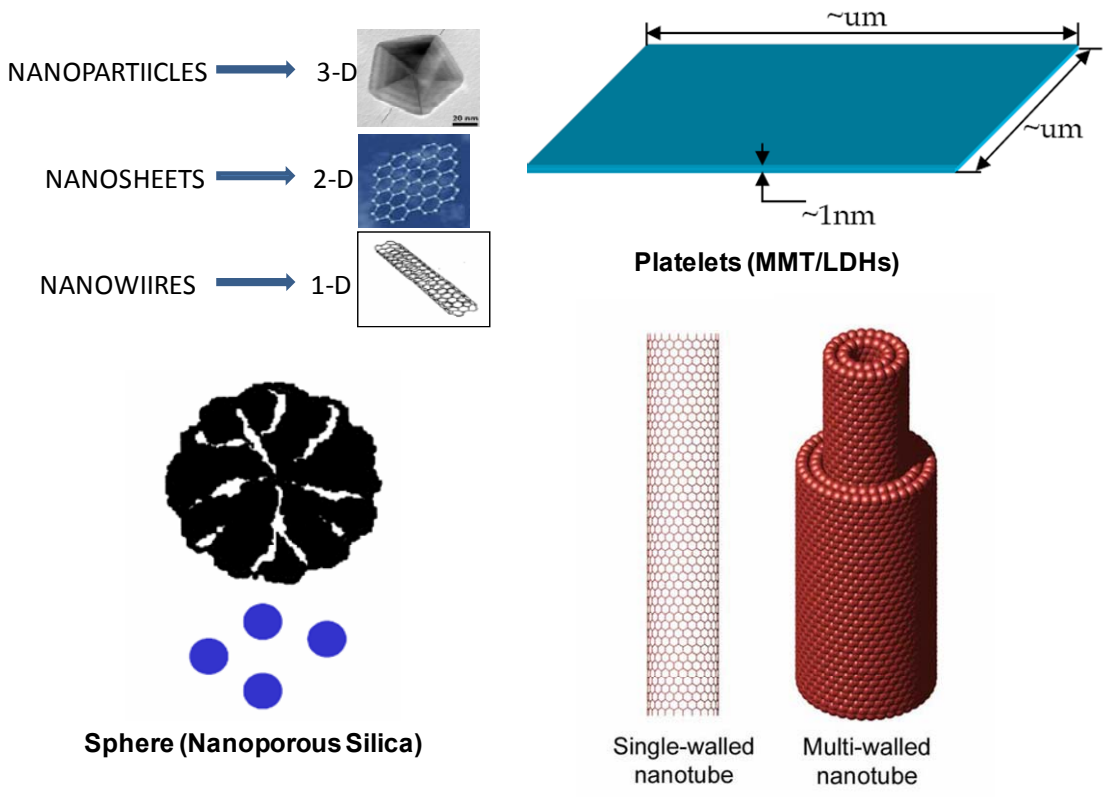

Figure 2.2: Different types of nanofillers in geometry [4]

Global manufacturing and development of nanofillers are demonstrated in **Table 2.2**. In particular, clay silicates (e.g. nanoclay) and carbon nanotubes are two most popular nanofillers under the wide investigation and commercialization. Nanotubes show the superior electrical and thermal conductive properties to fabricate the multifunctional polymer nanocomposites (PNCs), but are confronted with the limited usage owing to a much higher reported market value at US $100/g or $50/lb in masterbatch [5b].

Table 2.2 Worldwide commercially available nanofillers [5a]

Company	**Activity**
Altair Nanomaterials (Cody, WY)	Oxides
Argonide (Sanford, FL)	Metals
Cabot Corp. (Boston)	Oxides
Carbon Nanotechnologies (Houston)	Nanotubes
Carbolex (Lexington, KY)	Nanotubes
Degussa (Dusseldorf, Germany)	Oxides
Espin Technologies (Chattanooga,TN)	Nanofibers
Frontier Carbon (Tokyo)	Fullerenes
Hyperion Catalysis (Cambridge, MA)	Nanotubes
Nano-C (Westwood, MA)	Fullerenes
Nanogate (Saabrudeen, Germany)	Oxides
Nanocor (Arlington Heights, IL)	Nanoclay
Nanomaterials Research (Longmont, CO)	Oxides
Nanoproducts (Longmont, CO)	Oxides
Nanophase Technologies (Romeoville, IL)	Oxides

Nanopowder Enterprises (Piscataway, NJ)	Oxides
Nanopowder Industries (Caesarea, Israel)	Metals
Nanoscale Materials (Manhattan, KS)	Oxides
Nanotechnologies (Austin, TX)	Oxides, Metals
Nyacol Nano Technologies (Ashland, MA)	Oxides
Oxonica (Begbroke, U.K.)	Oxides
QinetiQ Nanomaterials (Farnborough, U.K.)	Oxides
Shin-Etsu (Tokyo)	Oxides
Southern Clay (Gonzales, TX)	Nanoclay
Sud-Chemie (Munich)	Nanoclay
Tosoh (Tokyo)	Oxides

In addition, the health hazards related to handling nanotubes are still uncertain though the laboratory-scaled techniques are available to prepare polymer/nanotube composites. Hence, much greater attention has been drawn to clay silicates since they are more cost-effective and eco-friendly with a reasonable price of US $ 2.25-3.25/lb [5b], and have broad utility in reinforcing common thermoplastics like polypropylene (PP), polyethylene (PE), polystyrene (PS), polyethylene terephthalate (PET) and nylon. More remarkably, the addition of layered nano-fillers helps to considerably enhance their mechanical, thermal, barrier and heat retardant properties. The most applicable polymers reinforced by nano clays to fabricate corresponding nanocomposites are listed in **Table 2.3.** Polyolefins are particularly well-known for their wide range of applications in automotive and packaging industries, especially PP and PE as the generally used commodity polymers.

Table 2.3: Types of applied polymers to fabricate nanocomposites [6].

Type of Polymers	**Specific Formulated Polymers**
Vinyl Polymers	Methyl Methacrylate (MMA), MMA Copolymers, Acrylic Acid, Acrylonitrile, Styrene (S), 4-Vinylpyridine, Acrylamide, Ethyl Vinyl Alcohol Copolymer, etc.
Condensation (Step) Polymers	Nylon6, Polyamides (PA), Poly(ethylene terephthalate), Polycarbonate (PC), Epoxidized Natural Rubber, Epoxy Polymer Resins (EPR), Poly(amic acid), Polyetherimide, etc.
Polyolefins	Polypropylene (PP), Polyethylene (PE), Polyethylene Oligomers, Poly (ethylene-*co*-vinyl acetate), Ethylene Propylene Diene Methylene Linkage Rubber (EPDM), etc.
Specialty Polymers	Polypyrrole (PPY), Poly(*N*-vinylcarbazole) (PNVC), Polyaniline (PANI), etc.
Biodegradable Polymers	Polylactide (PLA), Poly(butylene succinate) (PBS), PCL, Unsaturated Polyester, Polyhydroxy Butyrate, Aliphatic Polyester

2.3 Layered Double Hydroxide (LDH)

Layered double hydroxides (LDHs) belong to a general class of layered materials called anionic clay minerals. They can be of both synthetic and natural origin. LDHs are antitypes of 2:1clay minerals with positively charged metal oxide/hydroxide sheets comensated by anions in the interlayers. The most commonly known naturally occurring LDH clay is hydrotalcite having chemical formula Mg_6Al_2 $(OH)_{16}CO_3 0.4H_2O$. Hydrotalcite is the first mineral of this group whose structure and properties were studied extensively and often taken as the representative of the LDH clay materials. Hence, the LDHs are also known as hydrotalcite-like-compounds. The LDHs are the class of anionic clays represented by the general formula $[M^{II}_{1-x} M^{III}_{x} (OH)_2]^{x+}.[(A^{n-})^{x/n} . mH_2O]$ where M^{II} and are divalent such as Mg^{2+}, Zn^{2+}, Ca^{2+}, Co^{2+}, Ni^{2+}, Mn^{2+} or Cu^{2+} and M^{III} is a trivalent metal ion, such as Al^{3+}, Cr^{3+}, Co^{3+}, Fe^{3+}, V^{3+}, Mn^{3+}, Ni^{3+} or Ga^{3+}, respectively, and An^- is an anion, such as Cl^-, CO_3^{2-}, NO_3^- or SO_4^{2-} etc. The anions occupy the interlayer region of these layered crystalline materials. The M^{2+}/M^{3+} ratio generally ranges from 1 to 5 [7], the pure phase of LDH clays is usually obtained for a limited range as $0.2 \leq x \leq 0.33$ [8].

The structure of LDHs can best be explained by drawing analogy with the structural features of the metal hydroxide layers in mineral brucite or simply the $Mg(OH)_2$ crystal structure. Brucite consists of a hexagonal close packing of hydroxyl ions with alternate octahedral sites occupied by Mg^{2+} ions. The metal hydroxide sheets in brucite crystal are neutral in charge and stack one upon another by Van der Waal's interaction. The interlayer distance or the basal spacing in brucite has a value of about 0.48 nm. In LDH, some of the divalent cations of these brucite-like sheets are isomorphously substituted by a trivalent cation and the mixed metal hydroxide layers, $[M^{II}_{1-x} M^{III}_x(OH)_2]^{x+}$, thus formed acquire a net positive charge. This excess charge on the metal hydroxide layers is neutralized by the anions accumulated in the interlayer region. The interlayer region in LDHs also contains some water molecules for the stabilization of the crystal structure. . The presence of anions and water molecules leads to an enlargement of the basal spacing from 0.48 nm in brucite to about 0.77 nm in Mg-Al–LDH. A schematic representation comparing the brucite and the LDH structures is shown in **Figure 2.3.**

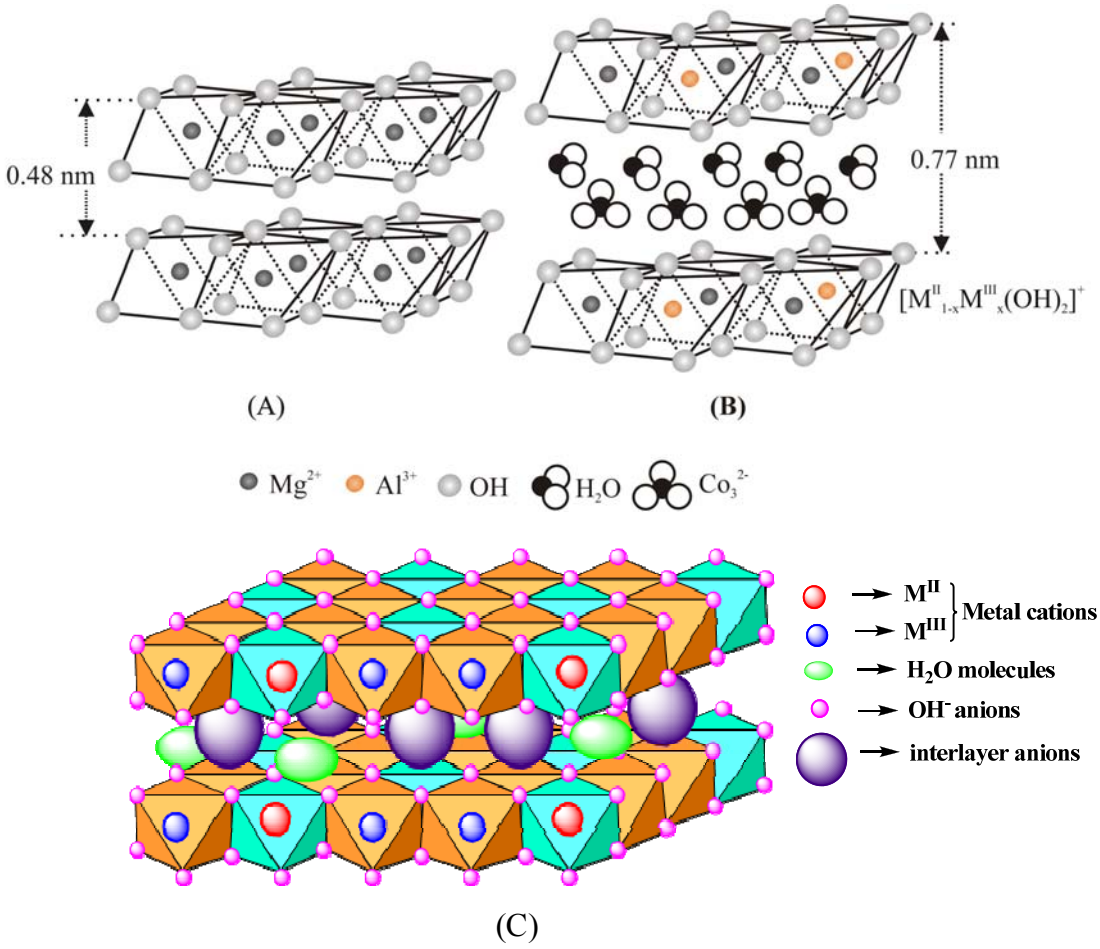

Figure 2.3: Schematic Representation comparing the crystal structure of brucite (A), LDH (B &C) [9, 10].

Although LDHs have layered structure like layered silicates, the two are quite significantly different from each other. While LDHs have positively charged layers with anionic interlayer species (so they are called anionic clay), the layered silicates have positively charged layers with cationic interlayer species (hence called cationic clay). In terms of compositions, geometry and layer thickness, LDHs are vastly different from layered silicates. In LDH, as described earlier, each crystal layer is composed of a single octahedral metal hydroxide sheet. Whereas, in layered silicates, it is a sandwiched structure of two or more sheets of metal oxides. For example, montmorillonite crystal layer is made up of three sheets. One octahedral sheet containing oxides of Fe, Al, Mg, etc remains sandwiched between two silica tetrahedral sheets as shown in **Figure 2.4 (a)**.

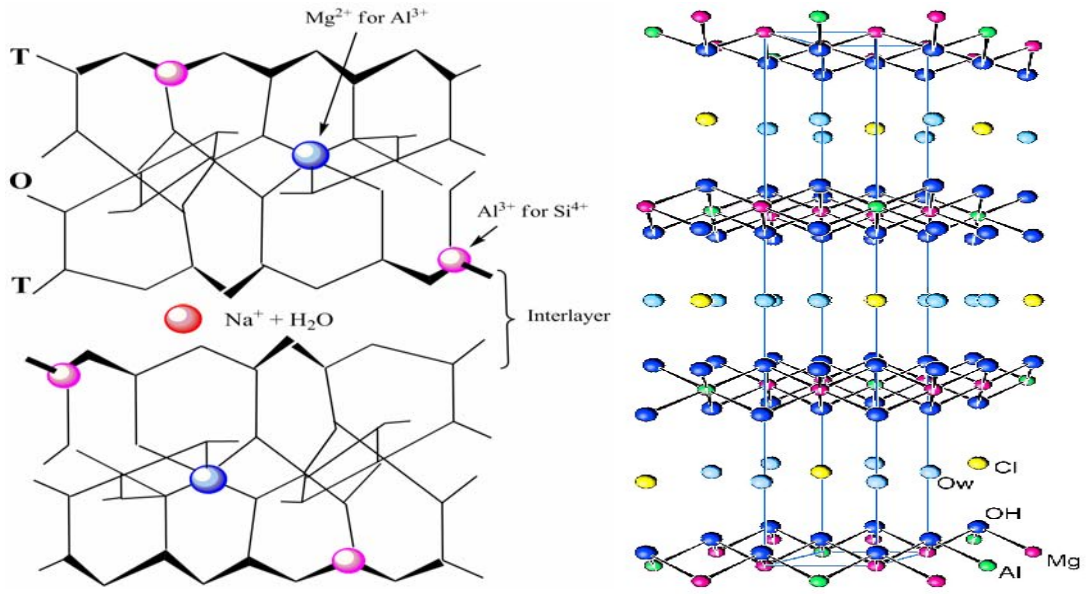

Figure 2.4: (a) Structure of MMT **(b)** Structure of LDH

This difference in layer structure results much lower crystal layer thickness and rigidity in case of LDHs. The charge density of hydroxide sheets in LDHs is in the range of 0.33 – 0.25 cm^{-2} (as high as in mica, 0.32 – 0.34 cm^{-2}) [7], which is much higher compared to that observed in various cationic clays of both natural and synthetic origin. However, the remarkable behavior of LDH is their high reactivity towards various organic anions, which can exchange as much as 80 – 100% of the interlayer anions in LDHs [7]. Many LDH materials show unique phenomenon called 'memory effect', which involves the regeneration of the layered crystalline structure from their calcined form, when the later is dispersed in an aqueous solution containing suitable anion [11]. This property is often used to synthesize and modify LDHs with different types of intercalating anions. Typically, LDHs containing carbonate anion are heated to a temperature in the range of 350–800 ˚C for several hours and the resultant mixed metal oxide (more precisely a solid solution of the two metal oxides) is then dispersed in an aqueous solution of the desired anionic species. The dispersion is overnight stirred mechanically at room temperature to ensure completion of the regeneration process. The regeneration property shown by LDHs is extensively reported in numerous literatures [8, 12-13]. LDHs can be readily

synthesized under laboratory conditions, with easily controllable chemical composition of the layer and interlayer domains [11, 14]. The co-precipitation method of LDH preparation involves co-precipitation of selected pairs of metal ions from their aqueous solution by a dilute NaOH or $NaHCO_3$ or Na_2CO_3 or NH_4OH solution. The pH of the reaction medium is maintained in the range of 8 to 10 depending on the nature of the metal ions. To obtain well crystallized materials the final suspension is subjected to hydrothermal treatment for a long period. The detail description of the process is available in numerous reports available in literature [15-19].

The homogeneous precipitation method using urea hydrolysis for synthesis provides LDH with a high degree of crystallinity and a narrow distribution of particle size. Usually, an aqueous solution of desired metal ions and urea in calculated molar ratio is heated at 90 ˚C to reflux condition for 24 – 36 hours. The urea molecules undergo decomposition producing ammonium carbonate, which finally causes the precipitation of LDH containing CO_3^{2-} as intercalating anion [20- 22]. The ion exchange method takes the advantage of exchangeable interlayer anions present in LDHs by other anionic species. Based on this property, the LDHs containing one type of intercalating anionic species can be synthesized from the LDHs containing another type of intercalating anion. Usually, the original LDH is dispersed in an aqueous solution of the desired anionic species and the dispersion is stirred at room temperature for several hours. However, some anionic species show more affinity to the inter gallery region of LDH than the other [23- 25]. Hydrothermal crystallization method involves the crystallization of amorphous $M^{III}_2O_3$ precursor in presence of a suitable $M_{II}O$, the latter acting as a crystallizing agent [26]. The precursor $M^{III}_2O_3$ is an amorphous hydrated oxide of the trivalent metal component of LDH whereas the crystallizing agent $M_{II}O$ is a reactive and basic oxide of the divalent metal component. The actual synthesis is carried out by hydrothermal treatment of an aqueous suspension of these two metal oxides in a pressurized vessel at elevated temperature for several days.

2.3.1 Organomodification of LDHs

Nano-clays may be called swellable-layered materials since they comprise planar layers arrayed in a co-herent, co-planar structure. The bonding within the layers is stronger than the bonding between the layers, such that they exhibit interlayer spacing in their intercalated compounds. As shown in **Figure 2.3**, swelling or compatibilizing agents may be introduced into the interlayer spaces by insertion, in the case of neutral molecules, ion exchange in the case of ions. LDH is normally very hydrophilic, therefore, is not compatible with most polymer resin like polypropylene. Usually, the clay materials include interlayers or exchangeable anions such as Cl^{-}, CO_3^{2-}, NO_3^{-} or SO_4^{2-} etc. Indeed, if LDH is placed in a solution of a given exchangeable long chain anionic organic-modifier i.e electrolyte, an exchange occurs between the ions of the clay (X^{-}) and those of the electrolyte (Y^{-}).

$$X.clay + Y^{-} \rightleftharpoons Y.clay + X^{-}$$

In the state, the unmodified clay does not delaminate in host polymer melts regardless of mixing, because the interlayer spacing usually too low to intercalate the macromolecular chains. A good intercalation is achieved for organomodified LDHs because higher inter -lamellar distance. Intercalation behavior of LDHs towards various organic anionic surfactants is extensively reported in literatures [7, 27- 29]. Carlino [29], reviewed different methods for modification of LDHs by long chain carboxylic acids. **Table 2.4,** summarizes different organomodified LDHs employed in fabrication of various polymer nanocomposites reported in the literature.

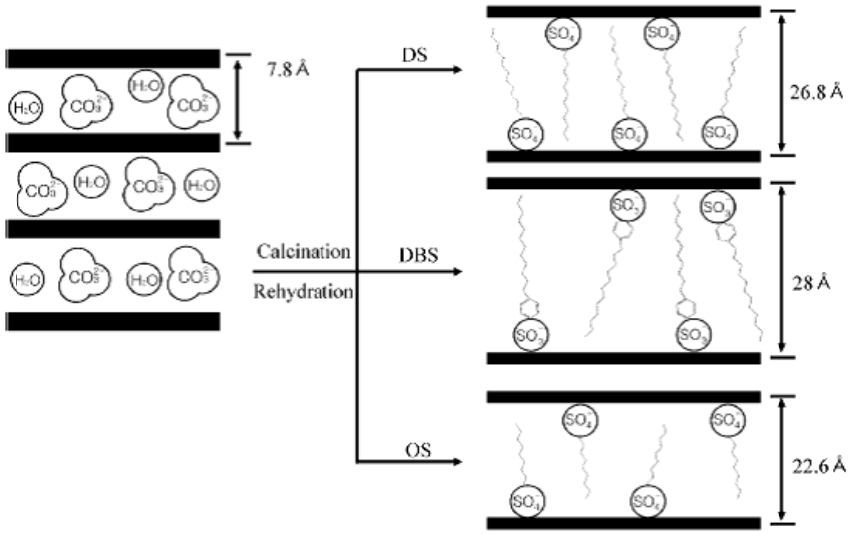

Figure 2.5: Schematic diagram of various organomodified LDHs. [30]

2.4 Structures of Polymer/LDHs Nanocomposites

Depending on the interactions and structures of constituents, polymer/layered nano-fillers nanocomposites can be classified as (i) phase separated or immiscible; (ii) intercalated; and (iii) exfoliated, exhibited in **Figure. 2.6.** When the polymer molecular chains are unable to intercalate clay platelets, indicated by no increase of interlayer spacing, immiscible composites are formed with the marginal property enhancement, known as "*microcomposites"*. Beyond this kind of classical composites, intercalated structure is obtained through the penetration of polymer molecular chains into the clay interlayers, as the result of a well-ordered multi-layer sandwich structure, built up with repeatable polymeric and inorganic layers. Hence, the interlayer expansion inevitably results in increasing the interlayer spacing. In the exfoliated nanocomposites, the individual clay platelets are peeled apart, completely and homogeneously dispersed in the continuous polymer matrix, so-called "*delamination"*. Either ordered or disordered exfoliated structure relies on the different clay platelet orientation states, arising from the secondary manufacturing processes (e.g. injection/compression moulding) after melt compounding of nanocomposites.

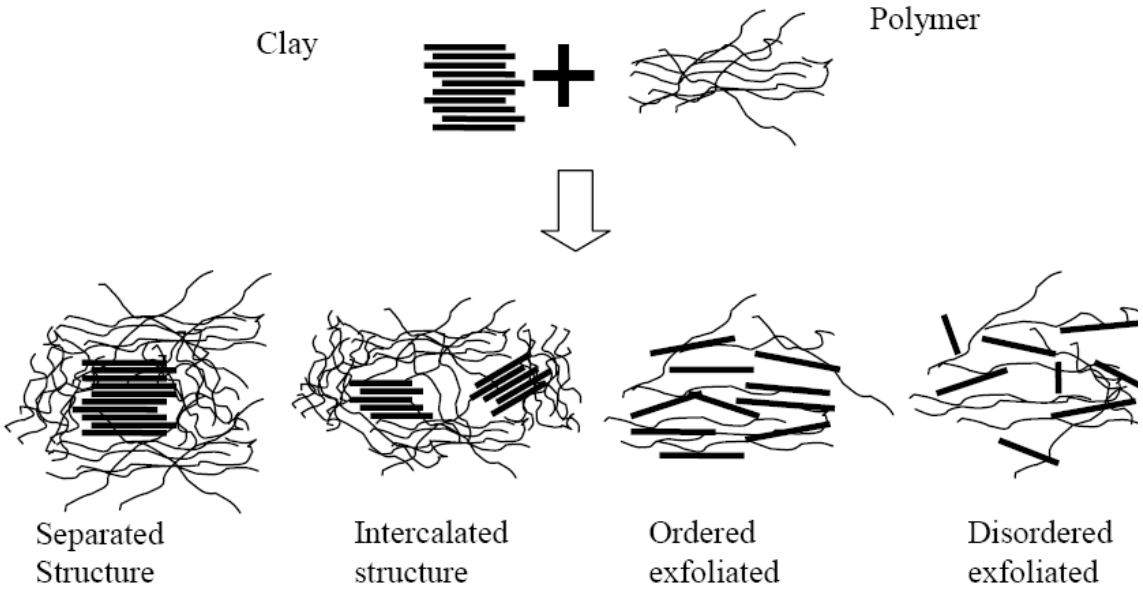

Figure 2.6: Nanocomposite structures based on the interaction of layered nano-fillers and polymers [31].

For instance, exfoliated clay platelets in the skin region of injection molded specimens of nylon 6/clay nanocomposites reveal a higher degree of alignment along the mould flow direction as opposed to the random orientation in the core area [32]. In the real morphology of polymer/clay nanocomposites, partially intercalated and exfoliated structure is practically available due to the limitation of conventional compounding methods and the difficult thermodynamic interactions in dispersing clay particles, which is mostly the case for PP/clay nanocomposites.

2.5 Processing Methods of Polymer/LDHs Nanocomposites

2.5.1 Preparation

The lamellar structure and anion exchange capacity of LDHs allow the formation of a wide range of host–guest complexes. Although the usages of LDHs in different fields, like catalysis, acid scavenger, controlled chemical release, etc. are well known, their potential as nanofillers in preparing polymer nanocomposites is very recently realized by researchers. In this regard, unlike conventional layered silicates (which is widely used so far as nanofiller in polymer), LDHs possess certain inherent advantages. For example, being mostly of synthetic origin, the presence of impurity in LDHs is far less and also a wide range of chemical compositions can be obtained by changing the type and molar ratio of the metal ion pairs during the synthesis process. Additionally, the positive nature of the crystal layers in LDHs provides a greater flexibility in selecting the suitable modifier from several groups of organic compounds, like fatty acid salts, sulfonates, sulfates, phosphates, etc [7, 33-34]. The LDHs apparently resemble many cationic clay minerals (like layered silicates) so far as the principle of polymer nanocomposite preparation is concerned. But, the major disadvantage of LDHs is the high charge density of layers, which firmly holds the metal hydroxide layers in the crystalline stacks and makes the intercalation of the polymeric materials into the interlayer region difficult. However, the strong affinity of LDHs for anion exchange reaction even with oligomeric anionic species gives an opportunity to convert these materials into suitable precursors for polymer nanocomposite preparation. In literatures, several methods for the preparation of polymer/LDH nanocomposites have been reported [35], which are described briefly in the following sections.

2.5.1.1 In-Situ Intercalative Polymerization

In this method, the layered nano filler is swollen within the liquid monomer or a monomer solution so the polymer formation can occur between the intercalated sheets. In-situ polymerization is the most widely referred technique for polymer/LDH nanocomposites preparation. This method is solution based and is usually carried out in an aqueous system. The scheme shown in **Figure 2.7** indicates the general principle for carrying out in-situ polymerization within the layers of LDH crystals. The primary step is

the preparation of monomer intercalated LDH hybrids, which are then subjected to excitation by heat [36, 37.], initiating chemicals [38], etc. for carrying out the polymerization reaction. Various methods of intercalation of monomers into the interlayer region of LDHs and their subsequent polymerization have been reported in literatures, which are summarized in **Figure 2.7.**

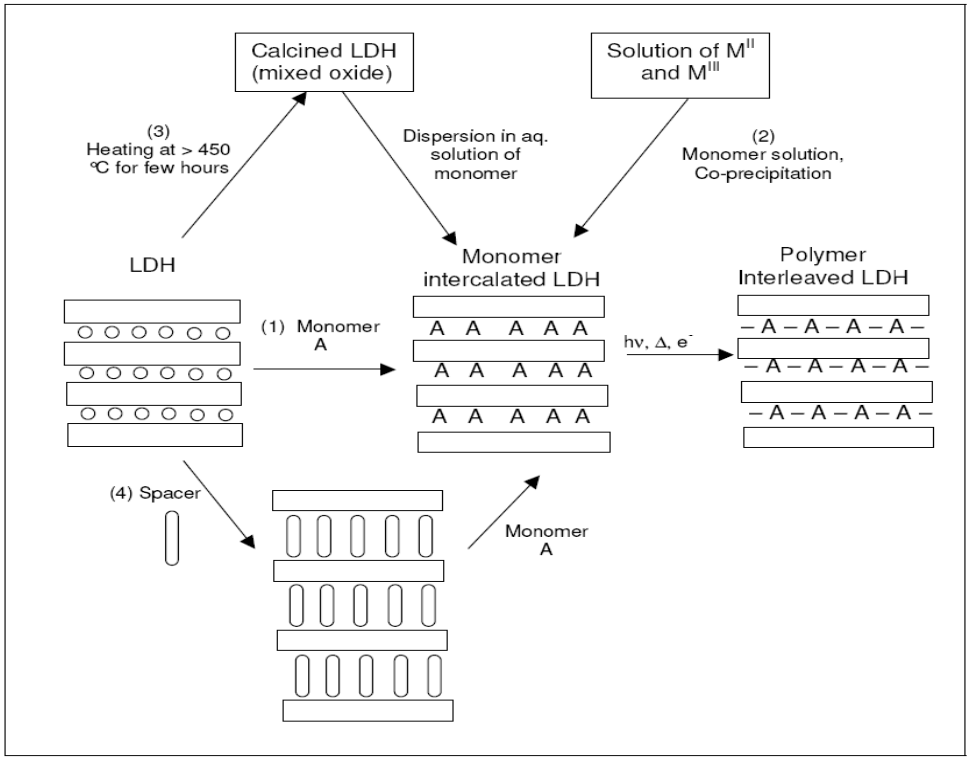

Figure 2.7: Schematic pathways of in-situ polymerization within LDH layers to synthesize polymer- LDH nanocomposites [9]

The anionic interchange method involve's the dispersion of LDHs into a monomer solution, most often in aqueous medium (path 1 in **Figure 2.7**) [39- 41]. The dispersion is then stirred for several hours with mild heating. The monomer molecules must have anionic functionality or strong nucleophillic sites in order to replace the interlayer anions in LDHs and to stabilize the layered stacking of the hydroxide sheets by neutralizing their excess positive charge. For example, acrylate anions can be easily intercalated into Mg-Al–LDH through ion exchanges with Cl^- or NO^{3-} present in LDH [41]. Other reports includes intercalation of amino benzoic acid [42], vinyl benzene sulfonate [40]. Recently, Lee and Chen have synthesized polyacrylate/LDH-based superabsorbent xerogels using in-situ suspension polymerization technique [38]. The most common and successful

method of preparation of monomer-LDH hybrid is synthesis of LDH by co-precipitation of metal ions from their mixed solution containing dissolved monomer (usually in form of salt) (path 2, **Figure 2.7**). To minimize the interference with CO_3^{2-}, the reaction mixture is often purged with nitrogen. The formation of hydroxide layers and the inclusion of monomer anion in the interlayer region take place simultaneously. Whilton and co-workers prepared polyamino acid/LDH based nanocomposites following this method [36]. An amino acid intercalated Mg-Al–LDH was prepared by reacting a mixed Mg and Al nitrate solution with a basic solution containing aspartate anion under nitrogen atmosphere. The aspartate-LDH hybrid thus obtained was subjected first to heating at 220 °C for 24 hours followed by the treatment with basic solution. The heat treatment in the first step provides condensation of the aspartate monomer within the interlayer region into polysuccinimide, which in the second step undergoes hydrolysis to form poly(ε–aspartate) [36]. Darder et al. demonstrated intercalation of various biomolecules during reconstruction of LDH phases. [43]. The other examples of the synthesis of polymer-LDH nanocomposites by co-precipitation method are intercalation and subsequent polymerization of styrene–4–sulfonate within Ca-Al–LDH [44], styrene sulfonate into Zn–Al and Ca-Al–LDH [42], 3–sulfopropyl methacrylate within Zn-Al–LDH [45], etc. The property of LDH materials to regenerate from an aqueous dispersion of their mixed oxide form is also applied to prepare the monomer-intercalated hybrids (path 3, **Figure 2.7**). This is called regeneration method, which is similar to that used for converting LDH containing CO_3^{2-} to the other forms. This method is very common for the modification of LDH materials with organic molecules, which are then used as a precursor for polymer intercalation by various methods. The organic/inorganic pillar method (path 4, **Figure 2.7)** differs from the anion exchange method in the sense that an anionic species (other than the monomers) is used in this method as a spacer or pillaring agent to increase the interlayer distance before the intercalation of monomer. Therefore, the monomers in this case interact with a pillared LDH species. Wang et al. [46] used 10-undecenoate pillared Mg-Al– LDH hybrid (prepared by co-precipitation method) as the precursor for methyl methaacrylate (MMA) intercalation into LDH and subsequently polymerized the intercalated MMA using a two-step bulk polymerization technique. Similarly, monomers like aniline [47], acrylonitrile [48] and acrylate [49] etc. have been successfully

intercalated in to LDH gallaries. Chan and co-workers [50] synthesized LDHs/epoxy nanocomposites using an active initiating agent poly(oxypropylene)–amindocarboxylic acid (POP–amido acid). The POP–amido acid modified Mg_2-Al–LDH was used as the curing agent precursor for intercalation of epoxy monomers (diglycidyl ether of bisphenol-A (DGEBA). The POP–amido acid/LDH epoxy networks were prepared by allowing initiating the epoxy self-polymerization. The possible mechanism of interlayer polymerization is shown in **Figure 2.8.** Also, the intercalated PMMA-MgAl LDH structure is obtained by similar method [51].

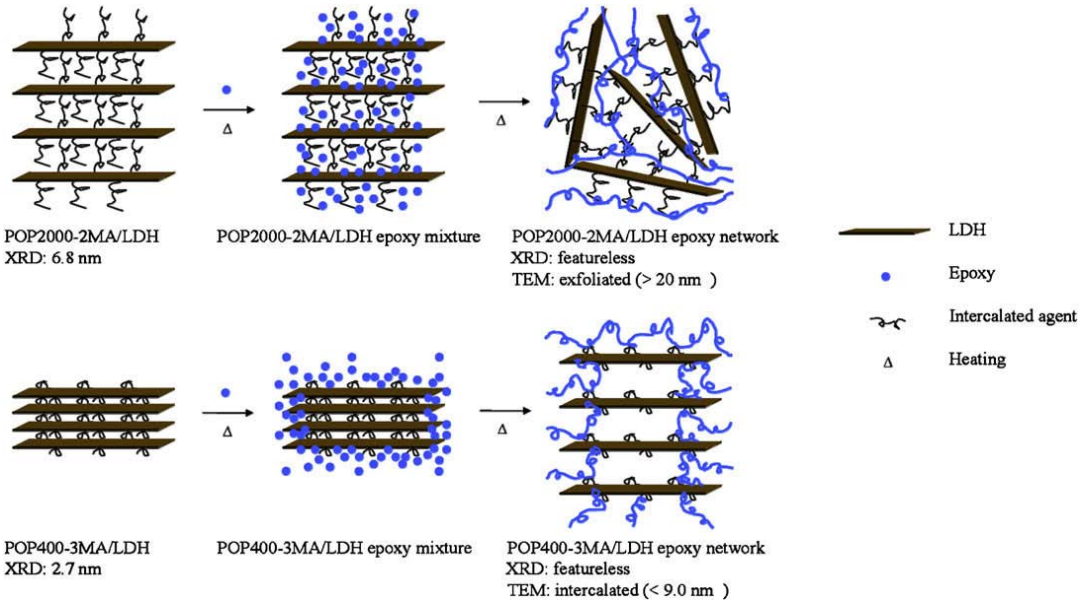

Figure 2.8: Conceptual diagram of POP–amido acid/LDH initiated epoxy polymerization to form the intercalated or exfoliated networks [50]

2.5.1.2 Solution Intercalation

This is based on a solvent system in which the polymer or prepolymer matrix is soluble and layered nano-fillers, are swellable. The layered filler is first swollen in a solvent such as water, chloroform or toluene. When the biopolymer and solution of swollen nanoparticles are mixed, the polymer chains intercalate and displace the solvent within the interlayer of the lamellas. Upon solvent removal, the intercalated structure remains, resulting in a polymer nanocomposite formation. The direct intercalation of the polymeric species having functional groups that can interact with the hydroxide layers of LDH is also an effective way to prepare polymer/LDH nanocomposites. Principally, the

methods used for intercalation of monomer or small oligomeric organic molecules into LDH, are also applicable for high molecular weight species. But, due to a very small interlayer distance and high charge density of the LDH layers, the direct intercalation of large polymeric chains is more difficult. Messsersmith and Stupp [52] prepared poly(vinyl alcohol) (PVA) intercalated Ca-Al–LDH by precipitating the later in the presence of dissolved PVA. The process involved mixing of a $Ca(OH)_2$/PVA solution to a solution containing $Ca(OH)_2$ and $Al(OH)_3$. It was suggested by them that the PVA molecules facilitate the nucleation and the growth of the metal hydroxide layers. Further, Oriakhi and co-workers [53], reported the incorporation of poly(acrylic acid), poly(vinylsulfonate) and poly(styrenesulfonate) into the LDHs, like $M_{1-x}Al_x\ (OH)_2\ x^+$ (where, M is Mg, Ca, Co) and $Zn_{1-x}M_x\ (OH)_2\ x^+$ (where, M is Al, Cr) by precipitating LDH from a deareated aqueous basic solution containing mixed metal nitrates and dissolved polymer. Other examples of polymer-LDH nanocomposites prepared by direct intercalation through co-precipitation technique are Mg-Al–LDH intercalated with poly(vinylsulfonate) [54], polyaspartate [36], poly(ethyleneoxide) derivatives [55], etc. Recently, Wu and co-workers [56] described fabrication of biodegradable Poly(L-lactide)/LDH nanocomposites by solution intercalation of PLLA into the galleries of PLA–COOH modified LDH (P-LDH) in tetrahydrofuran solution. Often for the intercalation of polymeric species in solution, organically modified LDH clays are used. Various anionic surfactants, like the salts of the fatty acids with different chain lengths, alkyl or alkylaryl sulfonates, etc are usually used for LDH modification. This modification involves the exchange of anionic species present in the unmodified LDH by a suitable organic anion, which is carried out by the similar methods used for LDH synthesis. The organically modified LDHs show higher interlayer separation and increased hydrophobicity, both of which make the polymer intercalation process easier. Qu and co-workers prepared and characterized polyethylene/LDH [57, 58] and polystyrene/LDH nanocomposites [59] by this method using dodecylsulfate modified LDH (LDH-DS). The nanocomposites were obtained by refluxing the mixture of LDH-DS and the polymers solution in xylene. Buniak and coworkers [60] also used LDH-DS to prepare poly(ethylene oxide) (PEO)/LDH nanocomposites. The modification of Mg-Al–LDH was carried out using ion-exchange method and the modified LDH was later

treated with aqueous solution of PEO to prepare the nanocomposite. Recently, Liao and Ye [61] prepared PEO/LDH based nanocomposite electrolyte by solution intercalation method. First, using the co-precipitation method they modified Mg-Al–LDH with two different types of anionic surfactants: alkyl 3-sulfopropyl ether salt (containing about 11 ethylene oxide/mole and C13 – C15 alkyl chain) and oligomeric hydroxy poly(ethylene oxide) phosphate. Then the nanocomposites were obtained by mixing PEO, the modified LDH and lithium perchlorate in anhydrous acetonitrile at 70°C with constant stirring for several hours. Further, Li and co-workers [62] prepared glycine intercalated Mg-Al–LDH and modified with formamide, which was then treated with an acetone solution of PMMA to form the nanocomposites. All these cases mentioned so far produce mostly polymer-intercalated LDH particle in the nanocomposite matrix. Hsuesh and Chen [63], reported the synthesis of exfoliated epoxy/LDH nanocomposites by treating amino laurate intercalated Mg-Al–LDH with a mixture of epoxy resin and curing agent. The resin and the curing agent diffused into the LDH interlayer region after heating the mixture for few hours. The thermal aging of this reaction mixture causes exfoliation of the LDH layers due to curing of the epoxy resin in between the layers, which results in formation of crosslined network of epoxy resin. The direct ion exchange with LDHs by the polymers having anionic functional groups is also a feasible method for the preparation of polymer/LDH nanocomposites. This method does not involve the organic modification of the pristine LDH. The other reports also show the intercalation poly(ethylene oxide) sulfate and poly(ethylene glycol) [64], dendrimers (carboxylate terminated polyamidoamide) [65] and poly(ethylene oxide) [55] in to LDH.

2.5.1.3 Melt Intercalation

This process involves annealing a mixture of the polymer and nanoparticles above the softening point of the polymer. While annealing, the polymer chains diffuse from the bulk polymer melt into the galleries between the nano layers. Perhaps the most challenging method of preparing polymer/clay nanocomposites is the melt compounding method. Melt intercalation is an environmentally friendly technique, as it does not require any solvent. It is also commercially attractive due to its compatibility with existing processing techniques. With non-polar polymers, like polyolefin, it becomes more

difficult due to high thermodynamic incompatibility between the non-polar matrix and the polar clay materials. There are not many reports available till today that exclusively deal with the preparation of polymer/LDH nanocomposites using melt-compounding technique. This method has definite technological advantage over the solution method as it can be easily adopted for industrial product manufacturing using conventional polymer processing equipments. Therefore, in spite of being most difficult method, melt-compounding method always finds special interest among researchers. Use of Mg-Al–LDH in the preparation of polymer composites using this method is very common, where it is treated as simple metal hydroxide whose basic nature and endothermic decomposition serves two-fold purpose: as acid scavenger in halogenated polymers [66, 67] and as flame-retardant [68]. However, in none of these applications any reference was made to exploit the efficiency of Mg-Al–LDH as nanofiller. The melt-compounding method used for the preparation of polymer/LDH nanocomposites is similar to that used for conventional polymer/clay nanocomposites. The organically modified LDHs are the suitable precursor for this process, which are mixed with molten polymer in the typical plastic processing equipments. Nichols and co-workers [69] first reported the melt-compounding method for preparing polymer/LDH nanocomposites. Very recently, researchers are showing more interests in this method to prepare nanocomposites based on different types of matrices. For examples, Zammarano *et al.* prepared polyamide 6/LDH nanocomposites using organically modified Mg-Al–LDH [70]. They observed that high degree of exfoliation of the LDH particles can be obtained using LDHs with low anion exchange capacity. Ardanuy *et al.* [71] prepared and characterized high-density polyethylene (HDPE)/hydrotalcite nanocomposites with a partially neutralized sodium ionomer of poly(ethylene-*co*-methacrylic acid) (EMAA) as a compatibilizer. Lee *et al.* [30] prepared poly(ethyleneterephthalate)/LDH nanocomposites with Mg-Al–LDH modified with various organic surfactants. They observed improved thermal and mechanical properties of these nanocomposite compositions compared to the unfilled polymer. The other reported polymer/LDH nanocomposites systems prepared by melt-compounding methods include polypropylene/Zn-Al–LDH [72], polyethylene/Mg-Al–LDH [73], polyethylene/Zn-Al–LDH [74], etc.

Apart from the four main techniques listed above, a few other techniques for the preparation of polymer nanocomposites include sonication [102] and miceller intercalation. [103]. **Figure 2.9,** shows flowchart of above mentioned three processing techniques for clay-based polymer nanocomposites and **Table 2.4** summarizes the various LDH reinforced polymer nanocomposites, type of organomodified LDH used and method of processing reported in the literature.

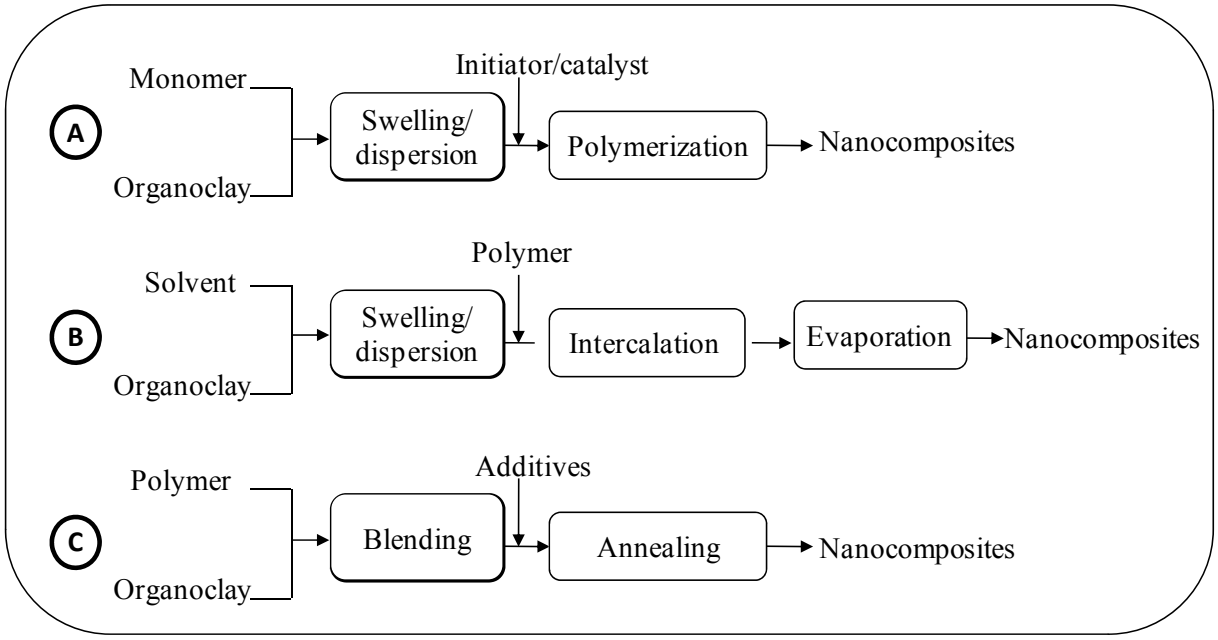

Figure 2.9: Flowchart of three processing techniques for clay-based polymer nanocomposites: A) *in-situ* polymerization, B) solution exfoliation and C) melt intercalation. [104]

Table 2.4: LDH based polymer nanocomposites and their method of processing.

Polymer Type	Layered double Hydroxide/Organic modifier	Processing Method	Reference
Polyamine-6	Co-Al LDH/SDS	In-situ polymerization	75
	Mg-Al LDH /DBS	Melt	70
	Zn-Al LDH/SDS	In-situ	76, 131, 77
Polystyrene	Zn-Al LDH/N-lauroyl-glutamate	In-situ	78
	Zn-Al LDH/ SDS & alfa-bromobutyrate	In-situ	79
PP	Ni-Al LDH/SDS	Melt	80
	Zn-Mg LDH/DS	Melt	72
PP-CO_3	Mg-Al LDH/SDS	Solution	108
	Mg-Al LDH/SDBS	Melt	81
Polyethylene (LDPE, LLDPE and HDPE)	Zn-Al LDH/SDS	Solution	73, 74 110
	Zn-Al LDH /SDS	Melt	82
	Mg-Al LDH /DS, DBS	Melt	83
	Mg-Al LDH/ Oligo(ethylene oxide)	Solution	61
Poly(ethylene oxide)	Cu2Cr(OH)(6)Cl	Solution	55
Poly (ethylene terepthalate)	Mg-Al LDH/ DS, DBS, and octylsulfate (OS)	Melt	30
Poly(butylene terephtahlate)	Mg-Al LDH/4-Sulfobenzoic acid potassium salt, SDS and dimethyl 5-sulfo isophthalate sodium salt	In-situ polymerization	84
PMMA	ZnAl LDH/SDS	In-situ	85
	Mg-Al LDH/SDS	In-Situ	51
EPDM	Mg-Al LDH/DS	Solution	86, 87
Polyurethane	Mg-Al LDH/ SDS	Solution	88
Thermoplastic polyurethane and nitrile butadiene rubber blends	Mg-Al LDH/ SDS	Solution	89
Poly (vinyl chloride)	Mg-Al LDH/ lauryl phosphate	Solution	90
Poly(p-dioxanone)	Mg-Al LDH/ DBS, HBS	Melt	91
Ethylene Vinyl Acetate	Mg-Al LDH/SDS	Solution	92
	Mg-Al LDH/SDS	Solution	93, 94, 95, 96

Nylon-6	Mg-Al LDH/SDS	Melt	97
Poly(l-lactide)	Mg-Al LDH/ (PLA–COOH)	Solution intercalation	133
Poly[(3-hydroxybutyrate)-co-(3-hydroxyvalerate)	Zn-Al LDH/stearate	Solution	98
Polycaprolactone	MgAl LDH NO_3	Solution	99
(ε-caprolactone)	Mg-Al LDH / 12-hydroxydodecanoic acid	Ball Milling	100
Satrch	ZnAl CO_3	Solution	101

2.6 Structure and Properties of Polymer/LDH Nanocomposites

2.6.1 Structural and Morphological Characteristics

The structural and morphological properties of well defined polymer/LDH nanocomposites have been successfully predicted by X-ray diffraction (XRD) and various microscopic techniques. Generally, complete exfoliation of layered nano-fillers in polymer matrix is indicated by the complete disappearance of the diffraction maxima or by their significant broadening in their XRD patterns. However, this can also occur due to other reasons, like extremely low concentration of clay materials in the composites, crystal defects, etc. The reports on polymer/LDH nanocomposites show that such hybrids result in exfoliated/intercalated or swollen nature of the clay structures. The disappearance or little presence of the basal reflections in the XRD patterns of such type of nanocomposites indicates that the LDH crystal structure is destroyed partially/completely. The shifting of their positions to lower 2θ values is interpreted as an expansion of the interlayer region by the polymer chains. Besides, broadening of the characteristic reflections in nanocomposites is often related to the defects in the crystal layer stacking caused by the interlayer polymeric species. The information on the arrangements of the polymer chains within the interlayer region can also be obtained from the XRD data, which suggest that, both bi-layer and mono-layer arrangements of polymer chains are possible depending on the nature of the chain backbone and the pendent functionalities. For example, **Figure 2.10** shows the XRD patterns of polystyrenesulfonate (PSS) and polyvinylsulfonate (PVS) intercalated Mg-Al–LDH nanocomposites. The theoretical calculations based on these XRD results and molecular dimensions reveal that the interlayer distance increases from 0.76 nm in the original LDH

to 1.27 nm to the LDH-PVS hybrid and to 2.10 nm in the LDH-PSS hybrid. The bi-layer thickness of these polymers based on molecular dimensions matches the expanded interlayer distance [53-54]. Again, the nature of arrangement of the pendent anionic functionality or electron rich moiety (like phenyl ring) on the polymer backbone can also influence the packing nature of the polymers in the interlayer region. For example, syndiotactic polystyrenesulfonate with alternating anionic groups projecting to the opposite sides of polymer backbone forms a monolayer arrangement in Ca–Al LDH host. The effect LDH concentration on dispersion state of LDH can be examined by basal peak positions in XRD [59]. **Figure 2.11** depicts the exfoliation of PS/ZnAl LDH nanocomposites with different contents of ZnAl(DS). It can be seen that the basal space of ZnAl(DS) component in the nanocomposites increases to more than 3.7 nm from the 2.54 nm of the original LDH layers with decreasing contents of ZnAl(DS) to 20 wt% from 100 wt%. The diffraction peak below 2θ =3° becomes weaker and broader with further decreasing the ZnAl(DS) contents. Upon loading of ZnAl(DS) below 10 wt%, no diffraction peak can be observed at 2θ =1.5 to 10°, as shown in **Figure 2.11 (**d and e). These data illustrate that the equilibrium between exfoliation and intercalation structures in the PS/ZnAl LDH nanocomposites can be driven toward to exfoliation by decreasing the content of LDH.

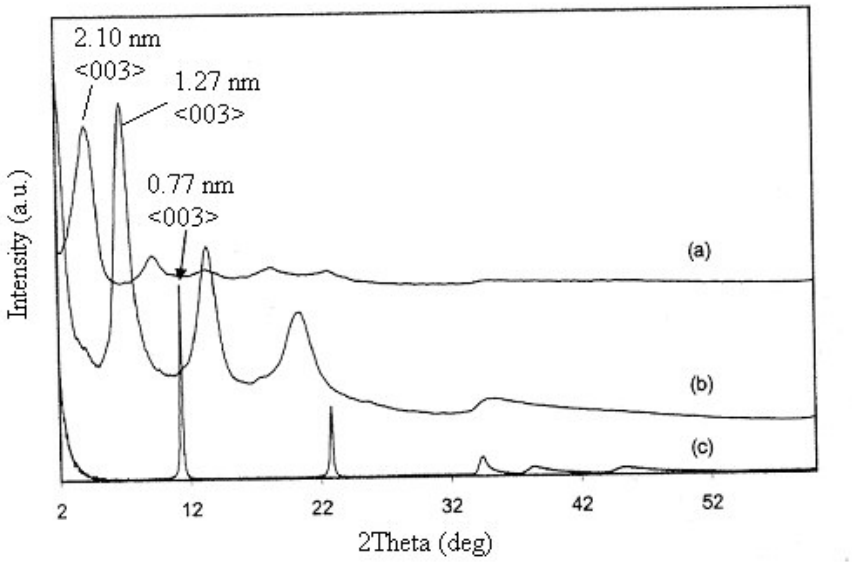

Figure 2.10: XRD patterns of LDH and LDH nanocomposites: (a) LDH-PSS, (b) LDH-PVS and (c) LDH-CO_3 [53].

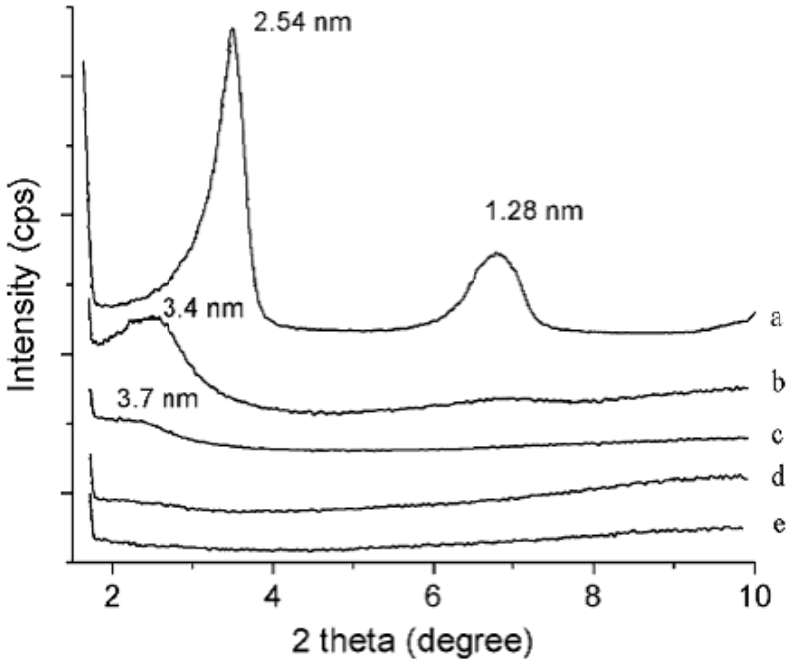

Figure 2.11: Change of XRD patterns with the different contents of ZnAl(DS) in the PS/LDH nanocomposite samples: (a)100 wt%, (b) 50 wt%, (c) 20 wt%, (d)10 wt%, (e) 5 wt%. [59]

The high degree of exfoliation of the LDH clay layers in polymer nanocomposites has also been reported by several groups [46, 63, 58, 105, 70, and 106]. The high degree of exfoliation is not only confirmed from the disappearance of all the characteristic peaks corresponding to LDH after expected conversion, but also from the large extent of polymer fraction unextractable by a suitable solvent from the resultant nanocomposite [106]. When the melt-compounding method is employed for polymer/LDH nanocomposites preparation, processing conditions such as temperature, degree of shearing, etc influence the degree of exfoliation of the LDH particles [70]. Besides, the concentration of LDH and the nature of polymer matrix also influence the state of particle dispersion in the nanocomposite. In general, with highly polar matrices, like epoxies, PMMA, polyimide, polyamide, etc the high degree of exfoliation of the LDH clay layers is achieved up to much higher LDH concentration compared to the relatively less polar or non-polar polymers. In later case, the high degree of exfoliation exists at lower concentration of LDH and with increasing concentration agglomerate formation takes place. Chen and co-workers reported that in polystyrene/LDH nanocomposites, fully exfoliated LDH particles are observed at the low concentrations of LDH whereas at high

concentrations, the LDH particles mostly have intercalated nature [57-59]. The analysis of the TEM micrographs of the polymer/LDH nanocomposites presents direct information about the nature of clay particle dispersion. In the exfoliated nanocomposites based on PMMA, epoxy and polyimide, the dispersed particles mostly exist as exfoliated layers or small tactoids (stacks of small number of single layer). This has been vividly demonstrated in **Figure 2.12**, where TEM images of the nanocomposites containing 5.0 wt% LDH in different matrices are shown at comparable magnification. In case polar matrix (epoxy, PMMA and polyamide), complete exfoliation of the LDH particles can be observed whereas in polystryrene matrix LDH particles are mostly intercalated. In addition to the polarity of matrix polymer, the method of preparation of the nanocomposites significantly influences the crystallinity and the morphology of the dispersed LDH particles.

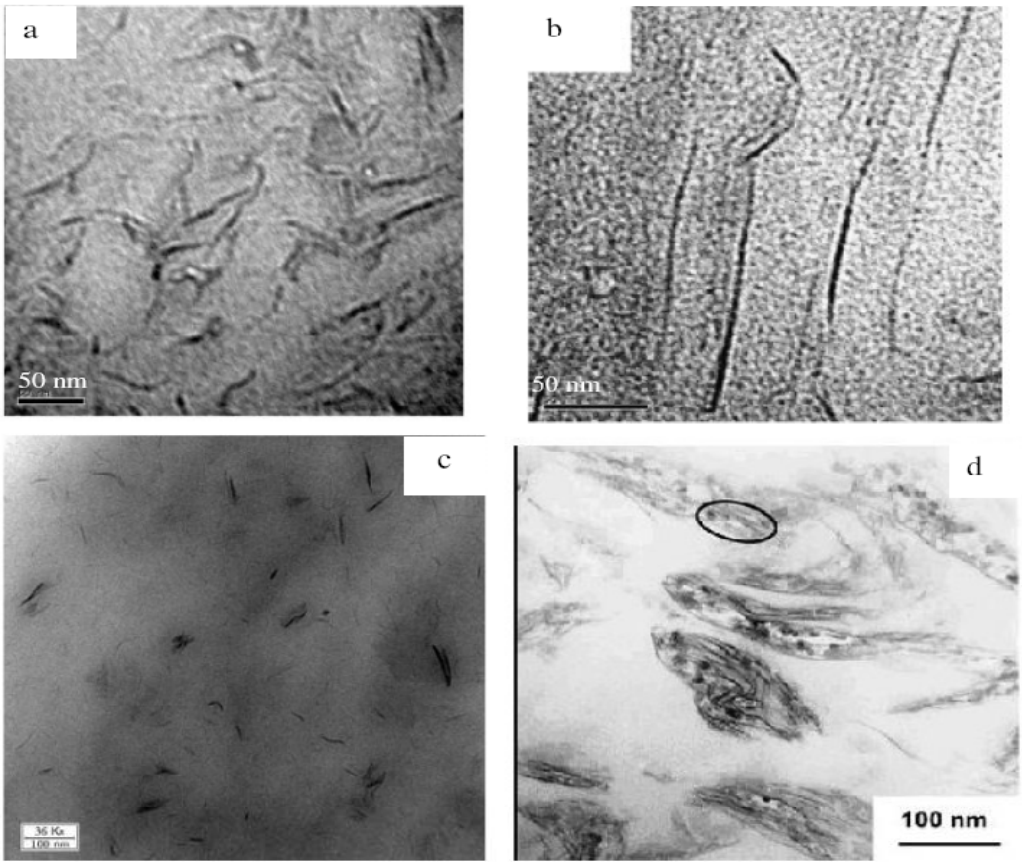

Figure 2.12: TEM micrographs showing LDH particle dispersion in different polymer (a) PMMA [46], (b) epoxy [63], (c) polyamide 6 [70] and (d) polystyrene containing 5 wt% LDH [59].

2.6.2 Properties of Polymer/LDH Nanocomposites

In general, when compared with the conventional polymer composites, polymer nanocomposites exhibit significant improvements in different properties at relatively much lower concentration of filler. Polymer–clay nanocomposites exhibit extremely large interfacial area due to the confinement of polymer chains within the galleries of clay platelets of large surface area per unit volume. It is believed that the confinement of polymer in clay galleries would affect the local chain dynamics to a certain extent. Since several chemical and physical interactions are governed by surfaces, polymer-clay nanocomposites can have substantially different properties from conventional polymer microcomposites. They usually differ from the conventional composites in different aspects, like size of the dispersed filler particles, nature and extent of interaction at the particle-polymer interface, etc. The efficiency of various additives in polymer composites can be increased many folds when dispersed in the nanoscale. This becomes more noteworthy when the additive is used to address any specific property of the final composites such as mechanical properties, conductivity, gas permeability, thermal stability, etc. In case of polymer/LDH nanocomposites, similar improvements are also observed in many occasions.

2.6.2.1 Mechanical Properties

The enhancement in mechanical properties of polymer nanocomposites can be attributed to the high rigidity and aspect ratio together with the good affinity between polymer and LDH. For instance, stronger interface interactions significantly reduce the stress concentration point upon repeated distortion which easily occurs in conventional composites reinforced by glass fibers and thus lead to weak fatigue strength.

The mechanical properties of epoxy/LDH nanocomposites are shown in **Figure 2.13.** It is evident that the presence of a small amount of LDH significantly increases the tensile strength and the modulus showing the strong reinforcing nature of LDH on the epoxy matrix. This highly reinforcing nature of LDH particles in epoxy is related to their exfoliated structure in the nanocomposite, where the highly anisometric LDH layers remain strongly attached to the polar epoxy matrix. This becomes possible due to favorable chemical and electrostatic interaction between LDH surface and oxygen rich

backbone of epoxy matrix. Thus, each individual exfoliated layer imparts reinforcing effect on the matrix. However, such strong interaction often acts negatively on the impact strength of the nanocomposites resulting sharp decrease in elongation at break after a certain level of LDH concentration. In case of relatively less polar polymer, aggregation of the dispersed particles leads to a reduction in the mechanical properties after an initial improvement observed at low concentration of LDH.

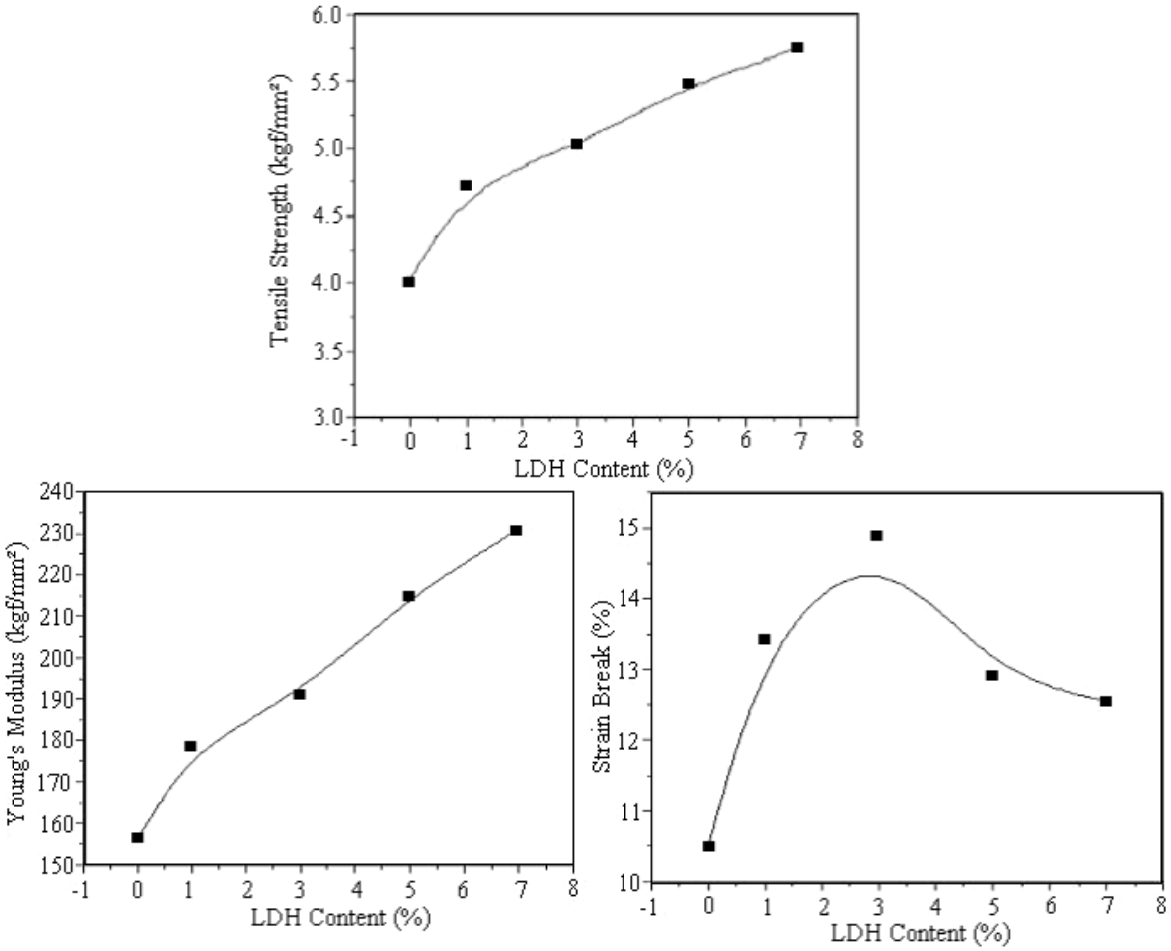

Figure 2.13: Effects of the LDHs content on the tensile properties (tensile strength, Young's modulus and strain at break) of the epoxy/LDH nanocomposites [63].

Hsueh and Chen [63] have observed this behavior in polyimide/LDH based nanocomposites. They reported that beyond 5 wt% LDH content, the dispersed nanolayers form aggregates and the tensile properties of the nanocomposites are reduced. The increase in modulus is believed to be directly related to the high aspect ratio of LDH

layers as well as the ultimate nanostructure. Moreover, a dramatic increase was also observed in exfoliated nanostructures such as LDH based exfoliated PMMA/LDH nanocomposites, Wang *et al.* [106] have observed a strong reinforcing nature of the exfoliated LDH clay particles. In presence of 5 wt% LDH, such composite shows above 60% and 80% increase in tensile strength and modulus, respectively, in comparison to unfilled PMMA. However, flexibility and the impact properties of such nanocomposites are significantly affected, which is reflected in over 50 % lowering in elongation at break during tensile testing. Similarly, mechanical properties of other LDH reinforced polymers have been reported by several authors [107-109].

2.6.2.2 Thermal and Flammability Properties

The improvement of thermal properties compared to the unfilled polymer is a very important aspect of polymer/LDH nanocomposites. The thermal stability of polymer composites is generally estimated from the weight loss upon heating which results in the formation of volatile products. LDHs contain large amount of bound water due to the presence of –OH group on the metal hydroxide sheets and some free water molecules in the interlayer region. The mechanism by which LDH clays improves the thermal stability and flammability of polymer matrix is similar to that observed in case of conventional metal hydroxide type fillers, like $Mg(OH)_2$ and $Al(OH)_3$. The endothermic decomposition of LDHs takes off heat from the surrounding and the liberated water vapor reduces the concentration of combustible volatile in the vicinity of the polymer surface. As a result, the decomposition temperature of the polymer is increased. Interestingly, such improvement is quite significant even at low concentrations of LDH. This is probably due to better dispersion of the LDH particles compared to that observed in conventional composites based on simple metal hydroxide. Again, when the more basic interlayer anions in the unmodified LDHs are replaced by less basic organo anionic species in the modified LDHs, the thermal stability of the metal hydroxide layers are enhanced [110]. Additionaly, the nanoscale dispersion of the clay materials in polymer nanocomposites improves the compactness of the char formed after burning of the surface region. This hinders the conduction of heat and the diffusion of oxygen into the bulk region [111,112]. The improved thermal stability of LDH based nanocomposites has been reported by many researchers [63, 28, 58, 59, 113,114]. In all these cases, thermogravimetric analysis

(TGA) showed significant increase in the temperature at which 50% weight loss occurs. The addition of 5 wt% LDH causes significant enhancement of the thermal stability of the composites, which is attributed to the nanoscale dispersion of the LDH hydroxide layers in the polyimide matrix. However, beyond 5 wt% LDH loading decomposition temperature does not change much with further increase in LDH concentration. The morphological analysis of these nanocomposites reveals that above 5 wt% concentration, the dispersed LDH particles form aggregates and remains mainly in the intercalated forms. This type of behavior has also been observed with other LDH based nanocomposites, like Zn–Al/polystyrene [59] and Zn–Al/polyethylene [58]. In these cases, decomposition temperature, though remain higher than the pure polymer, exhibits a decreasing trend after certain level of LDH content. Recently, Zang *et al.* [115], examined the effect of LDH containing different divalent metal cation on thermal stability of PP/IPR intumescent system. They showed, the thermal decomposition temperatures for the PP/IFR, PP/IFR/ZnAl-LDH, PP/IFR/CaAl-LDH, PP/IFR/CuAl-LDH, and PP/IFR/MgAl-LDH samples are 333.9, 379.2, 374.3, 385.9, and 386.1°C, respectively. It is obvious that the thermal decomposition temperatures of PP/IFR/LDH samples are 40–52°C higher than that of the PP/IFR sample without LDH, which indicates that the LDHs with different divalent metal cations possess the enhanced thermal stability of the PP/IFR system to some different degree.

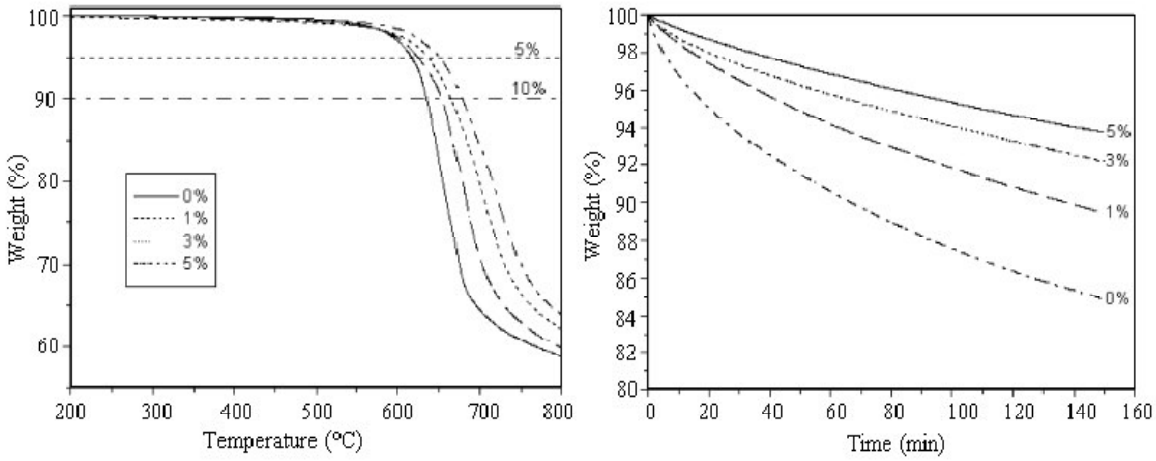

Figure 2.14: Left: TGA curves of LDH/polyimide nanocomposites with various LDH loadings, Right: Effects of LDH content on the decomposition temperatures at 5 and 10 % weight loss of LDH/polyimide nanocomposites [63].

The LHDs already proved as a potential flame retardant for polymeric systems. The flame retardant characteristics of LDH clays originate from their $Mg(OH)_2$ like

chemistry, which involves endothermic decomposition with the liberation of water vapor and often carbon dioxide. The residue of such combustion is the metallic oxides that impede the burning process by reducing the oxygen supply to the fresh surface beneath. The early report on the flame-retardant application of LDH was published by Miyata et al [68.]. In the recent years, many reports have been published that highlight the improved thermal and flammable properties of LDH clay based polymer nanocomposites. Recently, Zammarano and co-workers [116] have reported synthesis of self-extinguishing epoxy/LDH nanocomposites. They have also observed a synergistic effect between LDH clay and ammonium polyphosphate in such nanocomposites, where reduction of APP concentration from about 30.0 wt% to about 16.0 – 20.0 wt% can be tolerated in presence of a small amount of LDH without sacrificing the flammability performance. Recently, Manzi-Nshuti *et al.* [117] reported effect of LDH divalent metals on fire properties of polymers like PMMA and PE and interestingly it is observed that ZnAl performs well with PE, but not PMMA, while MgAl was the best system for PMMA but performs worse with PE as shown in **Figure.2.15.** The dripping behavior of unfilled PE (left) and PE/LDH nanocomposites has been investigated by Costa and co-workers [118] and show that burning rate of LDH filled PE is considerably slow compared to the unfilled PE. In addition, the potential of LDH as a flame retardant is also underlined by several authors [119-122].

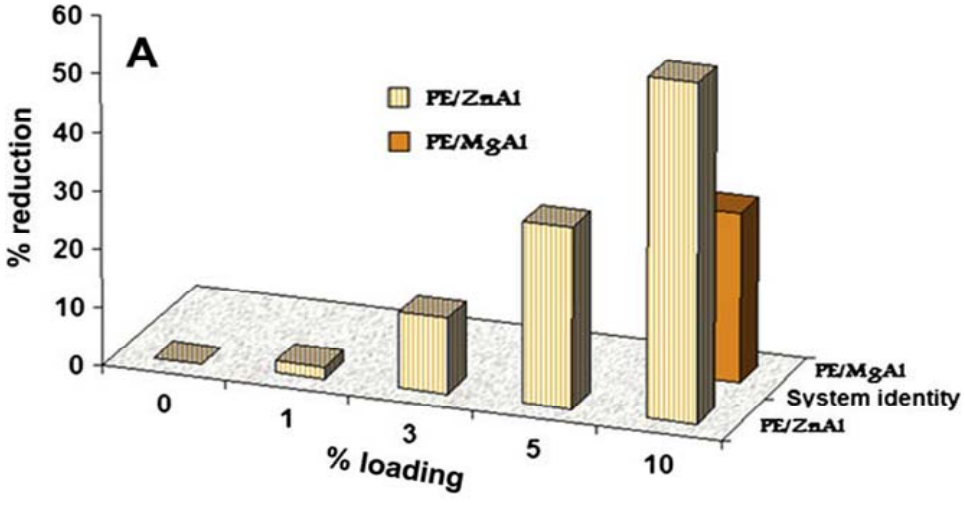

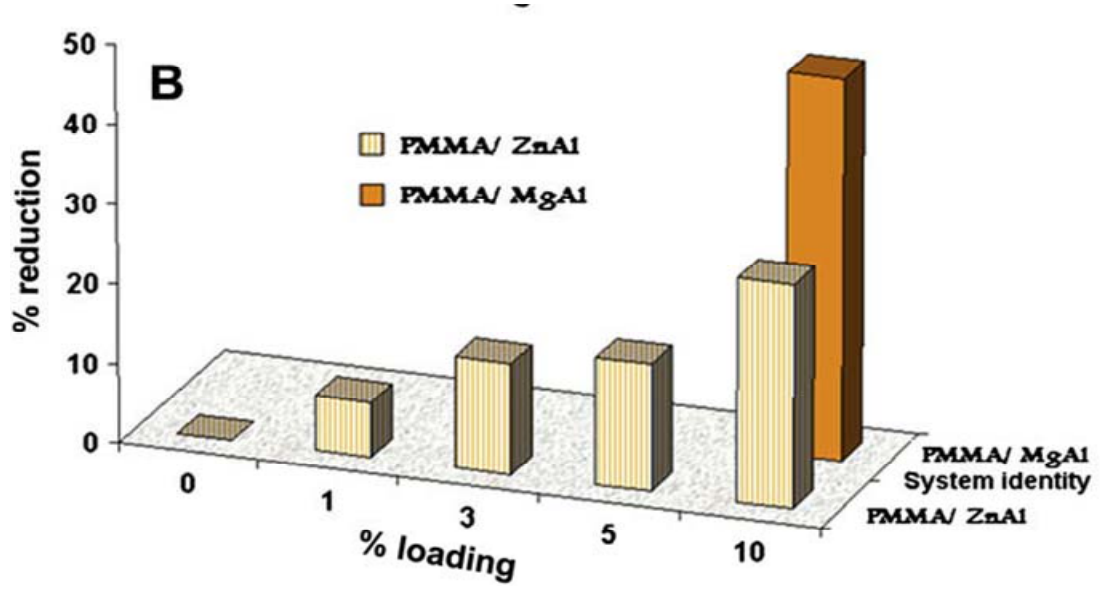

Figure 2.15: Comparison of the fire properties of polymeric systems of ZnAl and MgAl. The % reduction in PHRR is plotted vs. the LDH loading (wt.%) and the cone heat flux was set to 50 kW/m^2. (A) PE systems; (B) PMMA systems [117].

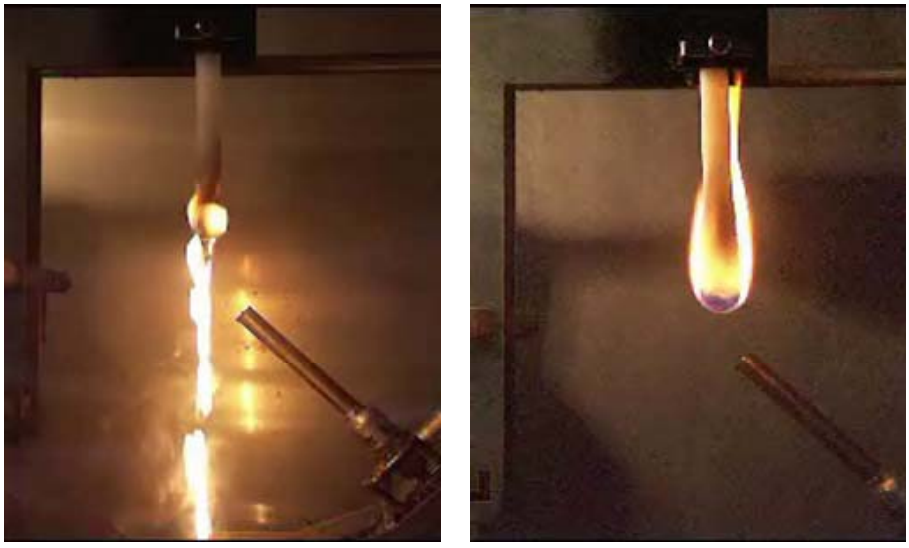

Figure 2.16: Dripping behavior of unfilled PE (left) and PE/LDH nanocomposites containing 12.75 wt% LDH (PE-LDH5) (right) (pictures were taken approximately after the same time period from the cessation of first 10 s flame application during UL94V test) [118].

2.6.2.3 Barrier Properties

Polymer nanocomposites exhibit excellent barrier properties against gases (e.g., oxygen, nitrogen and carbon dioxide), water and hydrocarbons. In this regard LDH nanofillers are relatively new but possess a great potential to improve the barrier properties of polymers because its high aspect ratio [123]. However, few reports still persist in literature on barrier properties of LDH reinforced polymer composites. Water vapor permeability (WVP) of dextrin-alginate/LDH nanocomposites is reported to decrease with organomodified LDH reinforcement **(Figure 2.17)** [124]. Kuila and co-workers [125] showed the influence of DS-LDH in the solvent (toluene) uptake properties on EVA-28/LDPE/DS-LDH nanocomposites. It is observed that the solvent uptake capacity decreases for EVA-28/LDPE blend nanocomposites containing 1 and 3 wt. % of DS-LDH. This is possibly due to the nano level dispersion of LDH particles offering whole surface area available for the interaction between the polymer and DS-LDH.

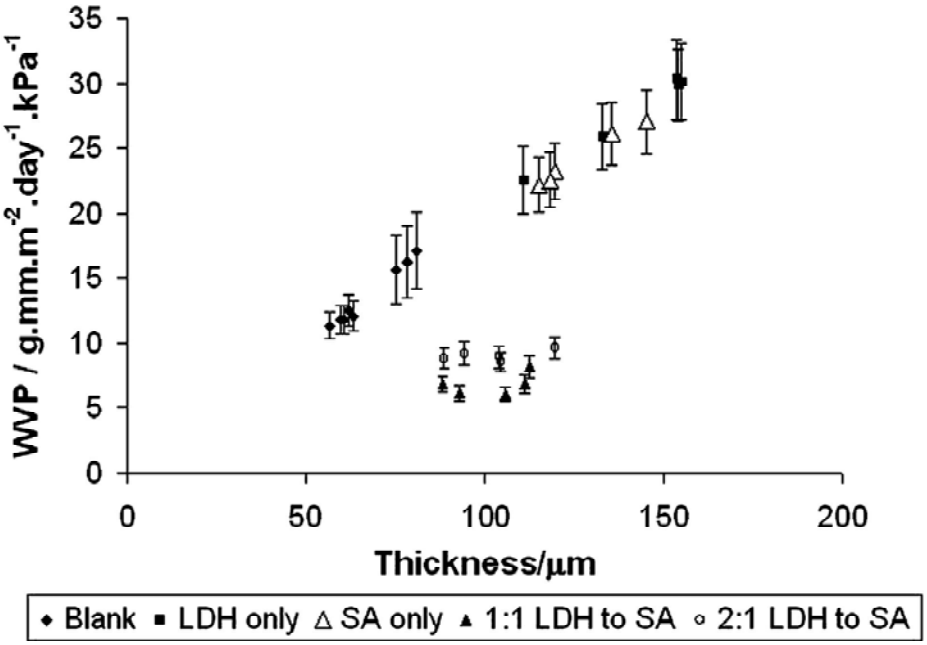

Figure 2.17: WVP of films with no filler, SA only or LDH only showing hydrophilic tendencies and those with combinations of SA and LDH showing hydrophobic tendencies [124].

Additionally, the high aspect ratio of LDH layers possessing the excellent barrier properties by the formation of polymer bridging flocculation in solvent also cannot be ruled out. Meanwhile, the increase in solvent uptake at higher DS-LDH contents may be due to the aggregation of DS-LDH layers in the polymer matrix.

The better barrier properties may also be attributed to the labyrinth or tortuous pathway model as proposed in **Figure 2.18** [125]. When a film of polymer nanocomposites is formed, the sheet-like clay layers orient in parallel with the film surface. As a result, gas molecules have to take a long way around the impermeable clay layers in polymer nanocomposite than in pristine polymer matrix when they traverse an equivalent film thickness. It is interesting to note that the enhancement of barrier properties does not arise from the chemical interactions since it does not depend on the type of gas or liquid molecules.

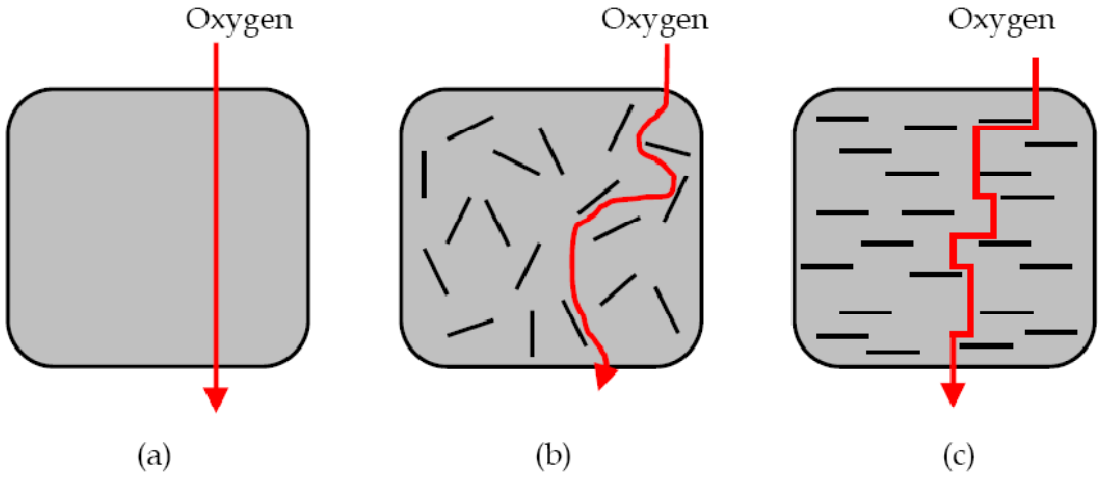

Figure 2.18: Barrier property improvement mechanism for polymer/clay nanocomposites: (a) straight path in unfilled polymers, (b) tortuous path in nanocomposites with random-oriented clay platelets and (c) zigzag path in nanocomposites with well-aligned clay platelets. [126].

2.6.2.4 Crystallization Behavior

Crystallinity and crystallization behaviour of a polymer affects the structure and property of the material. In the polymer–clay nanocomposites, the dispersed clay particles in a polymer matrix invariably act as a heterogeneous nucleating agent for the spherulite growth. However, such nucleating effect of nanoclays is more pronounced at very low loading levels, ca. 1–5 wt.%. Above these levels, nanoclays may hinder the

motion of polymers, thus retarding the crystallization rates. The restricted mobility of the chains imposed by higher clay content would not allow the growth of well developed lamellar crystals [127]. Nanoclays, thus, play two roles in the crystallizations, i.e. a nucleating agent to facilitate the crystallization and a physical hindrance to retard the crystallization [128]. For nanocomposites with low loading levels of fillers, the crystallization process can be either enhanced or inhibited depending on the nature or property of polymer employed. LDH is also know to accelerates the crystallization rates of polymers like PP [129], PET [130], poly(butylene terepthalate), syndiotactic PS [131], and PLLA [132,133] and poly(3-hydroxybutyrate [134,135] etc. The introduction of LDH hinders the crystallization of PLLA [133]. This is evidenced by a decrease of the spherulite growth and crystallization temperature on the basis of optical microscopy and DSC observations as shown in **Figure 2.19**.

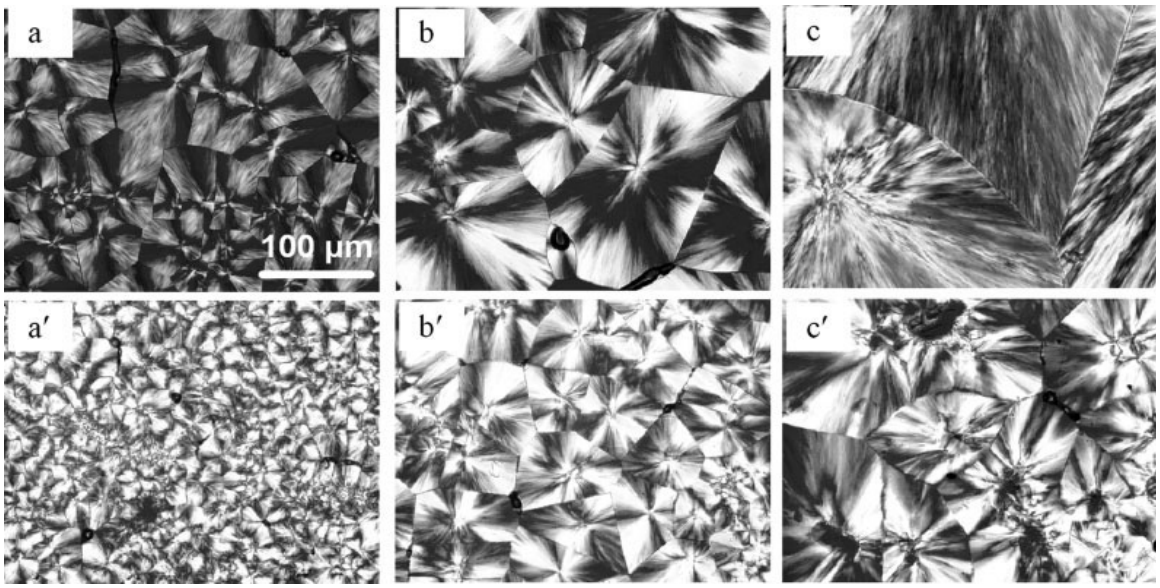

Figure 2.19: Polarized optical micrographs of neat PLLA (a, b, c) and PLLA/LDH2.5 composite (a', b', c') isothermally melt-crystallized at 120 ˚C (a, a'), 130 ˚C (b, b'), and 140 ˚C (c, c') [133].

Apart from enhancing the crystallization rate nano LDH platelets with large surface areas also enhance polymer–layered hydroxide interactions. In this regard, the addition of LDH fillers to polymers can stabilize a metastable phase and induce polymorphism.

2.6.2.5 Rheological Behavior

The linear dynamic mechanical properties of LDH reinforced nanocomposites have been examined in the melt state for polymer matrices like polyethylene [136,137]. Rheological behavior of the nanocomposite show peculiar characteristics as compared to conventional composites. The PE/LDH nanocomposites showed solid like rheological behavior at lower frequencies which was shown to be due to frictional interactions between the hydroxide layers **(Figure 2.20).** This behavior depends on the concentration of clay in the composite. It was shown that above a critical concentration of the clay, nanocomposites form percolated structure with the clay layers and show solid like behavior. Studies on the steady shear rheological behavior of show that for very low shear rates, clay platelets take a longer time to attain planar alignment along the flow direction, and hence, show a rheopexy behavior. At higher shear rates the nanocomposite shows time independent shear viscosity.

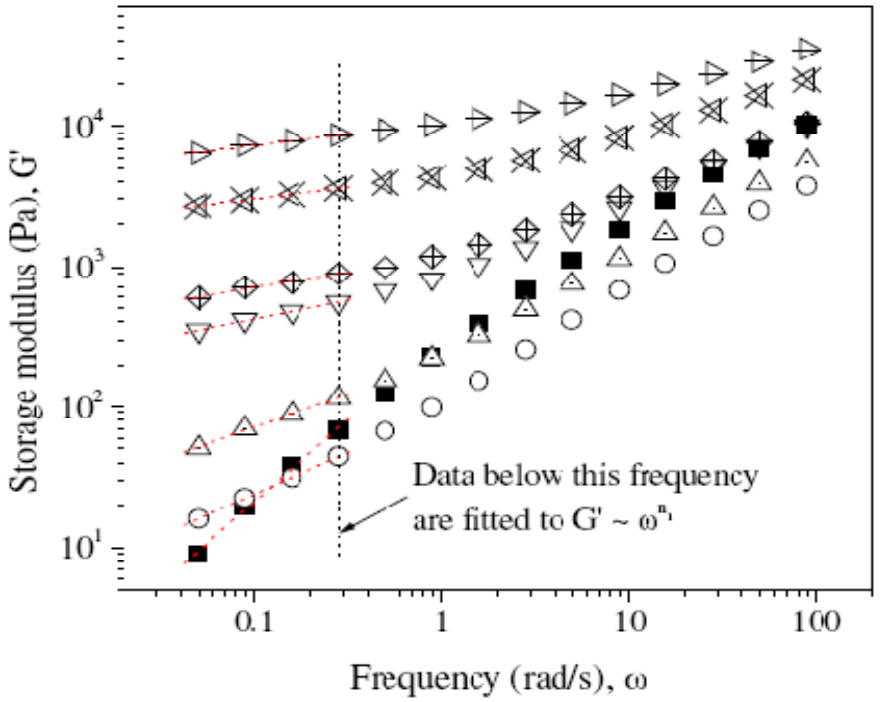

Figure 2.20: Storage modulus (G') versus frequency (ω) plots for unfilled PE and PE/LDH nanocomposite melts based on the results obtained from dynamic oscillatory measurements [136].

2.6.2.6 Photo-oxidative Behavior

Photo-oxidative degradation in polymer nanocomposites (PNC) materials caused by light and oxygen is an important issue concerning the use of these materials in outdoor applications e.g automotive, household and construction etc. The few studies concerning the photo-degradation of polymer nanocomposites based on layered silicates converge on showing an important result: the presence of the silicate causes a higher instability of PNCs to UV ageing with respect to the pristine polymers like PP [138, 139]. PS [140], EPDM [141], PE [142] etc. Relatively, very few reports on photo-oxidation behavior of LDH reinforced polymers were found [143, 144]. Leroux and co-workers [145] studied the photo-oxidative behavior of nanocomposites formed with polystyrene (PS) and organo-modified LDHs. It is observed that that the hybrid nanofiller do not modify the photo-oxidation mechanism of PS. The same products of oxidation were observed with the same proportions. A slightly higher oxidation rate was observed in the case of the sample with 5% of filler **Figure 2.21**.

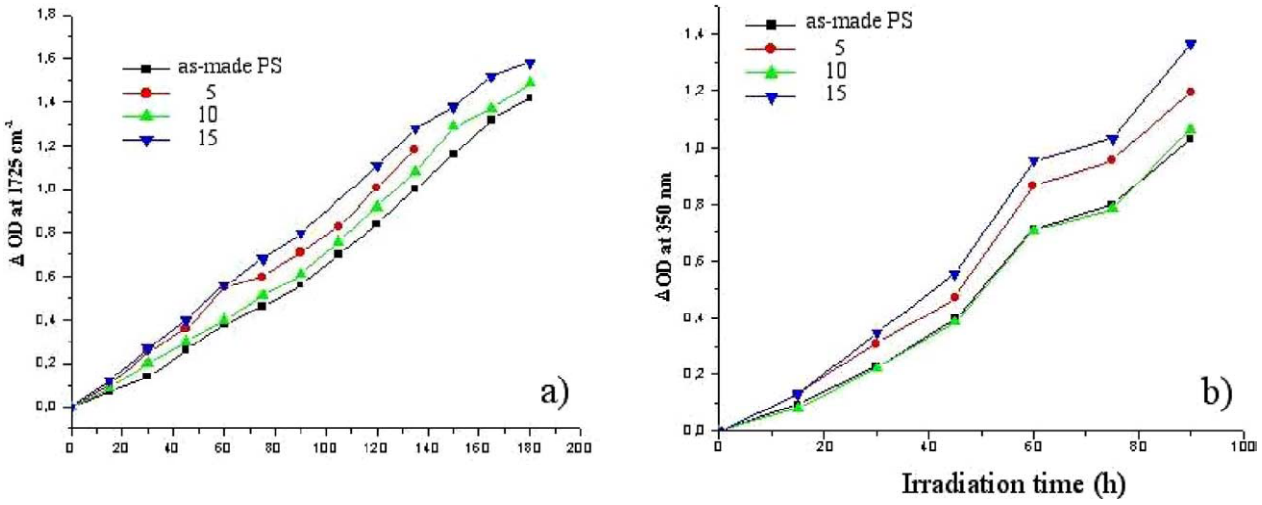

Figure: 2.21 .Variations in (a) IR absorbance at 1725 cm^{-1}, and (b) in optical absorbance at 350 nm for the as-made PS and the nanocomposite films SPMA/LDH:PS against irradiation time. The percentage of hybrid LDH is indicated [145].

2.7 Potential Applications of LDH Materials

LDHs provide a battery of advantages, like tunable chemical compositions and its purity, non-toxicity, large amount of bound water in their structure, possibility of modification by a large number of organic anionic species, etc. This makes them a potential candidate for various applications. Although the application of LDH clays or in general anionic clays is still in growing stage, their huge potential can be imagined from their properties. **Figure 2.22** shows an overview of various fields of application of LDH materials.

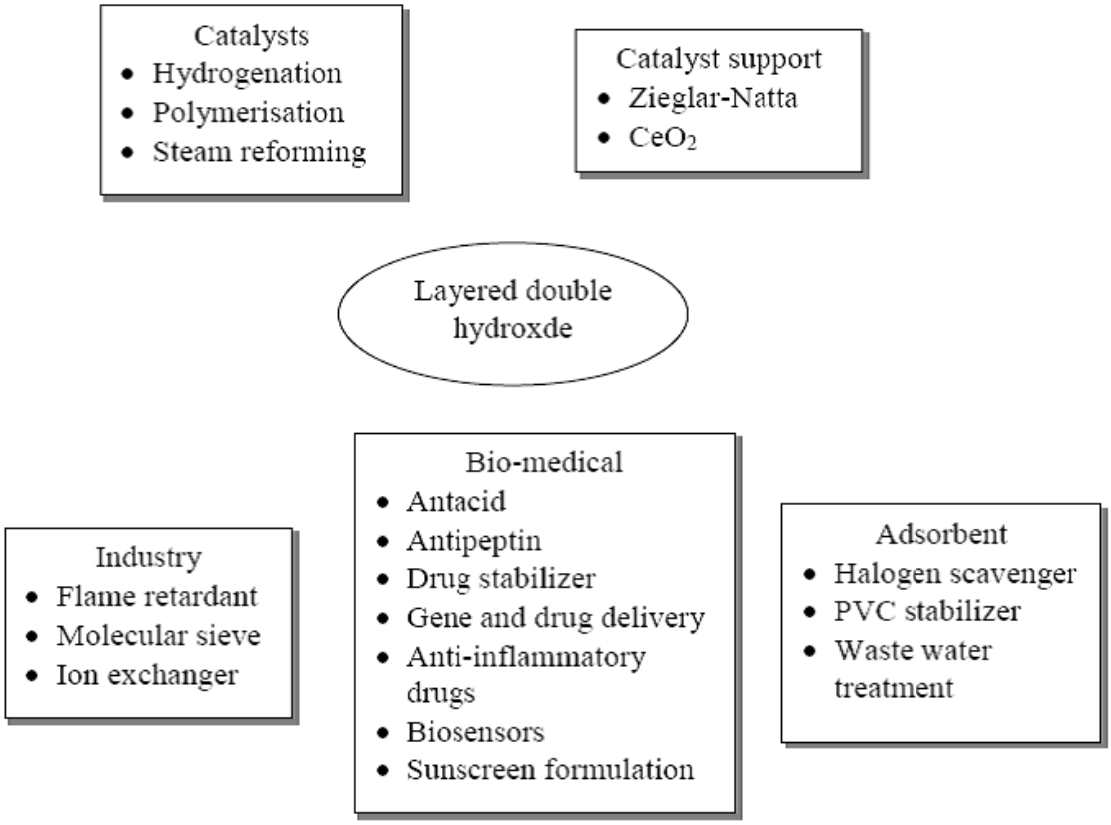

Figure 2.22: Various fields of application of LDH materials [146].

The use of LDH materials in the field of catalysis is well known and have been reported for basic catalysis (eg. Polymerization of alkene oxide, aldol condensation, transesterification reactions, etc), reforming of hydrocarbons with H_2O, hydrogenation (production of methane, alcohols, paraffins, olefins, etc), oxidation reactions, support for Zieglar-Natta catalysts during polymerization of olefins, etc [146, 147].

Because of bio-compatible nature, the use of LDH materials in bio-medical field is wide spread. One important and very promising field of application is the controlled release of drugs and various active chemical species. In this regard, the intercalation chemistry of LDH type clay is of special interest in stabilizing and sequestration of highly active or toxic molecules. Such bio-nanohybrid can then be administered into the body system, where the active ingredients are released at desired location via a chemical switch such as change in pH. For example, for controlled release of various inflammatory drugs the use of these techniques provides better results [148]. Recently, Lee and Chen [149] reported the drug release behavior of nanocomposite hydrogels prepared from Mg-Al–LDH and poly[acrylic acidco- poly(ethylene glycol methyl ethyl acrylate)]. LDH-organic hybrids can also be used in designing of electrochemical biosensors for various chemicals. For examples, polyphenylene oxidase intercalated Zn-Al–LDH hybrids for phenol determination [150], urease intercalated Zn-Al–LDH for urea detection [151] etc. The Mg-Al–LDH is also used as stabilizer and halogen scavenger in polyvinylchloride (PVC) formulation [152]. The incorporation of small amount of LDH into PVC significantly improves the thermal stability of the resin and suppresses its degradation. Evans et al. have made extensive investigation on the intercalation of various organic dyes and UV stabilizers within LDH [153, 154]. Such intercalated LDH-dye hybrids can also dispersed in polymer matrix, where the hybrid fillers simultaneously exhibit the functions of the nanofiller and the organic dye. The concept of nanotechnology in designing flame-retardant polymer composites is an upcoming field. It has already been established that polymer nanocomposites based on layered silicates type clays show certain improvements in flame retardancy of polymers. In many cases partially exfoliated and intercalated clay structure show better results compared to completely exfoliated one [112]. LDH clays, especially those based on Mg–Al and Zn–Al also have a definite potential as flame-retardant fillers. The mechanism by which they delay or restrict the burning process of polymer is similar to that followed by conventional metal hydroxides. But, the added advantages are their improved dispersion into polymer matrices and confinement of polymer chains within the metal hydroxide layers through intercalation. This can improve their efficiency as compared to the conventional metal hydroxides (like $Mg(OH)_2$ and aluminum trihydrate) by reducing the loading requirement for meeting

certain flame-retardancy rating. Another important aspect is the choice of clay modifying surfactants. Usually, in case of LDH clays, the amount of any surfactant used for such purpose is theoretically equivalent to the amount of interlayer anions present in the unmodified materials. Since the commonly used anionic surfactants for LDH clays posses oligomeric structure, their incorporation even in small percentage (of the amount required for complete replacement of the interlayer anionic species) produce organically modified LDHs that contain substantial amount of organic portion. Therefore, choice of these surfactants can be made in such a way that they serve a dual purpose, such as modification of unmodified clays by enlarging the interlayer region and the improvement of the flame-retardancy of the final composites. In this regard, organic surfactant containing phosphorous and aromatic moieties are the ideal candidates. The potential of LDH clays in preparing polymer nanocomposites with special properties has drawn considerable attentions among researchers in the recent years. The most widely reported a method in literature is solution intercalation process, which gives nanocomposites with intercalated to exfoliated clays structures. The melt-compounding method employed in the present study is still to be explored in details with these materials.

References

1. Mirabella M. Francis, Jr., (2004), "Polypropylene and TPO Nanocomposites", Dekker *Encyclopedia of Nanoscience and Nanotechnology*, **5**, p. 3015-3038.
2. Brydson, J.A. (1989). *Plastic Materials*. 5th ed. London: Mid-County Press. Inc.196-241.
3. Lieberman, R.B. and Barbe, P.C. (1990). Polypropylene. In: Corish, P.J. *Consice Encyclopedia of Polymer Processing & Application.* Oxford: Pergamom Press. 533-537.
4. C. Zeng, Synthesis, structure and properties of polymer nanocomposites, PhD dissertation, Ohio State University, Department of Chemical and Biomolecular Engineering, 2004.
5. A. Wood, "A Big Market Potential", *Chemical week* **164** (41) (2002), p.17-21.
6. L. M. Sherman, "Chasing nanocomposites", *Plastics Technology* (online article), November 2004. [Online]: http://www.ptonline.com/articles/200411fa2.html.
7. S. S. Ray and M. Okamoto. Polymer/layered silicate nanocomposites: a review from preparation to processing. *Progress in Polymer Science,* **28** (2003), p.1539- 1641.
8. M. Meyn, K. Beneke, and G. Legaly. Anionic-exchange reactions of layered double hydroxides. *Inorganic Chemistry*, **29** (1990), p. 5201 – 5207.
9. F. Cavani, F. Trifiro, and A. Vaccari. Hydrotalcite-type anionic clays: Preparation, properties and applications. *Catalysis Today*, **11**(1991), p.173 – 301.
10. F-R Costa, Mg-Al Layered Double Hydroxide: A Potential Nanofiller and Flame-Retardant for Polyethylene, PhD dissertation, Technical University Dresden, 2007.
11. S. P. Lonkar, S. Morlat-Therias , N. Caperaa, F. Leroux, J.L. Gardette, R.P. Singh. Preparation and nonisothermal crystallization behavior of polypropylene/layered double hydroxide nanocomposites. *Polymer*, **50** (2009), p.1505–1515.
12. S. Miyata. Physico-chemical properties of synthetic hydrotalcites in relation to composition. *Clays and Clay Minerals*, **28** (1980), p.50 – 56.
13. M. D. Arco, E. Cebadera, S. Gutierrez, C. Martin, M. J. Montero, V. Rives, J. Rocha, and M. A. Sevilla. Mg,Al layered double hydroxides with intercalated indomethacin: Synthesis, characterization, and pharmacological study. *Journal of Pharmaceutical Sciences*, **93** (2004), p.1649 – 1658.
14. T. S. Stanimirova, G. Kirov, and E. Dinolova. Mechanism of hydrotalcite regeneration. *Journal of Material Science Letter*, **20** (2001) p.453 – 455.

15. S. Miyata, T. Kumura. Synthesis of new hydrotalcite-like compounds and their physicochemical properties. Chemistry Letters. **8** (1973), p.843-848.
16. W. T. Reichle. Synthesis of anionic clay minerals (mixed metal hydroxides, hydrotalcite. *Solid State Ionics*, **22** (1986), p.135 – 141.
17. O. Clause, M. Gazzano, F. Trifiro, A. Vaccari, and L. Zatroski. Preparation and thermal reactivity of nickel/chromium and nickel/aluminium hydrotalcite-type precursors. *Applied Catalysis*, **73** (1991), p.217 – 236.
18. O. Clause, M. Gazzano, F. Trifiro, A. Vaccari, and L. Zatroski. Preparation and thermal reactivity of nickel/chromium and nickel/aluminium hydrotalcite-type precursors. *Applied Catalysis*, **73** (1991), p.217 – 236.
19. O. Clause, B. Rebours, E. Merlen, F. Trifir, and A. Vaccari. Preparation and characterization of nickel-aluminium mixed oxides obtained by thermal decomposition of hydrotalcite-type precursors. *Journal of Catalysis*, **133** (1992), p.231 – 246.
20. M. Sychev, R. Prihodko, K. Erdmann, A. Mangel, and R. A. van Santen. Hydrotalcites: relation between structural features, basicity and activity in the wittig reaction. *Applied Clay Science*, **18** (2001), p.103 – 110.
21. U. Costantino, F. Marmottini, M. Nocchetti, and R. Vivani. New synthetic routes to hydrotalcite like compounds- characterization and properties of the obtained materials. *European Journal of Inorganic Chemistry*, **21** (1998), p.1434 – 1446.
22. M. Ogawa and H. Kaiho. Homogeneous precipitation of uniform hydrotalcite particles. *Langmuir*, **18** (2002), p.4240 – 4242.
23. P. Yang, J. Yu, Z. Wang, Q. Liu, and T. Wu. Urea method for the synthesis of hydrotalcites. *Reaction Kinetics Catalysis Letters*, **83** (2004), p.275 – 282.
24. K. E. Malki, M. Guenane, C. Forano, A. De Roy, and J. P. Besse. Inorganic and organic anionic pillars intercalated in lamellar double hydroxides. *Material Science Forum,* **91 – 93** (1992), p.171 – 176.
25. R. P. Bontchev, S. Liu, J. L. Krumhansi, J. Voigt, and T. M. Nenoff. Synthesis, characterization, and ion exchange properties of hydrotalcite $Mg_6Al_2(OH)_{16}(A)_x(A')_{2-x}4H_2O$ (A,A' = Cl^-,Br^-, I^-, and NO_3^-, $2 \geq x \geq 0$) derivatives. *Chemistry of Materials*, **15** (2003), p.3669 – 3675.
26. G. Mascolo. Synthesis of anionic clays by hydrothermal crystallization of amorphous precursors. *Applied Clay Science*, **10** (1995), p.21 – 30.

27. Y. You, H. H. Zhao, and G. F. Vance. Surfactant-enhanced adsorption of organic compounds by layered double hydroxide. *Collides and Surfaces. A: Phys. Engg. Asp.*, **205** (2002), p.161 – 172.
28. Y. You, H. H. Zhao, and G. F. Vance. Hybrid organic-inorganic derivatives of layered double hydroxides and dodecylbenzenesulfonate: Preparation and adsorption characteristics. *Journal of Materials Chemistry*, **12** (2002), p.907 – 912.
29. S. Carlino. The intercalation of carboxylic acids into layered double hydroxides: A critical review of the different methods. *Solid State Ionics*, **98** (1997), p.73 – 84.
30. W.D. Lee, S.S. Im, H.M. Lim, Preparation and properties of layered double hydroxide/poly(ethylene terephthalate) nanocomposites by direct melt compounding. *Polymer*, **47** (2006), p.1364-1371.
31. H. L. Alejandro, Structure property and deformation analysis of polypropylene montmorillonite nanocomposites, PhD thesis, University of North Texas, Department of Materials Science, 2003.
32. T. D. Fornes and D. R. Paul, "Modeling properties of nylon 6/clay nanocomposites using composite theories", *Polymer* **44** (2003), p.4993-5013.
33. V. Prevot, C. Forano, and J. P. Besse. Hybrid derivative of layered double hydroxides. *Applied Clay Science*, **18** (2001), p.3 – 15.
34. S. Carlino. The intercalation of carboxylic acids into layered double hydroxides: A critical review of the different methods. *Solid State Ionics*, **98** (1997), p.73 – 84.
35. F. Leroux and J. P. Besse. Polymer interleaved layered double hydroxide: A new emerging class of nanocomposites. *Chemisty of Materials*, **13** (2001), p.3507 – 3515.
36. N. T. Whilton, P. J. Vickers, and S. Mann. Bioinorganic clays: synthesis and characterization of amino- and polyamino acid intercalated layered double hydroxide. *Journal of Materials Chemistry*, **7** (1997), p.1623 – 1629.
37. C. Vaysse, L. Guerlou-Demourgues, E. Duguet, and C. Delmas. Acrylate intercalation and in situ polymerization in iron-, cobalt-, or manganese-substituted nickel hydroxides. *Inorganic Chemistry*, **42** (2003), p.4559 – 4567.
38. W. F. Lee and Y. C. Chen. Superabsorbent polymeric materials. xiv. preparation and water absorbancy of nanocomposite superabsorbents containing intercalated hydrotalcite. *Journal of Applied Polymer Science*, **94** (2004, p.2417 – 2424.
39. E. M. Moujahid, J. P. Besse, and F. Leroux. Synthesis and characterization of a polystyrene sulfonate layered double hydroxide nanocomposite. in-situ polymerization vs. polymer incorporation. *Journal of Materials Chemistry*, **12** (2002), p.3324 – 3330.

40. J. P. Besse E. M. Moujahid, M. Dubois and F. Leroux. Role of atmospheric oxygen for the polymerization of interleaved aniline sulfonic acid in LDH. *Chemisty of Materials*, **14** (2002), p.3799 – 3807.
41. M. Tanaka, I. Y. Park, K. Kuroda, and C. Kato. Formation of hydrotalcite-acrylate intercalation compounds and their heat treated product. Bulletin Chemical Society Japan, **62** (1989), p.3442.
42. V. P. Isupov, L. E. Chupakhina, M. A. Ozerova, V. G. Kostrovsky, and V. A. Poluboyarov. Polymerization of m-$NH_2C_6H_4COO$ anions in the intercalation compounds of aluminium hydroxide $[LiAl_2(OH)_6][m\text{-}NH_2C_6H_4COO].nH_2O$. *Solid States Ionics*, **141-142** (2001), p.231 – 236.
43. M. Darder, M. Lopez-Blanco, P. Aranda. Bio-nanocomposites based on layered double hydroxides. *Chemistry of Materials,* **8** (2005), p.1969-1977.
44. L. Vieille, C. Taviot-Gueho, J. P. Besse, and F. Leroux. Hydrocalumite and its polymer derivatives. 2. polymer incorporation versus in situ polymerization of styrene-4-sulfonate. *Chemisty of Materials*, **15** (2003), p.4369 – 4376.
45. L. Vieille, E. M. Moujahid, C. Tavoit-Gueho, J. Cellier, J. P. Besse, and F. Leroux. In situ polymerization of interleaved monomers: a comparative study between hydrotalcite and hydrocalumite host structures. *Journal of Physics and Chemistry of Solids*, **65** (2004), p.385 – 393.
46. G. A.Wang, C. C.Wang, and C. Y. Chen. The disorderly exfoliated LDHs/PMMA nanocomposites synthesized by in situ bulk polymerization. *Polymer*, **46** (2005), p.5065 – 5074.
47. T. Challier and R. C. T. Slade. Nanocomposite materials: Polyaniline-intercalated layered double hydroxides. *Journal of Materials Chemistry*, **4** (1994), p.367 – 371.
48. Y. Sugahara, N. Yokoyama, K. Kuroda, and C. Kato. Preparation and properties of silica and silicate gels by the alkoxide, colloidal and amine-silicate methods. *Ceramic International*, **14** (1988), p.163 – 167.
49. S. O'Leary, D. O'Hare, and G. Seely. Delamination of layered double hydroxides in polar monomers: new LDH-acrylate nanocomposites. *Chemical Communication*, **14** (2002), p.1506 – 1507.
50. Ying-Nan Chan, Tzong-Yuan Juanga, Yi-Lin Liao, Shenghong A. Dai, Jiang-Jen Lin, Preparation of clay/epoxy nanocomposites by layered-double-hydroxide initiated self-polymerization, *Polymer*, **49** (2008), p.4796–4801.

51. W. Chen, L .Feng, B.J. Qu. In situ synthesis of poly(methyl methacrylate)/MgAl layered double hydroxide nanocomposite with high transparency and enhanced thermal properties. *Solid State Communications,* **130** (2004), p.259-263.
52. P. B. Messersmith and S. I. Stupp. High-temperature chemical and microstructural transformations of a nanocomposite organoceramic. *Chemisty of Materials,* **7** (1995), p.454 – 560.
53. C. O. Oriakhi, I. V. Farr, and M. M. Lerner. Incorporation of poly (acrylic acid), poly (vinylsulfonate) and poly (styrenesulfonate) within layered double hydroxides. *Journal of Materials Chemistry*, **6** (1996), p.103 – 107.
54. O. C. Wilson Jr., T. Olorunyolemi, A. Jaworski, L. Borum, D. Young, A. Siriwat, E. Dickens, C. Oriakhi, and M. Lerner. Surface and interfacial properties of polymer-intercalated layered double hydroxide nanocomposites. *Applied Clay Science*, **15** (1999), p.265 – 279.
55. F .Leroux, P. Aranda, J.P. Besse Intercalation of poly(ethylene oxide) derivatives into layered double hydroxides , *European Journal of Inorganic Chemistry,* **6** (2003), p.1242-1251.
56. M-F Chiang and T-M.Wu. Synthesis and characterization of biodegradable poly(l-lactide)/ layered double hydroxide nanocomposites. *Composites Science and Technology,* **70** (2010), p.110-115.
57. W. Chen and B. Qu. Structural characteristics and thermal properties of PE-g-MA/MgAl-LDH exfoliation nanocomposites synthesized by solution intercalation. *Chemisty of Materials*, **15** (2003), p.3208 – 3213.
58. W. Chen, L. Feng, and B. Qu. Preparation of nanocomposites by exfoliation of ZnAl layered double hydroxides in nonpolar LLDPE solution. *Chemisty of Materials*, **16** (2004), p.368 – 370.
59. L. Qui, W. Chen, and B. Qu. Structural characterisation and thermal properties of exfoliated polystyrene/ZnAl layered double hydroxide nanocomposites prepared via solution intercalation. *Polymer Degradation and Stability*, **87** (2005), p.433 – 440.
60. G. A. Buniak, W. H. Schreiner, N. Mattoso, and F. Wypych. Preparation of a new nanocomposites of $Al_{0.33}Mg_{0.67}(OH)_2(C_{12}H_{25}SO_4)_{0.33}$ and poly(ethyleneoxide). *Langmuir*, **18** (2002), p.5967 – 5970.
61. C.S. Liao, W.B. Ye. Structure and conductive properties of poly (ethylene oxide)/layered double hydroxide nanocomposite polymer electrolytes. *Electrochimica Acta,* **49** (2004), p. 4993-4998.

62. B. Li, Y. Hu, J. Liu, Z. Chen, and W. Fan. Preparation of poly(methyl methacrylate)/LDH nanocomposite by exfoliation-adsorption process. *Colloidal Polymer Science*, **281** (2003), p.998 – 1001.
63. H. B. Hsueh and C. Y. Chen. Preparation and properties of LDHs/epoxy nanocomposites. *Polymer*, **44** (2003), p.5275 – 5283.
64. Q. Z. Yang, D. J. Sun, C. G. Zhang, X. J.Wang, andW. A. Zhao. Synthesis and characterization of polyoxyethylene sulfate intercalated Mg-Al-nitrate layered double hydroxide. *Langmuir*, **19** (2003), p.5570 – 5574.
65. S. Costa, T. Imae, K. Takagi, and K. Kikuta. Intercalation of dendrimers in the interlayer of hydrotalcite clay sheets. *Progress in Colloidal Polymer Science*, **128** (2004), p.113 – 119.
66. L. van der Ven, M.L.M. van Gemert, L.F. Batenburg, J.J. Keern, L.H. Gielgens, T.P.M. Koster, and H.R. Fischer. On the action of hydrotalcite-like clay materials as stabilizers in polyvinylchloride. *Applied Clay Science*, **17**(2000), 25 – 34.
67. S. Miyata. Halogen-containing polyolefin composition, and methods for inactivating halogen therein. *US Patent*, **4 379 882**, 1983.
68. S. Miyata, T. Hirose, and N. Iizima. Fire-retarding thermoplastic resin composition. *US Patent*, **4 085 088**, 1978.
69. K. L. Nichols and C. J. Chou. Polymer composite comprising a inorganic layered material and a polymer matrix and a method for its preparation. *US Patent*, **5 952 093**, 1999.
70. M. Zammarano, S. Bellayer, J.W. Gilman, M. Franceschi, F. L. Beyer, R. H. Harris a, and S. Meriani. Delamination of organo-modified layered double hydroxides in polyamide 6 by melt processing. *Polymer*, **47** (2006) p.652 – 662.
71. M. Ardanuy, J.I .Velasco, M.L. Maspoch. Influence of EMAA Compatibilizer on the Structure and Properties of HDPE/Hydrotalcite Nanocomposites Prepared by Melt Mixing. *Journal of applied polymer science***,** **113** (2009), p.950-958.
72. P. Ding, B.J. Qu. Synthesis of exfoliated PP/LDH nanocomposites via melt-intercalation: Structure, thermal properties, and photo-oxidative behavior in comparison with PP/MMT nanocomposites *Polymer Engineering and Science*, **46** (2006) p.1153-1159.
73. L.C. Du, B.J. Qu . Structural characterization and thermal oxidation properties of LLDPE/MgAl-LDH nanocomposites. *Journal of Materials Chemistry*, **16** (2006), p.1549-1554.

74. U. Costantino, A. Gallipoli, M. Nocchetti, G. Camino, F. Bellucci, and A. Frache. New nanocomposites constituted of polyethylene and organically modified Zn Al-hydrotalcites. *Polymer Degradation and Stability*, **90** (2005), p.586 – 590.
75. H.D. Peng, W.C. Tjiu, L. Shen. Preparation and mechanical properties of exfoliated CoAl layered double hydroxide (LDH)/polyamide 6 nanocomposites by in situ polymerization. *Composites Science and Technology*, **69** (2009), p. 991-996.
76. Z .Matusinovic, M. Rogosic, J. Sipusic.Polymer nanocomposite materials based on polystyrene and a layered aluminate filler. *Polymer Engineering and Science*, **48** (2008), p.2027-2032.
77. P. Ding, B.J. Qu. Synthesis and characterization of polystyrene/layered double-hydroxide nanocomposites via in situ emulsion and suspension polymerization. *Journal of Applied Polymer Science*, **101** (2006), p.3758-3766.
78. P .Ding, B.J. Qu. Synthesis and characterization of exfoliated polystyrene/ZnAl layered double hydroxide nanocomplosite via emulsion polymerization. *Journal of Colloid and Interface Science*, **291** (2005), p.13-18.
79. L.Z .Qiu, W. Chen, B.J. Qu. Exfoliation of layered double hydroxide in polystyrene by in-situ atom transfer radical polymerization using initiator-modified precursor. *Colloid and Polymer Science*, **283** (2005), p.1241-1245.
80. B.X. Du, Z.H. Guo, Z.P. Fang.Effects of organo-clay and sodium dodecyl sulfonate intercalated layered double hydroxide on thermal and flame behaviour of intumescent flame retarded polypropylene. *Polymer Degradation and Stability,* **94** (2009), p. 1979-1985.
81. F.R. Costa, M .Abdel-Goad, U. Wagenknecht. Nanocomposites based on polyethylene and Mg-Al layered double hydroxide. I. Synthesis and characterization. *Polymer*, **46** (2005), p. 4447-4453.
82. P. Ding, B.J.Qu. Structure, thermal stability, and photocrosslinking characterization of HDPE/LDH nanocomposites synthesized by melt-intercalation. *Journal of Polymer Science Part B-Polymer Physics,* **44** (2006), p.3165-3172.
83. F.R. Costa, U. Wagenknecht, D. Jehnichen. Nanocomposites based on polyethylene and Mg-Al layered double hydroxide: characterisation of modified clay, morphological and rheological analysis of nanocomposites. *Plastics Rubber and Composites,* **35** (2004), p. 139-148.
84. C. Berti, M. Fiorini, L. Sisti. Synthesis of poly(butylene terephtahlate) nanocomposites using anionic clays. *European Polymer Journal*, **45** (2009), p. 70-78.

85. W. Chen, B.J. Qu. Enhanced thermal and mechanical properties of poly(methyl acrylate)/ZnAl layered double hydroxide nanocomposites formed by in situ polymerisation. *Polymer Degradation and Stability,* **90** (2005), p.162-166.
86. H, Acharya, S.K. Srivastava, A.K. Bhowmick. A solution blending route to ethylene propylene diene terpolymer/layered double hydroxide nanocomposites. *Nanoscale Research Letters,* **2** (2007), p.1-5.
87. H, Acharya, S.K. Srivastava, A.K. Bhowmick. Synthesis of partially exfoliated EPDM/LDH nanocomposites by solution intercalation: Structural characterization and properties. *Composites Science and Technology,* **67** (2007) p. 2807-2816.
88. M. Kotal, T. Kuila, S.K. Srivastava, Synthesis and Characterization of Polyurethane/Mg-Al Layered Double Hydroxide Nanocomposites. *Journal of Applied Polymer Science,* **114** (2009), p. 2691-2699.
89. M. Kotal, S.K. Srivastava, A.K .Bhowmick. Thermoplastic polyurethane and nitrile butadiene rubber blends with layered double hydroxide nanocomposites by solution blending. *Polymer International*, **59** (2010), p. 2-10.
90. N.H. Huang, J.Q. Wang .A new route to prepare nanocomposites based on polyvinyl chloride and MgAl layered double hydroxide intercalated with laurylether phosphate. *Express Polymer Letters*, **3** (2009), p. 595-604.
91. M. Zubitur, M.A. Gomez, M. Cortazar .Structural characterization and thermal decomposition of layered double hydroxide/poly(p-dioxanone) nanocomposites .*Polymer Degradation and Stability*, **94** (2009), p. 804-809.
92. T .Kuila, H. Acharya, S.K. Srivastava, Ethylene Vinyl Acetate/Mg-Al LDH Nanocomposites by Solution Blending. *Polymer Composites*, **30** (2009), p. 497-502.
93. T. Kuila, S.K. Srivastava, A.K. Bhowmick. Rubber/LDH Nanocomposites by Solution Blending, *Journal of Applied Polymer Science*, **111**(2009), p.635-641.
94. M, Zhang, P .Ding, L.C. Du. Structural characterization and related properties of EVA/ZnAl-LDH nanocomposites prepared by melt and solution intercalation. *Materials Chemistry and Physics*, **109** (2008), p. 206-211.
95. B. Ramaraj, K.R. Yoon. Thermal and physicomechanical properties of ethylene-vinyl acetate copolymer and layered double hydroxide composites . *Journal of Applied Polymer Science*, **108** (2008), p. 4090-4095
96. T. Kuila, H. Acharya, S.K. Srivastava. Synthesis and characterization of ethylene vinyl acetate/Mg-Al layered double hydroxide nanocomposites. *Journal of Applied Polymer Science*, **104** (2007), p.1845-1851.

97. L.C. Du, B.J. Qu, M. Zhang. Thermal properties and combustion characterization of nylon 6/MgAl-LDH nanocomposites via organic modification and melt intercalation. *Polymer Degradation and Stability*, **92** (2007), p. 497-502.
98. K.L .Dagnon, H.H. Chen, L.H. Lnnocentini-Mei, Poly[(3-hydroxybutyrate)-co-(3-hydroxyvalerate)]/layered double hydroxide nanocomposites. *Polymer International*, **58** (2009), p.133-141.
99. P. Mangiacapra, M .Raimondo, L .Tammaro, Nanometric dispersion of a Mg/Al layered double hydroxide into a chemically modified polycaprolactone. *Biomacromolecules,* **8**(2007) p. 773-779.
100. A. Sorrentino, G. Gorrasi, M. Tortora. Incorporation of Mg-Al hydrotalcite into a biodegradable poly (epsilon, caprolactone) by high energy ball milling. *Polymer,* **46** (2005) p.1601-1608.
101. H.M. Wilhelm, M.R. Sierakowski, G.P. Souza. The influence of layered compounds on the properties of starch/layered compound composites. *Polymer International,* **52** (2003), p.1035-1044.
102. J. S. Bergman, H. Chen, E. P. Giannelis, M. G. Thomas, G. W. Coates. Synthesis and characterization of polyolefin-silicate nanocomposites: a catalyst intercalation and in situ polymerization approach. *Chemical Communication,* **21** (1999), p.2179-2180.
103. J. P. Lemmon, J. Wu, M. M. Lerner. in Hybrid Organic-Inorganic Composites. ACS Symp. Series, 585 Mark, J. E.; Lee, C. Y. C.; Bianconi, P. A.; Eds. ACS: Washington D.C. **1995**.
104. Q. H. Zeng, A. B. Yu, G. Q. (Max) Lu, and D. R. Paul Clay-Based Polymer Nanocomposites: Research and Commercial Development. *Journal of Nanoscience and Nanotechnology*, **5** (2005) p.1574–1592.
105. B. Qu. Structural characterisation and thermal properties of exfoliated polystyrene/ZnAl layered double hydroxide nanocomposites prepared via solution intercalation. *Polymer Degradation and Stability*, **87** (2005), p.433 – 440.
106. G. A.Wang, C. C.Wang, and C. Y. Chen. The disorderly exfoliated LDHs/PMMA nanocomposites synthesized by in situ bulk polymerization: The effects of LDH-U on thermal and mechanical properties. *Polymer Degradation and Stability*, **91**(2006), p.2443 – 2450.
107. A. Du, B. Qu, Y. Meng, Q. Zhu. Structural characterization and thermal and mechanical properties of poly(propylene carbonate)/MgAl-LDH exfoliation

nanocomposite via solution intercalation, *Composites Science and Technology,* **66** (2006) p.913–918.

108. T. Kuila, H. Acharya, S. K. Srivastava, A. K. Bhowmick. Effect of Vinyl Acetate Content on the Mechanical and Thermal Properties of Ethylene Vinyl Acetate/MgAl Layered Double Hydroxide Nanocomposites, *Journal of Applied Polymer Science*, **108** (2008), p.1329–1335.
109. W.Chen and B. Qu. LLDPE/ZnAl LDH-exfoliated nanocomposites: effects of nanolayers on thermal and mechanical properties, *Journal of Material Chemistry*, **14** (2004), p.1705-1710.
110. J. C. A. A. Roelofs, J. A. van Bokhoven, A. Jos van Dillen, J. W. Geus, and K. P. de Jong. The thermal decomposition of Mg-Al hydrotalcites: effects of interlayer anions and characteristics of the final structure. *Chemical European Journal*, **8** (2002), p.5571 – 5579.
111. J. W. Gilman. Flammability and thermal stability studies of polymer-layered silicate (clay) nanocomposites. *Applied Clay Science*, **15 (**1999), p.31 – 49.
112. U. Wagenknecht, B. Kretzschmar, and G. Reinhardt. Investigation of fire retardant properties of polypropylene-clay nanocomposites. *Macromolecular Symposium*, **194** (2003), p.207 – 212.
113. W. Chen, L. Feng, B. Qu. In situ synthesis of poly(methyl methacrylate)/MgAl layered double hydroxide nanocomposite with high transparency and enhanced thermal properties. *Solid State Communications*, **130** (2004), p. 259–263.
114. J. Liu, G.M. Chen, J.P. Yang. Improved thermal stability of poly(vinyl chloride) by nanoscale layered double hydroxide particles grafted with toluene-2,4-di-isocyanate, *Materials Chemistry and Physics***, 118** (2009) p.405-409.
115. M.Zhang, P. Ding, B. Qu. Flammable, Thermal, and Mechanical Properties of Intumescent Flame Retardant PP/LDH Nanocomposites With Different Divalent Cations, , *Polymer Composites***, 30** (2009), p.1000 – 1006.
116. M. Zammarano, M. Franceschib, S. Bellayera, J. W. Gilmana, and S. Meriani. Preparation and flame resistance properties of revolutionary self-extinguishing epoxy nanocomposites based on layered double hydroxides. *Polymer,* **46** (2005), p.9314 – 9328.
117. C. Manzi-Nshuti, P. Songtipya, E. Manias, Maria M. Jimenez-Gasco, J.M. Hossenlopp, C. A. Wilkie. Polymer nanocomposites using zinc aluminum and magnesium aluminum oleate layered double hydroxides: Effects of LDH divalent

metals on dispersion, thermal, mechanical and fire performance in various polymers, *Polymer*, **50** (2009), p.3564-3574.

118. F.R. Costa, U. Wagenknecht and G. Heinrich. LDPE/Mg–Al layered double hydroxide nanocomposites: Thermal and flammability properties; Polymer Degradation and Stability, **92** (2007), p. 1813 –1823.
119. C.M.C. Pereira, M. Herrero, F.M. Labajos, A.T. Marques, V. Rives, Preparation and properties of new flame retardant unsaturated polyester nanocomposites based on layered double hydroxides, *Polymer Degradation and Stability*, **94** (2009), p. 939-946.
120. C. Nyambo, D. Chen, S. Su, C. A. Wilkie. Variation of benzyl anions in MgAl-layered double hydroxides: Fire and thermal properties in PMMA, *Polymer Degradation and Stability*, **94** (2009), p.496-50.
121. C. Nyambo, C. A. Wilkie. Layered double hydroxides intercalated with borate anions: Fire and thermal properties in ethylene vinyl acetate copolymer *Polymer Degradation and Stability*, **94** (2009) p.506-512.
122. M. C. Costache, M. J. Heidecker, E. Manias, G.Camino, A. Frache, G. Beyer, R.K. Gupta, C. A. Wilkie, The influence of carbon nanotubes, organically modified montmorillonites and layered double hydroxides on the thermal degradation and fire retardancy of polyethylene, ethylene–vinyl acetate copolymer and polystyrene *Polymer*, **48** (2007), p.6532-6545.
123. H. Tonnaer. New synthetic organoclays offer improved flame retardancy and gas barrier properties. *Plastics, Additives and Compounding*. **11** (2009), p.14-17.
124. E. P. Landman, W. W. Focke. Stearate intercalated layered double hydroxides: effect on the physical properties of dextrin-alginate films, *Journal of Material Science*, **41** (2006) p.2271–2279.
125. T. Kuila, S.K. Srivastava, A.K. Bhowmick, A.K. Saxena, Thermoplastic polyolefin based polymer – blend-layered double hydroxide nanocomposites *Composites Science and Technology*, **68** (2008) p.3234–3239.
126. K .Yano, A. Usuki. Synthesis and properties of polyimide-clay hybrid films. *Journal of Polymer Science. Part A: Poly. Chem.* **35** (1997), p. 2289-2294.
127. Maio E. D.; Iannace, S.; Sorrentino, L.; Nicolais, L., Isothermal crystallization in PCL/clay nanocomposites investigated with thermal and rheometric methods. *Polymer,* **45** (2004), p.8893-8900.

128. G. Zhang, D. Yan, Crystallization kinetics and melting behavior of nylon 10,10 in nylon 10,10-montmorillonite nanocomposites. *Journal of Applied Polymer Science* **88** (2003), p.2181-2188.

129. M. Ardanuy, J.I. Velasco, V. Realinho. Non-isothermal crystallization kinetics and activity of filler in polypropylene/Mg-Al layered double hydroxide nanocomposites. *Thermochimica Acta,* **479** (2008), p.45-52.

130. W.D. Lee, S.S. Im. Thermomechanical properties and crystallization behavior of layered double hydroxide/poly (ethylene terephthalate) nanocomposites prepared by in-situ polymerization, *Journal of Polymer Science Part B-Polymer Physics*, **45** (2007), p.28-40.

131. F-A.He, L-M. Zhang, F. Yang, L-S. Chen, Q. Wu. New Nanocomposites Based on Syndiotactic Polystyrene and Organo-Modified ZnAl Layered Double Hydroxide. *Journal of Polymer Research* **13** (2006), p.483-493.

132. P.J. Pan, B. Zhu, T. Dong. Poly (L-Lactide)/Layered Double Hydroxides Nanocomposites: Preparation and Crystallization Behavior, *Journal of Polymer Science Part B-Polymer physcis,* **46** (2008), p.2222-2233.

133. M.F. Chiang, T.M. Wu. Synthesis and characterization of biodegradable poly(L-lactide)/layered double hydroxide nanocomposites. *Composites Science and Technology***, 70** (2010), p.110-115 .

134. S.F. Hsu, T.M. Wu, C.S. Liao. Nonisothermal crystallization behavior and crystalline structure of poly(3-hydroxybutyrate)/layered double hydroxide nanocomposites. *Journal of Polymer Science Part B-Polymer Physics*, **45 (**2007), p.995-1002.

135. S.F. Hsu, T.M. Wu, C.S. Liao. Isothermal crystallization kinetics of poly(3-hydroxybutyrate)/layered double hydroxide nanocomposites, *Journal of Polymer Science Part B-Polymer Physics,* **25** (2006), p.3337-3347.

136. F. R.Costa, U. Wagenknecht, D. Jehnichen, M.. Abdel Goad and G. Heinrich. Nanocomposites based on polyethylene and Mg–Al layered double hydroxide. Part II. Rheological characterization, *Polymer* , **47** (2006), p.1649-1660.

137. M. Saphiannikova , F. R. Costa, U. Wagenknecht and G. Heinrich. Nonlinear behavior of polyethylene/layered double hydroxide nanocomposites under shear flow. *Polymer Science Series A*, **50**, (2008).

138. S. Morlat, B. Mailhot, D. Gonzalez, J-L. Gardette. Photo-oxidation of Polypropylene/Montmorillonite Nanocomposites. 1. Influence of Nanoclay and Compatibilizing Agent. *Chemistry of Materials*, **16** (2004), p.377–383

139. S. Morlat, B. Mailhot, D. Gonzalez, J-L. Gardette Photooxidation of Polypropylene/Montmorillonite Nanocomposites. 2. Interactions with Antioxidants. *Chemistry of Materials,* **17** (2005), p.1072–1078.

140. C. Remili , M. Kaci , S. Kachbi, S. Bruzaud , Y. Grohens. Photo-oxidation of polystyrene/clay nanocomposites under accelerated UV exposure: Effect on the structure and molecular weight. *Journal of Applied Polymer Science*, **112** (2009), p. 2868 – 2875.

141. S. Morlat-Therias, B. Mailhot, J.-L. Gardette , C. Da Silva, B. Haidar and A. Vidal. Photooxidation of ethylene-propylene-diene/montmorillonite nanocomposites. *Polymer Degradation and Stability,* **90** (2005), p.78-85.

142. S. Sánchez-Valdés , J. G. Martínez Colunga, M. L. López-Quintanilla, I. Yañez Flores, M. L. García-Salazar and C. González Cantu**.** Preparation and UV weathering of polyethylene nanocomposites. *Polymer International*, **60** (2008), p.829-836**.**

143. S. Bocchini, S.Morlat-Therias, J-L. Gardette, G. Camino, Influence of nanodispersed hydrotalcite on polypropylene photooxidation *European Polymer Journal,* **44** (2008), p.3473–3481.

144. B. Kumar, S. Rana, R. P. Singh Photo-oxidation of EPDM/layered double hydroxides composites: Influence of layered hydroxides and stabilizers *eXPRESS Polymer Letters.* **1** (2007), p.748–754.

145. F. Leroux, L. Meddar, B. Mailhot, S. Morlat-Therias, J-L. Gardette. Characterization and photooxidative behaviour of nanocomposites formed with polystyrene and LDHs organo-modified by monomer surfactant. *Polymer,* **46** (2005), p. 3571–3578.

146. F. Cavani, F. Trifiro, and A. Vaccari. Hydrotalcite-type anionic clays: Preparation, properties and applications. *Catalysis Today*, **11** (1991) p.173 – 301.

147. D. Tichit and B. Coq. Catalysis by hydrotalcites and related materials. Catalysis Technology, **7** (2003), p.206 – 217.

148. C. D. Hoyo. Layered double hydroxides and human health: An overview. *Applied Clay Science*, **36** (2007), p.103-121.

149. W. F. Lee and Y. C. Chen. Effect of hydrotalcite on the physical properties and drug-release behavior of nanocomposite hydrogels based on poly[acrylic acid-co-poly(ethylene glycol) methyl ether acrylate] gels. *Journal of Applied Polymer Science,* **94** (2004), p.692 – 699.

150. J. H. Choy, S. Y. Kwak, J. S. Park, Y. J. Jeon, and J. Portier. Intercalative nanohybrids of nucleoside monophosphates and dna in layered metal hydroxide. *Journal of the American Chemical Society*, **121 (**1999), p.399 – 1400.

151. J. V. de Melo, S. Cosnier, C. Mousty, C. martelet, and N. Jaffrezic-Renault. Urea biosensors based on immobilization of urease into two oppositely charged clays (laponite and zn-al layered double hydroxides). *Analytical Chemistry*, **74** (2002), p.4037 – 4043.

152. Y. Lin, J. Wang, D. G. Evans, and D. Li. Layered and intercalated hydrotalcite-like materials as thermal stabilizers in PVC resin. *Journal Physics and Chemistry of Solids*, **67** (2006), p.998 – 1001.

153. S. Guo, D. G. Evans, and D. Li. Preparation of C.I. pigment 52:1 anion-pillared layered double hydroxide and the thermo- and photostability of the resulting intercalated material. *Journal of Physics and Chemistry of Solids*, **67** (2006), p.1002 – 1006.

154. Y. Feng, D. Li, Y. Wang, D. G. Evans, and X. Duan. Synthesis and characterization of a UV absorbent-intercalated Zn-Al layered double hydroxide. *Polymer Degradation and Stability*, **91** (2006), p.789 – 794.

Chapter 3

EXPERIMENTAL AND CHARACTERIZATION TECHNIQUES

"Scientific innovations continually provide us with new means of analyzing the finds"

~Richard Leakey

3.1 Introduction

This chapter describes the experimental methods and characterization techniques used in the preparation of PP-LDH nanocomposites fabricated using the melt blending technique. The different characterization techniques used in the course of this work are discussed in this chapter. These nanocomposites have been characterized by a host of techniques for their microstructure using X–ray diffraction (XRD), transmission electron microscopy (TEM), and scanning electron microscopy (SEM). The filler–polymer interactions and photooxidative changes in nanocomposites were analyzed by Fourier transform infrared spectroscopy (FTIR). The mechanical property enhancements in the nanocomposites have been studied using dynamic mechanical thermal analysis (DMTA) and universal testing machine (UTM). Thermo gravimetric analysis (TGA) is used to elucidate the thermal stability of these nanocomposites. Crystallization behavior in nanocomposites is studied by differential scanning calorimeter (DSC). The spherulite growth was recorded under polarized optical microscopy (POM). Rheology is an important tool to understand the correlation between the mesostructure of nanocomposites and solid–state properties to create technologically important materials. Linear and non−linear rheological experiments were conducted to elucidate the durability of the nanocomposites structures under various conditions of shear and/or external stress. Accelerated photooxidative weathering was carried out in SEPAP 12/24.

3.2 Experimental

3.2.1 Melt Compounding

Melt processing technique is the most popular and economic method for thermoplastics and the composites based on them. In the present case, melt processing was carried out both in small scale using a micro-compounder and in large scale using a twin-screw extruder. There are several parameters associated with melt processing technique that control the quality of the processed materials. For example, temperature, mixing time, shear rate applied (speed of screw elements), design of the mixing equipments, etc all critically control the extrudate quality of thermoplastics. For preparing PP/LDH based nanocomposites, the similar processing conditions were maintained for all compositions. The nanocomposites were prepared using melt compounding technique. Two types of equipments are used for this purpose.

3.2.1.1 DSM Micro Extruder & Injection Molder

Various master batches of nanocomposites and the matrix polymer were prepared using the DSM micro-compounder (**Figure 3.1**). It is a twin-screw extruder, having a net barrel capacity of 5 CC (Model DSM Micro 5-DSM research, The Netherlands) and consists of a vertical barrel with two conical screws (screw diameter ranges from 0.43 to 1 cm, screw length = 10.75 cm. A brief overview of the different parts and processing were described using **Figure 3.1**.

3.2.1.2 Haake Polylab Batch Mixer

Haake Polylab batch mixer (shown in Figure 3.2) is a laboratory sized batch compounder and is suitable for preparing small batches of samples sufficient for carrying out most of the preliminary analysis required for material characterization. Haake Polylab batch mixer having 50g capacity is used for the compounding of nanocomposites of LDH and MMT nanoclays. The batch mixer is a Rheomix 600P equipped with roller rotors R600.

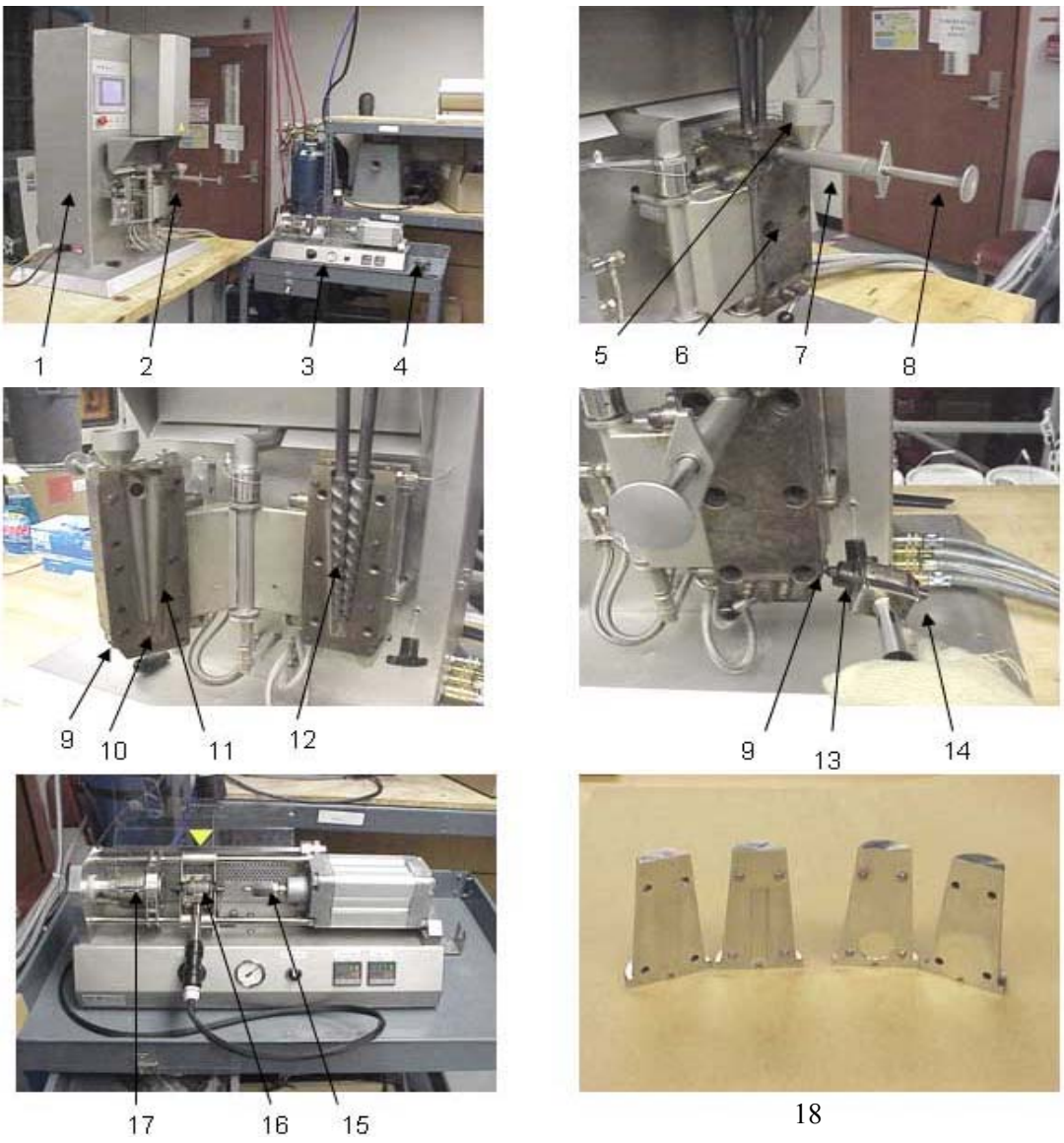

1-Microcompounder	2-Feeder	3-Mini-injuction molder
4-Transfer cylinder	5- Hopper	6-Extruder barrel
7- Transfer tube	8- Plunger	9-Die orifice
10- T gate	11-Recircullation canal	12- Screws
13-Melt cup	14-Mold plunger	15-Pneumatic ram
16-Molder cradel	17- The Mold	18- Dies

Figure 3.1: DSM micro-compounder and their parts

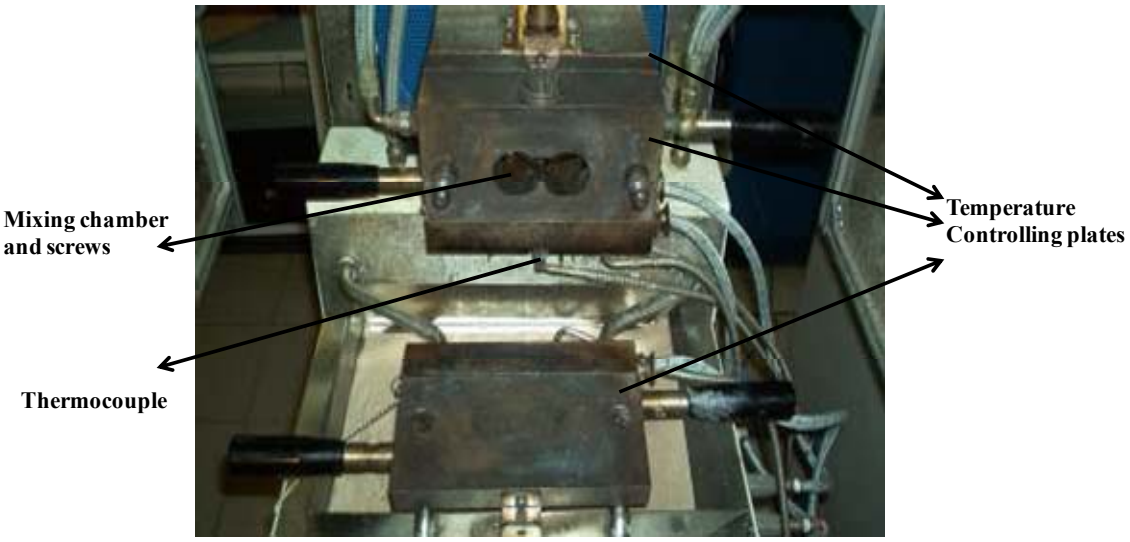

Figure 3.2 Haake Polylab batch mixer (Rheomix 600P)

3.2.2 Injection Molding

The extruded materials were injection molded following ASTM standard for tensile, flexural and Izod impact test specimens using a DSM injection-molding machine (**Figure 3.1**- part 15, 16 & 17) with barrel temperature of 180-220°C. All test specimens were allowed to condition under ambient environment for at least 48 hours prior to testing.

3.2.3 Compression Molding

The films are prepared by compression molding using Carver press model F – 15181. An appropriate quantity of material is taken and heated above melting temperature between metal sheets, which are sprayed using mold release spray. Nominal pressure is applied to get the required thickness of the film. Platens of carver press are then cooled using water circulation. These films are used for further characterization.

3.3 Characterization Techniques

3.3.1 Fourier Transform Infrared Spectroscopy (FT-IR)

Fourier transform infrared (FTIR) spectra for unmodified LDH, and organically modified forms were recorded over the wave number range 400 – 4000 cm^{-1} using Perkin-Elmer 16 PC FT-IR spectrophotometer, equipped with multiple reflectance accessories. The powdered samples were mixed with KBR in a 1:200 ratio of their weight and pressed in the form of pellets for measurement. For measuring FTIR of the polymeric composites thin films of thickness in the range 100 – 250 μm were compression molded.

Infrared spectra for the characterization and monitoring the functional group generation during photo-oxidation of PP/LDH nanocomposites were recorded with a Nicolet 5SX-FTIR spectrometer working with OMNIC software. Spectra were obtained using 32 scans and 4 cm^{-1} resolution. The rate of photo-oxidation of the UV degraded films was followed by measuring peak intensities in carbonyl and hydroxyl domains.

3.3.2 X-ray Diffraction Analysis (XRD)

The crystalline structure of LDH, the degree of swelling and the interlayer distance in layer structure of LDH and MMT in the nanocomposites were determined by Wide angle X-ray diffraction (WAXD). X-ray diffraction analysis (XRD) was carried out with a Rigaku (Japan) D/max-RB wide angle X-ray diffractometer (WAXD). X-ray diffraction was performed at accelerating voltage 30 kV with a current of 35mA at room temperature. The operation parameters were Cu-Kα radiation at a rotating anode generator operated at voltage of 40 kV and at current of 100 mA. The scanning rate was 2°/min at an interval of 0.02. Samples were in 1cm² pieces taken from compression-molded specimen. The diffraction patterns were recorded with a step size of 0.02º from 2θ = 2º to 60º. The calculation of the interlayer distance (d) was carried out from the measured value of diffraction angle 2θ by using the Bragg equation.

$$d = \frac{\lambda}{2\sin\theta} \qquad (3.1)$$

where, λ represents the wave length of the incident X-ray beam and *n* is a positive integer. XRD spectra were interpreted with respect to the position of the first order basal reflection < 003 >, which depends on the distance between two adjacent metal hydroxide sheets in the LDH crystal lattice (i.e. *d*). The higher order reflections of the same < *hkl* > series (i.e. < 006 >, < 009 > and so on) were also reported as they indicate the presence of repeating crystal planes and symmetry in a specific crystallographic direction.

3.3.3 Transmission Electron Microscopy (TEM)

Conventional optical microscopes can investigate structure to the resolution of few micrometers. But much higher resolution is required to study the fine structural details of the polymer nanoclay composites. Polypropylene nanocomposites were analyzed by transmission electron microscopy (TEM) in an effort to characterize the nanoscale dispersion of the LDHs. The samples for TEM imaging were sectioned using a Leica Ultracut UCT microtome at 80-100 nm thickness with a diamond knife at -100 °C. The sections were collected from water on 300 mesh carbon-coated copper grids. TEM imaging was done using a JEOL 1200EX electron microscope operating at an accelerating voltage of 100 kV. Images were captured using a charged couple detector camera and viewed using Gatan Digital Micrograph software.

3.3.4 Scanning Electron Microscopy (SEM)

SEM is designed for direct studying the surfaces of solid objects. By scanning with an electron beam that has been generated and focused by the operation of the microscope, an image is formed in much the same way as a television. Advantages of the SEM include higher resolution than optical microscopy with a much larger depth of field and focus, easy to operation and easy to prepare the sample. For this reason the SEM can produce an image that is a good representation of the three dimensional sample. In this thesis we have used SEM for observing the morphology of the organomodified LDHs and nanocomposites based on LDH, surface erosion studies after photo-oxidation of nanocomposites and to observe the fracture behavior. The SEM images were scanned under Leica Cambridge Stereoscan 440 model, electron microscope. The stained samples

were dried under vacuum for 24 h at 50°C and the gold-coated samples were examined for SEM.

3.3.5 Polarized Light Optical Microscopy (PLOM)

A microscope is a simple lens system for magnifying small objects. The first lens called objective has a short focal length of few millimeter and creates an image of the object in the intermediate image plane. This image is then viewed by another lens (eye - piece) that provide additional magnification. A polarized light beam is used to view the spherulitic morphology. A spherulite is a commonly observed spherically symmetrical morphological feature consisting of chain folded lamellae radiating from a central point. The spherulite growth formation in PP/LDH nanocomposites were observed under PLOM. Spherulitic morphology of the samples prepared was studied by OLYMPUS polarized optical microscope (POM) attached with a Mettler Toledo FP82HT hot stage under crossed polarizer. Thin slices were cut from the injection molded samples, inserted between two microscope cover glasses, melted at 200 °C. The slides were then transferred to the hot stage and melted at 200 °C then slides were held for one minute to ensure uniform melting. In subsequence, samples were cooled to room temperature at a constant rate of 10 °C /min. The course of non-isothermal crystallization was recorded by taking photomicrographs, using Olympus digital camera.

.

3.3.6 Thermogravimetric Analysis (TGA)

The determination of changes in chemical or physical properties of material as a function of temperature in a controlled atmosphere can be obtained by a thermal analysis. TGA is a good analytical tool to measure thermal decomposition of solids and liquids, solid-solid and solid - gas chemical reactions. TGA curve provides information concerning the thermal stability of the initial sample, intermediate compounds that may be formed and of the residue if any. In addition to thermal stability, the weight losses observed in TGA can be quantified to predict the pathway of degradation or to obtain compositional information. The thermogravimetric analysis (TGA) i.e. thermal stability and degradation behavior of LDHs and PP/LDH nanocomposites was done using TA instruments TGA-Q5000. The thermal stability and amount of LDH present in the

nanocomposites were determined from TGA. The samples were heated under flowing nitrogen atmosphere from 50 to 900 °C, at a heating rate of 10 °C /min. and the corresponding weight loss was recorded.

3.3.7 Differential Scanning Calorimetry (DSC)

Differential Scanning Calorimetry (DSC) is a frequently used technique for the thermal analytical investigation of polymeric materials. DSC measures the amount of energy (or heat) absorbed, cooled or maintained at a constant (isothermal) temperature, e.g. heat will be absorbed at both the Tg and the melting point of the sample. As a result, the melting and crystallization processes appear as peaks (endothermic or exothermic) and the area under the curve gives a direct measure of the heat of fusion or crystallization. The DSC test allows these thermal transitions to be identified for a plastic material by noting the absorption of heat from the plot of heat versus time as the sample is heated. Results identify the temperatures of the transitions. Non-isothermal, isothermal crystallization and crystal-to-crystal phase transformation of PP and the nanocomposites were studied by TA instruments Q10 differential scanning calorimeter (DSC) calibrated with indium. The samples of PP and PP/ LDH nanocomposite about 200 mm thick were obtained by hot compression molding, disk-like samples about 5 mg weight were taken for DSC measurements. Samples were heated to 200 °C at a rate of 10 °C/min under a nitrogen atmosphere and held for 5 min to destroy nuclei before cooling at the specified cooling rate. The exothermal curves of heat flow as a function of temperature were recorded to analyze crystallization process and the crystallinity of the samples was determined from the heat of crystallization. The crystallization temperatures T_c were recorded from the endothermic peak obtained during cooling from melt in the DSC.

3.3.8 Dynamic Mechanical Thermal Analysis (DMTA)

DMA is an important tool that provides invaluable insight into the structure–property relationships of polymers. DMTA probes essentially the relationships between the dynamic properties and the structural parameters including molecular weight, molecular orientation, crystallinity, crosslinking, copolymerization, plasticization etc. From a research perspective, suitability of innovative materials for new applications can

be assessed by considering, modulus, damping, glass transition, softening temperature and creep. DMTA measures the response of a given materials to a cyclic deformation (usually tension or three point flexion type deformation). DMTA results are expressed by three main parameters: (i) the storage modulus (*E'*), corresponding to the elastic response to the deformation; (ii) the loss modulus (*E''*), corresponding to the plastics response to the deformation and (iii) *tan δ*, that is the (*E'/E''*) ratio, useful for determining the occurrence of molecular mobility transitions such as the glass transition temperature.

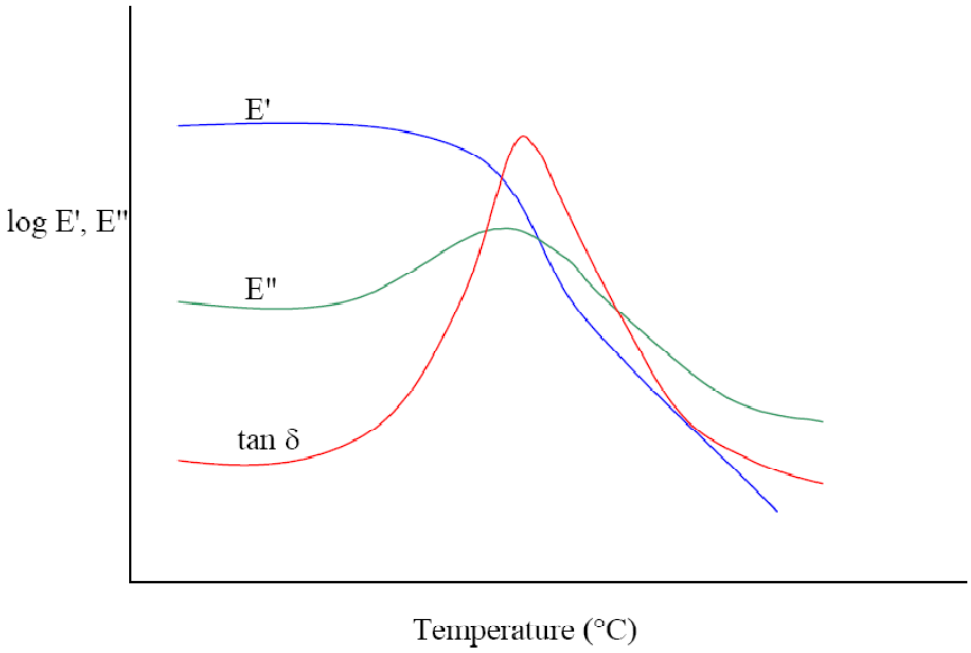

Figure 3.3: Typical DMA scan showing *E'*, *E''* and *tan δ* curves

Thus, the dynamic properties provide information at the molecular level to understanding the polymer mechanical behavior. The dynamic mechanical properties of the PP/LDH nanocomposites are studied using the TA Instruments Rheometric Series RSA III dynamic mechanical analyzer in the tensile mode. For the constant frequency, oscillatory test, temperature sweep is carried out from -60 to 120 ˚C and the sample is heated at a rate of 5 ˚C/min. The frequency is kept as 10 rad/s and the 0.02% strain is fixed suitably in the linear region, by carrying out strain sweep tests and noting that the force lies between the transducer limits.

3.3.9 Mechanical Properties

Most polymers are used in load-bearing capacity. The geometrical responses to loading lead to a wide range of mechanical properties required. However, nearly all can be grouped under stress-strain properties, viscoelasticity and failure properties. These properties are in turn largely determined by the polymer structure (i.e., molecular weight, crosslinking, branching, segmental structure and morphology) and the nature and extent of compounding. In addition, external conditions such as temperature, loading rate and environment must be considered when characterizing the mechanical behavior of a polymeric system.

3.3.9.1 Tensile Test

Tensile measurements were made on Dumbbell-shaped specimens (**Figure 3.4**) with thickness of 4 mm and a width of 10 mm at the center. **Figure 3.4** shows the dimension of the Dumbbell shape specimen. The tensile properties were measured at room temperature (27 ˚C) on a universal testing machine (Instron, UK, model 4204) according to ASTM D638. The specimen was pulled at a constant crosshead speed rate of 50mm/min. From the stress-strain curves, the instrument software calculated the following properties: tensile strength, Young modulus and elongation at break. Five specimens of each formulation were tested and the average values were reported.

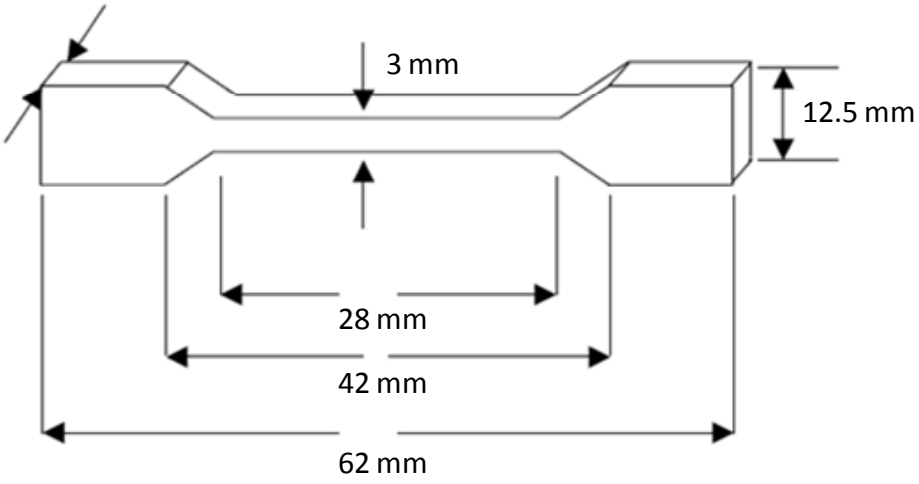

Figure 3.4: Specimen dimension of the dumbbell specimen

3.3.9.2 Flexural Test

Flexural test was carried out according to ASTM D790. The test procedure used was Test Method 1, Procedure A, i.e., three-point loading utilizing center loading. The reason to use three points bending as the evaluating technique was due to its ease in specimen preparation and similarity to impact loading exerted on the automotive parts. Sample for flexural test was placed on a simple supported beam. The distance between the spans was 100mm and the strain rate (compression speed) was 3 mm/min. Five specimens of each formulation were tested and the average values were reported.

3.3.9.3 Izod Impact Test

Izod impact strength (unnotched) was measured using an impact tester (Ceast, Italy) in accordance with the ASTM D256-93 standard test method for determining the pendulum impact resistance of unnotched specimens for plastic. Figure 3.3 shows the dimension of the Izod impact specimen. The test method covered the determination of the resistance of plastic to breakage by flexural shock as indicated by the energy extracted from standard pendulum type hammers. The notch was milled with a 45º angle and 2.5 mm depth with an Automatic Notcher Machine. Izod tests were carried out at room temperature. The test conditions used were as follows: Hammer energy = 7.5J, Velocity = 3.0 m/s and Angle = 150º.

3.3.10 Melt Rheology

An oscillatory shear experiment is the most commonly used method for determining the linear viscoelastic properties of polymer melts. In a typical oscillatory shear experiment, a sinusoidally varying small amplitude stress or strain is applied to the sample, and the response, i.e., either sinusoidally varying strain or stress respectively, is measured. A typical frequency response curve is shown in the Figure 2.7. At low frequencies (terminal region), G" > G' i.e., the behavior of polymer melt is liquid like. The slopes of G' and G" are 1 and 2 respectively. G' and G" increases with frequency until the crossover frequency is reached.

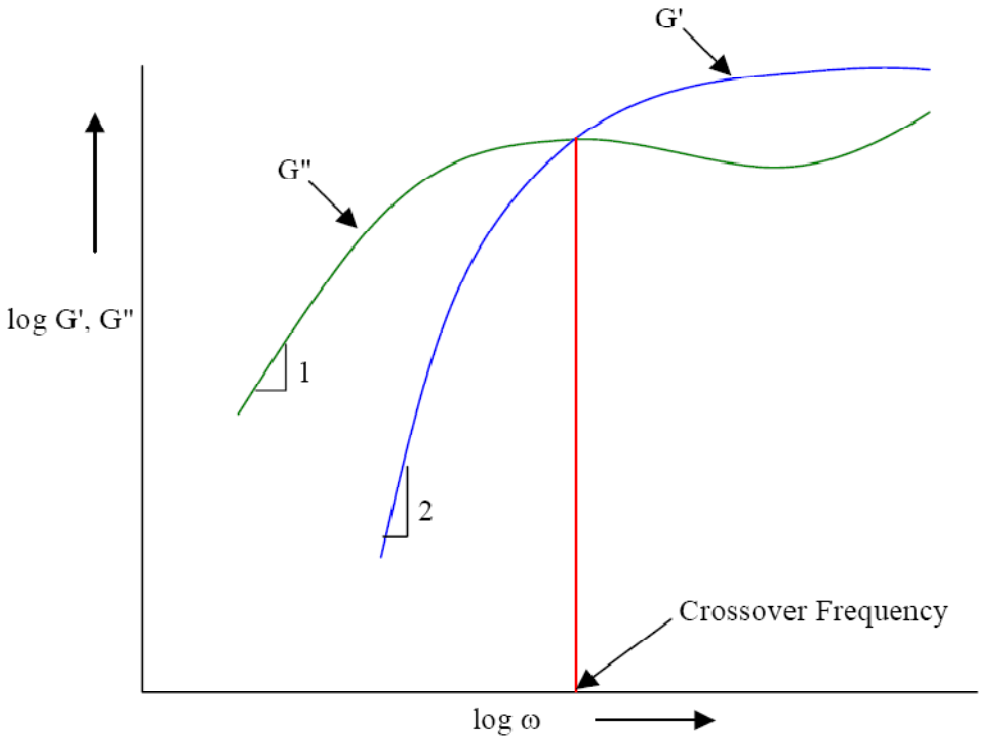

Figure 3.5: G' and G" behavior as the function of frequency

Reciprocal of crossover frequency gives the characteristic relaxation time of the material. After crossover, G' reaches a constant value in the intermediate frequencies called as the plateau modulus. Plateau modulus is independent of the molecular weight and depends only on the chemical nature of the polymer. In this region G" passes through a minimum. At higher frequencies or small time scales, response will be only due to the small parts of the polymer chains. The viscoelastic material functions are strongly dependent on temperature and frequency. No single experiment can cover the entire span of frequencies. Dynamic oscillatory frequency sweeps are carried out using Rheometric Scientific ARES rheometer in the frequency range of 0.1 to 100 rad/sec at temperatures 180 – 200 ˚C. Parallel plate geometry of 25 mm diameter is used for this purpose. The specimen thickness is about 0.5 mm. The strain sweep experiment is carried out to find the region of linear response. The strain value fixed at 5% ensuring that the measurements are carried out in linear region.

3.3.11 Limiting Oxygen Index (LOI)

LOI, the minimum oxygen concentration by volume for maintaining the burning of a material, is a very important parameter for evaluating the flame retardancy of polymeric material. The LOI is used to determine the minimum concentration (in a flowing mixture of nitrogen and oxygen) of oxygen required to sustain a candle-like burning process of any material. It is expressed by a number indicating percentage of oxygen in a nitrogen-oxygen mixture and gives a qualitative measure or indication of materials' susceptibility to continuous burning after ignition. In this test, the minimum amount of required oxygen to stabilize the flame of the samples is reported; the higher the LOI value, higher will be the resistance to flammability. The LOI value is obtained based on following equation:

$$LOI\% = \frac{V_{O_2}}{V_{O_2} - V_{N_2}} \qquad 3.2$$

where V_{O2} and V_{O2} are the minimum oxygen concentration in the inflow gases required to pass the ``minimum burning length'' criterion and the nitrogen concentration in the inflow gases respectively. LOI is often useful in comparative investigation and quality control during product design. Usually, a material having LOI value 21 or less burn spontaneously in air. So, the efficiency of a flame-retardant is often interpreted by the increase in the LOI value (from that in the pure polymer) when it is incorporated into a polymer. Although the relevance of this test to the real fire conditions is questionable, this test method is widely practiced both in industry and in academics because of inexpensive test equipments and a small sample requirement. The typical LOI test apparatus, as shown in Figure 3.3 consists of a glass tube of 75 to 100 mm in diameter and of 450 to 500 mm in height. A specimen with a specified dimension is supported inside the glass tube. A gas mixture of oxygen and nitrogen is supplied at the bottom of the tube and a small candle-like flame is applied to the top of the specimen in an attempt to ignite it. The composition of the gas mixture can be controlled (up to minimum 0.1 volume percent) by varying the flow pressure of the oxygen and nitrogen stream. The

LOI values of the LDH based composites were measured by a oxygen index tester from Veekay Testlab, Mumbai using injection molded strips (125 x 6.5 x 3.2 mm) according to ASTM 2863.

Figure 3.6: A typical LOI measuring instrument

3.3.12 Accelerated Photoageing

Accelerated weathering of PP/LDH nanocomposites were performed in SEPAP (**Figure 3.7**). This apparatus has been designed for the study of polymer photodegradation in artificial conditions corresponding to a medium acceleration of aging. It is a climate chamber equipped with 4 artificial lamps (mercury vapor : unit power 400W) with cut off of UV radiation below 300 nm and emitting a polychromatic light through borosilicate filters ; samples are continuously exposed without water sprinkling ; temperature is maintained at 60°C. The samples were rotated to assure homogeneous irradiation all over the exposed surfaces. Temperature is carefully

monitored by a thermal probe (Pt 1 0 0) connected to a sample. Advantage of accelerated weathering lays in robust identification of degradation mechanism due to rapid accumulation of photo-byproducts. Correlation with natural aging is valid as long as the chosen accelerated aging cycle is representative of climatic conditions found in tropical countries. SEPAP used in present study is SEPAP 12-24 weathering device from Atlas, Germany.

Figure 3.7: Accelerated Photoageing device (SEPAP 12/24)

Chapter 4

SYNTHESIS AND CHARACTERIZATION

"The important thing in science is not so much to obtain new facts as to discover new ways of thinking about them"

~William Lawrence Bragg

Sunil P. Lonkar, S. Morlat-Therias, F. Leroux, J-L. Gardette, R.P. Singh, ""*Preparation and Nonisothermal Crystallization Behavior of Polypropylene/Layered Double Hydroxide Nanocomposites*", ***Polymer,*** 50 (2009), p. 1505-1515.

4.1 Introduction

The basic reason for selecting LDH is their typical metal hydroxide-like chemistry and conventional clay-like layered crystalline structure with aspect ratios similar or even higher than that observed for aluminosilicates [1-2] and it makes LDH suitable for polymer nanocomposite preparation. However, in this type of clay the sheets have high charge density and hydrophilicity, which makes the intercalation of polymer chains into the gallery of LDHs difficult. Because of the hydrophilic nature of pristine LDHs, the formation of a thermodynamically homogeneous mixture of LDH with hydrophobic polymers at molecular level is difficult. Hence, to intercalate polymer chains into the galleries is of great challenge. Therefore, the surface treatment of LDHs sheets is necessary to render its surface more hydrophobic, which facilitates exfoliation. A typical way to enhance the interaction between the LDH and the polymer is by exchanging the interlayer anions with anionic surfactants having long hydrocarbon chains i.e organomodification. Three main benefits are normally obtained in the LDH by means of organomodification, related to potential use as nanocomposites precursors in polymer matrices: Firstly, the LDH basal space increases, making possible the interaction of macromolecular segments or molecules within the interlayer galleries. Secondly, the attractive forces between contiguous platelets decrease. As a consequence, the exfoliation of the platelets can be achieved more easily by means of shearing forces during the melt

mixing with the polymer. Finally, it gives organophilic character to the LDH particles, making them more compatible with polymer matrices. Thus, first step to prepare PP/LDH nanocomposites was the LDH organophillization.

In addition to the base matrix PP and the filler particles, the PP/LDH nanocomposite prepared by melt compounding contains a third component, namely compatibilizer. This compatibilizer is a functionalized polymer containing pendent maleic anhydride groups on a polypropylene backbone. The primary purpose of using a functionalized polymer (PP-g-MAH) is to improve compatibility between the non-polar PP matrix and the highly polar LDH particle surface. It is believed that the polar functional groups present in functionalized polymers (like maleic anhydride group in PP-g-MAH) can have favorable interaction with clay surface. The rigorous morphological characterization of a polymer/clay nanocomposite is necessary to understand the state of clay particle dispersion in polymer matrix. The primary approach is to study the changes in the interlayer separation of the clay crystals using X-ray diffraction analysis (XRD). However, the XRD analysis alone cannot be reliable to draw final conclusion about the dispersion state of clay particle in nanocomposites [3-4]. This is because of the fact that the nature of reflection (in terms of its position and intensity) in the XRD pattern not only depend on the interlayer separation, but also on several other factors, like concentration of the clay in the nanocomposites, symmetry in specific crystallographic directions, etc. Therefore, alongwith XRD analysis, electron microscopic investigations are often coupled to obtain a complete picture of dispersion of the clay particle in polymer nanocomposites. However, the morphological analysis using electron microscopy, like TEM also has certain inherent disadvantages so far as polymer nanocomposite is concerned. First, to view the nanoscopic particle distribution within a polymer matrix one needs to rely on high magnification images, which makes the scan surface area very small not necessarily representing the whole surface area of the sample. Second, it shows only the surface morphology of the particle distribution and not the bulk morphology. In case of molded articles or test specimen, the nature of particle distribution can be significantly different at the different sections of the samples [5]. To obtain the overview of particle dispersion over large surface area, images of different magnifications starting

from low magnification to high magnification should be investigated simultaneously on the same surface.

The study focuses here on is organophillization LDHs comprising different metal cations, which is realized by anionic exchange reaction with organic anions. The compositions and structures of the modified LDHs were analyzed by using different instrumental techniques such as FTIR, XRD and TEM analysis. Also, the thermal properties of such modified anionic clays have also been investigated. Afterwards, the modified LDHs have been successfully employed in fabrication of PP/LDH nanocomposites by melt intercalation using PP-g-MAH as a compatibilizer. It is believed that the maleic anhydride groups can react with the interlayer anionic groups of LDH. A series of samples were prepared in accordance with the aim of the study. Polymer intercalation within the LDH lamellar structure and dispersion of LDH particles were characterized by FTIR, TEM and WAXD analysis, respectively.

4.2 Materials Description

4.2.1 Layered Double Hydroxides

Three different types of LDHs have been used in this study comprising different metal cations. The M^+: Al (M^+ =Mg^{2+} and Zn^{2+}) ratio in the synthesized LDH is approximately kept to 2:1 and 1:1:1for Mg_2Al-DDS, Zn_2Al-DDS and ZnMgAl-DDS, respectively. For initial part of this study different phases of dodecyl sulfate modified (DDS) LDHs were obtained through courtesy of Dr.Fabrice Leroux, LMI, University of Blaise Pascal, France. Following similar literature procedure sizable amount of LDHs have been synthesized.

The various chemicals used for the synthesis of DDS modified LDHs were synthetic grade and are described below.

Metal Chlorides: Magnesium Chloride ($MgCl_2$), Zinc Chloride ($ZnCl_2$), and Aluminum Chloride ($AlCl_3$): All were in hexahydrated form with 98% purity and were purchased from Aldrich chemical company. NaOH is obtained from (Spectrochem, India).

Surfactant: Since the interlayer region of the LDHs clay accommodates anionic species, anionic surfactants are most suitable to modify for its modification. The sodium dodecyl

dulfate (DDS) was used as a surfactant for the modification of LDH to study its intercalation behavior. The choice of surfactants was made based on extensive literature survey, solubility in aqueous medium and structure of the hydrocarbon chain. The DDS (>98% $CH_3(CH_2)_{11}O\ SO_3Na$, Spectrochem, India) was used as received.

.

4.2.2 Montmorillonite

The montmorillonite type cationic clay is used for performance comparison with LDHs. In present study we have used Cloisite® 20A montmorillonite clay. It is a natural montmorillonite modified with a quaternary ammonium salt as shown in **Figure 4.1.**

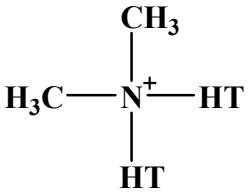

Figure 4.1: Chemical structure of the dimethyl dehydrogenated tallow quaternary ammonium chloride (C20A)

Cloisite® 20A: Where HT is Hydrogenated Tallow (~65% C18; ~30% C16; ~5% C14), Anion: Chloride, (1) 2M2HT: dimethyl, dehydrogenated tallow, quaternary ammonium

Table 4.1: Various technical details of the commercial clay used in the present study

Description	**Montmorrilonite**
Trade name	Cloisite® 20A
Producer	Southern Clay Products, USA
Density	1.77 g/cc
Bulk density	0.118 g/cc
Particle Size (by volume)	10%<2 μ, 50% <6 μ, 90%<13 μ
Color	Off white

4.2.3 Polymers

The main polymer matrix used in the whole study is polypropylene (PP), which is a commercially available general purpose grade of isotactic polypropylene with 2.5-3.0 MFI obtained from Exxonmobil Chemical Company, France. It is a high molecular weight grade with a high value of polydispersity index. Various characteristics of the virgin PP are given in **Table 4.2**.

Table 4.2 Description of the different polymeric materials used

Polymer	Density (g/cc)	Molecular weights (M_w)[a]	MFI[b] (g/10 min)	T_m[d] (°C)
PP	0.90	3,10,000	3.0	165
PP-g-MAH[c] (Polybond 3200)	0.91	42,000	115	157

[a]Measured by Gel Permeation Chromatography (GPC)
[b]Melt Flow Index, ASTM D 1238
[c]1% Maleic anhydride grafted polypropylene
[d]Measured by differential scanning calorimetry (DSC)

Maleic anhydride grafted polypropylene (PP-g-MAH) was used as a compatibilizer to obtain better dispersion of LDH clay particles in polypropylene matrix. The PP-g-MAH used was of lower molecular weight and of higher melt index compared to the base matrix. The details of these polymeric materials used are shown in **Table 4.2**.

4.2.4 Additives

In order evaluate the efficiency of antioxidants and light stabilizers in presence of LDH nanofiller in final nanocomposites, two types of commercially available additives are used namely, Irganox 1010 and Tinivin 770. These are obtained through courtesy from Ciba Chemical Co. Mumbai. Irganox 1010 (tetrakis[methylene 3-(3', 5'-di-tert-butyl-4'-hydroxyphenyl)-propionate]methane) is a hindered phenol type antioxidant, where as Tinuvin 770 (Bis(2,2,6,6-tetramethyl-4- piperidinyl) sebacate) is hindered amine type light stabilizer, their structures are depicted in **Figure 4.2.**

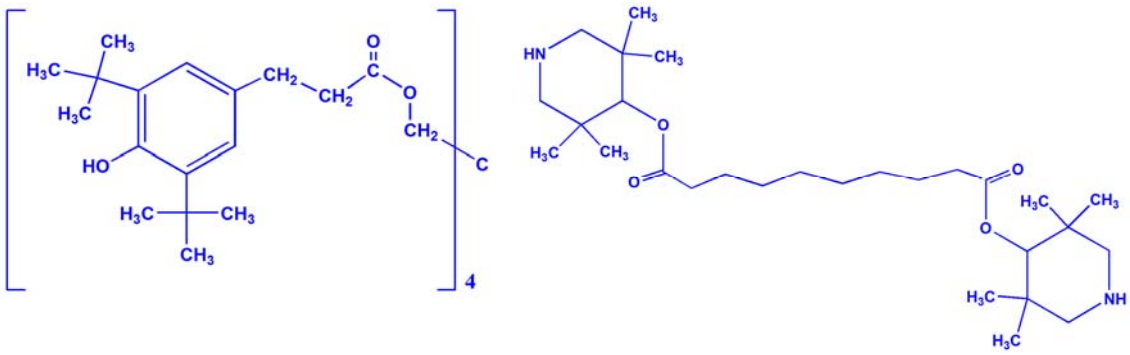

(A) **(B)**

Figure 4.2: Structure of (A) Irganox 1010 and (B)Tinuvin 770

4.3 LDH: Synthesis, Modification and Characterization

4.3.1 Synthesis

A series of hydrotalcite-type material Mg_2Al, Zn_2Al and ZnMgAl–Cl was prepared by simultaneously adding drop wise an aqueous solution of sodium hydroxide (2.0 M) and a mixed aqueous solution of magnesium chloride and aluminum chloride into a large plastic beaker containing 100 mL deionized water which had been boiled and stored under nitrogen before use. The total metal concentration of 1 M with a Zn^{2+}, Mg^{2+}/Al^{3+} molar ratio of 2.0 for Mg_2Al, Zn_2Al and 1.0 for ZnMgAl-LDH was used. Nitrogen was bubbled throughout the process to minimize dissolved carbonate. During the reaction, the temperature and pH of the reaction mixture were maintained at 25±1 °C and 10±0.2, respectively. The suspension was stirred for three hours, transferred to plastic bottles, and placed in an oven at 65 °C for 4 days. After cooling to room temperature, the suspension was centrifuged at 6000 rpm and the precipitate washed extensively using deionized water until free of chloride ($AgNO_3$ test). The samples were not subjected to any drying process, so as to preserve their morphology or particle size without any change. The products were dried at 65 °C and finely ground. This method has been described in literature and is suitable for synthesizing highly crystalline LDHs with narrow particle size distribution [6]. The conditions chosen for the synthesis provides Mg_2/Zn_2-Al–LDH with 'x' around 0.33, The detailed reaction set up is shown in **Figure 4.3**.

4.3.2 Modification

Like layered silicate based nanoclay materials, modification of layered double hydroxides is also an inevitable step in the preparation of polymer nanocomposites based on LDHs, especially when melt-compounding technique is used. Since, the hydroxide layers of LDH clays are positively charged, the modifying surfactants should contain at least one negatively charged functionalities or highly nucleophilic sites in their chemical structure. In the present work, three different LDHs have been modified by a surfactant having anionic functional group i.e. dodecyl sulfate (DDS) having n-C12 tail. The organo-modification was carried out by anion exchange reaction. SDS was introduced into the LDH interlayer at pH 6.5 and at a DDS: LDH ratio of 12 mmol/g. The mixture of LDH and water (1 g/20 mL) was homogenized by stirring before adding the SDS solution. The suspension was stirred at room temperature for 3 days under nitrogen and vigorous stirring. The resulting powder was washed several times with a mixture EtOH /H_2O (50/50), and then dried under vacuum. Similar procedure was employed by adjusting total metal concentration of 1 M with an Mg^{2+}/Al^{3+} molar ratio of 1 and Zn^{2+}/Al^{3+} molar ratio of 2 in order to obtain MgZnAl–DDS and Zn_2Al–DDS, respectively. The pristine and DDS modified LDH was characterized by X – ray diffraction, FT-IR, morphological and thermal studies.

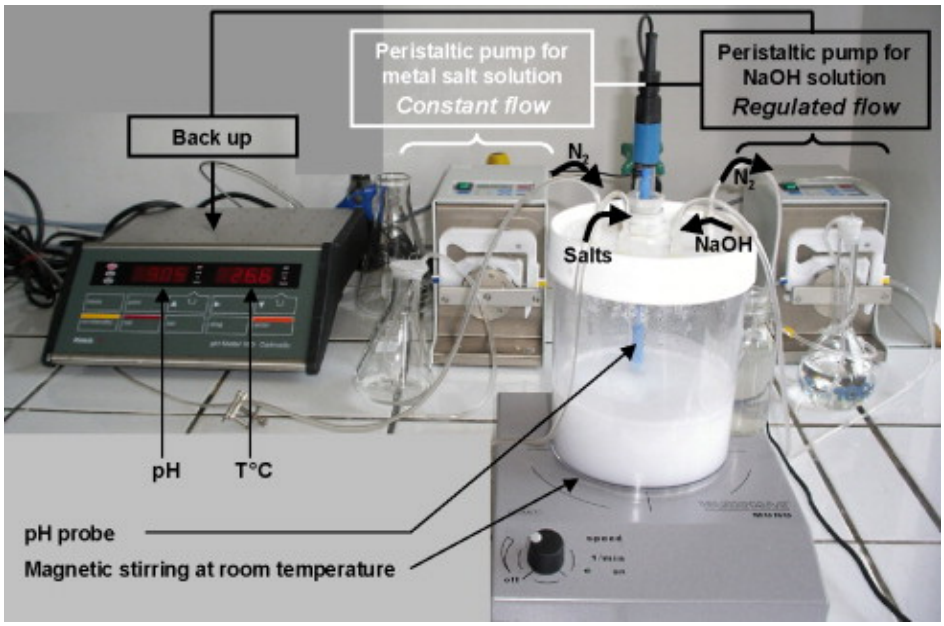

Figure 4.3: Reaction setup for layered double hydroxide preparation

Table 4.3: Composition of layered double hydroxides

LDH	Metal mole ratios			
code	Mg	Zn	Al	Ideal LDH formula
MA-Cl	2.0	0.0	1.0	$Mg_{2.0}Al(OH)_{6.00}$ (Cl). $2H_2O$
MA	2.0	0.0	1.0	$Mg_{2.0}Al(OH)_{6.00}$ ($C_{12}H_{25}O_4S$). $2H_2O$
ZMA	1.0	1.0	1.0	$Zn_{1.0}Mg_{1.0}Al(OH)_{6.00}$ ($C_{12}H_{25}O_4S$). $2H_2O$
ZA	0.0	2.0	1.0	$Zn_{2.0}Al(OH)_{6.00}$ ($C_{12}H_{25}O_4S$). $2H_2O$

4.3.3 Characterization

4.3.3.1 FT-IR Analysis

The FTIR spectra of LDH materials provide many important information, especially about the interlayer anions and their successful organo-modification, hence are very useful to understand the structure of these materials. **Figure 4.4** shows the typical FT-IR spectrum of both pristine and organo-modified LDHs. In the spectrum of both modified and unmodified LDHs, the broad and strong band in the range of 3600–3200 cm^{-1} centered at 3472 cm^{-1} which is due to the O–H stretching vibrations of surface and interlayer water molecule. A broad band or shoulder is observed in the range 1600 – 1640 cm^{-1}, which may indicate the presence of H_2O molecules as the band for its bending vibration appears in this region. The lattice vibration bands from the M-O and O-M-O (M=Zn, Mg, Al) groups appear in the 400-800 cm^{-1} region. Intercalation of DDS instead of Cl^- ions can be confirmed by the strong absorption bands in the range 2850–2950 cm^{-1} corresponding to the -CH_2- stretching vibration of the hydrocarbon tail present in DDS surfactant anion. Two strong absorption peaks appear at 1220 and 1471cm^{-1} can be assigned to the stretching vibrations of sulfate and methylene, respectively. The bands appear in the range 1000 – 1400 cm^{-1} are mostly due to the anionic functionalities present in the surfactants. These FT-IR assignments further confirm that dodecyl sulfate anion is successfully intercalated into the gallery of the LDH.

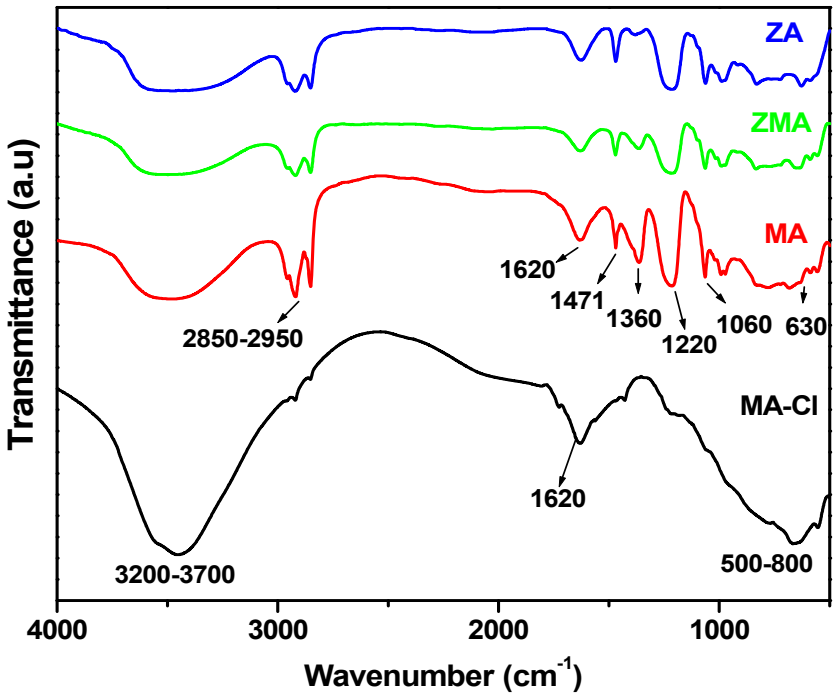

Figure 4.4: FT-IR spectra of unmodified and modified layered double hydroxides

Table 4.4 Assignment of FTIR bands in both modified and unmodified LDHs

Band Position (cm^{-1})	Type of vibration
3200-3700 cm^{-1}	ν_{-O-H}
2850-2950 cm^{-1}	ν_{-CH2-}
1620 cm^{-1}	ν_{-H2O} (bending)
1471 & 1360 cm^{-1}	ν_{-CH2-} (bending)
1220 cm^{-1}	$\nu_{-S=O}$ (symmetric)
1060 cm^{-1}	$\nu_{-S=O}$ (asymmetric)
630 cm^{-1}	ν_{-C-S}
500-800 cm^{-1}	$\nu_{-O-M / O-M-O}$ (M=Mg, Zn, Al)

4.3.3.2 XRD Analysis

The XRD patterns of the synthesized unmodified (MA-Cl) and its organomodified form (MA, ZMA and ZA) are shown in **Figure 4.5**. X-ray diffraction patterns indicated all the synthesized LDHs have typical, well-order layered structures with a high degree of crystallinity. It is observed that in MA-Cl XRD spectra, the first three reflections belongs to the common < *hkl* > series i.e. < 00*l* > and resemble to those reported in literature for synthetic Mg-Al–LDH [7] and hydrotalcite minerals [8]. It is found that the characteristic basal reflection < 003 > has the value of 2θ about 11.51°. By employing Bragg's equation, a basal spacing or interlayer distance is calculated to be about 0.76 nm, which is equal to the sum of the thickness of interlayer region and one metal hydroxide layer as shown in **Figure 4.6**.

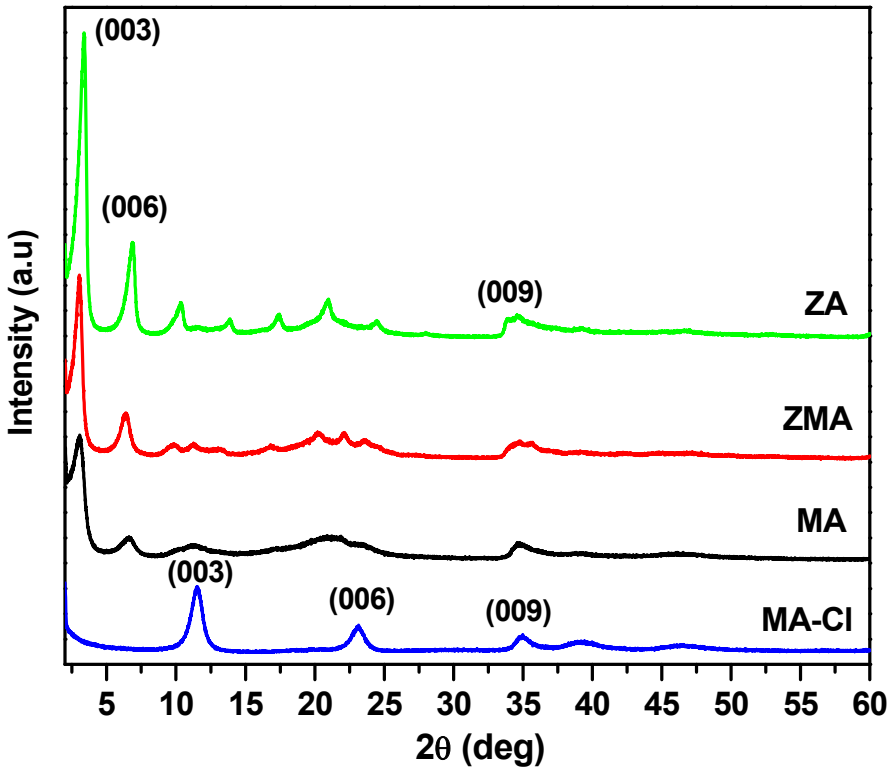

Figure 4.5: XRD patterns of unmodified and modified layered double hydroxides.

The XRD patterns of the DDS modified LDH is also shown in **Figure 4.5**. It can be seen that position of the first order basal reflection < 003 > in all modified samples is

shifted to a higher *d*-value indicating an expansion in the interlayer distance. After the ion-exchange with DDS solution, the first order basal reflection < 003 > of DDS modified LDH moved to the lower angle position (2θ = 3.03°), which corresponds to a *d*-spacing of 2.96 nm. These values were in good agreement with those reported in literature, obtained empirically by X-ray measures [9, 10] or determined from theoretical models [11]. Although none of the modified samples show distinct reflection at *d* = 0.76 nm, there exists a weak and broad reflection in the close vicinity, which may be either due to the presence of small fraction of the unmodified LDH or due to a higher order reflection in < *00l* > series in the modified samples. However, the first option seems most probable as the XRD pattern of all the modified sample show reflections corresponding to single < *00l* > series and no mixed < *hkl* > as compared to the unmodified LDH. The absence of reflection corresponding to mixed < *hkl* > series also indicates a loss of crystallinity of LDH after organic modification. This may be due to the presence of only small crystallites and/or the loss of coherent conditions for all other directions (i.e. no repeat units) in the sense of scattering. **Figure 4.6** illustrate how the DDS anions are placed within the interlamellar space in LDH by replacing the chloride anions.

Thus, the enlarged *d*-spacing of DDS-LDH indicates the successful intercalation of DDS chains into the layers of LDH, thus making LDH more organophilic and facilitating the intercalation and dispersion of organic materials.

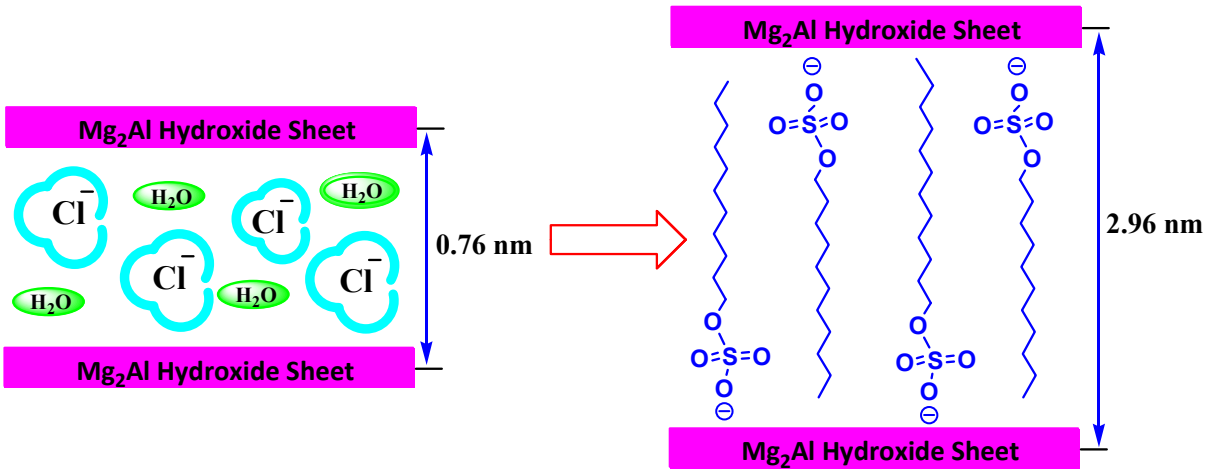

Figure 4.6: Schematic representation of surfactant intercalation in to LDH galleries

4.3.3.3 Morphological Analysis

The morphology of both modified and unmodified LDHs is examined using scanning electron microscopy. LDH clays have usually plate-like particle morphology. The size distribution of the particles depends mostly on the synthesis conditions and varies from few hundred nanometers to few micrometers in lateral dimensions. In **Figure 4.7**, the SEM micrograph of the synthesized LDH shows the particle geometry where the primary plate-like particles are characterized by distinct hexagonal shapes and sharp edges. The highly anisometric nature of these primary particles is also apparent. The lateral dimension of these plate-like particles varies within few micrometers whereas the thickness hardly exceeds few hundred nm. However, it is observed that the particle morphology are somewhat modified after organic modification. As can be observed from **Figure 4.7**, the well defined hexagonal particle shapes are lost. Instead plate-like particle morphology with irregular shapes and edges persist in the modified LDH. This could be because of the surfactant anions being much larger in size than simple inorganic anions perhaps hinder the large scale lateral growth of the LDH layer. Hence, the organo-modified LDH show prominent surface irregularities compared to the unmodified LDH. From **Figure 4.7**, it seems that in modified clay the particle surfaces is either perforated or contain structural features probably due to secondary layer growth. Also, they appear more floppy compared to unmodified LDH. The size of the surfactant anions may be a potential factor that influences the stacking and the growth of the metal hydroxide layers during regeneration process. However, more critical investigations are necessary for determining the exact mechanism of the regeneration process in presence of the organic surfactants.

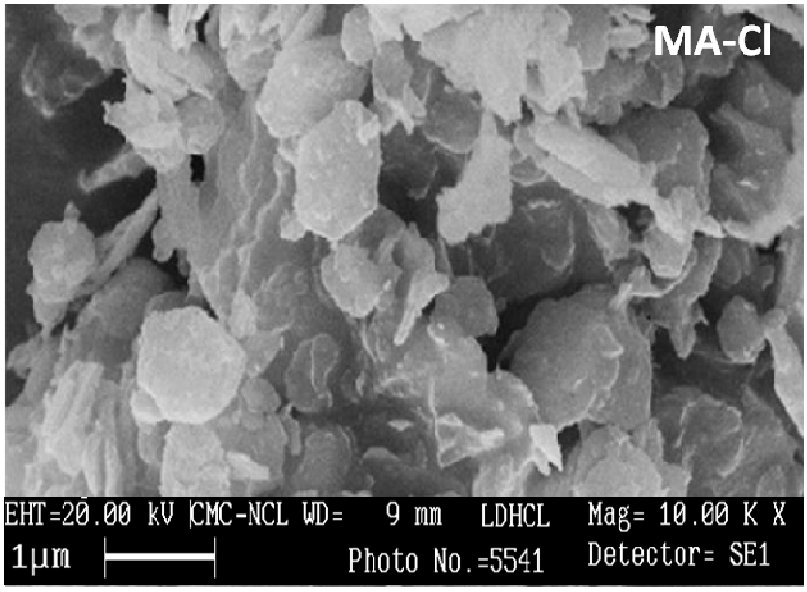

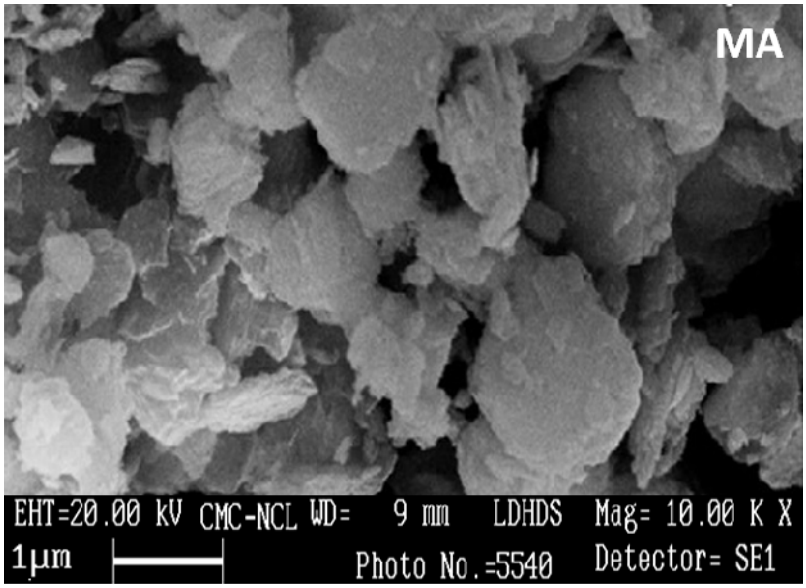

Figure 4.7: SEM micrographs of the unmodified and modified layered double hydroxides. (magnification bar 1µm)

4.3.3.4 Thermal Analysis

The thermal analysis of the modified LDH is primarily aimed to investigate the decomposition behavior of the organic fraction and also the metal hydroxide layers. This was carried out by identifying various decomposition stages and the corresponding temperature range in the TGA plots. The comparison of the TGA plots of the modified LDH with that of the unmodified one gives an indication of the interlayer surfactants anions influence on the decomposition of the host material. Thermal behavior of unmodified Mg-Al–LDH has been studied in details by several researchers. The most widely reported proposition suggests a two-stage decomposition process: a low temperature (up to about 225 °C) dehydration stage due to the loss of interlayer water and a high temperature decomposition (225 – 500 °C) stage due to the loss of interlayer anion and dehydroxylation of the metal hydroxide layer [12]. Often the high temperature decomposition occurs in two distinct steps depending upon the M^{2+}/Al^{3+} ratio [13, 14,15]. This tendency becomes more prominent as the M^{2+}/Al^{3+} ratio increases. At M^{2+}/Al^{3+} ratio equal to 2, these two steps are quite distinctly separated [16, 17] The first of these two peaks is attributed to the partial loss of OH^- from the brucite-like layer and the second one to the complete loss of OH^- and chloride ions [13]. However, it has also been observed that release of interlayer chloride starts as early as 250 °C and continues till 500°C [18].

The thermal decomposition and derivative analysis of the unmodified LDH and its modified forms is presented in **Figure 4.8**. It is observed that the decomposition of unmodified MA-Cl is divided into two steps. In the first one, at around 130-200°C, assigned for weight loss of 10.3% is due to the loss of physically adsorbed and interlayer water. In the second one, at around 333 - 430 °C, a weight loss of 31.2% can be ascribed to the dehydroxylation of the LDH layer and the elimination of interlayer Cl^- anion. The total weight loss for the region (50–700 °C) is observed about 40 %. For organomodified LDHs, the first decomposition for water occurs relatively early i.e around 90 °C. This may be because, after ion-exchange, LDH becomes more organophilic and the hydrogen bond interaction between water molecules decreases, resulting in a reduction of the decomposition temperature as it can be seen from thermogravimetry curves of MA, ZMA and ZA.

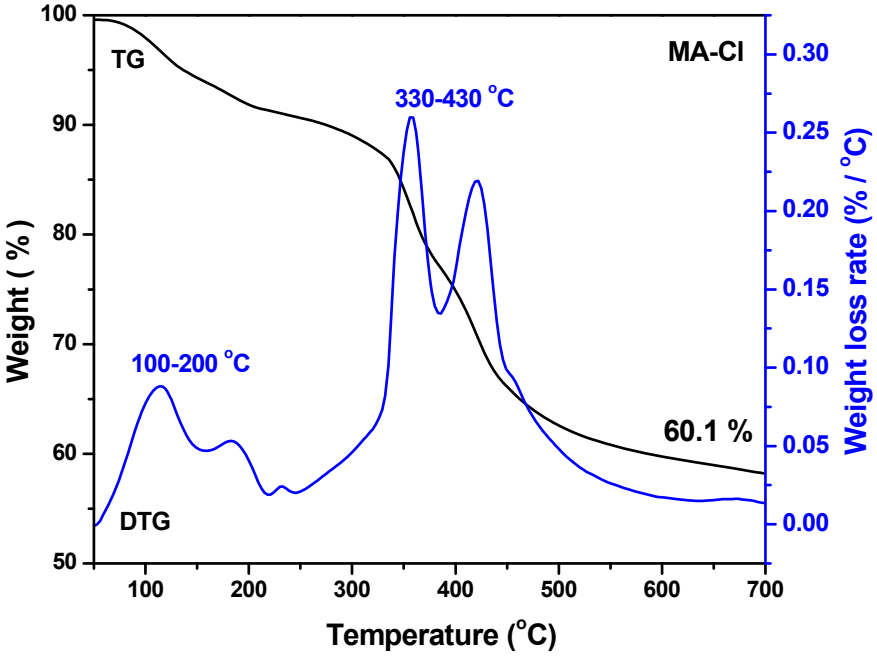
MA-Cl
TG
330-430 °C
100-200 °C
DTG
60.1 %
Weight (%)
Weight loss rate (% / °C)
Temperature (°C)

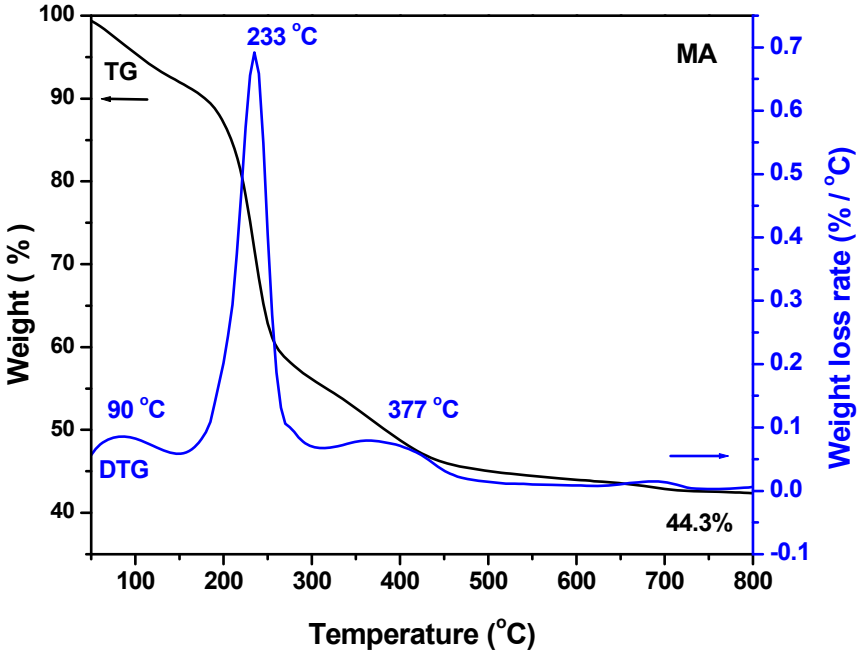
MA
TG
233 °C
90 °C
377 °C
DTG
44.3%
Weight (%)
Weight loss rate (% / °C)
Temperature (°C)

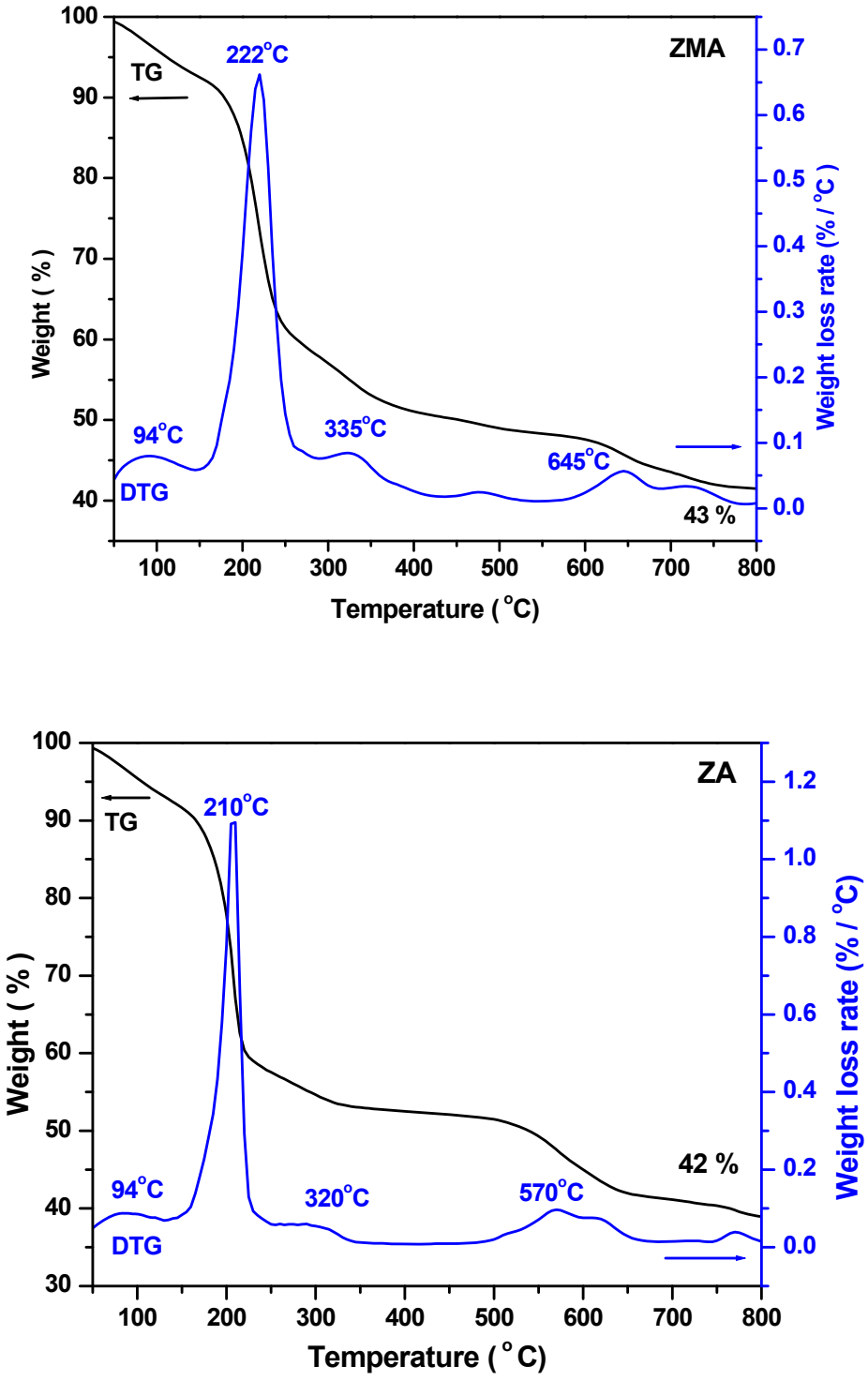

Figure 4.8: Thermogravimetry (TG) and Derivative Thermogravimetry (DTG) curves for LDH and its various modified forms showing major decomposition stages

In the second step, at around 210-230 °C, a weight loss of 35% is observed and can be ascribed to the degradation of DDS chain in the LDH layer. Around 10 °C incremental differences are seen for different LDHs that can be explained by the compositional difference and interactions of DDS chains with LDH layer. The third step, above 320 °C, is due to the dehydroxylation of LDH sheet, which is hindered by the second step. For ZMA, because of mixed metal composition the process of dehydroxylation may be retarded and as a result, the decomposition temperature increases. The total weight loss for the same region is around 55%, which is about 15% higher than that for unmodified LDHs. This remarkable difference is attributed to the differences in the molecular weight between the exchanged anions DDS (266 g mol^{-1}) and chloride (35.5 g mol^{-1}), and to the concentration in each sample.

Thus, overall thermal analysis gives detailed idea about degradation behavior of both unmodified and modified LDHs. Moreover, successful organomodification LDH is also evidenced, these results are in agreement with the FTIR and XRD measurements.

4.4 PP/LDH: Synthesis and Characterization

4.4.1 Nanocomposite Preparation

Nanocomposites of PP and LDHs were fabricated using PP-g-MAH as a compatibilizer by melt mixing techniques. A series of different set of nanocomposites were prepared in accordance with different property evaluation of PP/LDH nanocomposites and each method of preparation has been explained in detail in following sections:

4.4.1.1 PP/LDH Nanocomposites: Method 1

In this method PP/LDH nanocomposites were prepared in two steps using a co-rotating tightly inter-meshed twin-screw extruder (Haake Polylab Batch Mixer). All materials were dried at 80 °C under vacuum prior to mixing. All the samples were prepared by pre-mixing in a beaker polymers and filler in the right composition and then feeding the preheated hopper.

Step 1. Preparation of mastebatch:

DDS intercalated LDH (Mg_2Al-LDH) was mixed with PP-g-MAH in a weight proportion 1:2. The operation temperature was maintained at 160 °C for 5 min at 100 rpm rotor speed to prepare a master batch of filler in compatibilizer. All experiments were performed under inter atmosphere.

Step 2. Preparation of composites:

The designated amount of masterbatch was added to the molten PP and mixed at 180 °C for 5 min at 100 rpm rotor speed.

The PP/LDH nanocomposite in different compositions was prepared by above mentioned method was used for thermal, mechanical and rheological characterization (Chapter 5). **Table 4.5a** shows the different samples prepared and the designation of PP/LDH nanocomposite compositions.

Table 4.5a: Designation of PP/LDH nanocomposite compositions prepared by Method 1

Sample	PP (Wt %)	PP-g-MAH (Wt %)	LDH (Wt %)
PP	100	0	0
PPL1	97	2	1
PPL3	91	6	3
PPL5	85	10	5
PPL7	79	14	7
PPL10	70	20	10

4.4.1.2 PP/LDH Nanocomposites: Method 2

In this method PP/LDH nanocomposites containing 1, 3 and 5 % LDH nanoparticles were prepared by melt mixing in two steps using a co-rotating tightly intermeshed twin-screw extruder (DSM Micro-Compounder). All materials were dried at 80 °C under vacuum prior to mixing.

Step 1. Preparation of compatibilized PP:

Isotactic polypropylene was mixed with PP-g-MAH in a weight proportion in such way that final composite will have 5 Wt% of PP-g-MAH. The operation temperature was maintained at 180 °C for 5 min at 200 rpm rotor speed to prepare a master batch of compatibilizer in PP. All experiments were performed under inert atmosphere.

Step 2. Preparation of composites:

The designated amount of Mg_2Al-DDS LDH was added to the molten compatibilized PP and mixed at 180 °C for 5 min keeping other parameters as above.

The samples were abbreviated as PPL1, PPL3 and PPL5 as shown in **Table 4.5b.** These samples were used for investigation of crystallization behavior and kinetics study of PP/LDH nanocomposites (Chapter 6). In order to obtain better dispersion of LDH and avoid effect of varying content of PP-g-MAH on crystallization behavior the value of PP-g-MAH were kept constant to 5 Wt%.

Table 4.5b: Designation of PP/LDH nanocomposite prepared by Method 2

Sample	PP (Wt %)	PP-g-MAH (Wt %)	LDH (Wt %)
PP	95	5	0
PPL1	97	5	1
PPL3	91	5	3
PPL5	85	5	5

4.4.1.3 PP/LDH Nanocomposites: Method 3

In this method, masterbatch comprising MA-g-PP and LDH (MA, ZMA, ZA) in the ratio of 2:1 is prepared according to previous procedure as mentioned in **section 4.4.1.1**. For preparation of stabilized sample, the preweighed designated amount of stabilizer is well mixed (physically) with dry PP separately. In 2nd step the master batch and PP/stabilizer was melt blended in microcompounder under inert atmosphere at 180 ^{o}C for 5 min at 200 rpm screw speed. The series of samples prepared by this method and used for photo-oxidation and stabilization study (Chapter 7). In order to investigate the effect of different metal cations on photooxidation behavior PP/LDH nanocomposites and on efficiency of antioxidants, different LDHs are used and abbreviated as **A-** Mg_2Al, **B-** ZnMgAl and **C**- Zn_2Al LDH, **M-** OMMt. The sample abbreviation and compositions are listed in **Table 4.5c and 4.5d**, respectively.

Table 4.5c: Designation of PP/LDH nanocomposite compositions used for photo-oxidation and stabilization study (Chapter 7) and gas barriers and flammability study (Chapter 4).

Sample	% PP	%PP-g-MA	%LDH	% OMMt
PP	100	0	0	0
fPP	89.5	10.5	0	0
PPM5	85	10	0	5
PPLA5	85	10	5	0
PPLB5	85	10	5	0
PPLC5	85	10	5	0
PPM10	70	20	0	10
PPLA10	70	20	10	0
PPLB10	70	20	10	0
PPLC10	70	20	10	0

Table 4.5d: Designation of PP/LDH nanocomposite compositions used for stabilization study (Chapter 7)

Sample	Irganox 1010	Tinuvin 770
PPLA5a	**0.1**	0
PPLA5b	**0.6**	0
PPLA5c	**0.1**	**0.1**
PPLA5d	**0.6**	**0.6**
PPLB5a	**0.1**	0
PPLB5b	**0.6**	0
PPLB5c	**0.1**	**0.1**
PPLB5d	**0.6**	**0.6**
PPLC5a	**0.1**	0
PPLC5b	**0.6**	0
PPLC5c	**0.1**	**0.1**
PPLC5d	**0.6**	**0.6**
PPM5a	**0.1**	0
PPM5b	**0.1**	**0.1**
PPa	**0.1**	**0**
PPb	**0.1**	**0.1**
fPP1a	**0.1**	**0**
fPP1b	**0.1**	**0.1**

4.4.2 Nanocomposite Characterization

4.4.2.1 FT-IR Analysis

In present study, it is believed that the maleic anhydride groups can react with the interlayer anionic groups of LDH. Thus, the layered double hydroxides could chemically bind to the macromolecular polypropylene chains, resulting in the prevention of their agglomeration and the breakup of large stacking. Such interactions could improve the compatibility between the polymeric matrix and the nanoparticles, increasing the degree of dispersion of the particles, as shown in **Figure 4.9**. To verify the interactions that take place between the interlayer anions and the maleic anhydride groups of PP-g-MAH, FT-IR spectroscopy was used. **Figure 4.10** shows the typical FT-IR spectra and it is observed that the most characteristic peaks of PP-g-MAH, except those of PP, are the two peaks between 1700 and 1800 cm^{-1} corresponding to the anhydride groups. In the spectrum of PP/LDH nanocomposite, a strong absorbance at 1780 cm^{-1} has been intensively weakened and new band at 1715 cm^{-1} is observed, may be due to their reaction with the anhydride groups and this could be of evidence that such reactions take place. This shift is due to the result of the aforementioned interactions that facilitate polymer chains to intercalate into the lamellas.

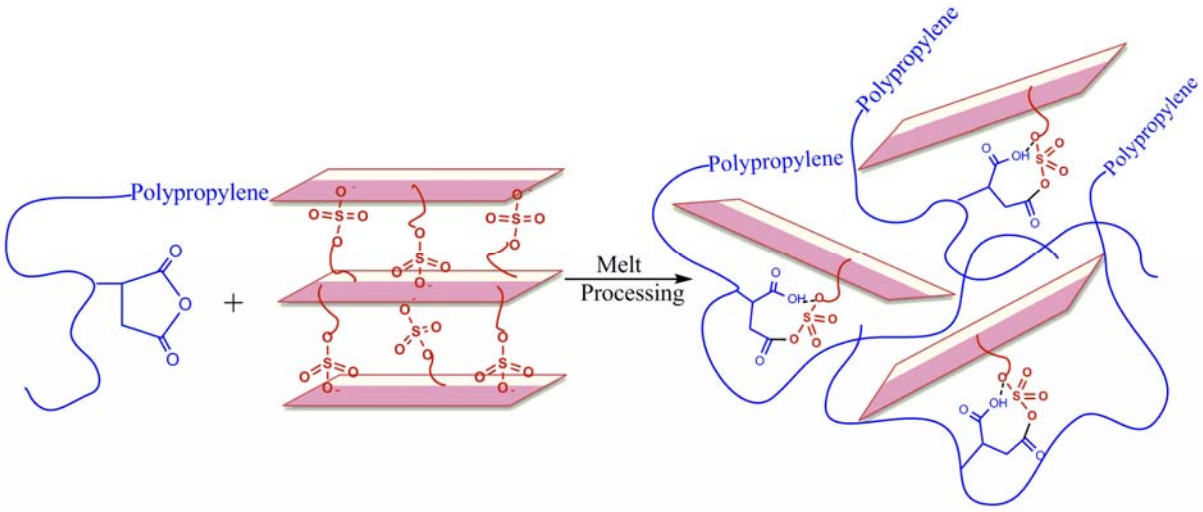

Figure 4.9: Conceptual diagram of PP-g-MAH/LDH interaction to form the intercalated /exfoliated networks

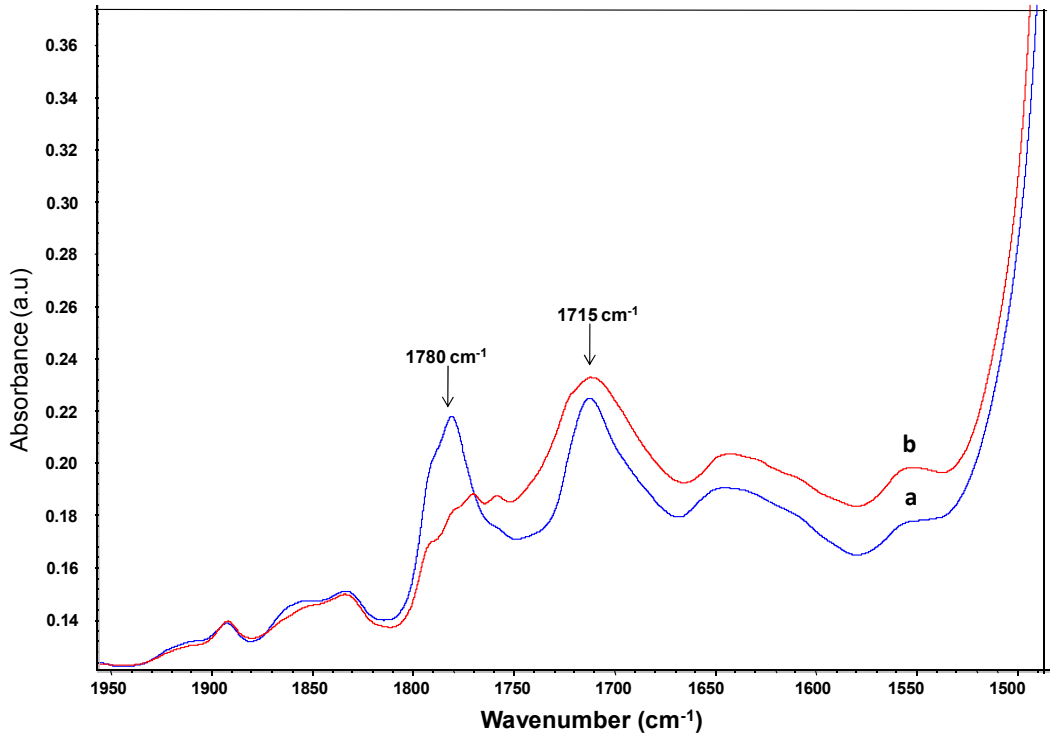

Figure 4.10: FTIR spectra of a) PP and b) PPL5 (Method-2)

4.4.2.2 X-ray Diffraction Analysis

In nanocomposites, the extent of intercalation of nanofillers having layered structure was analyzed by XRD technique. The complete disappearance of XRD peaks may reveal high degree of exfoliation or the presence of small diffracting volume as in the cases of low filler loading. Direct observation by TEM is then necessary to characterize an exfoliation state. **Figure 4.11** shows XRD analysis of PP and PP/LDH nanocomposites comprising varying content of LDH, a significant change in position of the basal peak is observed. The XRD patterns of these samples are characterized by the presence of the first order basal reflection (< 003 >).The characteristic crystalline basal position peak of Mg_2Al–DDS LDH at (< 003 >) has been completely disappeared in the case of PP/Mg_2Al–DDS LDH nanocomposites. However, for higher LDH loading peak become broad and shifted towards lower angle. Moreover, the higher order basal position peak at (< 006 >) has been shifted towards lower angle and their intensities are sharply reduced accompanied by peak broadening.

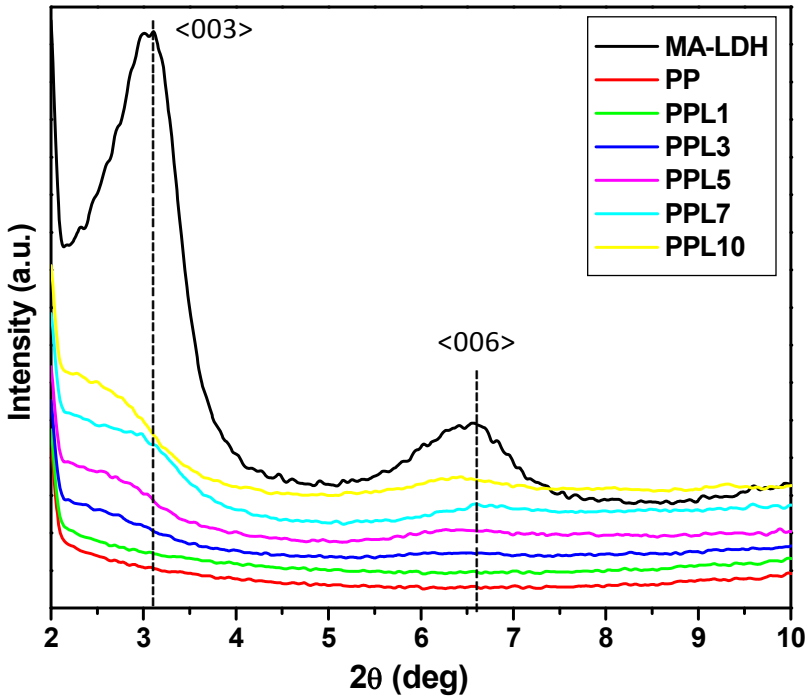

Figure 4.11: The X-ray diffraction patterns of MA-LDH, PP, PPL1, PPL3, PPL5, PPL7 and PPL10 in the range of 2θ = 2-10° (Method-1)

This may be due to intercalation of polymer chain segments into the interlayer region of LDH induced by the stronger shearing action during melt-mixing in the extruder. The overall XRD results suggested that the stacking layers of the Mg_2Al–DDS LDH in these samples were fully/partially separated and an exfoliated/intercalated PP/LDH nanostructure was formed. The XRD patterns of the nanocomposites with C20A and PP with PP-g-MAH as compatibilizer are shown in **Figure 4.12** As can be seen from this figure, the composites with 5 and 10% clay contents show an increase in intergallery spacing, as the d_{001} peak shifts to lower angles, showing that the intergallery distance was enlarged from 2.2 nm to around 3.5 nm. This clearly indicates that macromolecular links had intercalated into the interlayers of the modified clay. The higher order basal peak also shifted considerably towards lower angle indicating intercalated/exfoliated microstructure of PP/OMMt nanocomposites.

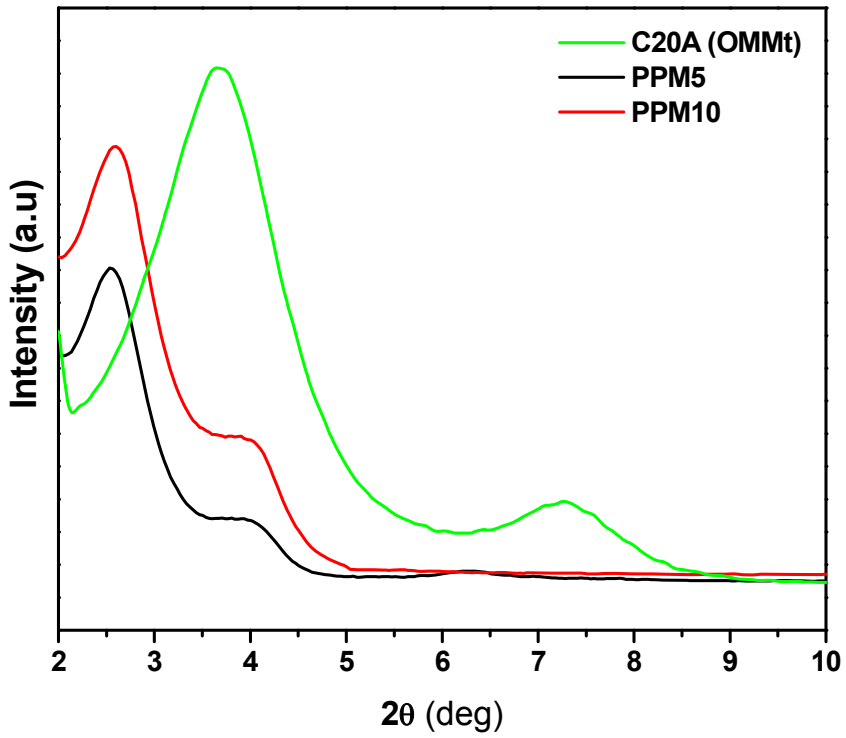

Figure 4.12: X ray diffraction patterns of nanocomposites of PP with C20A(OMMt)

4.4.2.3 Morphological Analysis

The complex morphological structures of polymer nanocomposites can be analyzed using TEM technique by thoroughly investigating the level of clay dispersion and the compatibilizing effect of PP-g-MAH, which can greatly affect the properties of nanocomposites.

In present study, the microstructure of the PP/LDH nanocomposites was investigated by TEM micrographs and is elaborately shown in **Figure 4.13 and 4.14**. The **Figure 4.13** shows the fine dispersion of 5 wt% Mg_2Al-DDS LDH in PPL5, comprising the LDH: PP-g-MAH ratio equal to 1:1 in lower and higher magnification. The micrographs show that LDH nano-layers are well dispersed and intercalated throughout the PP matrix. Dark lines in the micrograph represent the existence of single LDH layers. However, certain highly swelled tactoids are also observed. From the TEM observations at high magnification, it is clear that the delamination took place resulting in the presence of single double hydroxide layers as well as tactoids with reduced thickness.

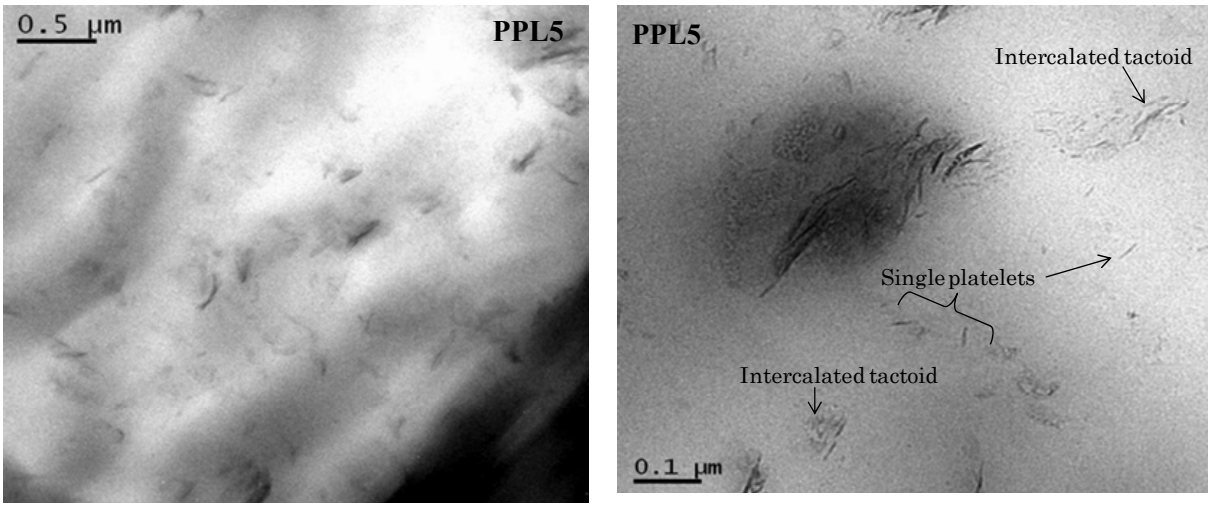

Figure 4.13: TEM micrograph of PPL5 in low and high magnification showing that LDH particles also undergo intercalation into tactoids and exfoliation into single layers (Method-2)

In **Figure 4.14**, the TEM micrographs of PP/LDH nanocomposites with ratio of LDH: MAH-g-PP (1:2) comprising various LDH contents between 3 wt% and 10wt% are demonstrated at high magnification. Evidently, PPL3 and PPL5 show homogeneous dispersions of LDH platelets and delamination of individual LDH platelets takes place. The observed single platelets reveal the lateral dimension of about 100-200 nm, which leads to the localized exfoliation in PPL3 and PPL5. However, PPL5 and PPL7, both of which still contain the some intercalated nanocomposite structures in the PP matrix. Furthermore, LDH agglomeration with intercalated tactoids has been detected in PPL10 nanocomposite. Those tactoids are surrounded with well dispersed LDH platelets, resulting in an "*island-like*" morphological structure. PPL7 and PPL10 show quite prevalent intercalated structures. Moreover, the micrograph of PPL7 visually demonstrates much larger interlayer galleries in the intercalated clay platelets compared to those in PPL10. Such stacked LDH tactoids representative of intercalated morphology, random clay platelets representative of exfoliated morphology and large dark structures occurring amongst some of the clay tactoids are visible.

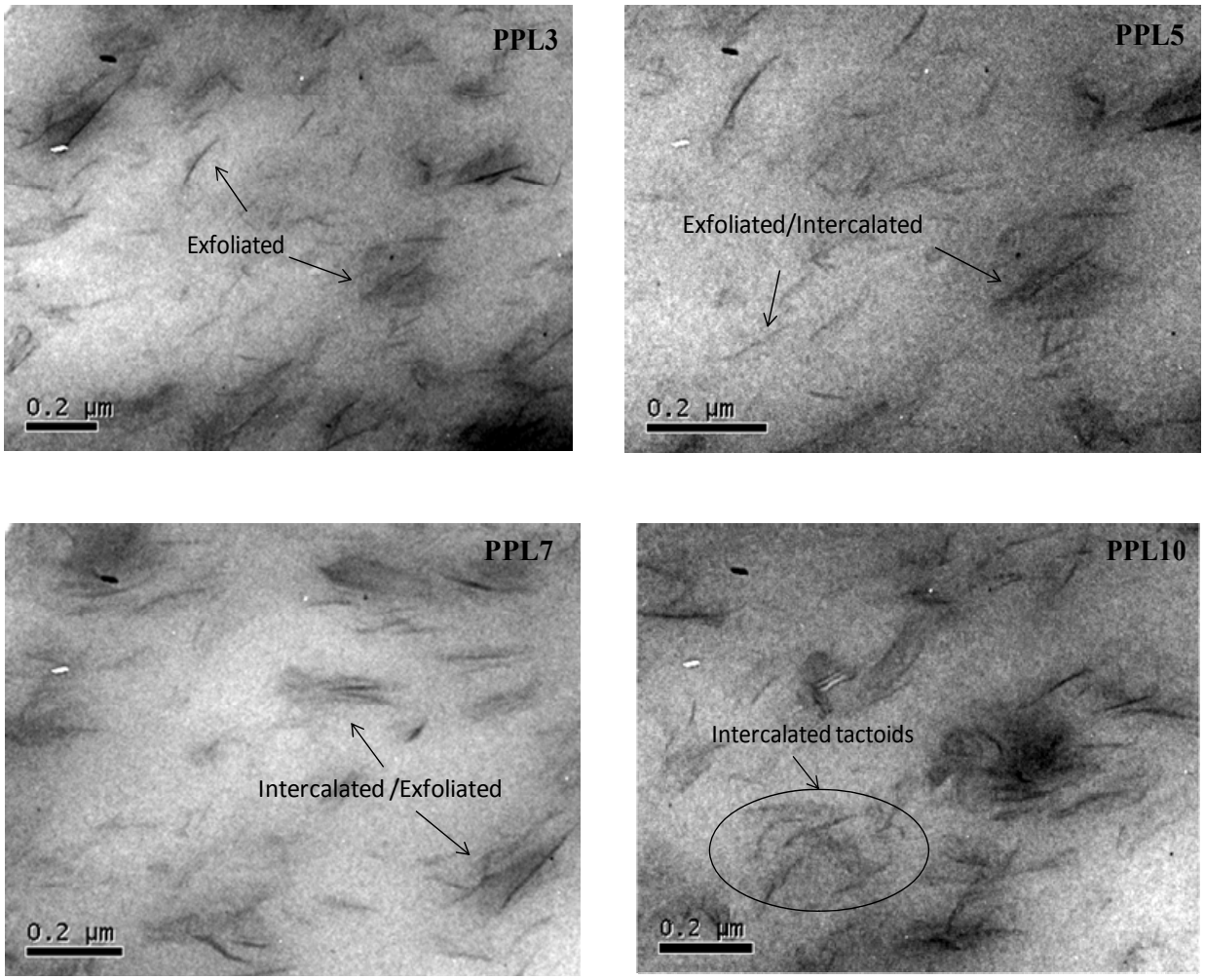

Figure 4.14: TEM images of PP/LDH nanocomposite (Method-1)

Overall finding is that the mixed morphologies of intercalated and exfoliated structures are in close proximity of each other. The closeness of these structures suggests that the polymer matrix is becoming increasingly reinforced. This phenomenon explains the increasing modulus and strength properties of LDH reinforced PP nanocomposites.

Therefore, TEM analysis provides complementary results for XRD analyses to validate the remarkable exfoliated/ intercalated structure in such nanocomposites.

4.5 Conclusions

In the present study, a series of hydrotalcite-type material i.e Mg_2Al, Zn_2Al and ZnMgAl–Cl are successfully prepared by co-precipitation method. To make the unmodified LDHs clay a suitable precursor for the preparation of polymer nanocomposite, modification by anionic surfactants is necessary. In this context, sodium dodecyl sulfate was used as an organic modified to modify LDHs in order to enlarge the interlayer distance and to render it more organophilic. The surfactant was selected based on their functionality, chain length, etc. The direct ion exchange method was employed for organic modification of LDH because of its higher efficiency and simple procedure. The characterization of the organically modified LDHs was carried out extensively using various analytical techniques, like XRD, FTIR, TGA and SEM. The XRD analysis of the modified clay indicated that the all synthesized LDHs have typical, well-order layered structures with a high degree of crystallinity. X-ray diffraction patterns reveal that the surfactant anions are arranged as monolayer within the interlayer region of LDHs and enlarge the interlayer distance according to the length of their hydrocarbon chain. It was observed that interlayer spacing is enlarged from 0.76 nm to 2.96 nm after organo-modification which is well enough to intercalate the macromolecular chains into the galleries. Thus, the enlarged *d*-spacing of DDS-LDH indicates the successful intercalation of DDS chains to the layers of LDH, thus making LDH organophilic and facilitating the intercalation and dispersion of organic materials. The FTIR spectra of LDH materials provide many important information, especially about the interlayer anions and successful organo-modification. The FT-IR assignments reveal that the dodecyl sulfate anion is successfully intercalated into the gallery of the LDH. It also gives the evidence for existence of some water molecules in the interlayer region in the modified LDH, which are usually arranged as monolayer in between surfactant and metal hydroxide sheet. The morphological analysis of both modified and unmodified LDHs showed that these materials posses a plate-like particle morphology having distinct hexagonal shapes and sharp edges. However, it is observed that the particle morphology are somewhat modified after organic modification and irregular shapes and edges persist in modified LDHs. The thermal analysis of unmodified and modified LDHs depict that the decomposition of unmodified MA-Cl is divided into two steps. The total weight loss

for the region (50–700 °C) is observed about 40 %. For organomodified LDHs, decomposition occurs in three steps and it is influenced by interlayer organic modifier and nature of metal cation composition. The total weight loss for MA, ZMA and ZA is observed is to be 56%, 57% and 58%, respectively, which is about 15% higher than that for unmodified LDHs. These results are in agreement with the FTIR and XRD measurements.

In second section, we have successfully prepared polypropylene/organomodified layered double hydroxide (LDH) hybrid nanocomposites by direct melt intercalation using PP-g-MAH as a compatibilizing agent and the conventional twin screw extrusion compounding process. A series of samples comprising varying content of LDHs and compatibilizer have been prepared in accordance with the aim of the study. The samples have been prepared for different property evaluation, crystallization studies and photo-oxidation behavior in PP/LDH nanocomposites. Moreover, nanocomposites based on PP/OMMt type conventional nanocomposites have also been prepared for comparison. The addition of PP-g-MAH as a compatibilizer results in a higher adhesion between the PP matrix and LDH nanolayers, due to the interactions that take place between the reactive groups. The FT-IR spectrum verifies the interactions that take place between the interlayer anions and the maleic anhydride groups of PP-g-MAH. The XRD analysis reveals, complete disappearance of first order peaks, for higher LDH loading peak become broad and shifted towards lower angle. Moreover, the higher order basal position peak has been shifted towards lower angle with intensities. These results conclude that the LDH layers were found to be dispersed at the nanometer level and the stacking layers of the LDH in these samples were fully/partially separated and an exfoliated/intercalated PP/LDH nanostructure was formed. TEM examinations provided direct evidence for the formation of intercalated and exfoliated nanocomposites. The TEM observations at high magnification showed that the delamination took place resulting in the presence of single double hydroxide layers as well as tactoids with reduced thickness.

References

1) F. Leroux. Organo-modified anionic clays into polymer compared to smectite-type nanofiller: Potential applications of the nanocomposites. *Journal of Nanoscience and Nanotechnology*, **6** (2006), p.303-315.
2) M. Meyn, K. Beneke, G. Lagaly. Anion-exchange reactions of layered double hydroxides. *Inorganic chemistry,* **29** (1990), p.5201-5207.
3) A. B. Morgan and J.W. Gilman. Characterization of polymer-layered silicate (clay) nanocomposites by transmission electron microscopy and x-ray diffraction: A comparative study. *Journal of Applied Polymer Science*, **87** (2003), p.1329 – 1338.
4) R. A. Vaia and W. Liu. X-ray powder diffraction of polymer/layered silicate nanocomposites: Model and practice. *Journal of Polymer Science, Part B: Polymer Physics*, **40** (2002), p.1590-1600.
5) K. Wang, S. Liang, R. Du, Q. Zhang, and Q. Fu. The interplay of thermodynamics and shear on the dispersion of polymer nanocomposite. Polymer, 45:7953 – 7960, 2004.
6) a) S Miyata, Physico-chemical properties of synthetic hydrotalcites in relation to composition *Clays and Clay Minerals,* **28** (1980), p.50-56. b) A-L Troutier-Thuilliez , C Taviot-Guéhoa, J. Cellier, H. Hintze-Bruening, F. Leroux, Layered particle-based polymer composites for coatings: Part I. Evaluation of layered double hydroxides, *Progress in Organic Coating,* **64** (2009), p.182–192.
7) U. Costantino, F. Marmottini, M. Nocchetti, and R. Vivani. New synthetic routes to hydrotalcitelike compounds- characterization and properties of the obtained materials. *Europian Journal of Inorganic Chemistry*, **15** (1998), p.1434 – 1446.
8) F. Cavani, F. Trifiro, and A. Vaccari. Hydrotalcite-type anionic clays: Preparation, properties and applications. *Catalysis Today*, **11** (1991), p.173 – 301.
9) F. Leroux, M. Adachi-Pagano, M. Intissar. Delamination and restacking of layered double hydroxides *Journal of Materials Chemistry,* **11** (2001), p.105-112.
10) R. Trujillano, M.J. Holgado, V.Rives. Alternative synthetic routes for NiAl layered double hydroxides with alkyl and alkylbenzene sulfonates *Studies in Surface Science and Catalysis,* **142** (2002), p. 1387-1394.
11) M.A. Drezon Synthesis of isopolymetalate-pillared hydrotalcite via organic-anion-pillared precursors. Inorganic Chemistry, 27**,** (1988), p.4628-4632.

12) E. Kanezaki. Effect of atomic ratio mg/al in layers of mg and al layered double hydroxide on thermal stability of hydrotalcite-like layered structure by means of in situ high temeperature powder x-ray diffraction. *Materials Research Bulletin*, **33** (1998), p.773 – 778.

13) F. Cavani, F. Trifiro, and A. Vaccari. Hydrotalcite-type anionic clays: Preparation, properties and applications. *Catalysis Today*, **11** (1991), p.173 – 301.

14) S. Miyata. Physico-chemical properties of synthetic hydrotalcites in relation to composition. *Clays and Clay Minerals*, **28** (1980), p.50-56.

15) E. Kanezaki. Effect of atomic ratio mg/al in layers of mg and al layered double hydroxide on thermal stability of hydrotalcite-like layered structure by means of in situ high temeperature powder x-ray diffraction. *Materials Research Bulletin*, **33** (1998), p.773 – 778.

16) S. Carlino. The intercalation of carboxylic acids into layered double hydroxides: A critical review of the different methods. Solid State Ionics, **98** (1997), p.73 – 84.

17) M. Meyn, K. Beneke, and G. Legaly. Anionic-exchange reactions of hydroxy double salts. *Inorganic Chemistry*, **32** (1993), p.1209 – 1215.

18) P. Bera, M. Rajamathi, M. S. Hegde, and P. V. Kamath. Thermal behavior of hydroxides, hydroxysalts and hydrotalcites. *Bulletin of Material Science*, **23** (2000), p.141 – 145.

Chapter 5

THERMAL, MECHANICAL AND RHEOLOGICAL CHARACTERIZATION

"Most of the fundamental ideas of science are essentially simple, and may, as a rule, be expressed in a language comprehensible to everyone"

~ Albert Einstein

Sunil P. Lonkar, S. Morlat-Therias, F. Leroux, J-L. Gardette, R.P. Singh, "*PP/LDH Nanocomposites: Thermal, Mechanical and Rheological Characterization" communicated to* ***Composites Science and Technologies***

5.1 Introduction

Nanocomposites consisting of a polymer and clay (modified or not) frequently exhibit remarkably improved mechanical and physical properties when compared to those of pristine polymers. Improvement includes thermal properties, higher modulus, increased strength and heat resistance, decreased gas permeability and flammability etc. Hence, it is very important to investigate these properties for new nanofiller in order to assess their feasibility in fabrication polymer nanocomposites with improved properties. The present chapter deals with the assessment of LDH type new nano-filler in property improvement of polypropylene such as thermal properties, mechanical properties, rheological behavior, gas barrier and flammability properties of these hybrid materials were investigated in detail. The thermal stability is one of the fundamental properties that can determine processing and application, especially when PP is used as general material. The thermal stability of PP can be changed by the presence of nanoclay in the polymer matrix [1-2]. Also, the chemical nature of the clay and the organic modifier may play an important role in the degradation pathway of the nanocomposite. The purpose of this work was to evaluate the thermal stability of PP/LDH nanocomposites based on Mg–Al layered double hydroxide. The effect of intercalation and exfoliation of the LDH on thermal stability will also be analyzed. Mechanical properties like tensile/flexural modulus, yield stress and toughness are measures that characterize the potential for improved end-use performance of a polymer

nanocomposite relative to the neat polymer or a traditional composite [3-4]. Well dispersed LDH can affect the mechanical properties of a semicrystalline polypropylene. The high modulus LDH inclusions of anisotropic shape can reinforce the PP. Thus in this view, the anisotropic shape of the LDH clay is important for mechanical property enhancement. Dynamic mechanical testing provides a method for determining the storage modulus (E') and loss modulus (E'') as a function of temperature. The analysis of the storage modulus, loss modulus and *tan* δ curves are very useful in ascertaining the performance of the sample under stress and temperature. DMTA not only measures the dynamic mechanical properties of a material, but also detects changes in the solid structure of a polymer after compounding with other materials. In addition, DMTA provides information on the compatibility [5-6], crystallinity and stiffness of the polymer [7] and it is useful as a relative comparison of the behavior blends. Rheological analysis of polymeric melts involves the study of the mechanical response of the melt under the action of external mechanical stress or strain. In case of filled polymeric systems, rheological behavior can be drastically different from that of the unfilled melts depending on the nature of filler particles (structure, size, shape, surface characteristics, etc) and the state of their dispersion in the polymer matrix [8-9]. In fact, rheological analysis is an important tool to investigate the state of filler particle dispersion in filled systems and their response under external force. Though an indirect method, rheological analysis can be treated as a complementary to the direct methods for morphological analysis, like XRD and electron microscopy, which altogether provide a complete picture of the state of filler particle dispersion in polymer matrix. Also, one of the important aspects of the present investigation is to study the efficiency of LDH nanofiller as a potential flame retardant for polypropylene. In this regards, the evaluation of the composite materials in terms of limited oxygen index (LOI) provides the first hand information on the effectiveness of fire retardant additives or so called flame-retardants [10]. Polypropylene finds extensive application in food and packaging because of its high distortion temperature and crystallinity. It offers a strong barrier to humidity but suffers from high oxygen permeability. Therefore, laminates of PP and other oxygen permeation resistant polymers are often employed in packaging applications. The commercial importance of PP has led to intense efforts in developing PP-layered silicate nanocomposites in order to

enhance its properties. The high aspect ratio of the LDH layers is expected to improve the oxygen-barrier properties by hindering the penetration of the gas molecules and increasing their average path length. The present study also focuses on the detailed investigation of oxygen barrier properties of PP/LDH nanocomposites.

Hence, the overall objective of present study is to investigate the effect of LDH nano clay and interlayer metal cations in PP matrix on thermal properties, mechanical properties, such as stiffness, strength, impact resistance, rheological behavior, flammability and oxygen permeability.

5.2 Thermal Analysis

Thermal analysis is essentially the study one of more properties of a material as a function of temperature. Thermal analyzer is the apparatus that allows automatic monitoring of the property with change in temperature. Three types of thermal analysis were used to analyze the thermal properties of PP/LDH nanocomposite that is thermogravimetrc analysis (TGA), dynamic mechanical thermal analysis (DMTA) and differential scanning calorimetry (DSC).

5.2.1 Thermogravimetric Analysis (TGA)

Thermogravimetric (TGA) analysis of the PP/LDH nanocomposites with different LDH content is shown in **Figure 5.1.** It can be seen that during the thermal degradation, the TGA curves displayed a single step degradation process for all samples produced. The thermal decomposition of pure polypropylene is characterized by major temperature region of weight loss in the temperature range 300 - 440 $^{\circ}$C. In the differential thermogravimetric (DTG) plot, **(Figure 5.2)**, this region appears as a sharp decomposition peak at about 406 $^{\circ}$C. It is observed that the presence of LDH causes distinct changes in the thermal decomposition behavior in comparison to the unfilled PP. With the addition of only 3 wt% LDH, the first decomposition stage in unfilled PP, is shifted to a higher temperature range (the decomposition peak in DTG shifts from about 406 $^{\circ}$C to about 440 $^{\circ}$C). With further increase in LDH concentration, the decomposition temperature is gradually increases up to 473 $^{\circ}$C for 10 wt% LDH.

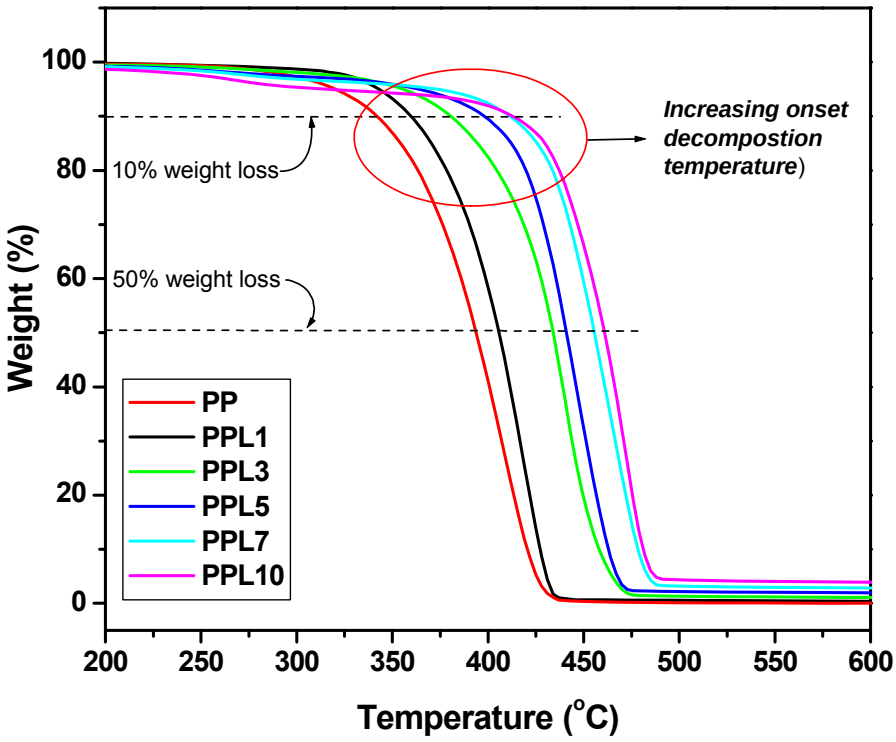

Figure 5.1: Thermogravimetric analysis of PP/LDH nanocomposites containing different LDH content

Usually, the comparison of thermal stability for polymeric materials from TGA plots is carried out in terms of two temperatures: one is the onset of decomposition temperature ($T_{0.10}$) referring to 10% weight loss and the other is the decomposition temperature ($T_{0.50}$) referring to 50% weight loss. **Figure 5.3** and **Table 5.1,** shows the comparison of these two temperatures for unfilled polypropylene and LDH filled nanocomposites. The incorporation of the LDH which is in a platelet form, resulted in significant improvement in the initial thermal stability of PP. The onset of decomposition is delayed significantly by the addition of 3 wt% LDH. In fact, with increasing LDH concentration, the onset decomposition temperature $T_{0.1}$ increases considerably but then stabilizes for 7 and 10 wt% LDH concentrations. The decomposition temperature, $T_{0.5}$ also drastically increases with increasing LDH concentration. With about 5 wt% LDH concentration, $T_{0.5}$ increases by about 50 °C as shown in **Figure 5.3**.

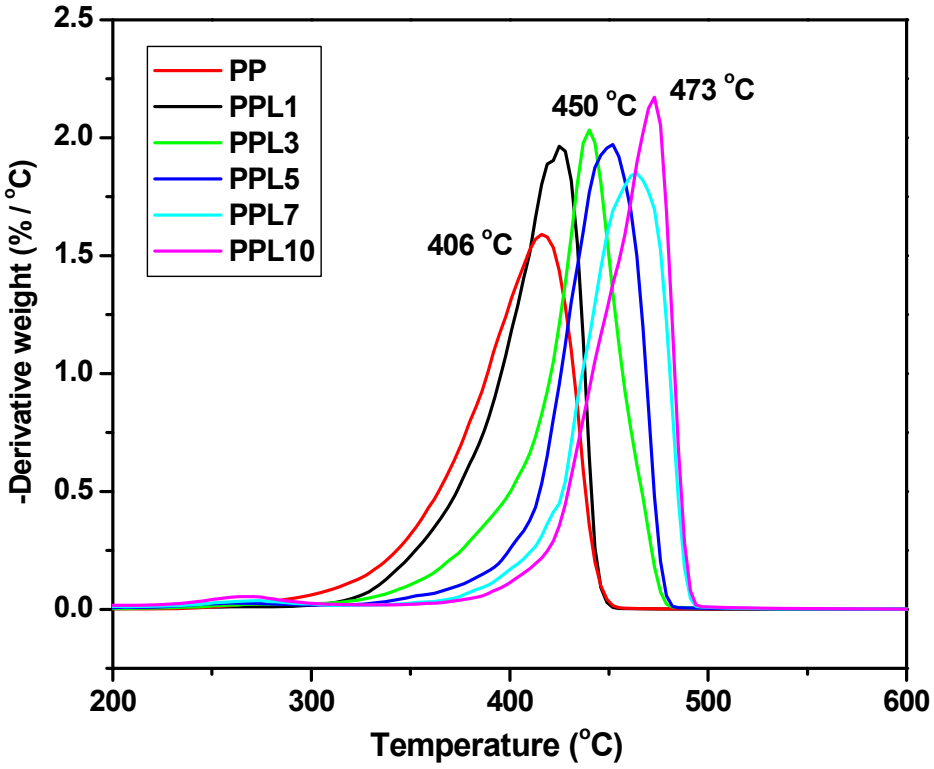

Figure 5.2: Derivative thermogravimetric analysis of PP/LDH nanocomposites containing different LDH content

Further additions of LDH up to 10 wt% led to a further improvement in the thermal stability of PP where the $T_{0.1}$ reached 415 ºC, which is about 25 % increment. Similarly, for $T_{0.5}$ such increment is up to 20%. The variation of $T_{0.1}$ and $T_{0.5}$ with LDH content is summarized in **Table 5.1**. Also, the sample weight percentage decreases continuously to a residual level after mass loss has commenced and given in **Table 5.1.** When the amount of the residues obtained under nitrogen and oxygen atmosphere during TGA experiments are compared, comparable numbers are obtained in case of filled system (**Table 5.1**).

Table 5.1: TGA data for PP containing different LDH content

Sample	$T_{0.1}$ (°C)	$T_{0.5}$ (°C)	Char Residue (%) in N_2	Char Residue (%) in air
PP	341	395	0	0
PPL1	359	405	0.46	0.43
PPL3	380	434	1.18	1.14
PPL5	398	443	2.22	2.25
PPL7	410	457	3.13	3.08
PPL10	413	463	4.35	4.33

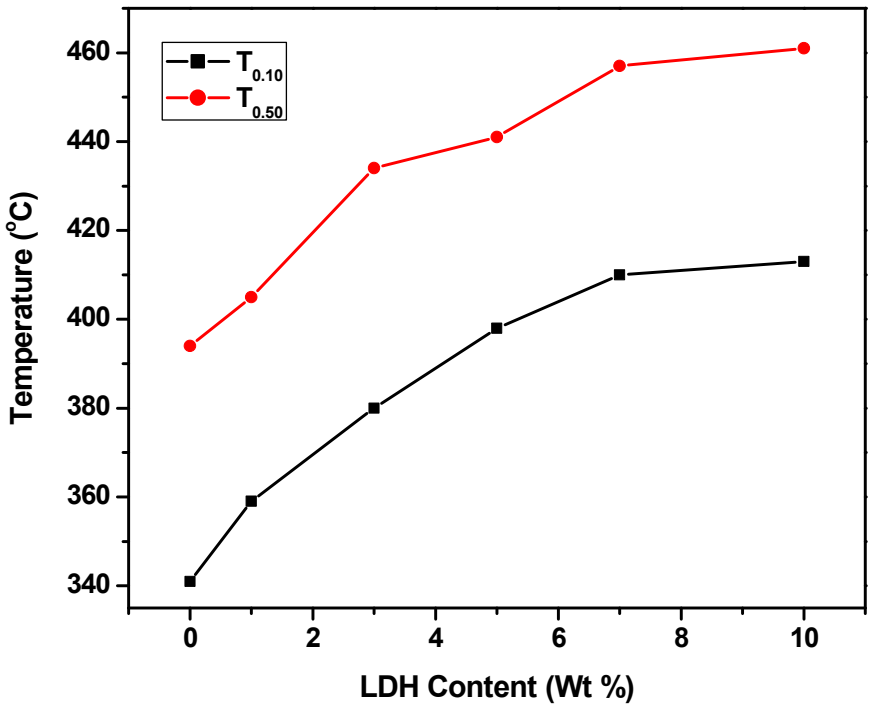

Figure 5.3: The influence of LDH concentration on (A) the decomposition temperatures at 10% weight loss ($T_{0.1}$) and 50% weight loss ($T_{0.5}$)

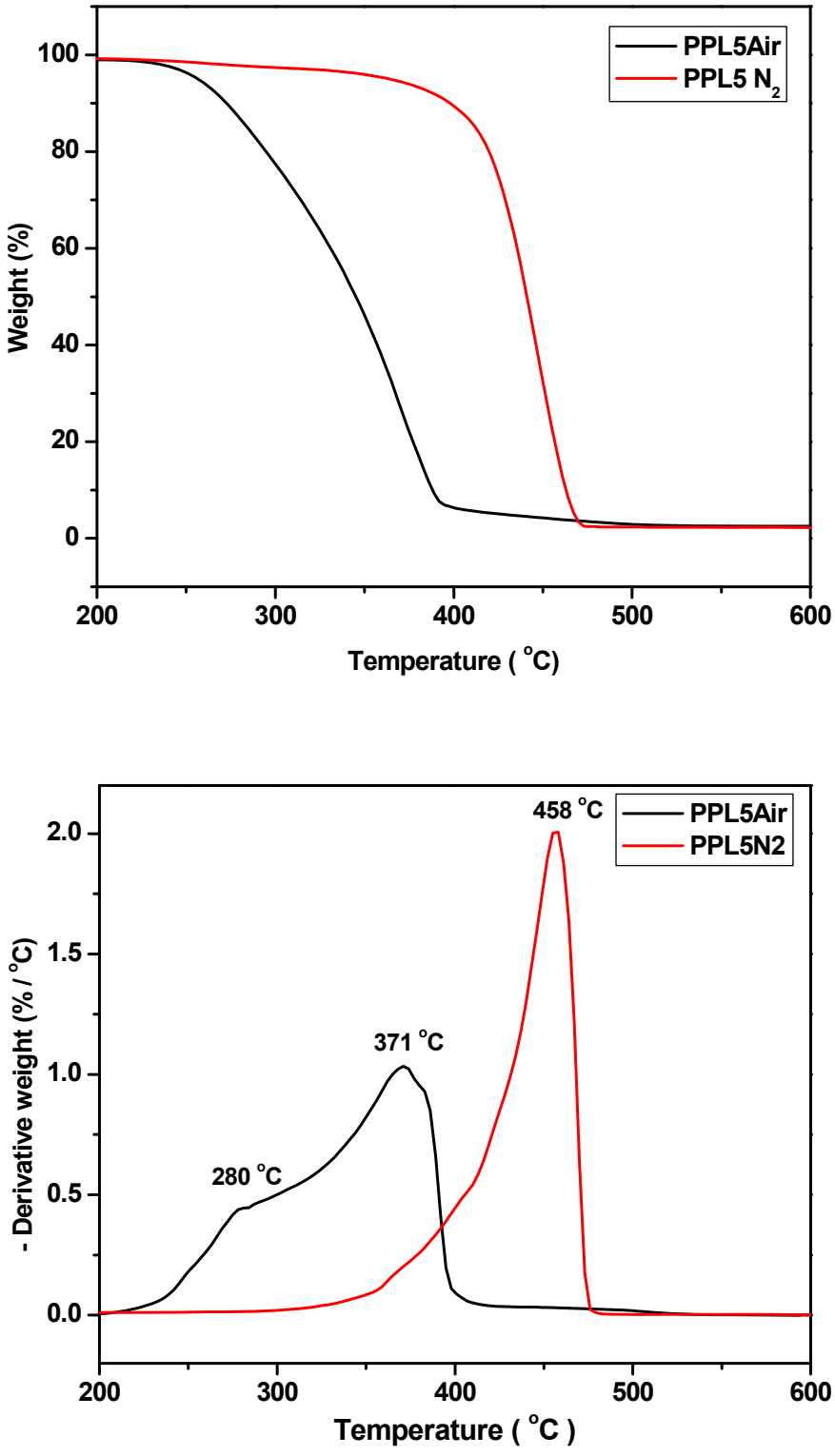

Figure 5.4 : Comparison of the Thermogravimetric analysis of PP/LDH nanocomposite under air and nitrogen atmosphere

The comparison of the DTG plots of nanocomposite composition PPL5 is shown in **Figure 5.4**. It is observed that under air atmosphere sample decomposition occurs at around 371°C along with a small hump around 280 °C, whereas under nitrogen atmosphere, a single-step decomposition occurs at 458 °C with the low temperature peak being completely suppressed. These findings reveal that the PP/LDH nanocomposites undergo diverse decomposition behavior under air and oxygen, respectively. It is obvious that the high amount of residue obtained under non oxidative atmosphere indicates the formation of carbonaceous char. Where perhaps the organic species (surfactant anion, polymer chain segments, etc) present within the interlayer region have delayed and therefore, less access of oxygen due to their encased position within metal hydroxide layer and the surrounding bulk polymeric matrix. Additionally, the endothermic decomposition of the metal hydroxide layers imparts a cooling effect, which may further affect the combustion process of these constraint organic species. As a result, incomplete combustion is more likely resulting in the formation of carbonaceous char even when combustion is carried out under oxygen atmosphere. In fact, such carbonaceous char formation within clay layers has earlier been proposed in case of combustion of polymer/layered silicate nanocomposites [11-12]. The basic difference between layered silicate and LDH during combustion is that the later undergoes endothermic decomposition liberating water and metal oxide, which makes reinforcement of the char less probable with LDH.

Overall results show that the LDH filled PP posses higher thermal stability compared with neat PP. The improvement in the thermal stability for PP/LDH nanocomposites is due to the formation of char which hinders the out-diffusion of the volatile decomposition products, as a direct result of the decrease in permeability of oxygen. The decrease in permeability is usually observed in intercalated or exfoliated platelets clay in the PP/LDH nanocomposites.

5.2.2 Dynamic Mechanical Thermal Analysis (DMTA)

Dynamic mechanical testing provides a method for determining the storage modulus (E') and loss modulus (E'') as a function of temperature. The analysis of the storage modulus, loss modulus and tan δ curves are very useful in ascertaining the performance of the sample under stress and temperature. The reinforcement effect due to the addition of LDH and the glass transition temperature (T_g) are of great interest in this study.

The dynamic storage modulus E' and loss tangent $tan\ \delta$ at various temperatures for the PP/LDH based nanocomposite is shown in **Figure 5.5**.

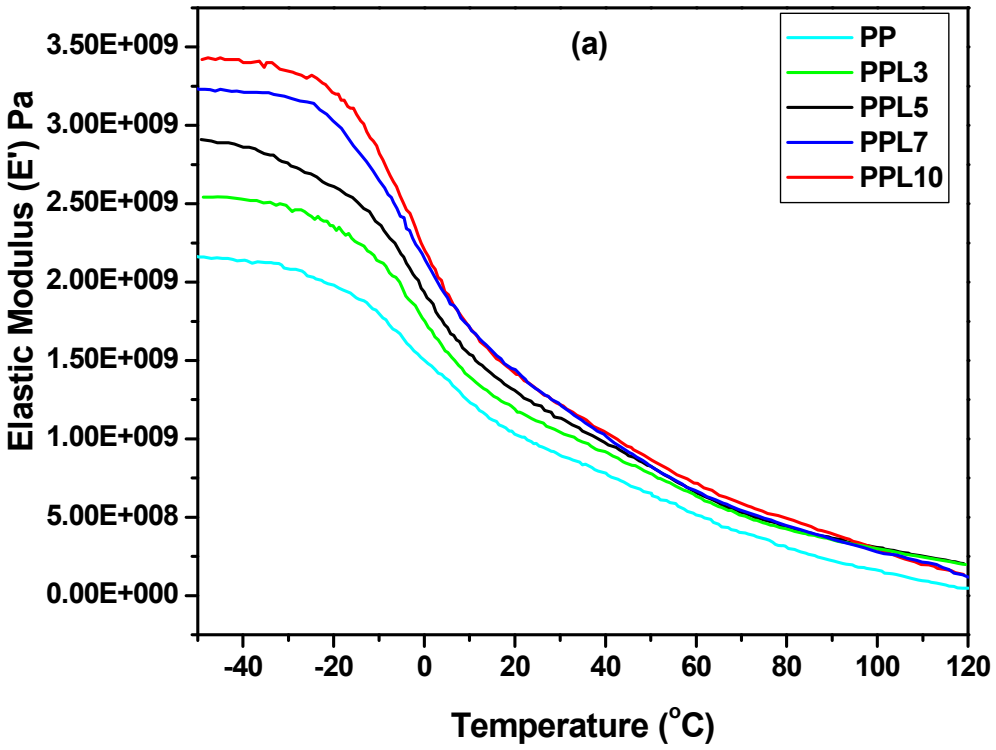

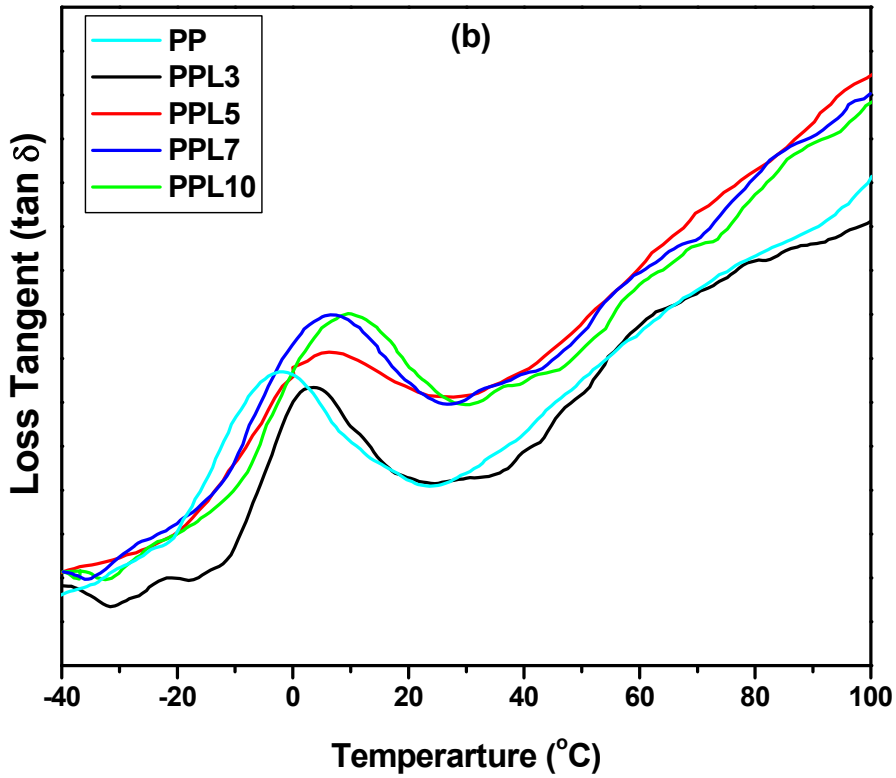

Figure 5.5: DMTA curves for PP/LDH nanocomposites (A) Dynamic elastic modulus (*E′*) and (B) loss tangent (*tan δ*)

The representative values of *E′* at five specific temperatures from -30°C to 75°C and T_g values are listed in **Table 5.2**.

It is noted that the incorporation of LDH into the PP matrix results in a remarkable increased in elastic modulus over the entire investigated temperature range especially at temperature below T_g (~0°C). It can be seen that the elastic modulus continues to be increased at clay content up to 5 wt% with the maximum improvements of 32% at 25°C for PPL3 and PPL5. Then, the modulus enhancement becomes dawdling when high LDH contents (7-10 wt %) are considered. In particular, such small enhancements of relative moduli observed at 25°C with increasing the LDH content, which is in good agreement with the corresponding mechanical properties, determined at the room temperature in **Section 5.3.** Moreover, a sharp drop in E' from ~ -20 °C and ~10 °C is observed which can be associated with the relaxation of the amorphous phase (α-

relaxation). Hence, an enormous reinforcement effect with the better magnitude of E' has been observed for PP/LDH based nanocomposites.

Table 5.2: Dynamic elastic moduli E' of PP/LDH nanocomposites at various temperatures and related glass transition temperatures (T_g)

Sample	Dynamic Elastic Modulus (E') (10^9 Pa=GPa)					T_g (°C)
	-30 °C	5°C	25 °C	50 °C	75 °C	
PP	2.09	1.38	0.95	0.65	0.36	-2.30
PPL3	2.45	1.51	1.08	0.73	0.44	3.82
PPL5	2.77	1.71	1.22	0.82	0.48	6.28
PPL7	3.18	1.91	1.31	0.81	0.49	7.14
PPL10	3.35	1.93	1.32	0.86	0.52	10.11

This indicates that the plastic and elastic responses of PP towards deformation are strongly influenced by the presence of LDH nano layers. The incorporation of LDH into the PP matrix remarkably enhances its stiffness and has good reinforcing effects. It is believed that the LDH became intercalated and a polymer layer formed around the layers. Here the chain mobility of the polymer molecules were reduced as the reinforcing effect of the organoclay platelets dominates. LDH layers affect the mobilization of PP macromolecular chains and share the stress transferred among the PP matrix. Restricted segmental motion at organic/inorganic interface and exfoliation of the clay galleries at the nanoscale level may be the possible cause for a phenomenal increase in the elastic modulus.

Figure 5.5B shows that the *tan* δ curves of neat PP and PP/LDH nanocomposites follow a similar pattern. The relevant representative T_g values are also listed in **Table 5.2**. Most nanocomposites demonstrate much higher T_g in contrast to PP (T_g = -2.30°C), and a further increase of T_g is shown by increasing the LDH content from 5 wt% to 10 wt%, reaching the maximum value of about 10 °C. The enhancement of T_g can be attributed to

the restricted segmental motions at the organic-inorganic interface in the neighborhood of intercalated compositions [13].

Also, this phenomenon mainly benefits from the uniform LDH dispersion and the strong interactions between PP molecular chains and intercalated clay particles. Even at a higher clay content of 10 wt%, the MA groups in PP-g-MAH can still break up the large clay agglomerates into much finer particles with increasing the degree of dispersion, as confirmed by the previous TEM study in **Section 4.4.2.2**. As expected, the more intercalated clay particles are, the higher restriction of PP chains mobility occurs, leading to the shift of T_g to a higher temperature. In addition, with increasing the LDH content, the elastic moduli of such nanocomposites are also significantly enhanced by over 32% below T_g. It is also observed that at higher temperatures above T_g, the elastic modulus continues to be increased at a low clay content up to 7 wt%. This indicates that the strong reinforcement effect can still take place in the rubbery plateau, depending on good clay dispersion and favorable interfacial interactions, which tend to be achieved more easily at low LDH contents.

5.2.3 Differential Scanning Calorimetry (DSC)

The influences of LDH and PP-g-MAH as compatibilizer on the crystallization temperature (T_c), melting temperature (T_m) and crystallinity content (X_c) of polypropylene were characterized by DSC thermal analysis. **Figure 5.6**(a) and (b) demonstrate the DSC curves of PP/LDH based nanocomposites. The corresponding characteristic parameters and calculated degree of crystallinity (X_c) are listed in **Table 5.3**. **Figure 5.6 (a)** shows the first DSC heating curves of the neat PP and nanocomposites. The thermograms showed that all materials exhibited a single melting endotherm at a relatively constant melting temperature at about 163 ºC. As can be seen from **Table 5.3**, T_m remained unaltered with the addition of either LDH or PP-g-MAH compatibilizer. More interestingly, the T_c of nanocomposites is gradually enhanced up to 124 ºC with addition of LDH, as compared to 115 ºC for PP. Such enhancement might be explained by a good balance between the positive nucleating effect of LDH and detrimental influence of the excessive PP-g-MAH with low crystallinity. Moreover, a better LDH dispersion leading to much stronger interfacial interactions may also induce more nucleating cores to

facilitate the crystallization with the better nucleating effect and the higher T_c. The higher T_c of such nanocomposites (>117 ºC) also indicates that a higher extent of segregation of dispersed clay particles takes place around the boundary of the spherulites or inter spherulites, resulting in the enhanced intercalation [13a], as confirmed by previous XRD and TEM results in Sections 4.4.2.2 and 4.4.2.3 of Chapter 4. The X_c of nanocomposites notably increases up to 69.9 % compared to that of PP (X_c =65.6%), which again implies the positive nucleating effect on crystallinity.

Therefore, it can be concluded that the introduction of LDH increased the crystallization rate of PP chains. The presence of LDH layers acts as heterogeneous nuclei of PP crystallization. Because the LDH layers are intercalated or exfoliated, the number of the heterogeneous nuclei in PP/LDH is much larger than that in pure PP. The further elaborative details on crystallization behavior and kinetic study of PP/LDH nanocomposites are discussed in Chapter 6.

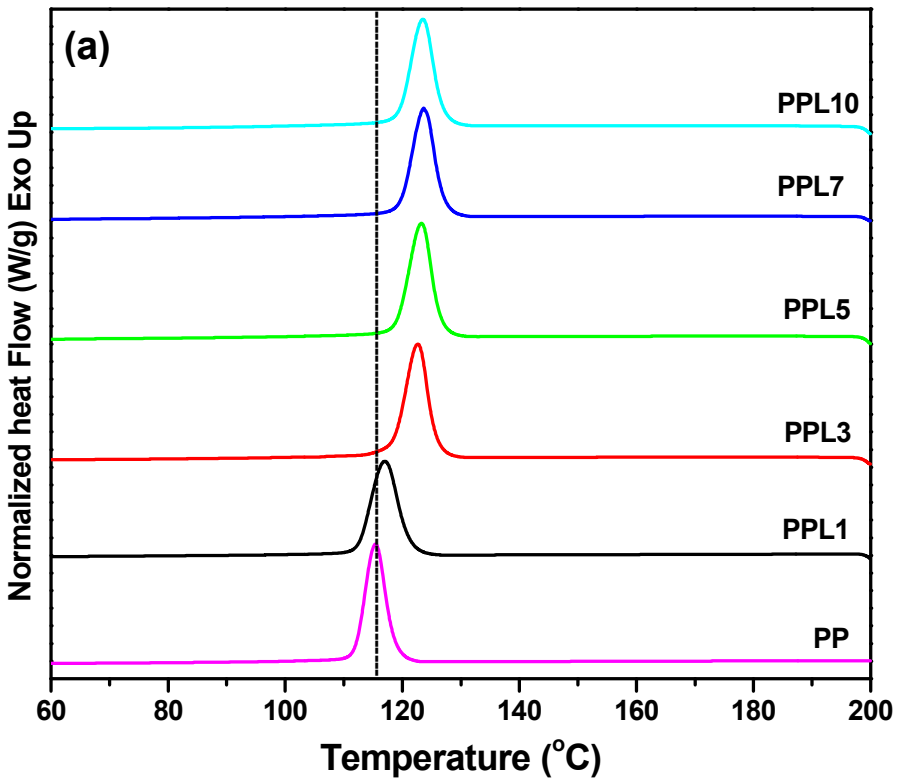

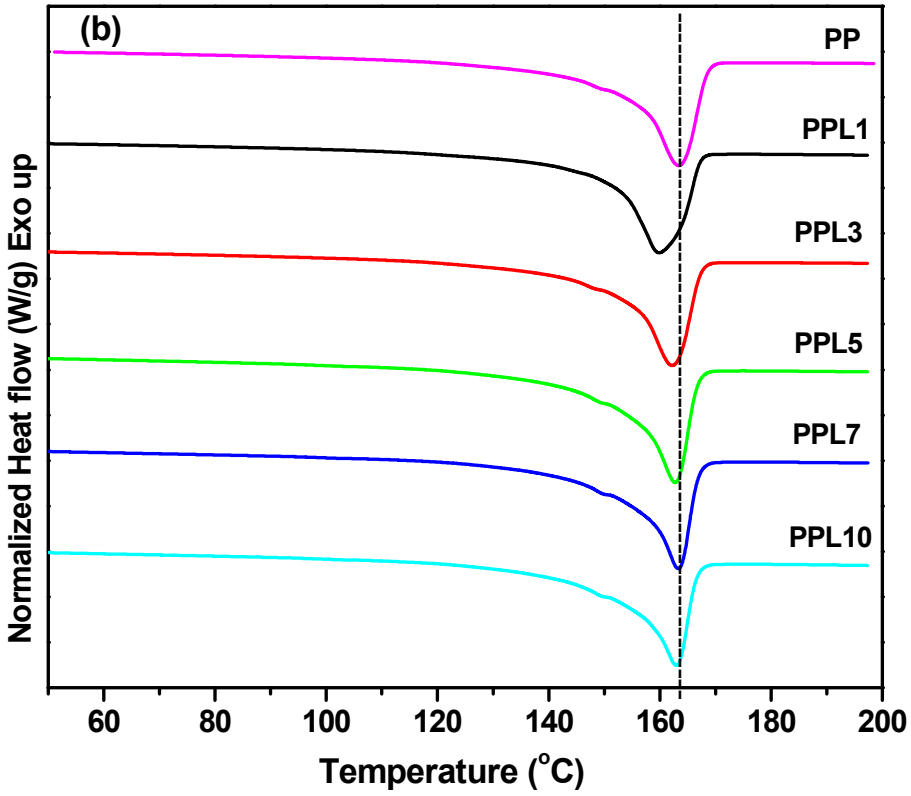

Figure 5.6 : DSC curves of PP/LDH nanocomposites (a) Heating scan (b) Cooling Scan

Table 5.3: DSC characteristic parameters and degree of crystallinity of PP/LDH nanocomposites

Sample	T_m (°C)	T_c (°C)	ΔH_m (J/g)	X_c (%)
PP	163.1	115.4	102.3	65.60
PPL1	161.1	117.0	97.63	66.00
PPL3	162.7	122.7	105	68.96
PPL5	162.7	123.4	105.1	68.76
PPL7	163.3	123.7	99.52	69.54
PPL10	163.0	123.5	112.6	69.89

5.3 Mechanical Properties

Mechanical properties such as tensile, flexural and impact properties reflect the macroscopic behavior of nanocomposites in relation to the clay dispersion and interfacial adhesion under different physical testing mechanisms. Hence it is of paramount importance to investigate the various mechanical properties of such materials which are summarized in following sections.

5.3.1 Tensile test

The tensile test data obtained were used to plot stress-strain curves for the various nanocomposite structures. **Figure 5.7** and **Figure 5.8** shows the average tensile stress-strain and tensile modulus data computed for virgin polypropylene and PP/LDH nanocomposite specimens.

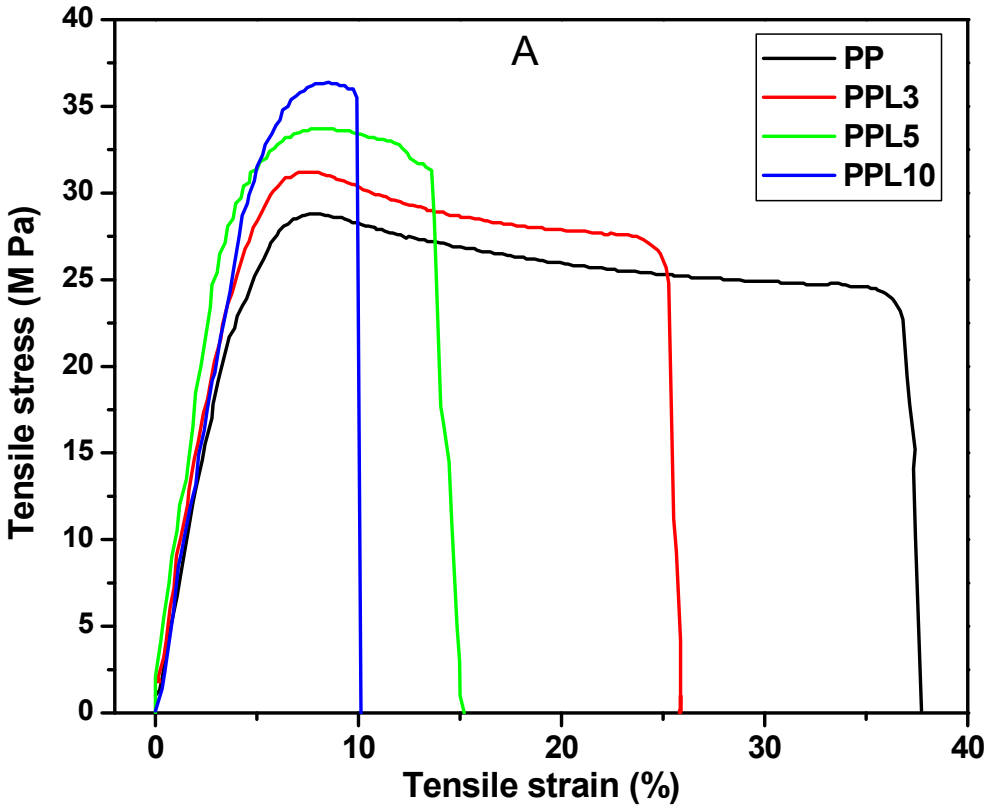

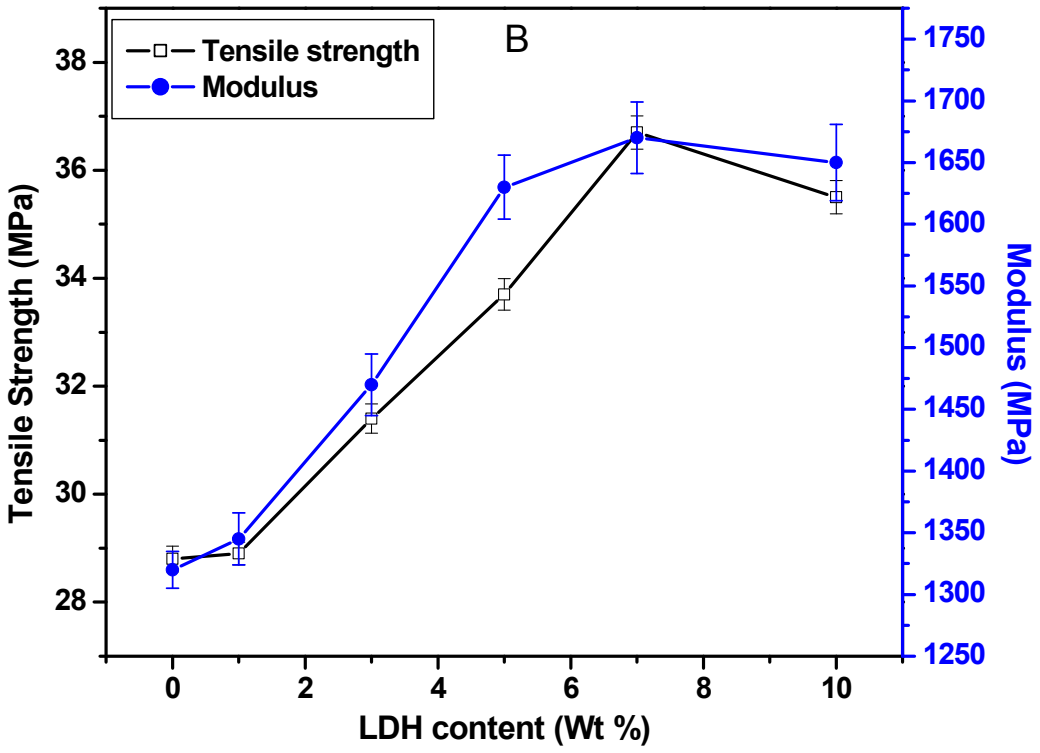

Figure 5.7: A typical stress-strain curve for PP and PP/LDH nanocomposites (A) and Tensile strength and modulus as a function of LDH content (B).

As shown in **Figure 5.7 and Table 5.4,** the tensile strength of neat PP is 28.8 MPa and it is remarkably affected by LDH loading. The tensile strength values gradually increase up to 7 wt.%, but beyond this threshold, they more or less level off regardless of the LDH addition. Such behavior might be attributed to a higher level of intercalation/exfoliation in the LDH dispersion and better improvement of the interfacial adhesion, especially for the low clay content (≤ 5 wt %), as illustrated in **Figure 5.7.** This is also due to the tendency of agglomerations above a specific concentration and higher level of compatibilization. The excess amount of PP -g-MAH plasticize the interface between the LDH and PP matrix and the tensile strength of compatibilized nanocomposites were found to be the lowest at high concentrations. At optimum compatibilization, better exfoliation of LDH and better adhesion at the interface compensate the plasticizing effect of PP -g-MAH.

Figure 5.7 shows the elastic modulus and tensile strength as a function of LDH concentration. Both the tensile strength and the modulus increase in tandem up to 7 wt % LDH concentration, thereafter significant degradation occurs. The average highest modulus is found for 7 wt. % structures is approximately 1670 MPa which is about 27% higher than that of virgin PP as shown in **Table 5.4**. A sharp increase in modulus up to 7% LDH loading is observed and then dropping to 10% (1650 MPa). A similar trend for the ultimate tensile strength is shown in **Figure 5.7**. Such behavior may be due to the uniformly dispersed LDH tactoids and intercalated structures. The organically modified LDH is intercalated by the PP chains and confines the segmental movement of the PP macromolecules. As a result, the modulus of the PP nanocomposites increases with LDH loadings. A fraction of intercalated structure decreases with increasing LDH content. At higher LDH concentrations, aggregation of the nanoclays and plasticization effect of MAH-g-PP may occur decreasing the tensile strength and modulus.

5.3.2 Flexural Tests

The flexural properties of PP/LDH nanocomposites are illustrated in **Figure 5.8**. It is observed that the flexural strength and moduli are significantly improved with increasing the LDH content, the maximum enhancements of flexural strength and moduli reach 31MPa and 1510 MPa, respectively. More interestingly, there is a sharp increasing tendency in flexural modulus for a LDH content of less than 5 wt%, followed by a much slower increase between 7 wt% and 10 wt%, similar trend is observed for tensile modulus. The flexural strengths is also increased by maximum 32%. Remarkable strength increasing trends are also very consistent for LDH contents less than 5 wt%, but beyond this threshold, they more or less level off regardless of the LDH content. Such flexural properties from PP/LDH nanocomposites might be attributed to a higher level of intercalation/exfoliation in the clay dispersion and better improvement of the interfacial adhesion, especially for the low clay content (≤ 5 wt%), as illustrated in **Figure 5.8.**

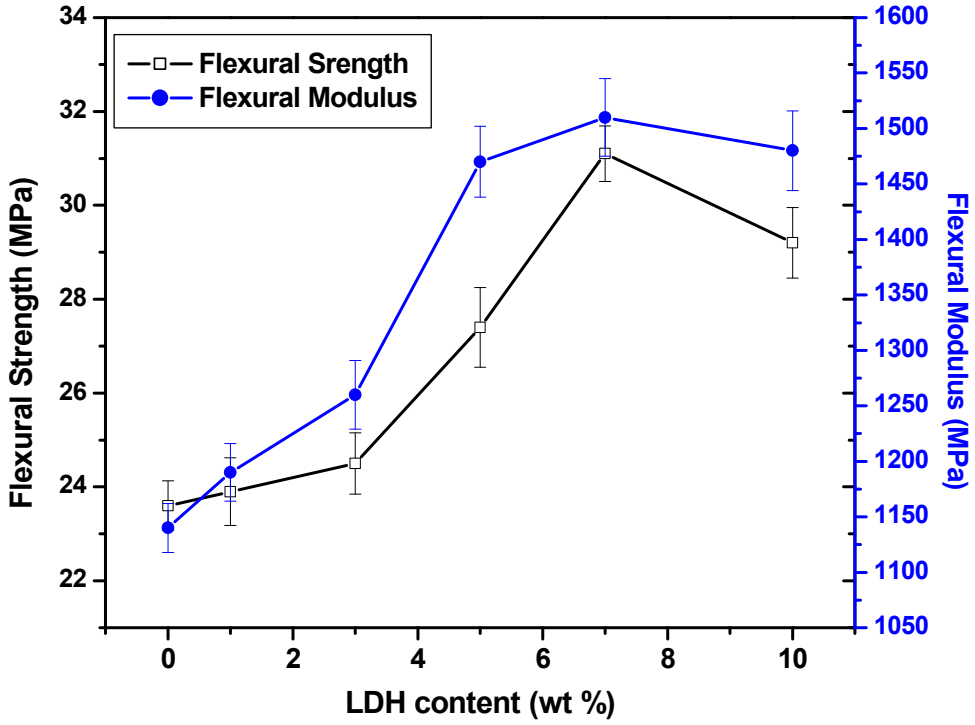

Figure 5.8: Flexural strength and modulus as a function of LDH content

5.3.3 Izode Impact Tests

The influence of LDH content on the relevant impact properties is depicted in **Figure 5.9**. Initially, with an increase of LDH content, the impact strength is considerably enhanced by maximum 25% when increasing up to 5 wt% LDH, and then drops off in a similar way until it levels off at a high LDH content of about 10 wt%, comparable to that of neat PP. The higher impact strength at a lower LDH content possibly benefits from more uniform LDH dispersion, leading to the better level of intercalation/exfoliation. As mentioned earlier, the reduction of impact strength often occurs at higher nanoclay content due to the induced material brittleness from the proportional amount increase of nanoclay and PP-g-MAH that is more brittle than neat PP itself [14-15]. Similar trend is also observed in case of PP/LDH nanocomposites.

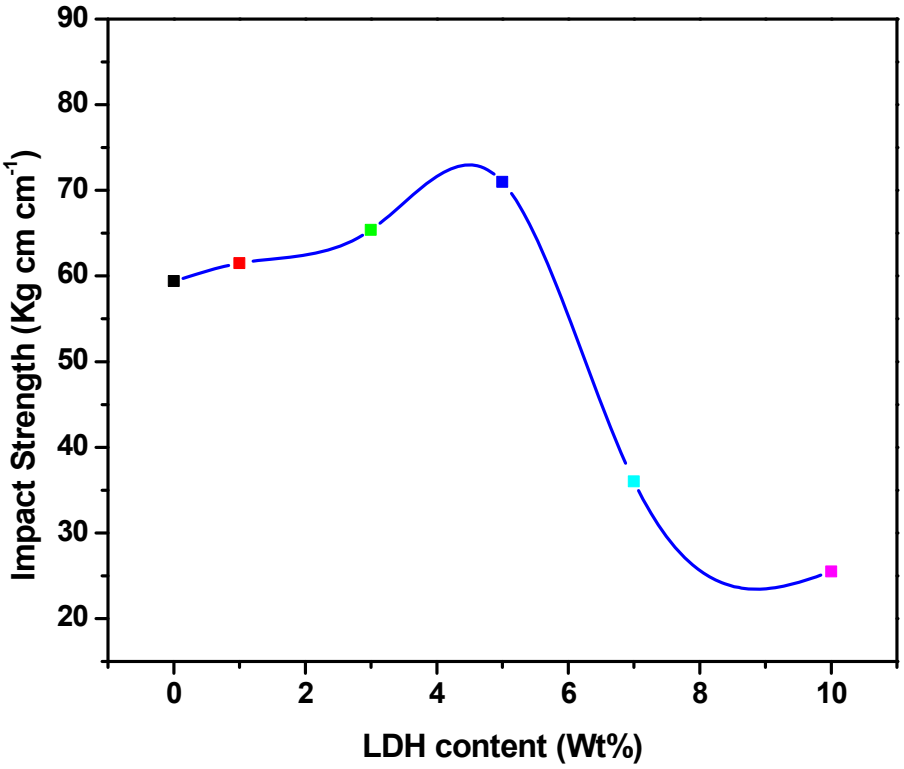

Figure 5.9: Izode impact strength as a function of LDH content in PP/LDH nanocomposites

5.3.4 Elongation at break

The effect of LDH loading on elongation of PP is also studied as shown in **Figure 5.6 and 5.10**. It can be seen that the EB values remarkably decreased due to the presence of LDH platelets in PP structure. This may be due to the restraints on mobility of the polymer chains caused by the intercalated/exfoliated LDH platelets; this is also associated with reduced chain mobility that causes reduction in ductility.

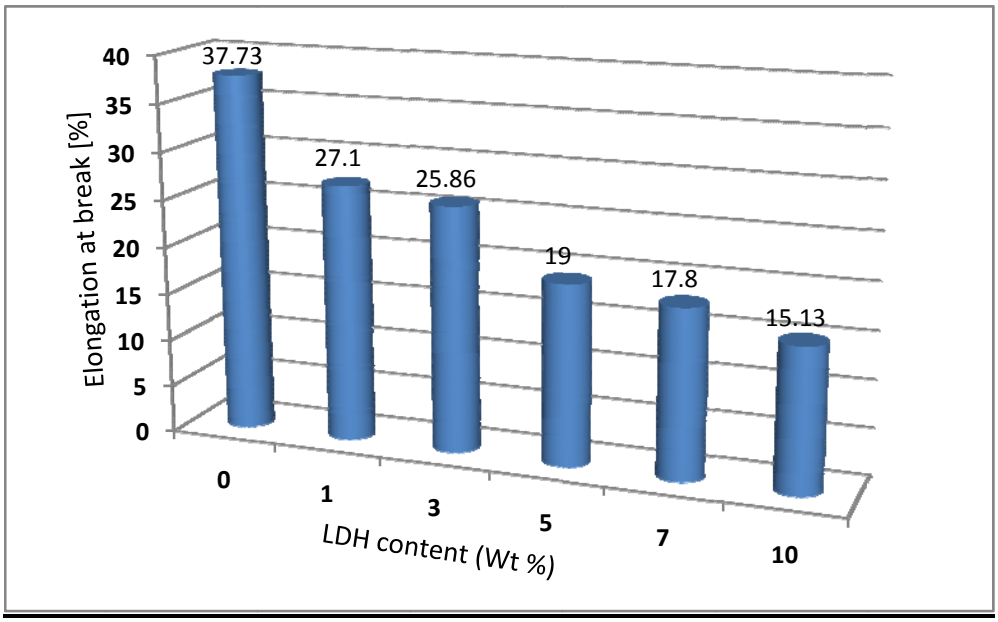

Figure 5.10: Elongation at break as a function of LDH content in PP/LDH nanocomposites

Table 5.4: Mechanical properties of PP/LDH nanocomposites

Sample	Tensile Strength (MPa)	Young's Modulus (MPa)	Flexural Modulus (MPa)	Flexural Strength (MPa)	Elongation at break (%)	Izode Impact strength (Kg cm cm^{-1})
PP	28.8±0.24	1320±15	23.6±0.53	1140 ± 22	37.7±0.45	59.4
PPL1	28.9±0.21	1345±21	23.9±0.72	1190 ± 26	27.1±0.32	61.5
PPL3	31.4±0.27	1470±25	24.5±0.65	1260 ± 31	25.8±0.35	64.4
PPL5	33.7±0.29	1630±26	27.4±0.85	1470 ± 32	19.0±0.27	70.1
PPL7	36.7±0.31	1670±29	31.1±0.59	1510 ± 35	17.8±0.24	37
PPL10	35.5±0.31	1650±31	29.2±0.75	1480 ± 36	15.3±0.19	25.5

5.4 Rheological Analysis

The linear viscoelastic response of PP/LDH nanocomposites are studied using dynamic oscillatory measurements with a sinusoidal strain input at a constant strain amplitude of 5% and frequency sweep from 0.05 rad/s to 100 rad/s. The temperature range used was 180–200°C. The linear viscoelastic responses of all the nanocomposite compositions are qualitatively similar in this temperature range but, the time-temperature superposition principle is not fulfilled for the nanocomposites, especially in the low frequency region. This is mainly because of the reason that the modulus shift factors are found to change with LDH concentration [16]. Therefore, construction of the master curve is not possible. All the oscillatory shear experiment data presented in this section corresponds to the measurements carried out at a fixed temperature of 200°C. The material response is interpreted in terms of various parameters, like storage modulus (G'), complex viscosity (η*), *tan δ*, etc. **Figure 5.11** shows the typical features of linear viscoelastic response of the unfilled polypropylene and a nanocomposite melt containing varying content of LDH during such a frequency sweep experiment. Within the experimental frequency range, the storage modulus of the unfilled PP is lower than its loss modulus. It means that the viscous component has a dominant effect on the flow behavior of the unfilled PP melt in this frequency range. With increasing frequency, the storage modulus increases more compared to the loss modulus and at some higher frequency (which is larger than the highest value of frequency used in the present experiment) G' crosses G" indicating increasing contribution of the elastic response. This is typical behavior of unfilled thermoplastic melt [17]. On the contrary, PP/LDH nanocomposites having high LDH content show completely different behavior. The storage modulus always remains higher than the loss modulus within the experimental frequency range indicating dominant elastic character of the material. This is typical behavior observed in crosslinked polymer or polymer gel, where viscous flow is restricted by chemical constraints. In the present case, high concentration of LDH particles both in nano- and microscales creates strong physical barrier against the mobility of the polymer chains.

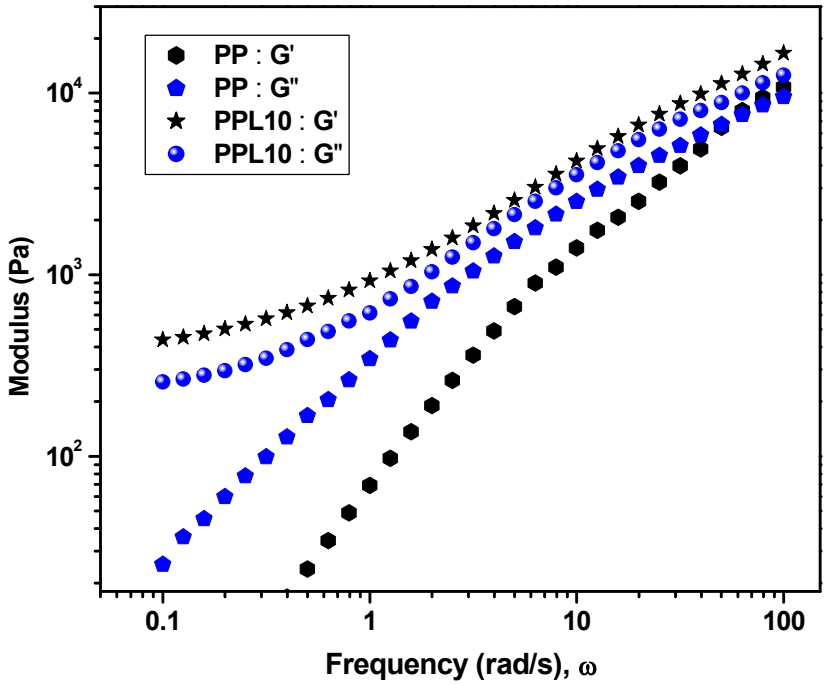

Figure 5.11: Difference in the viscoelastic response (storage modulus, G' and loss modulus G") of unfilled polypropylene and high LDH filled nanocomposite in a dynamic oscillatory frequency sweep experiment

The influence of increasing LDH concentration on linear viscoelastic response as discussed in the following sections shows how liquid-like melt is gradually transforms into a solid-like melt. **Figure 5.11** also shows that the difference in viscoelastic response between unfilled melt and the nanocomposite strongly depends on the frequency region at which they are compared. In the high frequency range, due to a small time period in each shear cycle, the dispersed filler particles can not fluctuate in phase with the oscillating shear force field and appears virtually static. As a result their influence is minimized and materials behavior is solely determined by the matrix behavior [18]. On the other hand, at low frequencies the influence of the filler particles can be realized as they get more time to follow the oscillating shear force field and if they interfere with flowability of the materials strong effects like that presented in **Figure 5.11** are observed. Therefore, in discussing the linear viscoelastic behavior of nanocomposites, the low frequency data are of prime importance. The ability to store energy by any polymeric melt during shearing

depends on its chain relaxation behavior. Lower the relaxation time for a system faster it dissipates the energy and hence shows lower value of storage modulus. In storage modulus versus frequency plot (**Figure 5.12**), the low frequency data for unfilled polypropylene reflect this fact. At low frequencies due to longer time period of shear cycles polymer chains get sufficient time to relax nearly completely showing low value of G'. This is the typical behavior of Newtonian liquids. The addition of LDH filler causes an upward shift of the low frequency G' values, which becomes more prominent with increasing LDH concentration ultimately leading to a virtually plateau behavior or frequency independence (**Figure 5.12**). The extent by which LDH particles influence the storage modulus can be measured semi quantitatively by the relaxation exponent (n_1) obtained by fitting the low frequency data to power law equation

$$G' \propto \omega^{n_1} \qquad 5.1$$

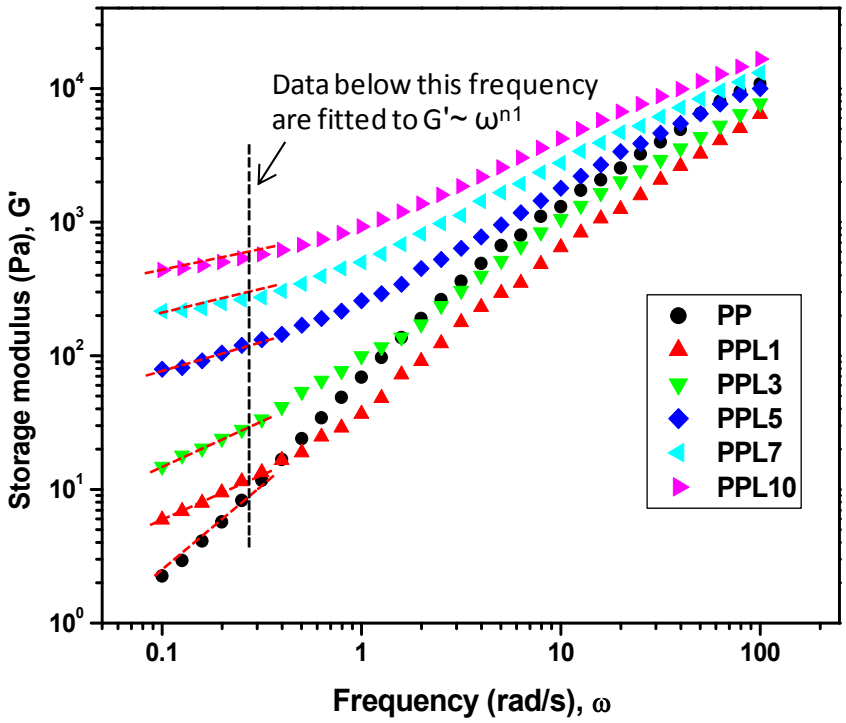

Figure 5.12: Storage modulus (G') versus frequency (ω) plots for unfilled PP and PP/LDH nanocomposite melts based on the results obtained from dynamic oscillatory measurements.

In case of homopolymers, the complete relaxation at low frequencies results in a characteristic terminal behavior with the value of n_1 equal to 2 [19-20]. **Figure 5.12** shows how n_1 changes with LDH concentration in case of PP/LDH nanocomposites. The **Table 5.5** shows the relaxation exponents obtained by fitting low frequency data to the power law model. The unfilled polypropylene does not show typical homopolymer-like low frequency behavior and it may be due to its high molecular weight associated with long chain branching and high polydispersity index. Still the value of 1.32 for n_1 indicates high extent of chain relaxation when compared to LDH filled compositions. While the presence of small amount of LDH (3 wt %) changes n_1 significantly, the corresponding change in G' is not much. This is attributed to the presence of low molecular weight functionalized polypropylene (PP-g-MAH) as compatibilizer, which lowers the matrix viscosity. Similar effects have also been observed in case of layered silicate based polymer nanocomposites containing a functionalized polymer of lower molecular weight [21]. However, with the further increase of LDH concentration (say beyond 5 wt %), the both n_1 and G' at low frequency are changed significantly due to strong influence of LDH particles on the flow behavior of the melt. It is apparent that with increasing LDH concentration, G' shows decreasing frequency dependency in the low frequency region and at very high LDH level (above 7 wt %) a virtually plateau region is reached. This means that the system develops more and more solid-like behavior with increasing resistance against relaxation through viscous flow of the polymer chains and segments. This low frequency non-terminal viscoelastic response observed in PP/LDH nanocomposites resembles the layered silicate based exfoliated nanocomposites, where the polymer chain ends are inter-locked at the surface of the highly anisotropic exfoliated silicate layers [22]. On the contrary, such non-terminal behavior is not observed when the polymer chains do not interact with the exfoliated clay layers [23-24]. It is suggested that the adsorption of polymer chain segments on a rigid surface creates an energetic barrier against the repetition of the polymer chains. As a result, the chain relaxation process is delayed (increasing the relaxation time) and shifts the terminal behavior to very lower frequencies. Interaction between LDH clay surfaces with polymer chains through maleic anhydride groups present in functionalized polymer has been observed. The morphological analysis of the PP/LDH nanocomposites at different loadings discussed

earlier and the fracture surface analysis of these nanocomposites show that polymer chains are indeed adsorbed on the LDH particle surface and are also entrapped within loose particle clusters [25]. The highly anisometric exfoliated LDH layers remains randomly dispersed in the matrix and in the vicinity of larger particle agglomerates. With increasing LDH concentration, the number density of the exfoliated layers increases, which decreases the average inter-particle distance. This may lead to formation of localized domains of physical networked structure, where the nanostructured particles may orient themselves in some preferential direction [26-28]. The shearing in low frequency region can not generate sufficient force to destroy such structured domain resulting in fluctuation of individual particles to oscillate with the shear force field. Also, close proximity and strong particle-particle interaction cause a kind of physical jamming leading to extremely slow relaxation of the particle phase as well. As a result, this causes strong reinforcement of the melt producing high elastic modulus compared to unfilled melt.

Table 5.5: Values of n_1 in $G' \sim \omega^{n_1}$ and n_2 in $\eta^* \sim \omega^{n_2}$

Sample	n_1	n_2
PP	1.32	0.04
PPL1	0.81	0.35
PPL3	0.67	0.48
PPL5	0.50	0.78
PPL7	0.34	0.83
PPL10	0.20	0.89

The variation of complex viscosity (η*) with frequency and LDH concentration is shown in **Figure 5.13**. The unfilled PP melt is characterized by a low frequency Newtonian flow behavior, which transforms to shear thinning characteristic in the high frequency region. This is typical behavior of unfilled polymeric melts (with only differences observed in the frequency region at which transition from Newtonian to shear thinning behavior takes place depending on the molecular weight and the molecular

architecture). The presence of nanostructured LDH particles in the melt not only enhances the melt viscosity but also induces shear thinning character in the low frequency region. The frequency independent viscosity of unfilled melt in the low frequency region is an indication that the shear force applied in this region is not sufficient to disentangle the polymer chains and align them in the flow direction. Such Newtonian behavior at low frequencies or low shear rate is also common in polymer composites containing non interactive filler particles, even at very high filler concentration. Like an unfilled melt, these composite melts are also characterized by the absence of yield stress. However, in case of PP/LDH nanocomposites, completely different low frequency behavior is observed. Like typical polymer/clay based nanocomposites, beyond certain critical concentration of LDH, the low frequency Newtonian behavior changes into a shear thinning behavior. The extent of deviation from the low-frequency Newtonian flow behavior is measured by a term called shear thinning exponent (n_2) obtained by fitting the low frequency data in **Figure 5.13** to the power law equation:

$$\eta^* \propto \omega^{n_2} \qquad 5.3$$

In case of unfilled PP, the value of n_2 is expected to be zero. But, polypropylene used in the present study shows a small negative value (-0.04) of n_2. The high molecular weight and long chain branching are the factors causing this small increase in shear thinning exponent. In the case of PP/LDH nanocomposites, the negative value of n_2 increases significantly at a very small LDH concentration and steadily increases with further increase in LDH concentration as shown in **Figure 5.13**.

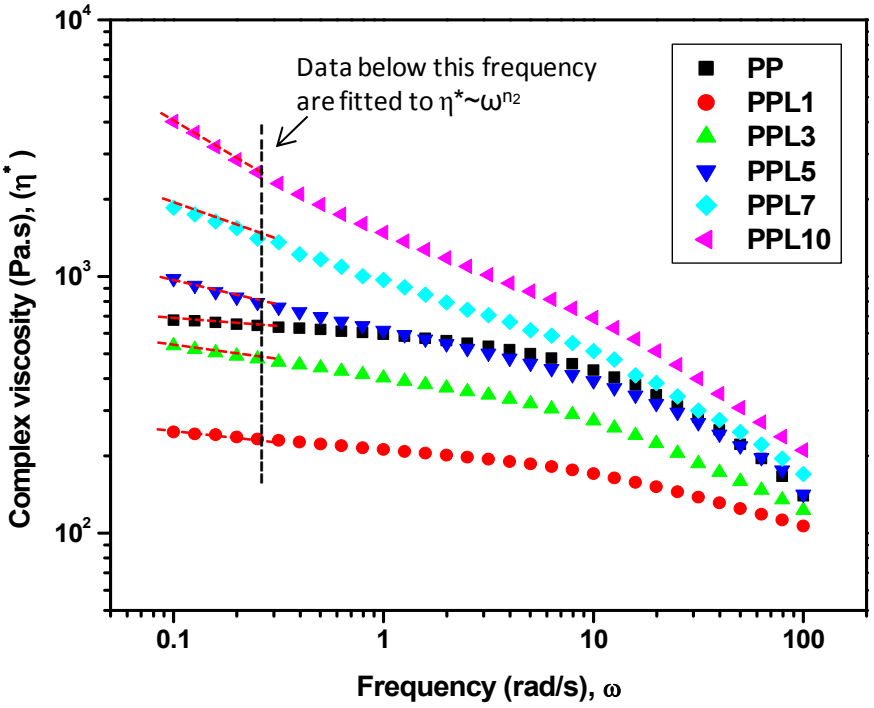

Figure 5.13: Complex viscosity (η*) versus frequency (ω) plots for unfilled PP and PP/LDH nanocomposite melts obtained from a dynamic oscillatory shear experiments.

Recently, Wagner *et al.* have proposed this shear thinning exponent as a semi-quantitative measure of degree of exfoliation of the clay particles in polymer/clay nanocomposites [29]. It is suggested that polymer nanocomposites containing exfoliated clay particles show much higher value of n_2 compared to conventional composites, where clay particles form big agglomerates. They observed no change in low frequency complex viscosity with temperature of the melt, while high-frequency viscosity decreased with increasing temperature. However, the similar explanation does not hold for the PP/LDH nanocomposites and the results are shown in **Figure 5.13**. The PP/LDH nanocomposites melts show weaker temperature dependency of the low-frequency complex viscosity compared to that of the high-frequency complex viscosity indicating stronger influence of the dispersed particle in the low frequency response. This behavior is in agreement with the XRD and TEM results of LDH based nanocomposites qualitatively showing significant enhancement in the degree of exfoliation of LDH

particles with increasing LDH concentration. Therefore, the change in the shear-thinning exponent as shown in **Figure 5.13** is may be due to enhancement of degree of exfoliation. Rather, the increasing LDH concentration brings about two changes in the system, firstly, more number of polymer chains/segments get interlocked on the LDH platelets surface or in the interlayer region. Secondly, the average distance between the dispersed particles is decreased. These two factors contribute though different mechanisms to the final properties of the nanocomposites. The interlocking of the polymer chains on LDH platelets certainly restricts their mobility and hence delays their relaxation process. This is reflected in so called zero shear viscosity of the melts. In case of unfilled PE and the nanocomposites containing low amount of LDH, the well defined zero shear viscosity can be determined (**Figure 5.13)** by extrapolating the viscosity versus frequency curve to zero frequency. However, this does not work at high LDH concentration as the complex viscosity versus frequency curves diverge as frequency approaches zero indicating the presence of a yield stress value. The formation of network structure (more specifically, sub network structures due to the formation of structured domains) by the nanostructured clay particles beyond certain critical filler concentration induces solid-like behavior in the melt showing high viscosity and elastic modulus. During low-strain and low frequency oscillatory shearing, matrix mobility is severely restricted by such particulate domain. However, as the shearing become more intense with increasing frequency or strain, the network structures start getting disturbed and at sufficiently high frequency or shear rate they may be completely destroyed with shear induced alignment of the clay particles in the flow direction. As a result, melt rheology at this stage is solely influenced by the matrix showing strong temperature dependence. The elastic nature of the melt is also reduced by such alignment [27]. Additionally, the polymer chains which are entrapped between particle clusters or constrained by the clay particles through intercalation and adsorption, experience larger effective strain compared to unconfined chains [30]. This can lead to enhanced shear thinning behavior of the nanocomposite melts at low shear rate experienced during low frequency oscillatory measurements [21, 31].

5.5 Gas Barrier Properties

The permeability of a nanocomposite system normally depends on the clay content, length-to width ratio, relative orientation, and degree of dispersion (intercalated, exfoliated, or intermediate state) of the nano-layers. In particular, a high length to width or aspect ratio of the clay lamellae is a key factor in maximizing tortuosity. Because of its layered crystalline structure and high aspect ratio, layered double hydroxide (LDH) can be useful in lowering gas permeation when high dispersion is achieved in polymeric system. The objective of the present investigation is to study the effect of different LDH loadings on oxygen-barrier properties of PP/LDH nanocomposites. **Table 5.6** shows the oxygen transmission rate (OTR) measurements for various PP/LDH systems, which indicate that the gradual decrease in gas permeation with addition of LDH to the PP matrix with optimized compatibilizer is observed. Improvements in the oxygen barrier properties are obtained for higher concentrations of the LDH, about 35 % reduction in oxygen permeation is observed in 7 % LDH filled PP in comparison of pristine PP. This effect can be explained by changes in the arrangement of the LDH platelets and by the state of the amorphous domains. The insertion of inorganic particles into the homopolymer matrix is likely to decrease the mobility of the amorphous phase, which in turn is directly related to the gas diffusivity. Amorphous chains located in the vicinity of the rigid particles do not entangle with one another and become locally oriented and strained, thereby hindering the permeation of gas molecules. When the compatibilizer is included, the polymer– clay interactions become stronger and the stack configuration is modified, as shown by TEM images. The smaller clay aggregates and individual platelets are then dispersed in the matrix, increasing tortuosity and induce the partial alignment of nearby amorphous chains; these combined actions lead to an overall improvement in the barrier properties. While there is no any significant difference in oxygen permeability rate is observed for nanocomposites fabricated using LDH comprising different metal cations as shown in **Table 5.6.**

Table 5.6: Oxygen permeability properties of PP/LDH nanocomposites

Sample	Oxygen permeability mL/m^2 per day	Sample	Oxygen permeability mL/m^2 per day
PP	567 ±1	PPLA	406 ±11
PPL1	535±9	PPLB	411±13
PPL3	482±8	PPLC	402±11
PPL5	403±6	PPLM	440±16
PPL7	365±5		
PPL10	385±5		

Moreover, from these values it is clear that the PP/LDH nanocomposites have lower OTR values than PP/OMMt nanocomposites indicating PP/LDH nanocomposites have lower oxygen permeability. This may be due to higher aspect ratio of LDH clay over OMMt clay, after uniform dispersion resulting in high tortuosity in nanocomposites.

5.6 Flame Retardancy

The effect of LDH type nanofillers as a flame retardant in PP was investigated by LOI. The LOI value is merely expressed as a number indicating the minimum percentage of oxygen required for self-sustained combustion of a polymeric material, this test method can also be used to analyze how the materials burn at oxygen concentration corresponding to LOI value and also close (from lower side) to it. During the LOI test measurements, flame propagates vertically downwards along the burning test specimen. The propagation first takes place through the surface layer and then finally reaches the core of the sample. The values of limited oxygen indices for PP nanocomposites based on LDH containing different metal cations are shown in **Figure 5.14**. In this test, the minimum amount of required oxygen to stabilize the flame of the samples is reported; the higher the LOI value is, the higher the resistance to flammability will be. Obviously, the LOI values of different PP/LDH nanocomposites increased to different extents in the

range of 17.6 to 22.5, because better dispersion of LDH nano-layers in the PP matrix and layer of metal oxide formed made flame retardant sample more difficult to ignite and consequently needed a higher oxygen concentration to support burning of the samples. The LOI value of PP is 17.6% that indicates relatively high flammability. The addition of small amount of LDH (PPL5) results in small change in the LOI value. In addition, small variation in LOI values was also observed for depending on interlayer metal cations. Incorporation of higher amount LDH into PP increases LOI value up to 22.5% for PPLC10 and the order of flame retardant is found to be decreased in following order PPLC10>PPLB10>PPLA10. Since the LOI value is higher than 21 %, the PPM10 sample is also classified as a material with average flammability. The higher LOI of PPLC10 reduces the activity of free radicals and makes them inactive. Thus, a higher amount of oxygen will be needed to stabilize the flame. The basic difference between burning of unfilled PP and PP/LDH nanocomposites is that in case of former no char/burn residue is formed. Consequently, a reinforced charred structure is formed. The produced structure acts as an insulator and both the heat transfer flux to the underneath layers and volatilization of gaseous products into the gas phase reduces. Sufficient heat energy from the flame-front must be conducted through the char layer to the melt region for sustaining the burning process. Thus, the char layer acts as a physical barrier against the propagation of the flame downward along the LOI sample. At low LDH concentration (PPL5), the amount of char layer is formed and hence its thickness on the burning surface is very small. As a result, the char can not provide efficient barrier effect and the test piece burns quite easily at similar oxygen concentration as that for unfilled PP. With the increasing LDH concentration, both thickness of the char layer and the endothermic decomposition contribution of the clay increases. This makes the self-sustained burning of the sample more and more difficult at low oxygen concentration, thus increasing the LOI value with LDH concentration. At low LDH concentration, the viscosity of melt is not sufficient to hold the residue on the vertically placed test specimen. As a result, it falls down and a fresh unburnt surface is continuously exposed to flame resulting in spontaneous burning of the test specimen at relatively lower oxygen concentration.

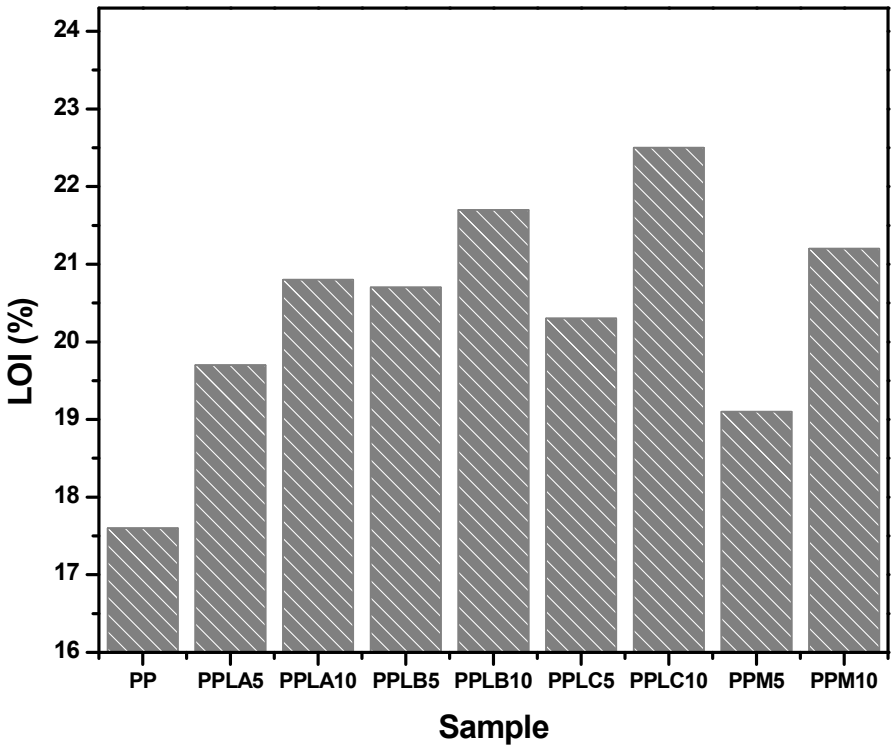

Figure 5.14: Limited oxygen index (LOI) of PP/LDH nanocomposites

However, at higher LDH concentration, the high viscosity of the melt prevents the easy slippage of the char layer from the sample stock. Therefore, the melt viscosity plays an important role in determining the LOI value of the PP/LDH nanocomposites. In fact, this is also true for the conventional polyolefin/metal hydroxide type flame-retardant composites. The PP/LDH nanocomposites posses higher LOI values then PP/OMMt nanocomposites. Such behavior may be due to the endothermic decomposition of the LDH particles as it reduces the supply of heat for the combustion process. As a result, more oxygen is required to sustain the flame, i.e. the LOI value increases. While burning at oxygen concentration lower than that indicated by the LOI value of the respective nanocomposite sample, the test piece though catches the flame, but the flame is extinguished. Conversely in PP/OMMt nanocomposites the relatively less stable silicate char is formed. Hence, PP/LDH nanocomposites show higher flame retardancy in comparison to PP/OMMt nanocomposites.

5.7 Conclusions

Based on this research devoted to study the thermal, mechanical, rheological, gas barrier and flammability properties of an LDH reinforced PP; the following conclusions can be drawn:

The TGA analysis showed that the incorporation of the LDH which is in a platelet form resulted in a significant improvement in the initial thermal stability of PP. Presence of LDH causes distinct changes in the thermal decomposition behavior in comparison to the unfilled PP. The thermal degradation temperature tended to increase as the interaction between the LDH and polypropylene matrix was improved via organic modification and PP-g-MAH compatibilization. LDH reinforcement significantly enhances the thermal stability of the composites. The onset of decomposition $T_{0.1}$ is delayed significantly by the addition of LDH. $T_{0.50}$ also increases with LDH concentration. Two step decomposition was observed under air in contrast to the single step in N_2. These results show that the PP/LDH hybrid posses remarkable enhanced thermal properties. DMTA measurements reveal that the addition of LDH can contribute to the reinforcement effect by increasing the elastic modulus E'. This indicates that the plastic and elastic responses of PP towards deformation are strongly influenced by the presence of LDH. The nanocomposites achieve the significant reinforcement level with the modulus improvement of about 40% at a high LDH content (7-10 wt%) and temperatures below T_g. Such tendency is conversely well maintained at a low LDH content ($\leq$ 5 wt%) in the rubbery plateau. The glass transition temperatures (T_g) of most nanocomposites are increased compared to that of the corresponding neat PP, implying that these nanocomposites benefit from the intercalation structures which restrict the mobility of PP molecular chains. The thermal analysis results showed that the crystallization temperature of neat polypropylene was increased due to the nucleation effect of LDH in the nanocomposite structure. An increase about 8^oC was recorded in 10 wt.% LDH /PP-g-MAH/PP nanocomposite. On the other hand, no significant effect on melting temperature was observed by LDH loading. Moreover, the crystallinity of LDH is found to increase with addition of LDH, which implies the positive nucleating effect on crystallinity of PP.

In mechanical properties, both the tensile strength and the modulus increases with LDH content, while the rate of increase at higher loading is less pronounced. About 27.5 % and 35 % increase in average modulus and tensile strength for 7 wt. % PP/LDH hybrid is observed, similar trend is observed in flexural properties. The improvement in modulus and strength parameters is due to the PP-g-MAH to be associated with the functionality of the LDH which promotes the interaction between the LDH and PP matrix. Stiffness gradually increases from 1 wt. % to 7 wt. % with a decrease occurring for 10 wt. % specimens. The study also shown that the impact strength and tensile elongation at break of PP nanocomposites decrease steadily as the LDH content increased from 0 to 10 wt. %.

The melt rheological analysis of PP/LDH nanocomposite shows flow behavior typical of polymer/layered silicate nanocomposites. This was not only helpful to understand the flow behavior of the composite melts under different shearing conditions, but was also useful in understanding the nature of LDH particle dispersion and possible filler-filler and filler-polymer interaction in the nanocomposites. The dynamic oscillatory shearing in linear viscoelastic regime reveals that with increasing LDH concentration, the nanocomposite melts progressively deviate from the low-frequency Newtonian behavior to a strong shear thinning behavior. Also the pseudo-solid like behavior becomes more and more prominent with the appearance of apparent yield stress. Such deviation in the low frequency flow behavior is caused by the dispersed LDH particles and their physical networked structures, which creates an energy barrier against the relaxation of the polymer chains. This also gives indirect evidence that polymer chains are interlocked on the LDH particle surface or within clusters. The morphological analysis shows that the dispersed LDH particles form physically associated structures in different scales. As a result, the response of these nanocomposite melts during shearing in non-linear regime differs significantly from that of the unfilled PP melt. It is observed that steady shearing causes breakdown of the filler structures until a steady state is reached. This is manifested in the form of stress overshoot at the start-up flows during steady shear. Such behavior is also observed in unfilled PP melt, but the time scale and magnitude of stress overshoot differ drastically from the nanocomposites.

The incorporation well dispersed LDH into PP shows improved oxygen barrier properties. Moreover, the PP/LDH nanocomposites exhibits fairly better barrier performance than PP/ OMMt nanocomposites. While there is no any significant difference in oxygen permeability rate is observed for nanocomposites fabricated using LDH comprising different metal cations. The flammability studies of the PP/LDH nanocomposites showed improved flame retardancy in comparison to the unfilled PP. The LOI value was progressively improved with increasing LDH concentration. PP/LDH nanocomposites show higher LOI in comparison to PP/OMMt. For different LDH, LOI increases in the following order Zn_2Al-LDH > ZnMgAl-LDH > Mg_2Al-LDH. The results indicate that the LDH act as effective flame retardant for PP.

The improvements obtained in PP/LDH nanocomposite structure and properties can make this commercial thermoplastic polymer more suitable for automotive, construction and packaging applications.

References

1. A. Leuteritz, D. Pospiech, B. Kretzschmar, M. Willeke, D. Jehnichen, U. Jentzsch, K. Grundke, A. Janke. Progress in Polypropylene Nanocomposite Development, *Advanced Engineering Materials*, **5** (2003), p.678 – 681.
2. J. Zhang, D. D. Jiang, C. A. Wilkie. Thermal and flame properties of polyethylene and polypropylene nanocomposites based on an oligomerically-modified clay, *Polymer Degradation and Stability,* **91**, (2006), p.298-304.
3. J-Y. Lee. Polymer Nanocomposites: The "Nano" Effect on Mechanical Properties, *Polymer Reviews*, **47** (2007), p.217 – 229.
4. S.C. Tjong, Structural and mechanical properties of polymer nanocomposites *Materials Science and Engineering: R: Reports,* **53** (2006), p.73-197.
5. R.E. Wetton, P.J. Corish, DMTA Studies of Polymer Blends and Compatibility. *Polymer Testing*, **8** (1989), p. 303-312.
6. J.J. Scobbo, Dynamic Mechanical Analysis of Compatibilized Polymer Blends. *Polymer Testing*. **10** (1991), p.279-290.
7. W.J. Sichina, P.S. Gill (1986). Characterization of Composites by Thermal Analysis. *31st International SAMPE Symposium*. Wilmington: Concord Plaza. April. 7-10. Choudhury et al., 1991c.
8. H. A. Barnes. Thixotropy - a review. *Journal of Non-Newtonian Fluid Mechanics*, **70** (1997), p.1 – 33.
9. A. I. Leonov. On the rheology of filled polymers. *Journal of Rheology*, **34** (1990), p.1039 – 1068.
10. S. M. Lomakin and G. E. Zaikov. Modern Polymer Flame Retardancy. VSP Publishers, Netherlands, 2003.
11. J. W. Gilman, A. B. Morgan, and R. Harris (Jr.). Polymer layered silicate nanocomposites: Polyamide-6, polypropylene and polystyrene. In Proc. New Advances in Flame Retardant Technology. Proceedings. Fire Retardant Chemicals Association, Lancaster, PA, USA, pages 9 – 22, 1999.
12. M. C. Costache, M. J. Heidecker, E. Manias, G. Camino, A. Frache, G. Beyer, R. K. Gupta, C. A. Wilkie. The influence of carbon nanotubes, organically modified montmorillonites and layered double hydroxides on the thermal degradation and fire retardancy of polyethylene, ethyleneevinyl acetate copolymer and polystyrene, *Polymer*, **48** (2007), p.6532-6545.

13. M. Alexandre and P. Dubois, "Polymer-layered silicate nanocomposites: preparation, properties, and uses of a new class of materials", *Mater. Sci. Eng.*28 (2000), p.1-63. 13a) P. Maiti, P. H. Nam, M. Okamoto, N. Hasegawa and A. Usuki, "Influence of crystallization on intercalation, morphology, and mechanical properties of polypropylene/clay nanocomposites", *Macromolecules* **35** (2002), p.2042-2049.
14. S. Coiai, E.Passaglia, A. Hermann, S.Augier, D. Pratelli, R. C. Streller The Influence of the Compatibilizer on the Morphology and Thermal Properties of Polypropylene-Layered Double Hydroxide Composites, *Polymer Composites*, **31** (2009), p.744 – 754.
15. J. Pascual, E. Fages, O. Fenollar, D. García and Rafael Influence of the compatibilizer/nanoclay ratio on final properties of polypropylene matrix modified with montmorillonite-based organoclay, *Polymer Bulletin,* **62** (2009), p.367-380.
16. J. Ren, A. S. Silva, and R. Krishnamoorti. Linear viscoelasticity of disordereed polystyrenepolypropylene block copolymer based layered-silicate nanocomposites. Macromolecules, **33** (2000), p.3739 – 3746.
17. C. W. Macosko. *Rheology Principles, Measurements and Applications*. VCH Publishers, USA, 1993.
18. H. A. Barnes. Thixotropy - a review. *Journal of Non-Newtonian Fluid Mechanics*, **70 (**1997), p.1 – 33.
19. R. Krishnamoorti, R. A. Vaia, and E. P. Giannelis. Structure and dynamics of polymer-layered silicate, nanocomposites. *Chemisty of Materials*, **8** (1996), p.1728 – 1734.
20. K. M. Lee and C. D. Han. Effect of hydrogen bonding on the rheology of polycarbonate/ organoclay nanocomposites. *Polymer*, **44** (2003), p.4573 – 4588.
21. M. J. Solomon, A. S. Almusallam, K. F. Seefeldt, A Somwangthanaroj, and P. Vardan. Rheology of polypropylene/clay hybrid materials. *Macromolecules*, **34** (2001), p.1864 – 1872.
22. R. Krishnamoorti and E. P. Giannelis. Rheology of end-thethered polymer layered silicate nanocomposites. *Macromolecules*, **30** (1997), p.4097 – 4102.
23. R. Krishnamoorti, R. A. Vaia, and E. P. Giannelis. Structure and dynamics of polymer-layered silicate, nanocomposites. *Chemistry of Materials*, **8** (1996), p.1728 – 1734.

24. R. Krishnamoorti and E. P. Giannelis. Rheology of end-thethered polymer layered silicate nanocomposites. *Macromolecules*, **30** (1997), p.4097 – 4102.
25. F.R. Costa, B.K. Satapathy, U. Wagenknecht, R. Weidisch, and G. Heinrich. Morphology and fracture behaviour of polyethylene/MgAl layered double hydroxide (LDH) nanocomposites. *European Polymer Journal*, **42** (2006), p.2140 – 2152.
26. R. Krishnamoorti and E. P. Giannelis. Rheology of end-thethered polymer layered silicate nanocomposites. *Macromolecules*, **30** (1997), p.4097 – 4102.
27. J. Ren, A. S. Silva, and R. Krishnamoorti. Linear viscoelasticity of disordereed polystyrenepolypropylene block copolymer based layered-silicate nanocomposites. *Macromolecules*, **33** (2000), p.3739 – 3746.
28. F.R. Costa, B.K. Satapathy, U. Wagenknecht, R. Weidisch, and G. Heinrich. Morphology and fracture behaviour of polyethylene/MgAl layered double hydroxide (LDH) nanocomposites. *European Polymer Journal*, **42** (2006), p.2140 – 2152.
29. R. Wagner and T. J. G. Reisinger. A rheological method to compare the degree of exfoliation of nanocomposites. *Polymer*, **44** (2003), p.7513 – 7518.
30. A. Subbotin, A . Semenov, E. Manias, G. Hadziioannou, and G. ten Brinke. Rheology of confined polymer melts under shear flow: Strong adsorption limit. *Macromolecules*, **28** (1996), p.1511 – 1515.
31. R. Krishnamoorti, J. Ren, and A. S. Silva. Shear response of layered silicate nanocomposites. *Journal of Chemical Physics,* **114** (2001), p.4968 – 4973.

Chapter 6

CRYSTALLIZATION BEHAVIOR AND KINETIC STUDY

"If I have seen further it is by standing on the shoulders of giants"

~Sir Isaac Newton

Sunil P. Lonkar, S. Morlat-Therias, F. Leroux, J-L. Gardette, R.P. Singh, *"Preparation and Nonisothermal Crystallization Behavior of Polypropylene/Layered Double Hydroxide Nanocomposites"*, ***Polymer,*** 50 (2009), p. 1505-1515.

Sunil P. Lonkar and R.P. Singh, *"Isothermal Crystallization and Melting Behavior of Polypropylene/Layered Double Hydroxide Nanocomposites"*, ***Thermochimica Acta,*** 491 (2009), p. 63-70.

6.1 Introduction

Polymer crystallinity is one of the important properties of all polymers. Polymer exists both in crystalline and amorphous form. **Figure 6.1**, shows the arrangement of polymer chain forming crystalline and amorphous regions [1]. It can be seen that part of molecules are arranged in regular order, these regions are called crystalline regions. In between these ordered regions, molecules are arranged in random disorganized state and these are called amorphous regions. The study of crystallization phenomena is of great importance in polymer processing. In particular, the study of crystallization kinetics of polymers as a function of the processing conditions, from a macro-kinetic point of view, is very important for the analysis and design of processing operations. On the other hand, physical properties of polymeric materials such as hardness, modulus, tensile, stiffness and melting point etc. are strongly depend on their microstructure and crystallinity, since it is at this microscopic level where failure of the materials takes place. Polypropylene (PP) is semicrstalline polymer and is well known that the physical and mechanical properties of semicrystalline PP depend on the morphology and structure of the crystal and on degree of crystallization. Also, the final properties of PP based composites in engineering applications are critically dependent on the extent of crystallinity which in

turn depends on the processing conditions. The study of the kinetics of crystallization is necessary for optimizing industrial process conditions and establishing the structure-property correlations in polymer nanocomposites [2]. The crystallization process consists of two steps such as nucleation and growth. When the nucleation occurs spontaneously only due to the supercooling and no second phase or other nuclei exists, such type of nucleation called as homogeneous nucleation. While in presence of any other second phase such as foreign particle or surface from the same polymer nuclei/crystal, then the nucleation is referred as heterogeneous nucleation. The nucleation, growth and kinetics of development of these crystalline regions are of both profound fundamental and pragmatic interest. These characteristics are directly linked to understanding of the morphological details of crystalline regions. Crystallization of long chain flexible molecules of sufficient structural regularity is widely observed for a large number of polymers.

The crystallization ability of the polypropylenes and isothermal and non-isothermal crystallization kinetics in presence of different fillers have been extensively reported in the literature [3-8]. It has been found that the degree of crystallinity, crystal size, and shape morphology and crystallization kinetics of the polypropylene matrix is strongly affected by the presence of nano-scale particulates. Recently, Chen *et al.* [9] calorimetrically studied the isothermal crystallization behavior of PP/polyhedral oligomeric silsesquioxane (POSS) nanocomposites and found that POSS nanoparticles could accelerate the overall crystallization of PP and suggested a three-dimensional growth with heterogeneous nucleation. Maiti *et al.* [6] investigated how crystallization controls the fine structure and morphology of the PP/clay nanocomposites. They concluded that the clay platelets act as a nucleating agent and lower the size of the PP spherulites. To our knowledge, only few articles report the use of such inorganic/organic (I/O) LDH/surfactant assemblies as filler for polymers and their effect on the iso or non-isothermal crystallization behavior and the subsequent effect on changes of the microstructural parameters [10-12]. However, there was no literature on studies of LDH induced crystallization and melting behavior of polypropylene.

The prime objective of this research is to investigate the influence of LDH type nanometric anionic clays, organo-modified by surfactant molecules as filler on the

crystallization behavior of PP in PP/LDH hybrid nanocomposites. A special focus will be on the ability of these materials to crystallize from the melt. Morphology development and melting behavior of PP/LDH hybrids, with respect to the recrystallization from various melt conditions will be discussed. Crystallization kinetics of such melt processable hybrids is extremely important from both a practical and fundamental standpoint and results in the literature will be discussed in this regard. The data obtained from differential scanning calorimetry were employed for measuring crystallization kinetic parameters and subsequent melting. The crystallization kinetics was achieved by confronting different models, namely Ozawa, Avrami and Liu *et al.* Another important feature frequently exhibited by these polymers is the multiple melting behavior. Melting behaviors following the isothermal crystallization process were also discussed. The possible explanations of this phenomenon put forward in the literature will be highlighted. The spherulitic growth rate and the effective energy barrier of iso/non-isothermal crystallization were explained by an isoconversional approach. The spherulitic growth rate was used to obtain data on the specific surface free energies for the PP and all nanocomposites. The microcrystalline dimensions (D_{hkl}) of crystal growth and spherulitic morphology were investigated by WAXD and optical polarising microscopy (POM), respectively.

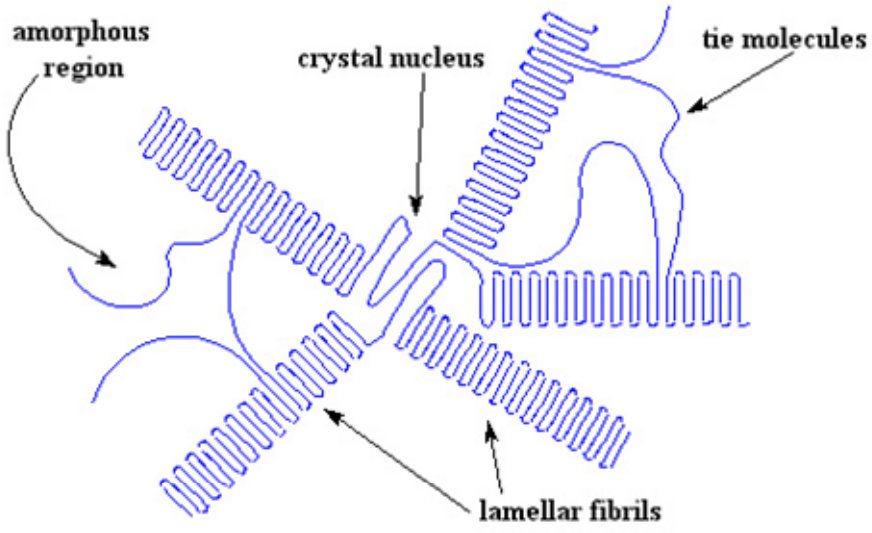

Figure 6.1: A polymer crystalline spherulite

6.2 Nonisothermal Crystallization Behavior and Kinetics

A study of non-isothermal crystallization of polymer nanocomposites is of pragmatic significance because in processing, crystallization occurs under non-isothermal conditions. It has been reported that the nanoscale clay layers bring about significant changes in the crystallization behavior and polymorphic nature in semicrystalline polymers. The crystallization behavior of PP and PP/LDH nanocomposites was studied at cooling rates (α) between 2.5 and 20 °C/min. **Figure 6.2 (a)**, shows typical nonisothermal crystallization thermograms of polymer. From these curves, some useful parameters for the nonisothermal crystallization analysis, such as the onset temperature of crystallization (T_o), the crystallization temperatures, e.g. the exothermic peak maxima (T_p) and the end temperature of crystallization (T_∞) can be obtained.

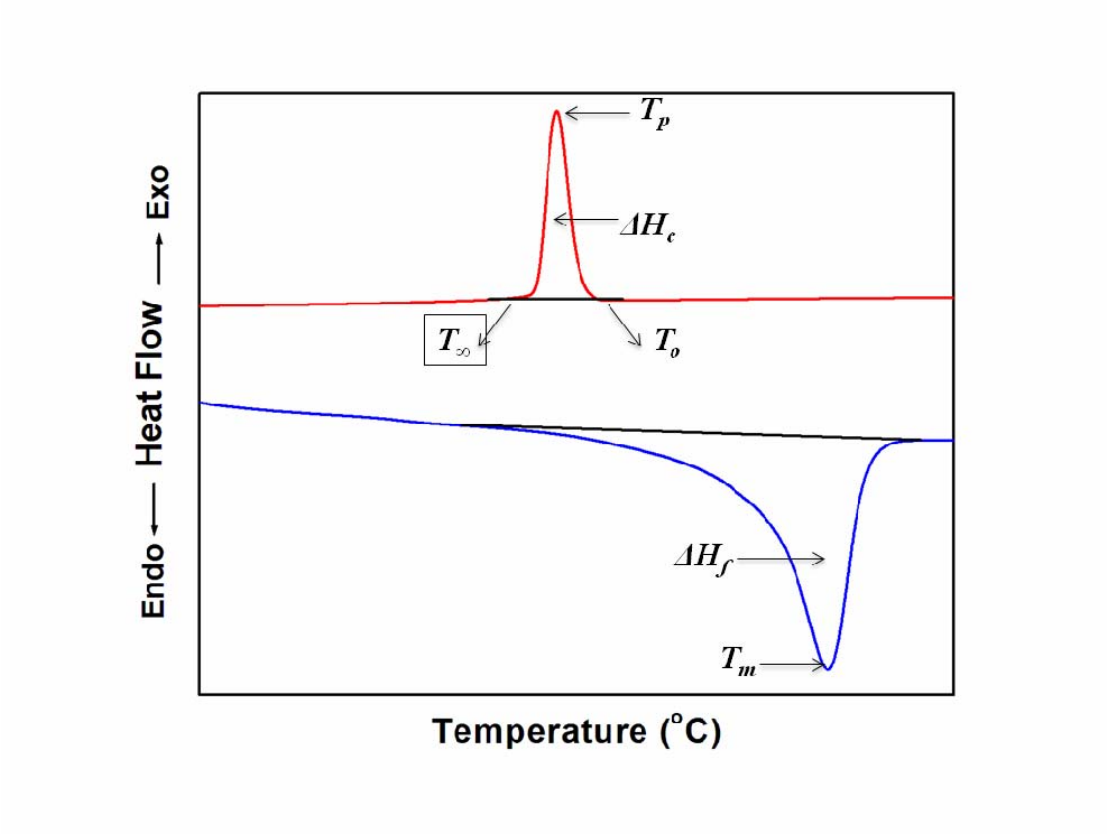

Figure 6.2: A typical a) non-isothermal crystallization curves, heating (lower curve) and cooling (upper curve)

Figure 6.3 (a-d), shows typical nonisothermal crystallization thermograms of PP and PP/LDH nanocomposites. The various crystallization parameters obtained from these curves e.g crystallization temperature (T_p) and the percent crystallinity (X_c) etc. of the PP phase are listed in **Table 6.1** The enthalpy of crystallization (ΔH_c) has also been calculated from the enthalpy of crystallization normalized to the PP content, assuming that the thermodynamic contribution of the LDH phase is negligible. The percent crystallinity (X_c) of pure PP and the PP nanocomposites was determined by Eq.6.1, where the value of the heat of crystallinity of pure crystalline PP (ΔH_c^0) was assumed to be 146.5 J/g. [13]

$$X_c = \frac{\Delta H_c}{\Delta H_c^0} \times 100 \qquad (6.1)$$

From DSC thermograms [**Figure 6.3 (a-d) and Table 6.1**] at various cooling rates (2.5, 5, 10 and 20 °C), it is clear that the crystallization peak temperature, for nanocomposites are higher than those of pure PP and decreases with increasing cooling rates. The faster the cooling rate, the lower the temperature range at which the crystallization occurs. At a slower cooling rate, there is sufficient time to activate nuclei; therefore, the crystallization can occur at a higher temperature [7]. For example, the crystallization temperature of PP increased by 15 °C in presence of LDH nano particles whereas decreased when the cooling rate was increased.

The plots, which show the variation of the peak temperature with cooling rates, for the PP/LDH nanocomposites are shown in **Figure 6.4**. It is obvious that the peak temperature at a given cooling rate increases with increasing LDH content, this phenomenon can be explained by the heterogeneous nucleation effect of Mg_2Al-DDS LDH nanoparticles on PP macromolecular segments which can be easily attached to the surface of the Mg_2Al-DDS LDH, which leads to the crystallization of PP to occur at a higher crystallization temperature.

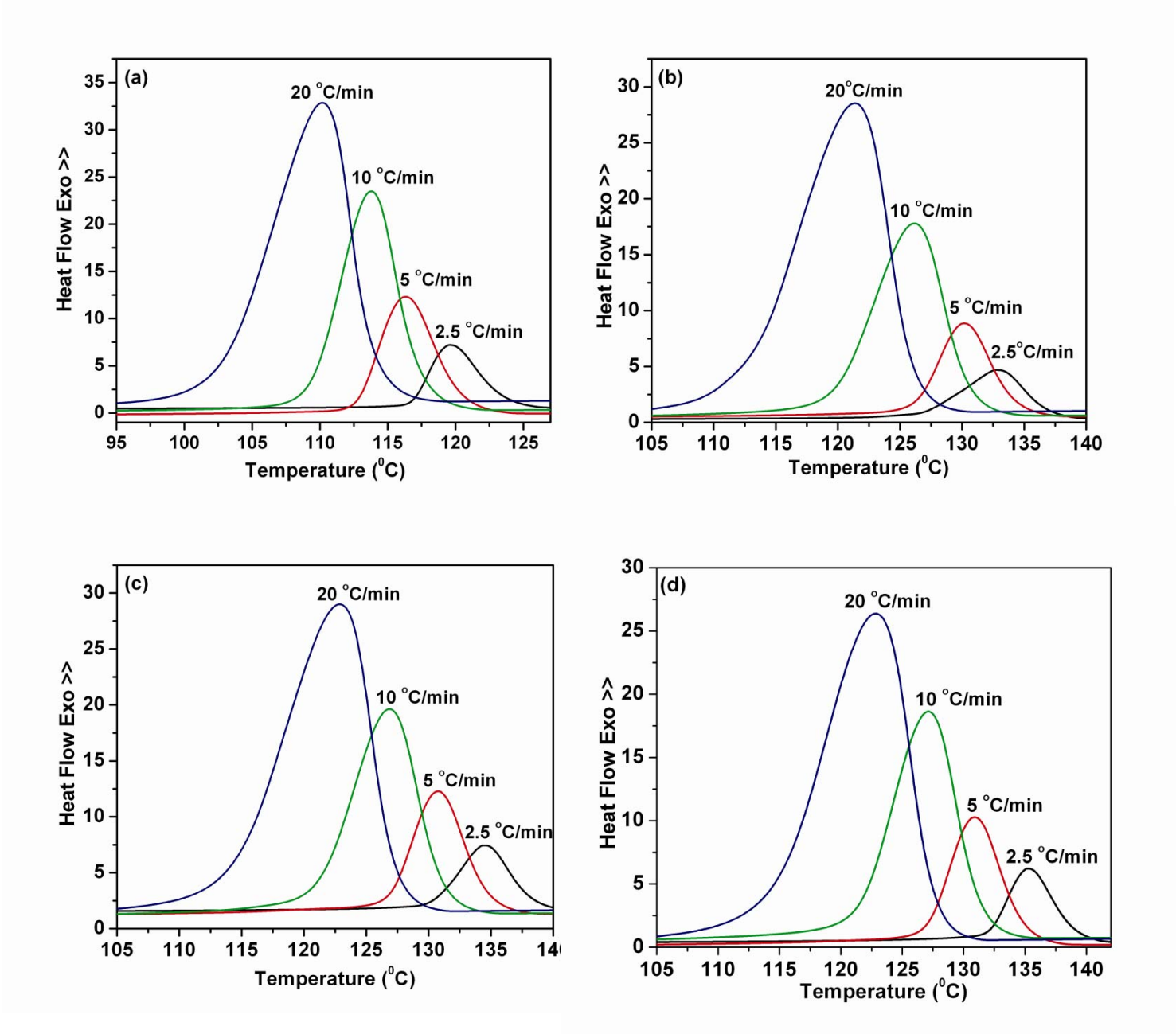

Figure 6.3: DSC thermograms of nonisothermal crystallization at different cooling rates: (a) PP, (b) PPL1, (c) PPL3, and d) PPL5.

Table 6.1 Crystallization temperature and maximum percent crystallinity of PP /LDH nanocomposites for cooling rates of 2.5, 5, 10 and 20 °C/min.

Sample	2.5 °C/min		5 °C/min		10 °C/min		20 °C/min	
	T_p (°C)	X_c %	T_p (°C)	X_c %	T_p (°C)	X_c %	T_p (°C)	X_c %
PP	119.60	66	116.33	67	113.81	66	110.15	62
PPL1	132.74	63	129.18	64	125.16	66	121.32	67
PPL3	134.44	65	130.75	69	126.85	68	122.85	66
PPL5	135.24	67	131.89	64	128.17	65	123.85	66

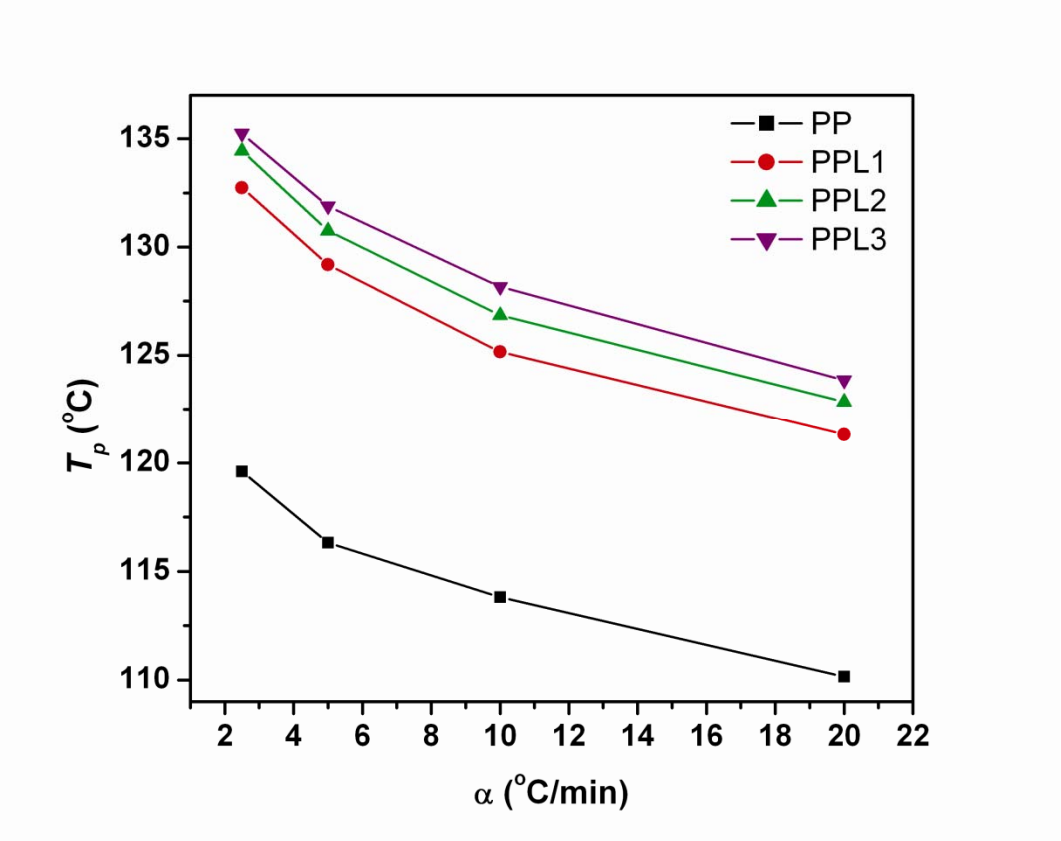

Figure 6.4: Crystallization peak temperature versus cooling rate for PP and PP/LDH nanocomposites.

6.2.1 Nonisothermal Crystallization Kinetics

In order to further analyze the nonisothermal crystallization process, the crystallization kinetics of PP and PP/LDH nanocomposites is compared. From dynamic crystallization experiments, data from the crystallization exotherms as a function of temperature; dH_c/dT can be obtained, for each cooling rate.

The relative degree of crystallinity as a function of temperature, X_T, can be calculated according to the equation following equation:

$$X_T = \frac{\int_{T_o}^{T} (dH_c / dT)dT}{\int_{T_o}^{T_\infty} (dH_c / dT)dT} \tag{6.2}$$

where, T_o and T_∞ are the temperature at which crystallization starts and ends, and dH_c/dT is the heat flow rate. The development of relative degree of crystallinity X_T as a function of temperature, T, for PP and its nanocomposites at various cooling rates is shown in **Figure 6.5**. The plots of X_T versus T for PP and PP/LDH nanocomposites are similar and all these curves have the same sigmoidal shape, implying that only a lag effect of cooling rate on crystallization is observed.

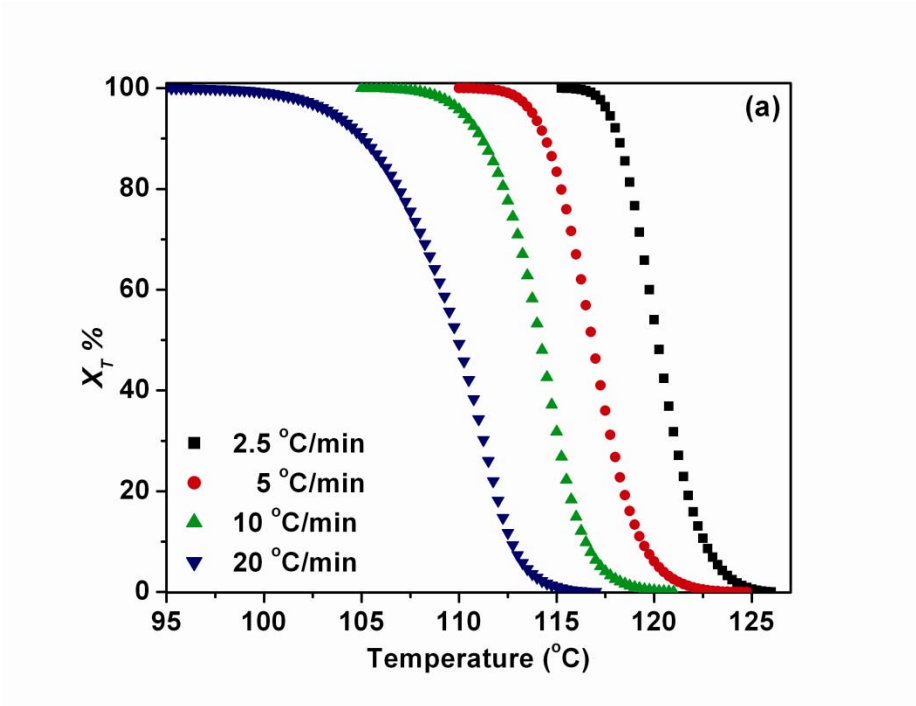

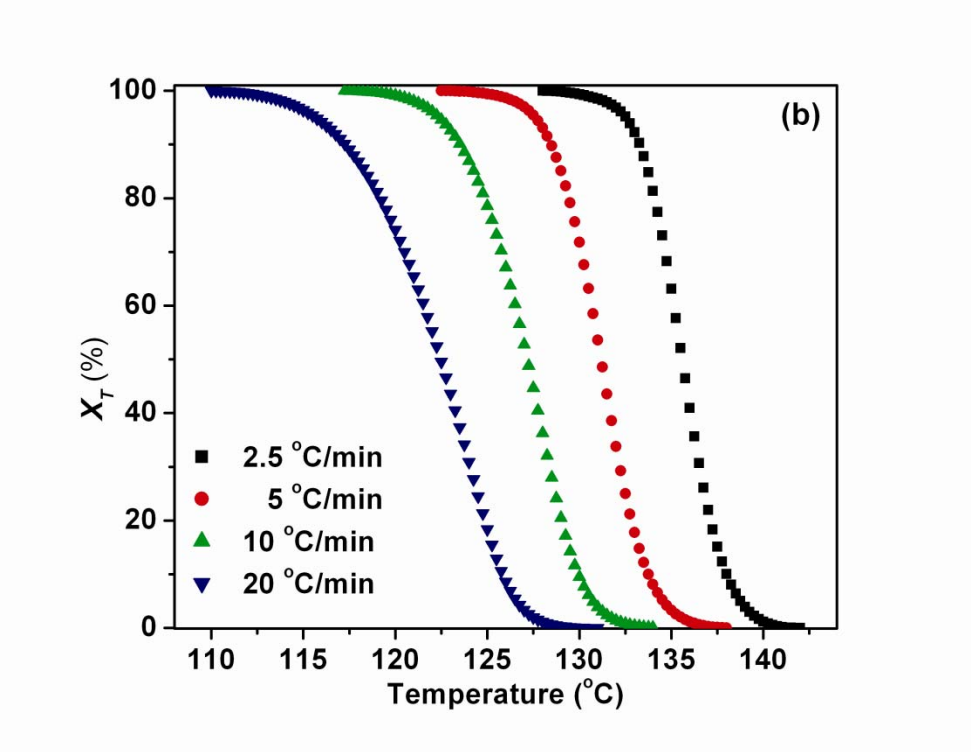

Figure 6.5: The relative degree of crystallinity with temperature for the crystallization of (a) PP and (b) PPL5 at different cooling rates.

In nonisothermal crystallization, the temperature can be related to crystallization time scale by using the following equation:

$$t = \frac{(T_o - T_p)}{\alpha} \tag{6.3}$$

(where, T_o is the onset temperature at a crystallization time $t = 0$, T_p is the temperature at crystallization time t, and α is the cooling rate). The results show that the higher the cooling rate, the shorter the time for completing crystallization. According to Eq.6.3 the value of T on the X-axis can be transposed into the crystallization time (t) as shown in **Figure 6.6**.

.

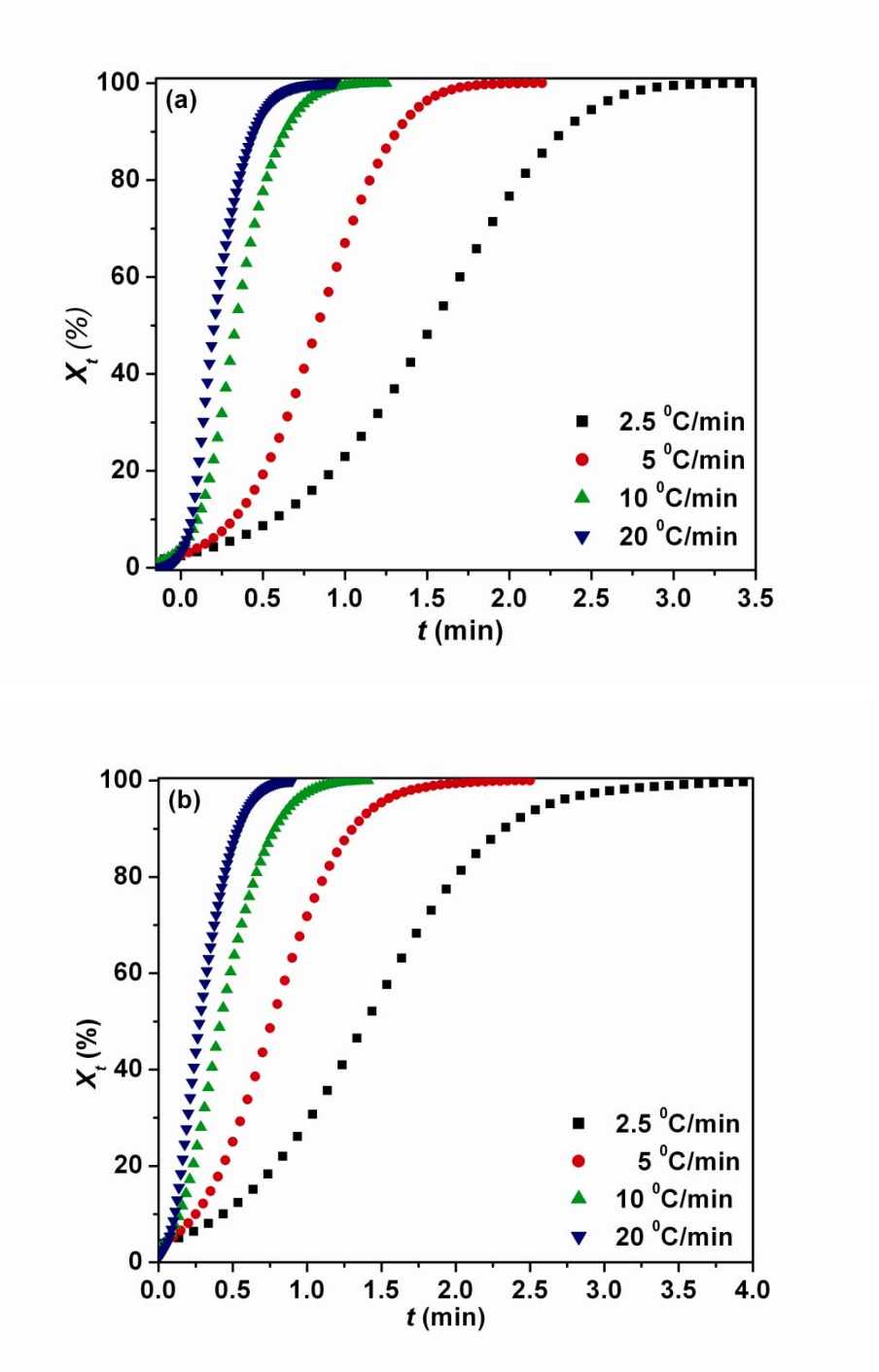

Figure 6.6: The relative degree of crystallinity with time for the crystallization of (a) PP and (b) PPL5 at different cooling rates.

The half crystallization time ($t_{1/2}$) is defined as the half period (i.e 50 % crystallization), from the onset of crystallization and the end of crystallization. The t and $t_{1/2}$ values for PP and its nanocomposites can be obtained from **Figure 6.8**, and the results are listed in **Table 6.2.** It is apparent that the value of $t_{1/2}$ decreases with increasing cooling rate. Moreover, at a given cooling rate, the $t_{1/2}$ value for PP/LDH nanocomposites is lower than that for PP and even decrease with increasing LDH content. These results signify that addition of Mg_2Al-DDS LDH particles could act as heterogeneous nucleating agents to facilitate the overall crystallization process. Such a similar trend was observed in the case of PHB/LDH nanocomposite [10].

Table 6.2: Non-isothermal crystallization parameters T_p, T_o, t and $t_{1/2}$ for PP and its nanocomposites at various cooling rates.

Sample	α (°C/min)	T_p (°C)	t (min)	T_o (°C)	$t_{1/2}$ (min)
PP	2.5	119.60	1.59	123.58	2.10
	5	116.33	0.818	120.42	1.03
	10	113.81	0.359	117.40	0.57
	20	110.15	0.1875	113.92	0.41
PPL1	2.5	132.74	1.7	136.99	1.82
	5	129.18	1.018	134.27	0.89
	10	125.16	0.538	130.54	0.54
	20	121.32	0.237	126.06	0.34
PPL3	2.5	134.44	1.572	138.37	1.55
	5	130.75	0.806	134.78	0.81
	10	126.85	0.424	131.09	0.50
	20	122.85	0.225	127.30	0.33
PPL5	2.5	135.24	1.54	139.09	1.37
	5	131.89	0.602	134.90	0.78
	10	128.17	0.308	131.35	0.48
	20	123.85	0.167	127.59	0.30

In order to understand fully, the evolution of crystallinity during the nonisothermal crystallization, the Ozawa, the Avrami and the Liu model (modified Avrami-Ozawa method) were employed to analyze the nonisothermal crystallization kinetics of PP and its nanocomposites.

6.2.1.1 Nonisothermal Crystallization Kinetics by Using the Ozawa Model

According to Ozawa theory [14], the non-isothermal crystallization process is a result of infinitesimally small isothermal crystallization steps. According to this model, the degree of conversion at temperature *T, X_T,* can be written as a function of cooling rate:

$$1 - X_T = \exp(-K(T)/\alpha^m) \tag{6.4}$$

where, *K(T)* is the function of cooling crystallization, α is the cooling rate and *m* is the Ozawa exponent that depends on the dimension of crystal growth. The double logarithmic form of Eq. 6.4**:**

$$\ln[-\ln(1 - X_T) = \ln K(T) - m \ln \alpha \tag{6.5}$$

A plot of ln[-ln (1-X_T)] versus ln α at a given temperature should result in a straight line if the Ozawa method is valid. The kinetic parameters, *m* and *K(T)* can be obtained from the slope and the intercept, respectively. Ozawa plots for dynamic crystallization of the PP and PPL5 are shown in **Figure 6.7**. The curves in the plot of PP show better linear relationship but PP nanocomposite containing 5% LDH deviates from linearity and an increase in curvature was observed. These results shows that PP/OMMT nanocomposites can be analyzed by the Ozawa method which is in agreement with previously reported [15] but the nanocomposite, PP/LDH cannot be fit by Ozawa Model. The reason for this difference is that, Ozawa in his approach ignored secondary crystallization, dependence of the fold length on temperature [16] and also the constant value of cooling function over the entire crystallization process [17]. Thus, the Ozawa method was found to be inapplicable for the nonisothermal kinetic modelling of PP/LDH nanocomposites.

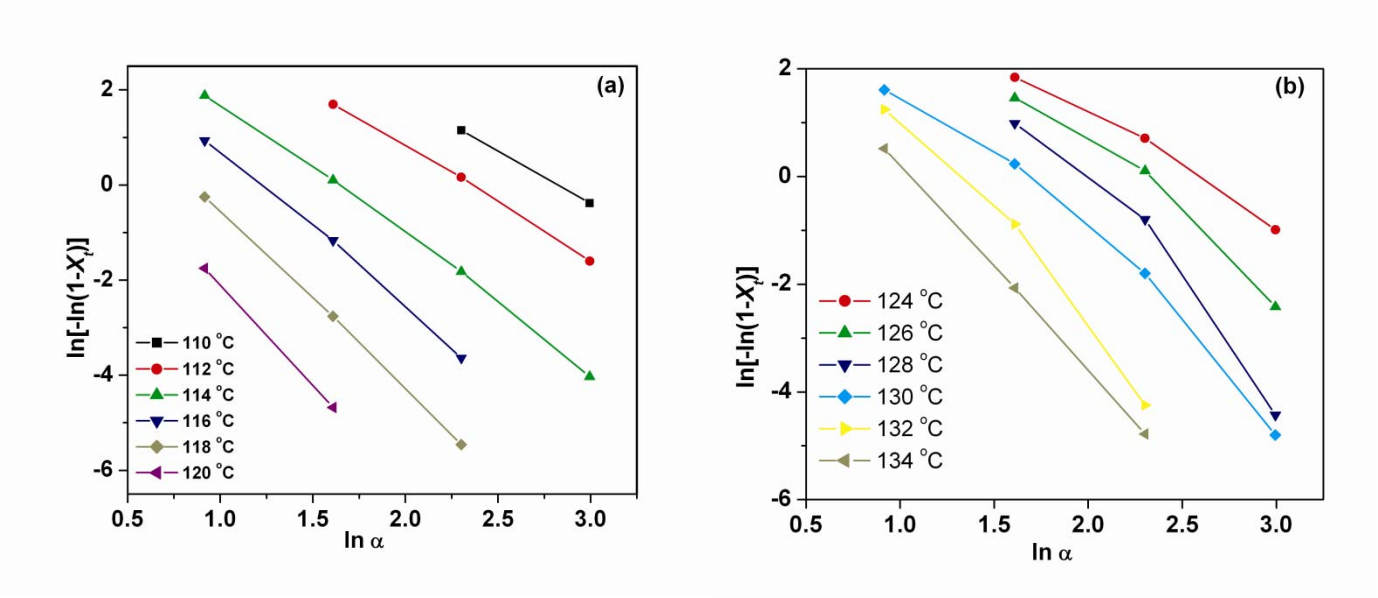

Figure 6.7: Ozawa plots of ln[-ln(1-*Xt*)] versus ln α during nonisothermal crystallization process: (a) PP and (b) PPL5 nanocomposite.

6.2.1.2 Nonisothermal Crystallization Kinetics by Using Avrami Model

Generally isothermal crystallization kinetics is explained by Avrami equation [18] but the Eq. (6.6), was also adopted as an alternative approach [19], according to which the equivalent time dependent crystallinity X_t can be expressed as,

$$X_t = 1 - \exp(-Z_t t^n) \qquad (6.6)$$

Where X_t is relative degree of crystallinity at crystallization time t, n is the Avrami exponent and Z_t is the crystallization rate constant involving both nucleation and growth rate parameters. As before Eq.6 can be liberalized in its double logarithmic form to give Eq.6.7.

$$\ln[-\ln(1 - X_T) = \ln Z_t + n \ln t \qquad (6.7)$$

By fitting the experimental data to Eq.6.7, the values of n and Z_t can be obtained from the slope and intercept of the plots of ln[-ln (1-X_t)] versus ln t for each cooling rate as shown in **Figure 6.8.** From this figure it can be seen that the straight lines are obtained in each cooling rate. It should be taken into account that in nonisothermal crystallization, Z_t and n do not have same physical significance as in isothermal crystallization because under nonisothermal crystallization, the temperature changes constantly. Since the rate of nonisothermal crystallization depends on the cooling rate, Jeziorny [20], suggested that

the rate parameter Z_t should be corrected for the influence of cooling rate α of the polymer. The parameters characterizing the kinetics of nonisothermal crystallization was given as follows:

$$\ln Z_c = \ln Z_t / \alpha \tag{6.8}$$

The results obtained from the Avrami plots and the Jeziorny methods are listed in **Table 6.3.**

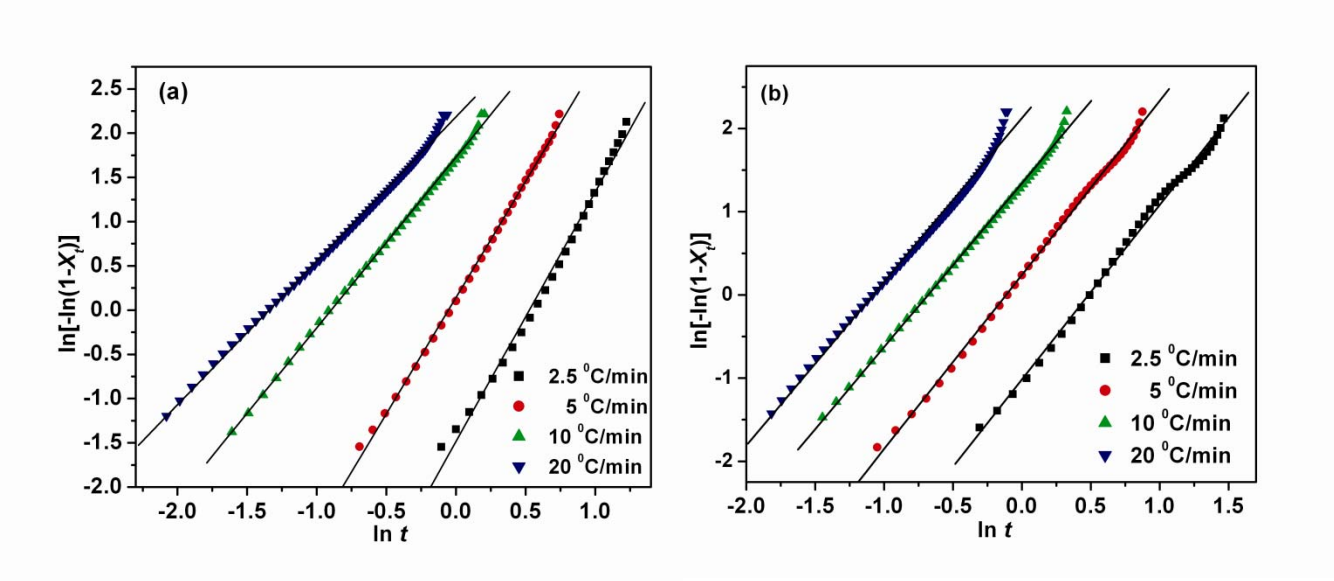

Figure 6.8: Avrami plots of ln[-ln (1-X_t)] versus ln t for nonisothermal crystallization process for (a) PP and (b) PPL5 nanocomposite.

The Avrami exponent is known to be influenced by the molecular weight, nucleation type, and secondary crystallization, and in general, not much influenced by the temperature. The values of the Avrami exponent for PP-LDH nanocomposites are higher (varied from 1.9 to 2.9) than that for pure PP (varied from 1.6 to 2.8) for given cooling rate, indicating that LDH nano-layers act as nucleating agents and governs a typical heterogeneous nucleation mechanism in the crystallization kinetics of PP-LDH nanocomposites. The Z_c values of the PP-LDH nanocomposites are, as expected, higher than that of the pure PP as the same cooling rate, showing that incorporation of nano LDH could crystallize PP at quicker rate. These results are similar to other 2D reinforcing PP nanocomposites [7, 21].

Table 6.3: Nonsiothermal crystallization parameters obtained by Avrami and Jeziorny methods

Sample	α (°C/min)	ln Z_t	Z_c	n
PP	2.5	0.84	2.52	2.82
	5	1.48	2.40	2.62
	10	1.72	1.74	1.92
	20	2.18	1.55	1.62
PPL1	2.5	0.85	2.55	2.81
	5	1.48	2.41	2.09
	10	1.77	1.79	1.87
	20	2.14	1.52	1.62
PPL3	2.5	0.87	2.61	2.85
	5	1.52	2.50	2.28
	10	1.67	1.70	1.93
	20	2.16	1.54	1.70
PPL5	2.5	1.01	2.99	2. 95
	5	1.63	2.78	2. 95
	10	1.83	1.86	2.06
	20	2.12	1.58	1.96

6.2.1.3 Nonisothermal Crystallization Kinetics by Liu Model (Modified Avrami–Ozawa Models)

Liu and coworkers [22] developed a method by combining the Ozawa and Avrami equations to describe the nonisothermal crystallization kinetics which is applicable in many nanocomposites systems [7, 23]. Therefore, the corresponding kinetic equation was used here to study the nonisothermal crystallization behavior of the PP-LDH nanocomposites. As the degree of crystallinity was related to the cooling rate α and the crystallization time t (or temperature T), the relation between α and t could be defined for a given degree of crystallinity. Consequently, using equation (6.3) and combining equations (6.5) and (6.7), a new kinetic model is derived for nonisothermal crystallization:

$$\ln Z_t + n \ln t = K(T) - m \ln \alpha \tag{6.9}$$

At given crystallinity X_t, Eq.6.9 can be rearranged to

$$\ln \alpha = \ln F(T) - a \ln t \tag{6.10}$$

where, $F(T) = [K(T)/Z_t]^{1/m}$ refers to the value of cooling rate that must be selected within a unit of crystallization time when the measured systems reaches a certain degree of crystallinity; and a is the ratio of Avrami exponent n to Ozawa exponent (m) that is n/m. It can be seen that $F(T)$ has a definite physical and practical meaning. Indeed, according to eq.6.10, at a given degree of crystallinity, plotting ln α versus ln t should yield a linear relationship. The kinetic parameters $F(T)$ and α are determined from the intercept and slope of the lines, respectively. Plots of ln α vs ln t at various degree of crystallinity for PP and PP/LDH nanocomposites are presented in **Figure 6.9**. It can be seen that these plots show good linearity, which verifies the advantage of the combined approach applied in this case. The values for a and $F(T)$ are listed in Table 4. The value of a varies from 1.08 to 1.19 for pure PP and from 1.10 to 1.25 for PP/LDH nanocomposites. Almost all a values of neat PP are lower than those of its nanocomposites at the same relative degree of crystallinity. This phenomenon is similar to the earlier reports of PP/SiO_2 [24], PP/clay [25] and PP/CNT [3].

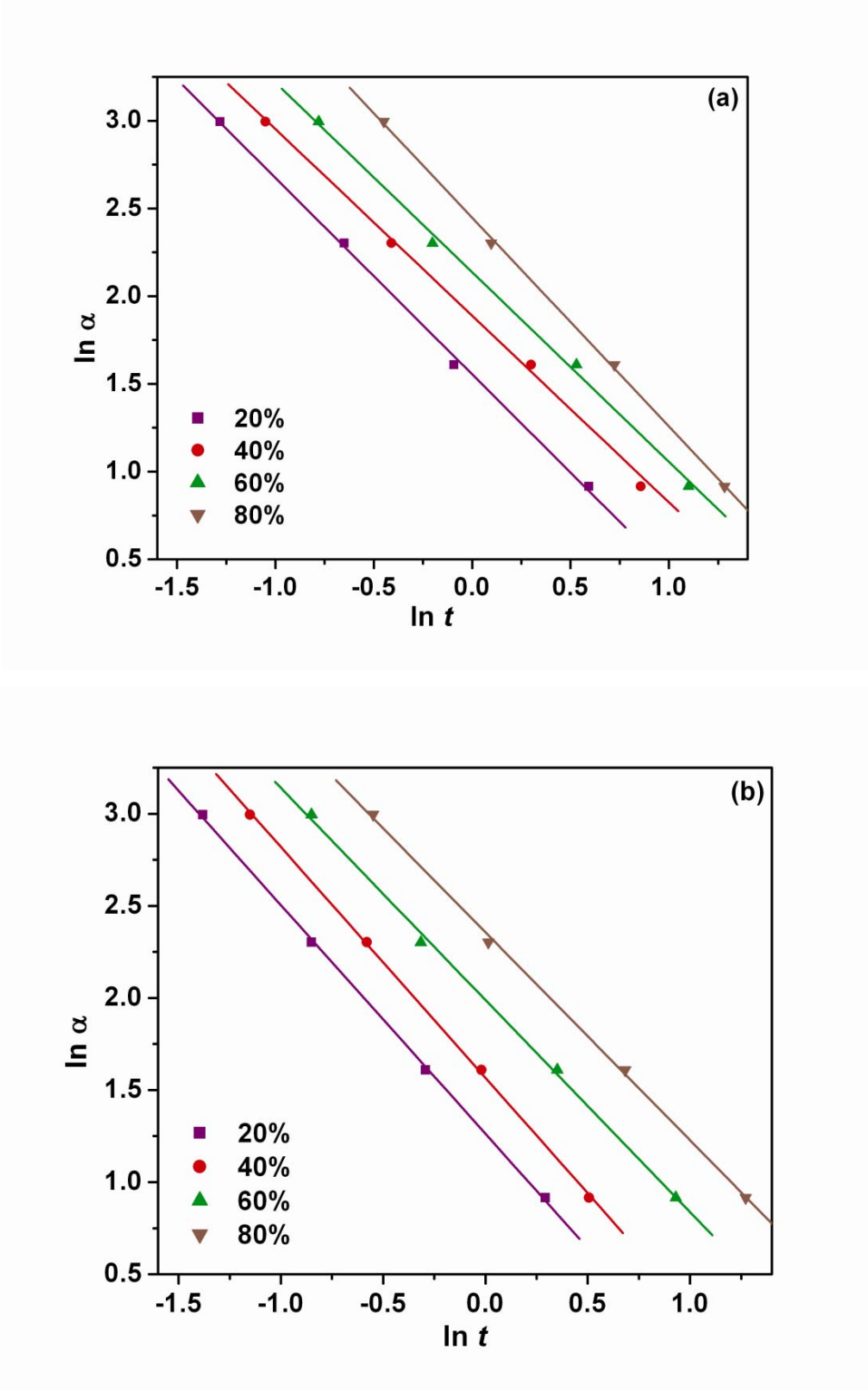

Figure 6.9: Plots of ln α versus ln t during the nonisothermal crystallization process for (a) PP and (b) PPL5 nanocomposite.

The values of $F(T)$ systematically increase with increasing relative degree of crystallinity and are lower in the presence of nano-scale reinforcement as reported for other nano-scale reinforcements [3-4, 8, 24-25,] which indicates that PP/LDH nanocomposites crystallize at a faster rate than PP.

Table 6.4 Kinetic parameters for the PP and PP–LDH nanocomposites at different relative degrees of crystallinity by Liu method.

Sample	X_t *(%)*	a	F(T)
PP	20	1.08	4.71
	40	1.06	6.55
	60	1.12	8.41
	80	1.19	11.47
PPL1	20	1.10	4.52
	40	1.13	6.11
	60	1.12	8.15
	80	1.17	11.03
PPL3	20	1.12	3.85
	40	1.13	5.63
	60	1.19	6.87
	80	1.23	10.74
PPL5	20	1.12	3.52
	40	1.15	4.75
	60	1.24	7.24
	80	1.25	10.48

6.2.2 Nucleation Activity

Dobreva and Gutzow [26] suggested a simple method for calculating the nucleation activity of foreign substrates in a polymer melt. Nucleation activity (Φ) is a factor by which the work of three-dimensional nucleation decreases with the addition of a foreign substrate. If the foreign substrate is extremely active, w approaches 0 while for inert particles Φ approaches 1. The nucleation activity is calculated from the ratio:

$$\Phi = \frac{B^*}{B} \qquad 6.11$$

The parameter *B* can be experimentally obtained from crystallization experiences through the following relationship proposed by Dobreva and Gutzow:

$$\log \alpha = \text{const} - \frac{B}{2.303 \Delta T^2} \qquad 6.12$$

where *q* is the crystallisation rate, ΔT is the undercooling (T_m- T_c), T_m the polymer melting temperature and T_c the crystallisation peak temperature. In Eq. (2) B^* represent the value of B when the polymer crystallizes in presence of a nucleation substrate, and B when there is no nucleation agent. The value of Φ can vary from 1 to 0. It decreases as the nucleation activity increases. The approach was successfully applied to evaluate nucleating rate differences of PP containing different mineral fillers [27-31].

From the definition of B, the polymer crystal surface energy (σ) can be estimated:

$$B = \frac{16 \pi \sigma^3 V_m^2}{3 n k T_m \Delta S_m^2} \qquad 6.13$$

and the lamella thickness (L), from the variant of the Gibbs-Thomson equation for a crystal of large lateral dimensions and finite thickness:

$$T_m = T_m^0 \left[1 - \frac{2\sigma_e}{L\Delta H_m} \right] \qquad 6.13$$

In the above equations, *k* is the Boltzman's constant, T_m the PP melting temperature, ΔH_m the PP melting enthalpy and σ_e the specific surface energy. The polypropylene molar volume (V_m) can be taken equal to 28 cm^3 mol^{-1}, the molar entropy (ΔS_m) 24.2 JK^{-1}, the Avrami exponent n=3, and the melting temperature at equilibrium (T_m^0) 479 K [29].

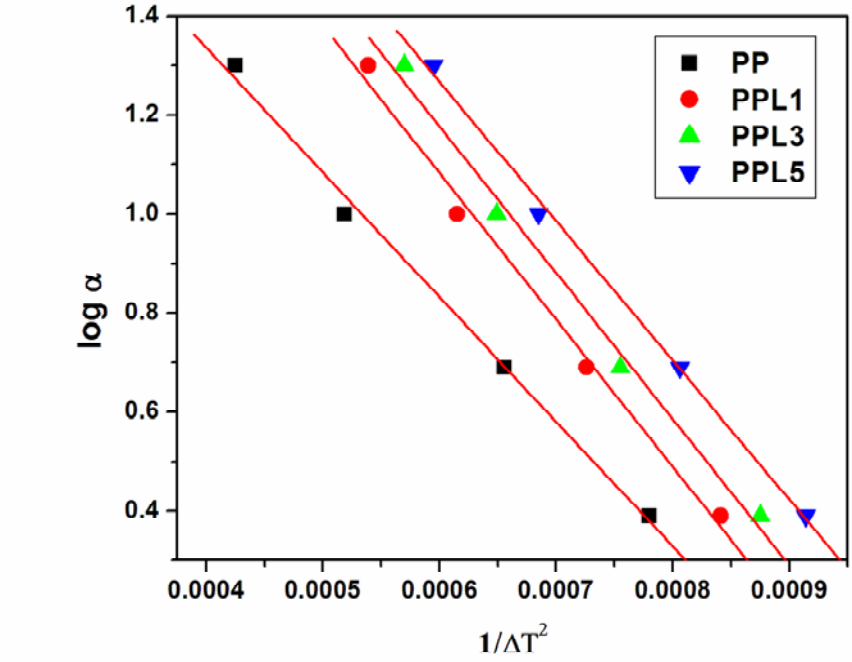

Figure 6.10: Plot of log α vs. 1/ ΔT^2 for PP and PP/LDH nanocomposites.

The slopes, B* and B of linear plots of log φ vs $1/\Delta T^2$ (**Figure 6.10**) are used to determine Φ. The values of nucleating activity calculated are 0.83, 0.75, and 0.69 for PPL1, PPL3, and PPL5 nanocomposites, respectively. This result shows that organomodified LDH is an effective nucleating agent for polypropylene. The LDH layers are the active substrates for the heterogeneous nucleation. With the presence of the active substrates, the free energy opposing primary nucleation can be decreased.

6.2.3 Effective Activation Energies for Nonisothermal Crystal Growth

Apart from the aforementioned macroscopic kinetic models, it is also interesting to evaluate the effective activation energy ΔE for a non-isothermal crystallization process. Considering the variation of the peak temperature with the cooling rate α, several mathematical procedures have been proposed in literature for the calculation of ΔE [32, 33]. Among them Kissinger's method [34] was one of the most popular approach of evaluating effective activation energy of non-isothermal crystallization:

$$\frac{d[\ln(\alpha/T_p^2)]}{d(1/T_p)} = -\frac{\Delta E}{R} \qquad 6.14$$

Values of the effective activation energy were calculated using the Kissinger's method for all nanocomposites listed in **Table 6.5.,** with the data obtained from the plot of (a) $\ln(\alpha/T_p^2)$ versus $1/T_p$ and (b) $\ln(\alpha)$ versus $1/T_p$ by multiplying the slope by gas constant R as shown in **Figure.6.11** which are approximately linear.

The results show that the activation energy is strongly dependent on the LDH content. In Kissinger approach, it is observed that the activation energy of PP is 314.2 kJ/mol, which drastically decreases with the presence of 1 wt% LDH (PPL1) in PP/LDH nanocomposites (259.3 kJ/mol) and then increases with increasing LDH content (268.3 kJ/mol for 3 wt% LDH (PPL3) and 297.9 kJ/mol for 5 wt% LDH (PPL5) in PP/LDH nanocomposites. These results indicate that the addition of 1 wt% LDH into PP probably induces the heterogeneous nucleation (lower ΔE*)*. The addition of more LDH into the PP matrix causes more heterogeneous nucleation, which is expected to produce a lower ΔE but the addition of more LDH also reduces the transportation ability of polymer chains and prevents the PP macromolecule segment from rearranging, and as a result, increases the activation energy during crystallization process.

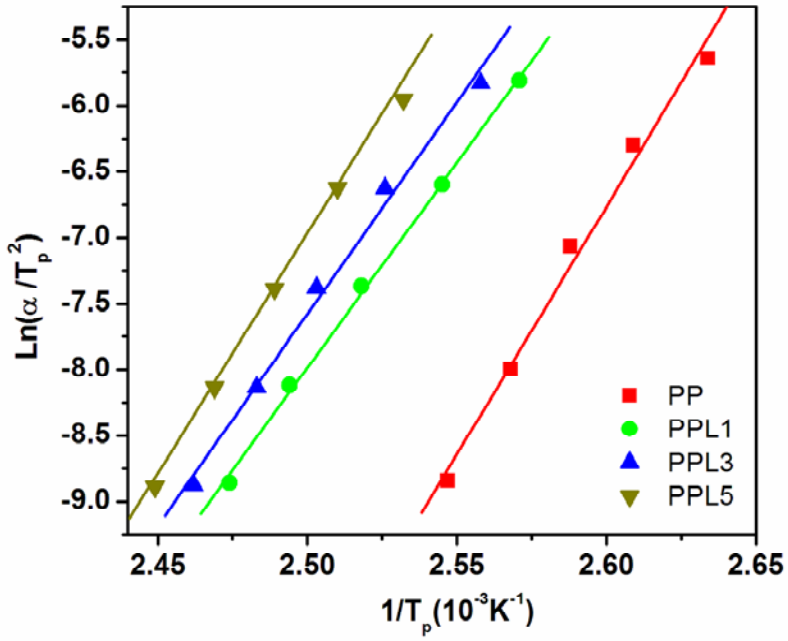

Figure 6.11: Determination of crystallization activation energy ΔE for PP and PP/LDH nanocomposites based on Kissinger approach

Recently, a major concern has been raised for the use of these procedures in obtaining ΔE, since they have been formulated for heating experiments (i.e., positive values of α). Vyazovkin [35] has demonstrated that dropping the negative sign for a is a mathematically invalid procedure that generally makes the Kissinger equation inapplicable to the processes that occur on cooling. Moreover, the use of this invalid procedure may result in erroneous values of the effective energy barrier, ΔE. The use of multiple heating rate methods such as isoconversion methods is recommended. An isoconversion method can in principle be applied to non-isothermal crystallisations for evaluating the dependence of the effective activation energy on conversion and temperature. Such dependencies have been quite helpful in detecting and elucidating complex kinetics in polymeric systems. The more popular representatives of these methods are the advanced isoconversion method of Vyazovkin and Sbirrazzuoli [36] and the differential isoconversion methods of Friedman, Flynn and Wall, and Ozawa [14, 37-38]. However, the latter is likely to be inapplicable to melt crystallisation because it

requires calculation of the logarithm of the heating rate, which is negative for a cooling process. Therefore, the differential isoconversion method of Friedman [37] and the advanced integral isoconversion method of Vyazovkin [39] are the most appropriate. In this investigation, the method of Friedman was used. According to the differential isoconversion method of Friedman, different effective activation energies are calculated for every degree of crystallinity from:

The Friedman equation is expressed as:

$$\ln(dX/dt)_X = \text{Constant} - \frac{\Delta E_X}{RT_X} \quad (6.15)$$

where, dX/dt is the instantaneous crystallization rate as a function of time at a given conversion X. According to this method, the X_t function obtained from the integration of the experimentally measured crystallization rate is initially differentiated with respect to time to obtain the instantaneous crystallization rate, dX/dt. Furthermore, by selecting appropriate degrees of crystallinity (i.e. from 2 to 98%) the values of dX/dt at a specific X are correlated to the corresponding crystallization temperature at this X, i.e. T_X. Then, by plotting the left hand side of Eq.13 with respect to $1/T_x$ a straight line must be obtained with a slope equal to $\Delta E_X/R$. Plots of ln(dX/dt) versus $1/T_{X,}$ at different relative crystallinity are obtained as a straight lines, permitting thus, the calculation of the effective energy barrier at different degrees of crystallinity. The correlation coefficient obtained were always greater than 0.980.

Furthermore, the dependence of the effective activation energy on the context of relative crystallization of the PP and PP/LDH nanocomposites is presented in **Figure 6.12 (a).** As it can be seen, ΔE is strongly dependant on the LDH content and increases with the increase in relative degree of crystallinity for all nanocomposites and neat PP at $X > 20\%$. In all the cases, ΔE takes great negative values at lower extent of conversion that corresponds to temperature closer to the melting point. For the nanocomposites, it is observed that 1% LDH show lower values of ΔE and then increases with increasing LDH content. These results indicate that the addition of 1% LDH in to PP causes more heterogeneous nucleation (lower ΔE). The addition of more LDH expected to cause more heterogeneous nucleation but higher the content of LDH also reduces transportation ability of polymer chains and prevents the PP macromolecule segment from rearranging,

and as a result, increases the ΔE during crystallization process. Accordingly, the addition of LDH may accelerate the overall nonisothermal crystallization process of PP.

Furthermore, according to recent reports, the effective activation energy barrier can be plotted as a function of temperature by taking an average temperature associated with certain α value [40], such plots can be seen in **Figure.6.12 (b).** It can also be seen, again at given crystallization temperature, the 1% LDH nanocomposite exhibits lower value of the effective activation energy while the 5% LDH shows higher ΔE. The values of ΔE were negative, indicating that the rate of crystallization increased with decreasing temperatures. The absolute value of ΔE for 5% nanocomposites were higher than that of PP, which revealed that polypropylene segments require more energy to rearrange in presence of LDH, since LDH nano layers might hinder the mobility of chain segments. These plots also can be used in evaluating Lauritzen-Hoffman parameters, K_g and U^*. The temperature dependence of the effective activation energy is defined as:

$$E_\alpha(T) = U^* \frac{T^2}{(T - T_\infty)^2} + K_g R \frac{T_m{}^2 - T^2 - T_m T}{(T_m - T)^2 T} \qquad (6.16)$$

By performing the non-linear curve fitting based on Levenberg-Marquardt method [54,55] to the experimental data, the parameter K_g can be evaluated. The estimated values of K_g are listed in **Table 6.5**. and found linearly decrease with LDH %. The values of K_g are found to be close to those reported for isothermal crystallization and are used for determination of surface free energy by using Eq.12. Herewith, isconversional method has been successfully employed for non-isothermal crystallization behavior of PP/LDH nanocomposites.

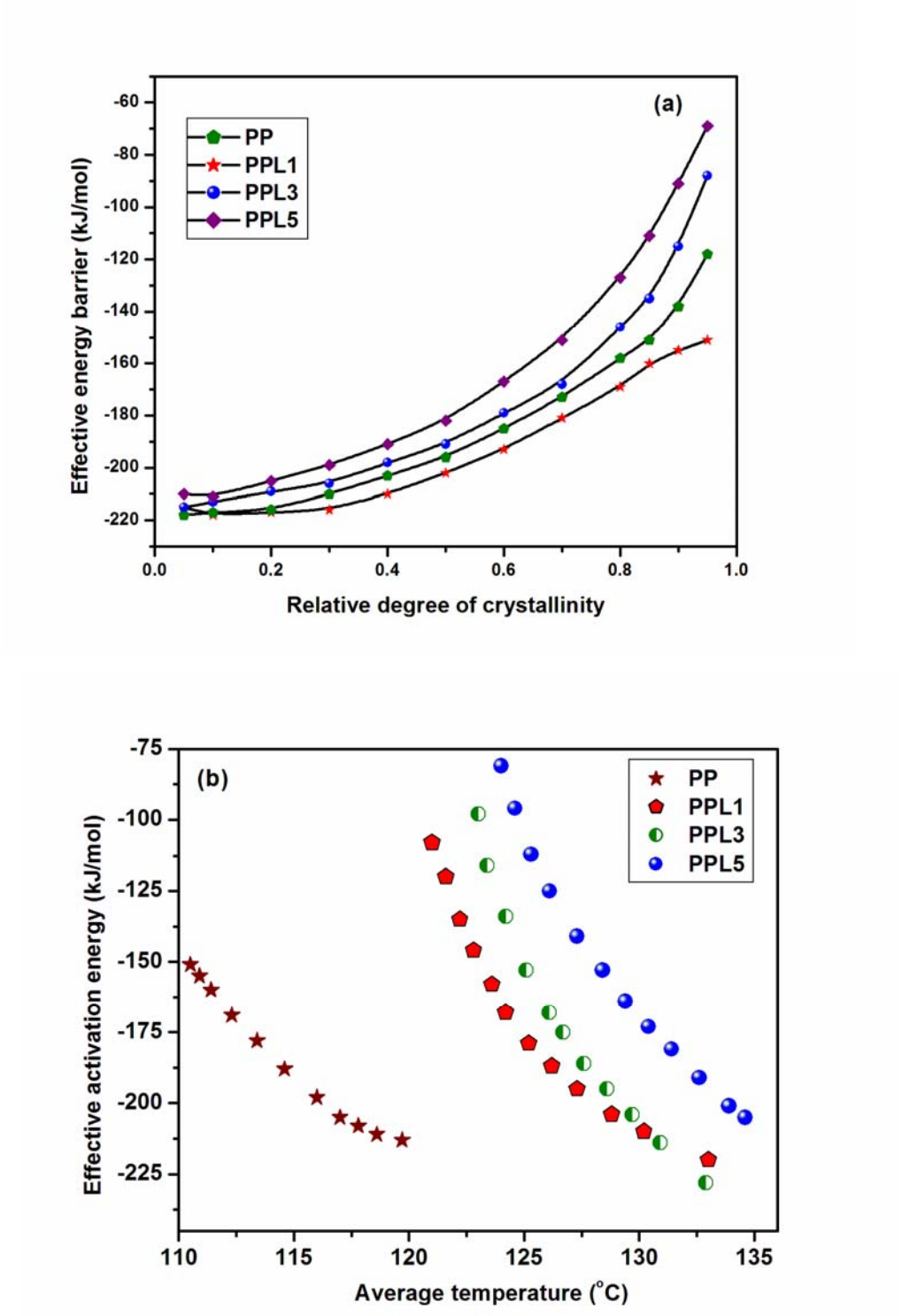

Figure 6.12. Dependence of the effective activation energy on the extent of a) relative crystallization b) average temperature (isoconversional analysis) for the PP and PP/LDH nanocomposites.

Table 6.5 Interfacial free energies (σ_e) and kinetic parameter (K_g) under different crystallization processes.

Sample	ΔE (kJ/mol)	K_g (10^5 K^2)[a]	σ_e (erg/cm^2)[a]	K_g (10^5 K^2)[b]	σ_e (erg/cm^2)[b]
PP	314.2	10.21	125.3	10.18	124.9
PPL1	259.3	9.57	108.4	9.61	108.8
PPL3	268.3	8.85	94.2	8.87	94.4
PPL5	297.9	7.91	87.8	7.86	87.2

[a]Isothermal crystallization
[b]Isoconversional approach/non-isothermal crystallization

6.3 Isothermal Crystallization Behavior

To analyze the effect of temperature on the crystallization of the PP/LDH nanocomposites, the DSC crystallization isotherms at different crystallization temperatures were obtained. Samples were heated to 200 °C at a rate of 10 °C/min under a nitrogen atmosphere and held for 5 min to destroy any residual nuclei. Then it was rapidly cooled to certain isothermal crystallization temperatures (T_c), and held to allow complete crystallization. After the isothermal crystallization was finished, the samples were heated to 200 °C at a rate of 10 °C /min to estimate melting profile of the samples.

The **Figure 6.13** shows the typical isothermal crystallization exotherm. The curve shows induction time (t_i) and total crystallization time (t_c). The induction time is the time required to initiate the isothermal crystallization while the total crystallization time is total time required to complete the crystallization process.

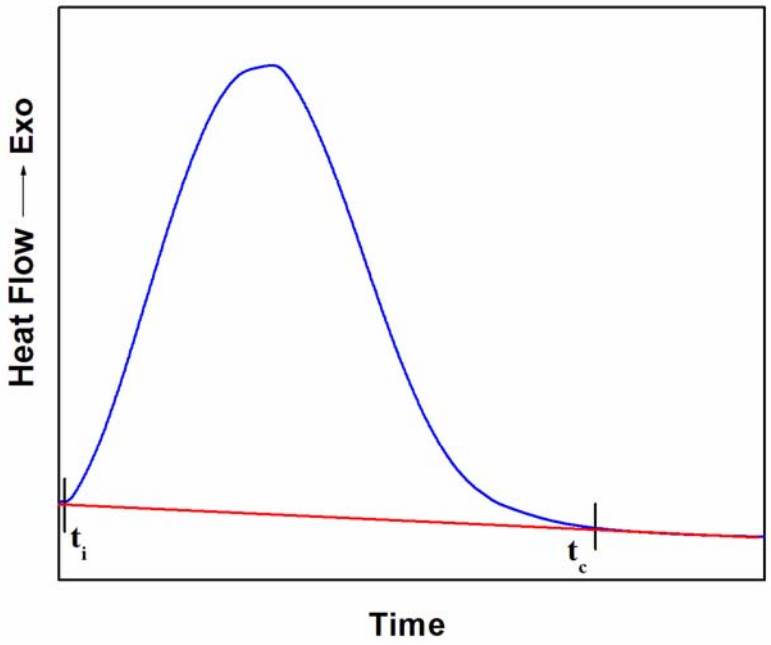

Figure 6.13: A typical isothermal crystallization exotherm

The crystallization kinetics of PP and PP/LDH nanocomposites were studied by differential scanning calorimetry (DSC). **Figure 6.14**, shows the DSC crystallization exotherms for PP and PP/LDH nanocomposites that had been isothermally crystallized

at different crystallization temperatures (T_c). It was observed that as the supercooling, i.e the difference between the melting and crystallization temperature, decreases and the exothermal peak becomes broader which implies that the crystallization rate is reduced as the T_c increases. Thus, the induction time of the exotherm increases. The position of the crystallization peaks of PP/LDH nanocomposites appeared earlier than that of PP. It is evident that the crystallization rate of PP can be enhanced greatly by adding layered double hydroxides type nano fillers. In the case of PP, the interval was between 118-126 °C and in the case of PP/LDH; this interval shifts to higher crystallization temperatures 122-130 °C. This shift revealed that the LDH nano particles are acting as nucleating agent during the course of isothermal crystallization of PP/LDH nanocomposite. This phenomenon is in agreement with earlier reports describing the effect of nano-fillers on crystallization behaviors of polypropylene [8, 42]. However, the crystallinity value of PP in the nanocomposites is found to be almost independent of LDH content. Therefore, it can be concluded that the incorporation of the LDH increased the crystallization rate of PP chains without increasing the level of crystallinity.

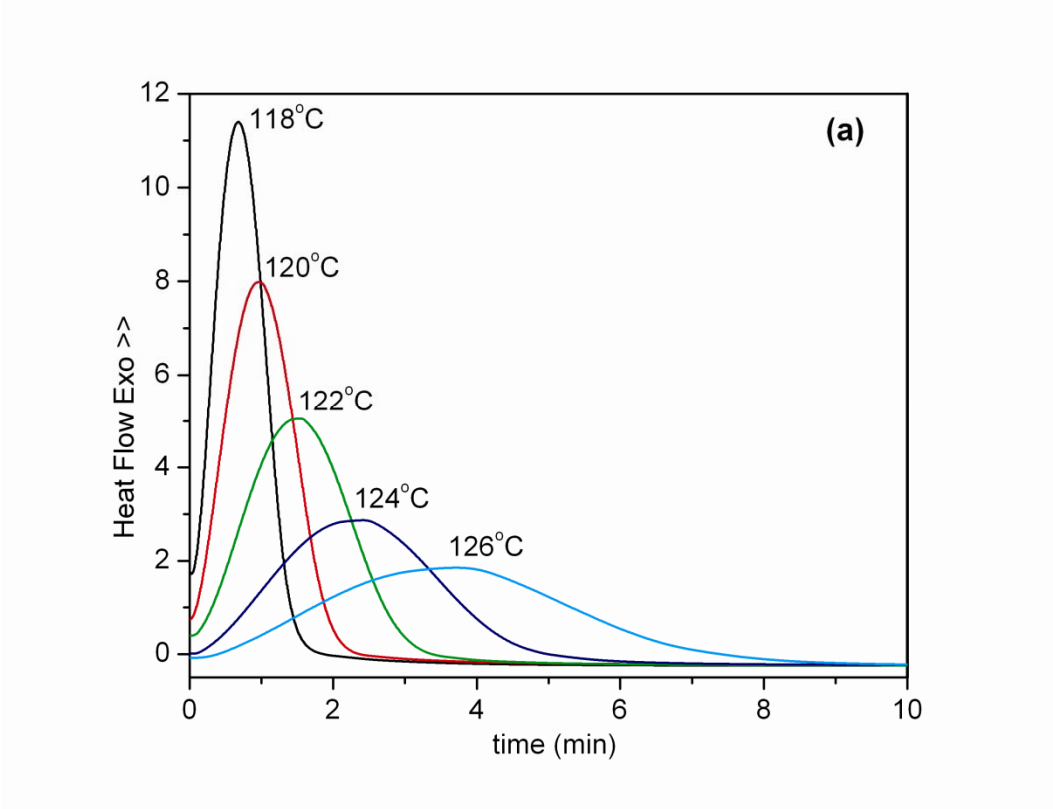

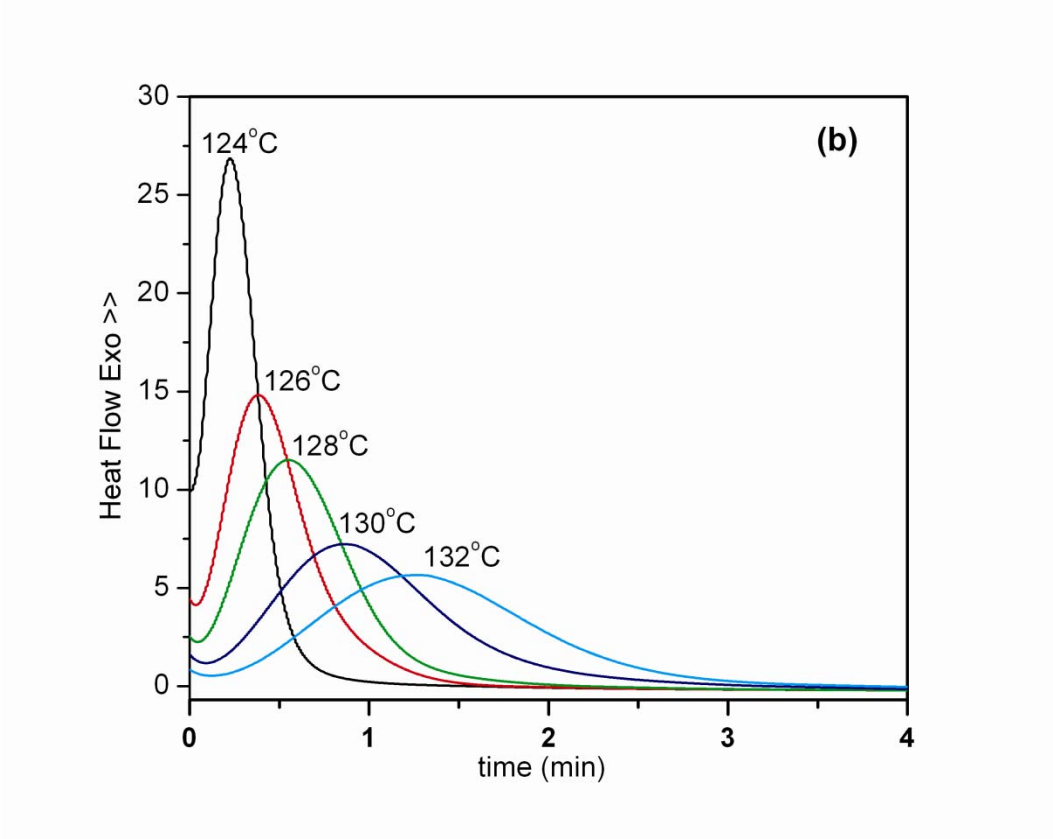

Figure 6.14: DSC thermograms of isothermal crystallization at different crystallization temperature: (a) PP, (b) PPL5

In order to further analyze the isothermal crystallization process, the crystallization kinetics of PP and PP/LDH nanocomposites is compared. From dynamic crystallization experiments, data from the crystallization exotherms as a function of temperature; dH_c/dt can be obtained, for each crystallization temperature. The relative degree of crystallinity as a function of temperature, X_t, can be calculated according to the following equation:

$$X_t = \frac{\int_0^t (dH_c/dt)dt}{\int_0^\infty (dH_c/dt)dt} \qquad (6.17)$$

Where, dH_c denotes the measured enthalpy of crystallization during and isothermal time interval dt. The limits t and ∞ denotes the elapsed time during the course of crystallization and at the end of the crystallization process, respectively.

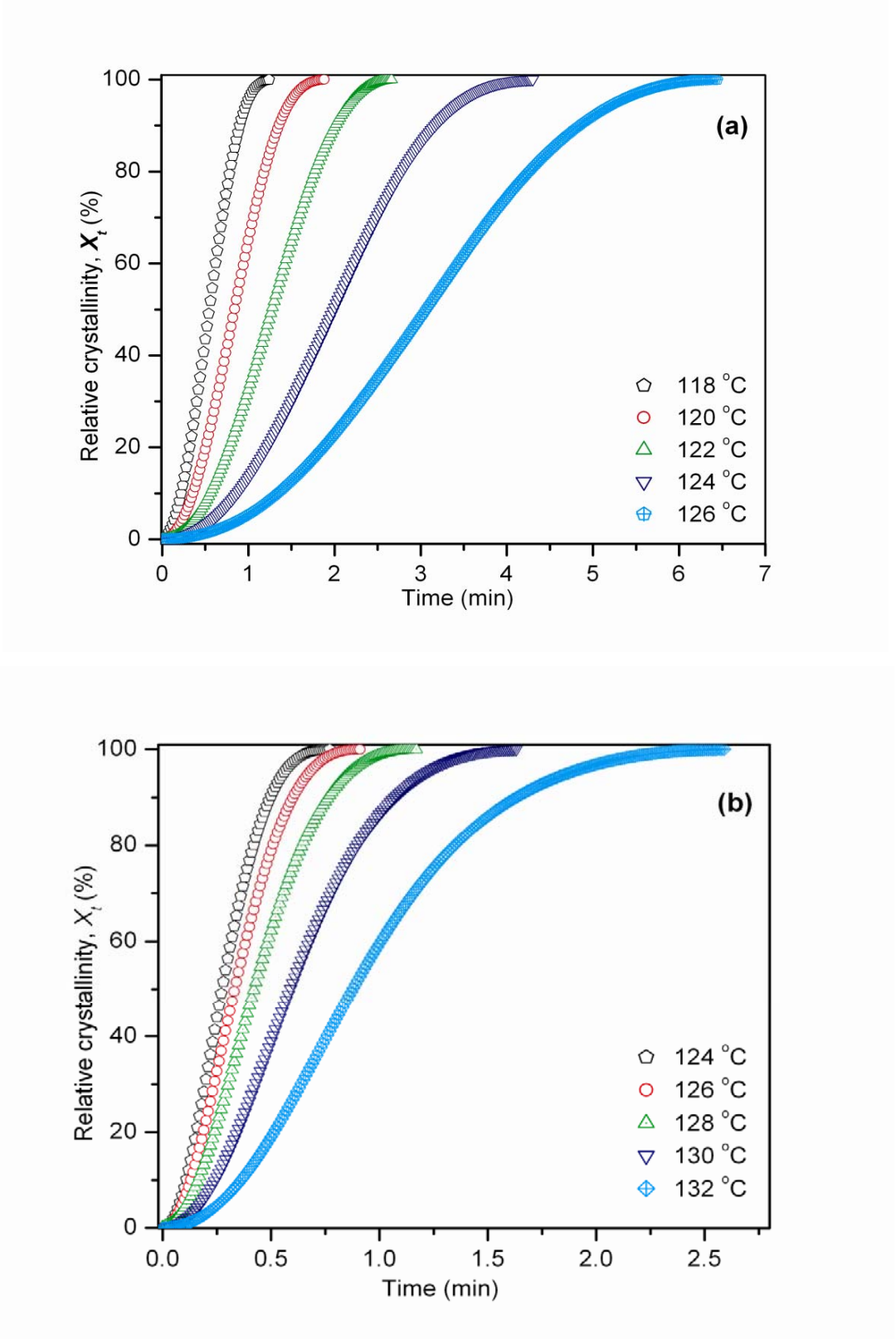

Figure 6.15: The relative degree of crystallinity with time for the crystallization of (a) PP and (b) PPL5 at different crystallization temperatures.

The development of relative degree of crystallinity X_t as a function of time, *t,* for PP and its nanocomposites at various crystallization temperatures is shown in [**Figure 15(a-b)**]. The plots of X_t versus time for PP and PP/LDH (5%) nanocomposites are similar and all these curves have the same sigmoidal shape, implying that only a lag effect of temperature on crystallization is observed. The half crystallization time ($t_{1/2}$), which is direct measure of rate of crystallization can be defined as the half period (i.e 50 % crystallization), from the onset of crystallization and the end of crystallization.

The $t_{1/2}$ values for PP and its nanocomposites can be obtained from **Figure 6.15**, and the results are listed in **Table 6.6**. It is apparent that the value of $t_{1/2}$ decreases with increasing crystallization temperature. Moreover, at a given crystallization temperature, the $t_{1/2}$ value for PP/LDH nanocomposites is lower than that for PP and even decrease with increasing LDH content. The kinetic constant (k) of the PP/LDH hybrid is higher than that of PP at give crystallization temperature. These results signify that addition of Mg_2Al-DS LDH particles act as heterogeneous nucleating agents to facilitate the overall crystallization process.

6.3.1 Isothermal Crystallization Kinetics

In order to understand fully, the evolution of crystallinity during the isothermal crystallization, the Avrami model [18] was employed to analyze the isothermal crystallization kinetics of PP and its nanocomposites. As we know, the Avrami theory has been widely and successfully used for the interpretation of isothermal crystallization processes, according to which the equivalent time dependent crystallinity X_t can be expressed as shown in eq. 6.6 and 6.7. By fitting the experimental data to these equations, the values of n and k can be obtained from the slope and intercept of the plots of log [-ln (1-X_t)] versus log t for each cooling rate shown in Figure 6. The experimental data appear to fit very well with the Avrami equation at the primary crystallization stage, and plots of log [-ln (1-X_t)] versus log t at different T_c values and LDH content. As it can be seen the straight lines are obtained showing good relationship at each cooling rate.

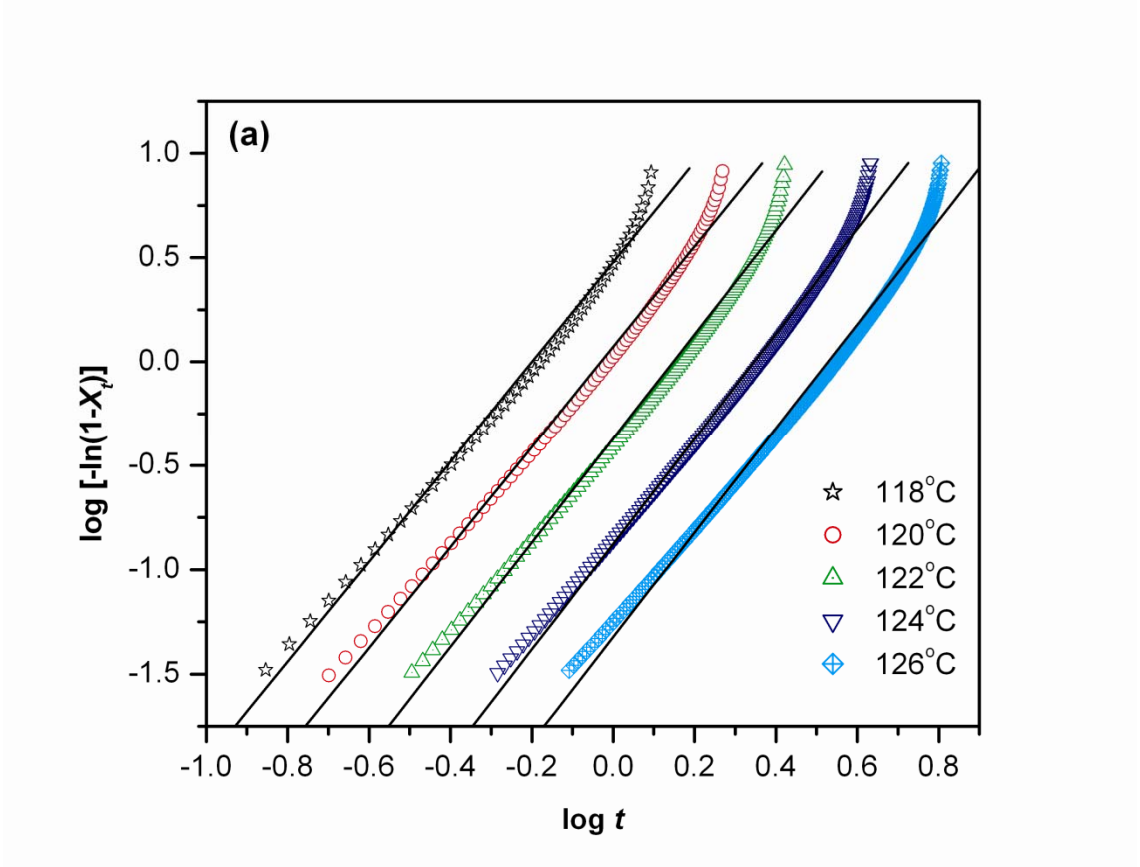

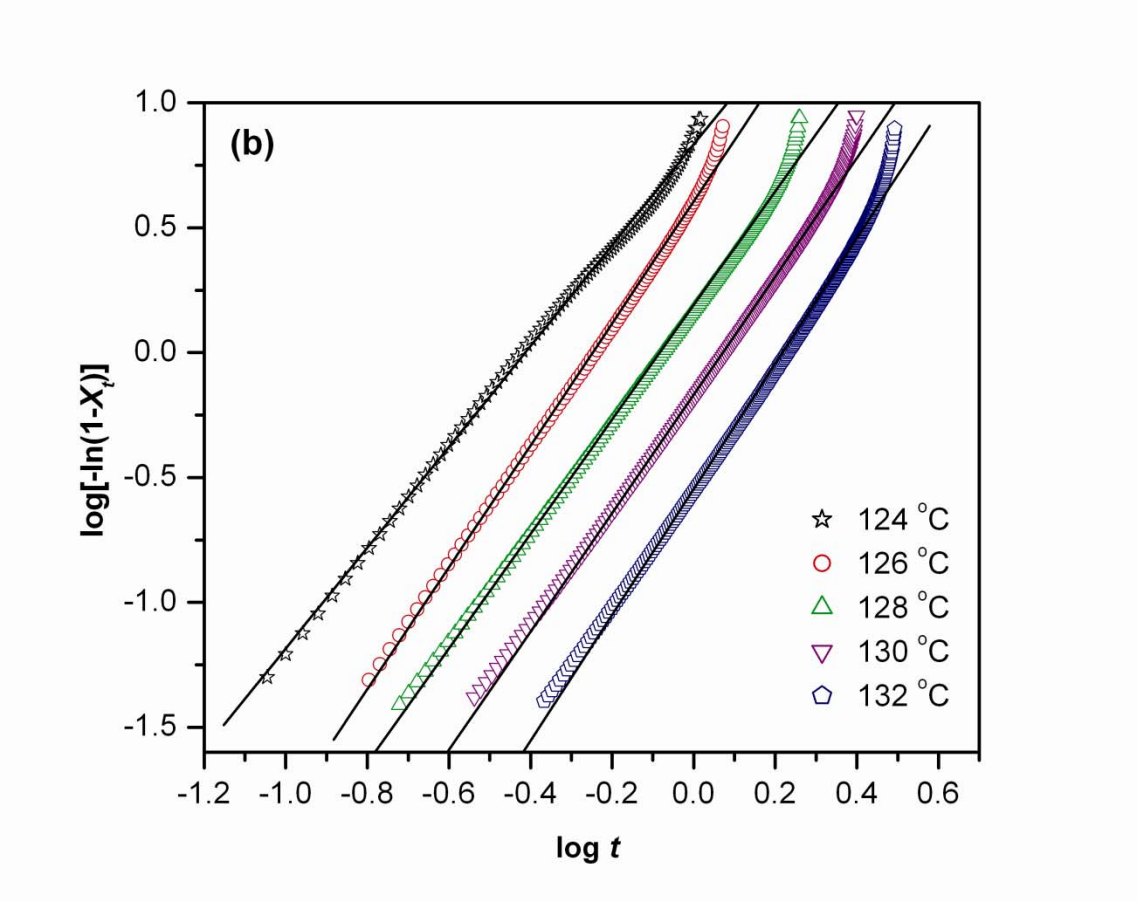

Figure 6.16: Avrami plots of log [-ln (1-X_t)] versus log t for isothermal crystallization process for (a) PP and (b) PPL5 nanocomposite.

Table 6.6 The Avrami parameters for Isothermal Crystallization of PP/LDH nanocomposites

Sample	T_c (°C)	*n*	k x 10^{-2} (min^{-n})	T_m (°C)	$t_{1/2}$ (min)
PP	118	2.39	2.99	157.3	0.55
	120	2.40	1.17	157.5	0.84
	122	2.49	0.43	158.0	1.28
	124	2.52	0.134	158.7	2.0
	126	2.50	0.047	157.8	3.08
PPL5	124	2.01	28.18	163.2	0.33
	126	2.44	6.67	163.9	0.42
	128	2.28	3.98	164.1	0.59
	130	2.36	0.69	164.6	0.88
	132	2.51	0.28	165.1	1.09

6.3.2 Crystallization Activation Energy

The crystallization thermodynamics and kinetics of the nanocomposites have been analyzed on the basis of the theory of Hoffman–Lauritzen [42-43]. Accordingly, the linear crystal growth (*G*) of polymer spherulites can be expressed as the following:

$$G = G_0 \exp\left[-\frac{U^*}{R(T_c - T_\infty)}\right]\exp\left[-\frac{K_g}{T_c \Delta T f}\right] \tag{6.18}$$

$$\ln G + \left[\frac{U^*}{R(T_c - T_\infty)}\right] = \ln G_0\left[-\frac{K_g}{T_c \Delta T f}\right] \tag{6.19}$$

where G_0 is the pre-exponential factor, U^* is the activation energy of the segmental jump, the first exponential term contains the contribution of diffusion process to the growth

rate, while second exponential term is contribution to the nucleation process; U^* and T_∞ are the Vogel-Fulcher-Tamman-Hesse (VFTH) parameters describing the transport of polymer segments across the liquid /crystal interphase, $\Delta T = T_m - T_c$ the under cooling, $f = 2T_c(T_m + T_c)$ the correction factor. The universal values used for the VFTH parameters are U^* =1500 cal/mol (6300 J/mol) and T_∞=(T_g -30) K [43]. In this study, the T_g value of PP used was 270K [44] and the equilibrium melting temperature T_m was set equal to 212.1 °C. This value found by Marand and coworkers [45] using nonlinear Hoffman-Weeks extrapolation. The kinetic parameter i.e nucleation constant, K_g is the term connected with the energy required for the formation of the nuclei of critical size and can be expressed as:

$$K_g = \frac{nb\sigma\sigma_e T_m}{\Delta h_f k_B} \tag{6.20}$$

where n is the variable that considers the crystallization regime and assumes the value n = 4 for regime I and III and n = 2 for regime II [46]. In the present work, the crystallization is assumed to take place in regime III according to Marand et al.[45], b is the distance between two adjacent fold planes taken as 6.26 x 10^{-10} m assuming (110) growth front [45], σ and σ_e the lateral and fold surface free energy per unit area of the surfaces of the lamellae parallel and perpendicular to the chain direction, respectively, k_B the Boltzmann constant (k_B = 1.38 x 10^{-23} J/K), Δh_f = 1.93 x 10^8 is the heat of fusion per unit volume of crystal [47]. To confirm an isoconversional method for non-isothermal crystallization of PP/LDH nanocomposites, the values of K_g for PP and PP/LDH hybrid composites were obtained from DSC data on isothermal crystallization using Eq. 6.11, in which the values of G and G_0 were substituted with $(1/t_{1/2})$ and $(1/t_{1/2})_0$, respectively [48]. The plots of ln $G + U^*/(R\,(T_c - T_\infty))$ versus $1/(T_c - T_f)$ are shown in **Figure 6.17**. and shows that the experimental data can be reasonably fitted with straight lines. The values of K_g and σ_e were calculated from **Figure 6.17** and listed in table **Table 6.5.** It is found that the value of σ_e is 125.3 erg/cm^2 for PP, and this very close to that obtained isoconversional method. There is clear tendency for σ_e to decrease with as the LDH content is increased. As is well known, a foreign surface frequently reduces the nucleus size needed for crystal

growth, because the creation of the interface between polymer crystal and substrate may be less hindered than the creation of the corresponding free polymer crystal surface [49]. The decrease of σ_e could indicate an increase in the entropy of folding and therefore, the formation of less homogeneous and regular folding surface. As the composites have a higher melt viscosity than neat PP, the chain movements are restricted during crystallization and will form a less regular folding pattern in the crystals. Based on the results of PP/LDH nanocomposites, we conclude that the addition of LDH at nanometric level reduces the creation of new surface, hence leading to faster crystallization rate.

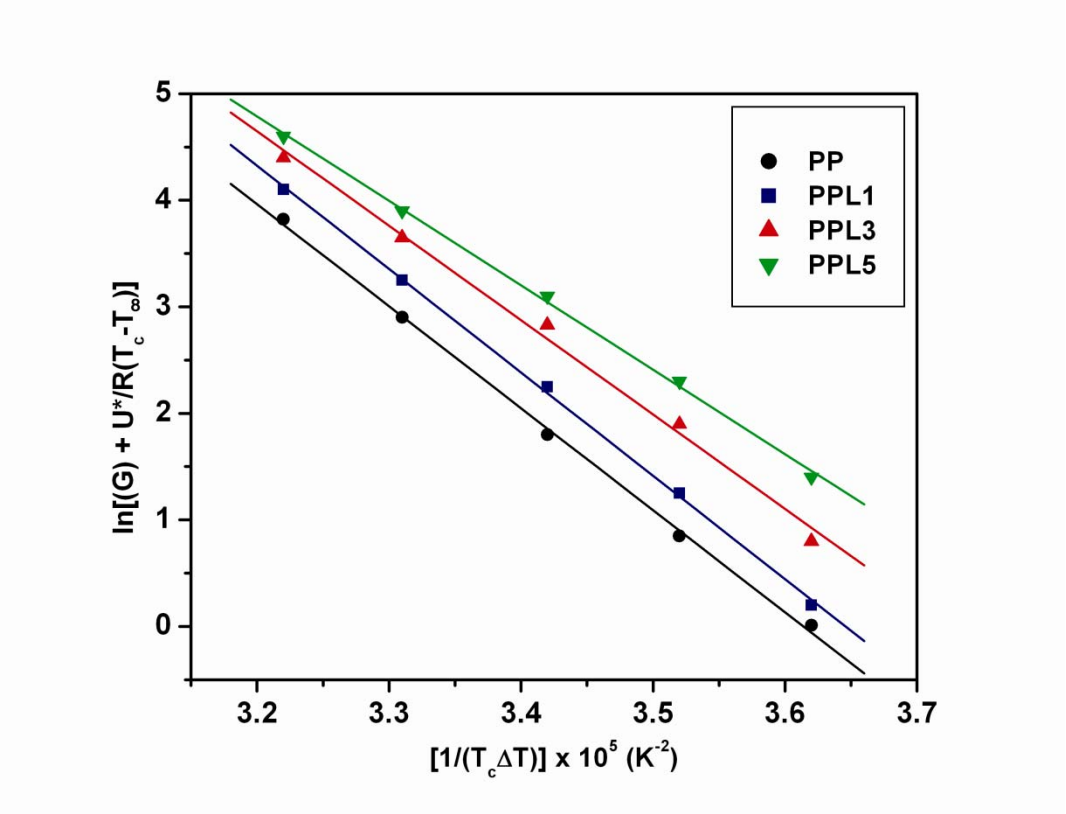

Figure 6.17: The plots of ln $G + U^*/(R\ (T_c - T_\infty))$ versus $1/(T_c - T_f)$ for PP and PP/LDH nanocomposites

6.3.3 Crystalline Structure of PP/LDH Nanocomposites

The crystalline form and crystal size, markedly affects the mechanical properties of semicrystalline polymers like polypropylene. To investigate the influence of the LDH on the crystalline structure and crystallinity of PP, we performed WAXD experiments on both neat PP and the PP/LDH nanocomposites. The **Figure 6.18**, shows the WAXD intensity profiles of PP/LDH nanocomposites after isothermal crystallization at 128 °C. The X-ray diffractograms show nearly the α-crystalline form of PP after isothermal crystallization. The monoclinic α reflections of PP can be found at 2θ angles of 14.19° (110), 16.98° (040), 18.68 ° (130), 21.25° (111) and 21.91° (131 and 041) crystalline planes [50-51]. These observations confirm that the addition of LDH does not affect the crystalline polymorph of PP. However, the crystallization rate of PP is accelerated by the addition of LDH, as shown in the development of the WAXD crystalline reflections as a function of the crystalline time. In **Figure 6.18**, it is also observed that the intensity of (110) plane decreases with increasing LDH content accompanied by increase in the intensity of (040) plane in case of nanocomposites. The intensity of (040) peak of PP in nanocomposites was found to increase because the surfaces of well- dispersed exfoliated LDH layers modified with organic modifier seems to induce the crystal growth in (040) direction. It is known that the ratio between the (110) and (040) gives the information on crystal growth orientations in *a* and *b* axes of α-phase [52]. The peak intensity of (110)/ (040) in PP/LDH nanocomposites is not due to the possible change in the crystal forms, from α to γ form with addition of nano filler like LDH which is in agreement with reports of Kim et al.[18] in case of maleated PP/MMT nanocomposites. The degree of perfection of the α-phase i.e crystalline size (D_{hkl}) can be calculated from the full width at half maximum (FWHM) of the (110) face using the Debye-Scherrer equation:

$$D_{hkl} = \frac{K\lambda}{\beta \cos\theta} \tag{6.21}$$

where D_{hkl} is the microcrystalline dimensions (nm), β is the half width of the diffraction peak in radian [β= (β1-0.2) x π/180°)] , K is equal to 0.9, θ is the Bragg angle, and λ is the wave length of the X-rays (λ=0.154 nm). The crystal sizes of the (110) planes of PP and its LDH hybrids obtained this equation are listed in **Table 6.7**. As can be seen, compared to PP, the crystal size of the composites is reduced, indicating that the packing order of

the α-phase decreased in PP/LDH nanocomposites. This is in agreement with results of the POM study, which showed small size crystal formed with low degree of perfection.

Table 6.7. The crystalline size D_{110} of PP and PP/LDH hybrids

Parameter	PP	PPL1	PPL3	PPL5
2θ (^{0})	14.2	14.15	14.15	14.19
***β1* (radian)**	0.59	0.66	0.73	0.82
***β* (radian)**	0.0068	0.0080	0.0092	0.010
D_{110} (nm)	20.45	19.16	15.15	13.67

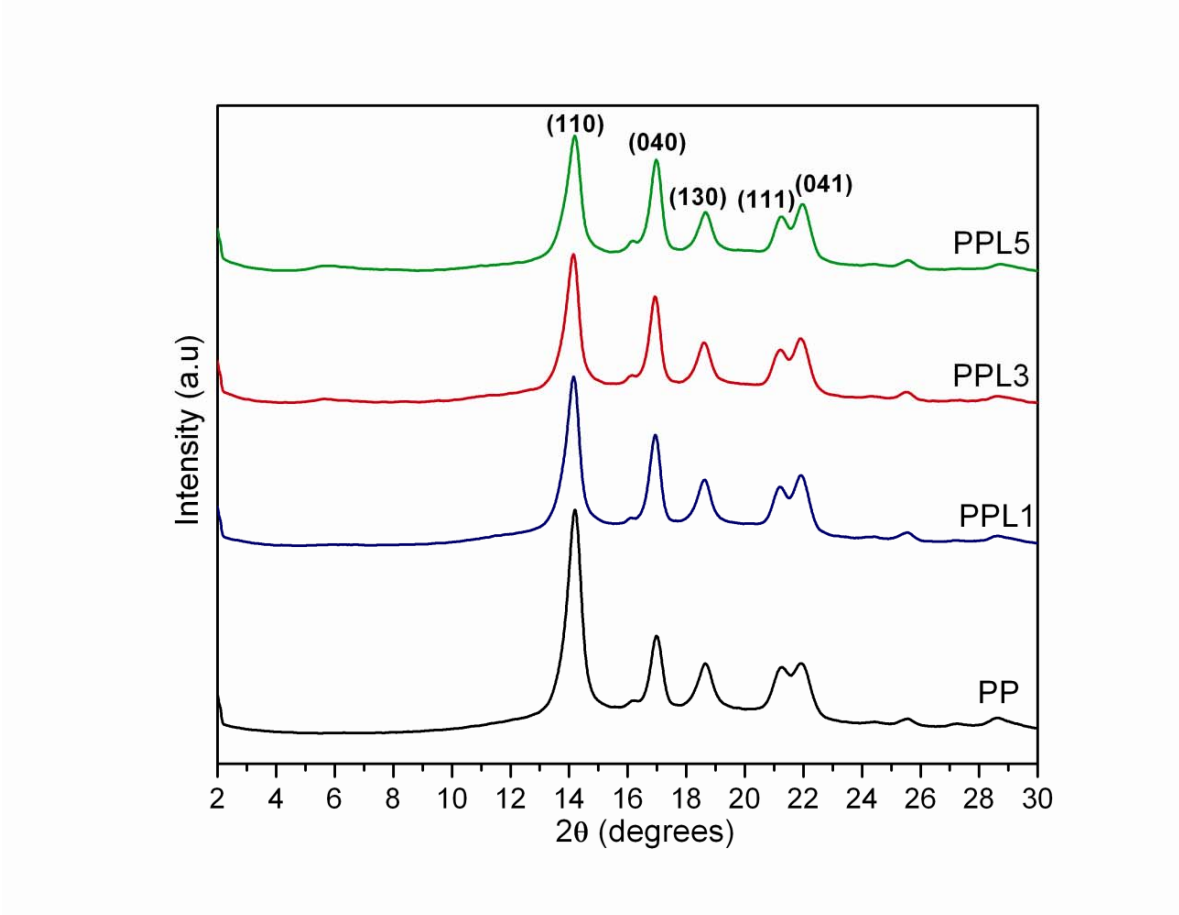

Figure 6.18: X-ray diffractograms of isothermally crystallized nanocomposites: (a) PP, (b) PPL1, (c) PPL3 and (d) PPL5 at 128 °C.

6.3.4 Development of Spherulitic Morphologies

In order to investigate the influence of LDH nano-particles on the morphology development and size of spherulites of PP, POM characterization was carried out. Figure 8 shows the micrographs of PP and PPL5 after isothermally crystallizing at 128 °C for 15 min. One can observe well-defined spherulites with a 'Maltese-cross' structure for PP **Figure 6.19**.

Figure 6.19: Polarized microscopy pictures of isothermally crystallized nanocomposites : (a) PP, (b) PPL1, (c) PPL3 and (d) PPL5 at 128 °C.

Two kinds of optically different areas can be seen as separate phases. The dark and bright areas might be amorphous and crystal regions, respectively. Comparably, the morphology development of spherulites for PPL1, PPL3 and PPL5 shows the instantaneous nucleation process and there is little indication of any regular structure and have relatively small or less perfect Maltase crosses. Clearly, the dimensions of the

spherulites decreases with LDH contents and only very tiny crystallites can be seen. This is due to the effect of the nano-dispersed LDH layers, which may act as seeds crystallization and may change the crystallization process during the formation of PP crystallites. Therefore, a gradual decrease in crystal growth and perfection has been observed with increasing LDH nano-layers in PP matrix.

6.3.5 Melting Behavior and Equilibrium Melting Points

The DSC heating thermograms of neat PP and the PP/LDH nanocomposite sample are presented in **Figure. 6.20 (a-b)**, respectively. It is observed that the PP/LDH nanocomposite DSC thermograms possess two melting peaks in contrast to the single melting peak of neat PP. However, the nature of the peak changes slightly with increasing crystallization temperature. While up to now, some discrepancies still existed in the origin and mechanism of the presence of multiple thermograms, it is generally believed that different thermal history leads to crystals with different perfection [53]. The cause of the first peaks in the scans is assumed to be due to the melting of the smallest lamellae produced by secondary crystallization and in the inter-lamellar layers between the larger crystallites. As such, this growth should not develop until after the primary stage is complete. Since the last peak is less dependent on the crystallization temperature and is much larger that the first one, it might be considered to be originated from the melting of the major crystals formed in the primary crystallization process [54]. As seen from **Table 6.7**, the crystallization temperature barely affected the melting profile of neat PP and its melting points were approximately at 157.6 $^{\circ}$C at different crystalline temperature, whereas, the melting points of PP/LDH nanocomposites found higher than neat PP and was related to crystallization temperature. The melting of PPL5 crystallized at 132 $^{\circ}$C was higher than that at 124 $^{\circ}$C. Generally, the perfection of the crystalline, or high-temperature melting peaks increased with crystallization temperature, which was confirmed by the fact that the higher-temperature melting peaks shifted to higher temperatures with higher crystallization temperature. Relatively imperfect crystals would be formed at lower crystallizations, and would melt at a lower temperature. This result indicates that the isothermal crystallization temperature influences the melting behavior of PP/LDH hybrid nanocomposites. The significant increase in melting points of

nanocomposites could be ascribed due to possible interaction between LDH nano-layers and PP molecular chains.

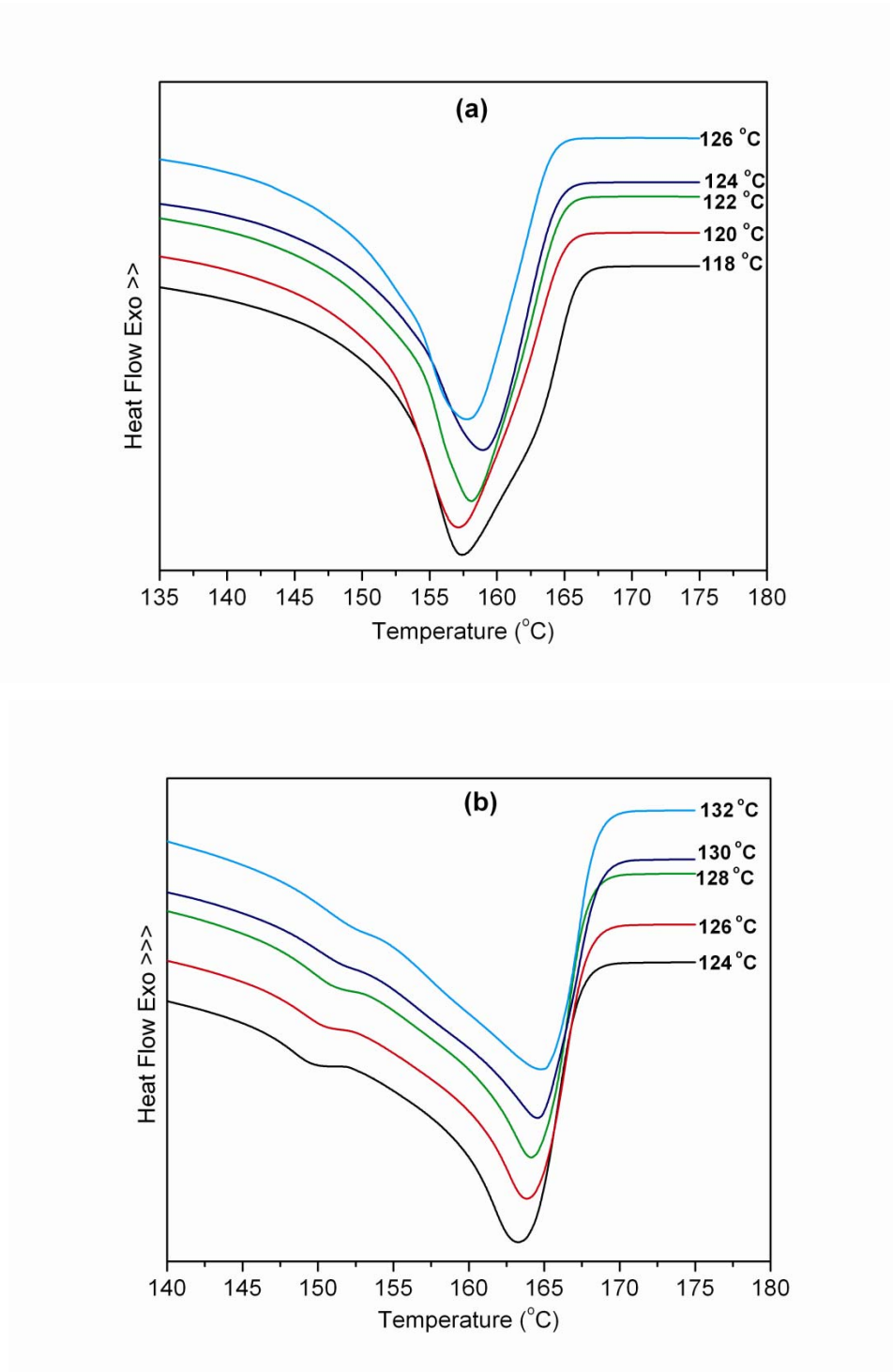

Figure 6.20: Melting DSC curves of a) PP and b) PPL5 at different T_c.

6.4 Conclusions

In this study we have systematically investigated the effect of organically modified LDH on the both nonisothermal and isothermal crystallization behaviors and their respective kinetics of PP.

The nonisothermal crystallization kinetics of PP and PP-LDH nanocomposites was studied by means of DSC technique by cooling the melt at various cooling rates. The Ozawa, modified Avrami and combined Ozawa- Avrami approaches were used for the investigation. The Ozawa model failed to adequately describe the nonisothermal crystallization behavior probably due to inaccurate assumption in the approach regarding secondary crystallization, dependence of lamellar thickness on crystallization temperature and the constant value of cooling function over the entire crystallization process.The Avrami plots of PP and PP/LDH nanocomposites showed good linearity and were able to explain crystallization kinetics for these systems. The values of Avrami exponent *n* varies from 1.9 to 2.9 for neat PP and PP/LDH nanocomposites, suggesting spherulitic crystal growth mechanism with heterogeneous nucleation at the low cooling rates. The Avrami analysis modified by Jeziorny was also successful for describing the nonisothermal crystallization process of PP/LDH nanocomposite. The half-time $t_{1/2}$ and Z_c showed that the crystallization rate of PP and PP/LDH nanocomposite increased with increasing cooling rates, but the crystallization rate of PP/LDH nanocomposite was faster than that of PP at a given cooling rate. This behavior is ascribed to the nucleating effect of clay nanoparticles. The method developed by Liu et al. was able to describe the nonisothermal crystallization kinetics of PP and PP/LDH nanocomposites satisfactorily. Different kinetic parameters determined from these models proved that in the nanocomposites, LDH was efficient to start crystallization earlier by nucleation but crystal growth decreased in nanocomposites due to intercalation of polymer chains in the galleries. Different kinetic parameters determined from these models proved that in the nanocomposites, LDH was efficient to start crystallization earlier by nucleation but crystal growth decreased in nanocomposites due to intercalation of polymer chains in the galleries. Furthermore, the activity of nucleation of LDH is determined with the values in the range of 0.85 to 0.69 by using Dobreva's method. It indicates that the hydroxide layers of LDH are active substrates for heterogeneous nucleation, which results in the

increase of the crystallization rate and the decrease of the degree of surpercooling required for crystallizing nucleation. The isoconversional analysis was successfully employed to determine the effective energy barrier for non-isothermal crystallization. It was found to vary with conversion and altered by LDH addition. In addition, in the analysis of the activation energy of crystallization, it was shown that the fold surface free energy σ_e of PP chains decreased with increasing LDH content. Different kinetic parameters determined from these models proved that in the nanocomposites, LDH was efficient to start crystallization earlier by nucleation but crystal growth decreased in nanocomposites due to intercalation of polymer chains in the galleries. Consequently, these analyses showed that the addition of a small amount of LDH enhances the PP nucleation mechanism but also hinders the crystallite growth.

The isothermal crystallization kinetic study of PP/LDH nanocomposites showed that the addition of LDH nano-layers remarkably affected the crystallization and melting behavior of PP/LDH hybrids. The isothermal crystallization kinetics of the PP and PP/LDH nanocomposites was systematically studied by Avrami model using calorimetric data at various crystallization temperatures. The Avrami plots of PP and PP/LDH nanocomposites were found to obey the linearity and were able to explain crystallization kinetics for these systems. The values of Avrami exponent *n* varies from 2 to 2.5 for neat PP and PP/LDH nanocomposites, suggesting spherulitic crystal growth mechanism with heterogeneous nucleation. The melting behavior of PP is also altered by addition of LDH, a significant increase and two peaks in melting endotherm are observed. The existence of double melting endotherms may be due to simultaneous melting-reorganization-remelting and due to possible interaction between LDH nano-layers and PP molecular chains. Moreover, the WAXD profile of PP hybrids corresponds to monoclinic α-form which implies the addition of LDH does not change the overall crystalline structure of PP matrix. However, a slight decrease in microcrystalline dimensions is observed in case of PP/LDH hybrids. On the other hand, the LDH layers acted as heterogeneous nuclei in the nucleation of crystallization, causing a dramatic increase of the crystallization rate and decrease of the spherulite size with the increase of LDH content. The perfect spherulites cannot form for colliding and compacting of a large number of small spherulites in a limited space. The nucleus density increased with the increase of LDH content, leading to

a positive effect on the crystallization, which is in good agreement with the result that the interfacial free energy per unit area perpendicular to PP chains in PP/LDH nanocomposites decreased with increasing LDH content due to nucleating effect of LDH.

Overall results conclude that the LDH at nanometer level can act as effective nucleating agent and accelerating crystallization rate of PP. Finally, it can be concluded that the type of nucleation, growth and geometry of PP crystals markedly change in the presence of nano-sized LDH nanoparticles. It is our belief that such shifts in the mechanism of crystal nucleation and growth leading to the development of a fine grain micron-sized structure for the PP/LDH composites should improve the overall physical properties of such hybrid material.

References

1) R. Gowarikar, N. V. Viswanathan, Jayadev Sreedhar " *Polymer Science*" Published by New Age International (P) Ltd., p, 173, 1986.
2) L. Mandelkern, ''*Crystallization of polymers*,'' McGraw-Hill, New York, 1964, pp 67–71.
3) B.P. Grady, F. Pompeo, R.L. Shambaugh, D.E. Reasasco .Nucleation of polypropylene crystallization by single-walled carbon nanotubes *Journal of Physical Chemistry B*, **106** (2002), p.5852-5858.
4) D.J.Y.S. Page, T.G. Gopakumar. Properties and crystallization of maleated polypropylene/graphite flake nanocomposites. *Polymer Journal*, **38** (2006), p. 920-929.
5) J.H. Chen , B.X. Yao , W.B. Su , Y.B. Yang. Isothermal crystallization behavior of isotactic polypropylene blended with small loading of polyhedral oligomeric silsesquioxane. *Polymer*, **48** (2007), p.1756-1769.
6) P. Maiti, P.H. Nam, M.Okamoto, N. Hasegawa, A. Usuki. Influence of crystallization on intercalation, morphology, and mechanical properties of polypropylene/clay nanocomposites, Macromolecules **35**, (2002) p.2042-2049.
7) W.B. Xu, M.L.Ge, P.S.He. Nonisothermal crystallization kinetics of polypropylene / montmorillonite nanocomposites. *Journal of Polymer Science Part B- Polymer Physics*, **40** (2002), p. 408-414.
8) M. Mucha, J. Marszalek, A. Fifrych. Crystallization of isotactic polypropylene containing carbon black as a filler. *Polymer*, **41** (2000), p.4137-4142.
9) J.H. Chen , B.X. Yao , W.B. Su , Y.B. Yang. Isothermal crystallization behavior of isotactic polypropylene blended with small loading of polyhedral oligomeric silsesquioxane. *Polymer*, **48** (2007), p.1756-1769.
10) S.F. Hsu, T.M. Wu, C.S. Liao. Nonisothermal crystallization behavior and crystalline structure of poly(3-hydroxybutyrate)/layered double hydroxide nanocomposites. *Journal of Polymer Science Part B- Polymer Physics*, **45** (2007), p. 995-1002.
11) W.Chen, B. Qu. Structural Characteristics and Thermal Properties of PE-g-MA/MgAl-LDH Exfoliation Nanocomposites Synthesized by Solution Intercalation *Chemistry of Materials*. **15** (2003), p. 3208-3213.

12) P. Pan, B. Zhu, T. Dong, Y. Inoue, Poly(L-lactide)/layered double hydroxides nanocomposites : Preparation and crystallization behavior. *Journal of Polymer Science Part B: Polymer Physics*. **46** (2008), p.2222-2233.

13) M. Eder, A. Wlochowicz, Kinetics of non-isothermal crystallization of polyethylene and polypropylene; *Polymer*, **24** (1983), p.1593-1595.

14) T. Ozawa. A new method of analyzing thermogravimetric data. *Bulletin of the Chemical Society of Japan***, 38** (1965), p.1881-1986.

15) W. Xu, G. Liang, W. Wang, S. Tang, P.He, W.P. Pan. Poly(propylene)-poly(propylene)-grafted maleic anhydride-organic montmorillonite (PP-PP-g-MAH-Org-MMT) nanocomposites. II. Nonisothermal crystallization kinetics. *Journal of Applied Polymer Science,* **88** (2003), p.3093-3099.

16) M.L. Addonizio, E. Martuscelli, C. Silvestre. Study of the nonisothermal crystallization of poly(ethylene oxide) poly(methyl methacrylate) blends. *Polymer,* **28** (1987), p.183-188.

17) A. Joshi, B.S. Butola. Studies on nonisothermal crystallization of HDPE/POSS nanocomposites, *Polymer* **45** (2004), p. 4953-4968.

18) M.J.Avrami. Kinetics of phase change. II. Transformation-time relations for random distribution of nuclei. *Journal of Chemical Physics,* **8 (**1940), p.212–224.

19) G.X. Chen and J.S. Yoon. Nonisothermal crystallization kinetics of poly(butylene succinate) composites with a twice functionalized organoclay. *Journal of Polymer Science Part B- Polymer Physics*, **43** (2005), p. 817-826.

20) A. Jeziorny. Parameters characterizing kinetics of nonisothermal crystallization of poly(ethylene-terephthalate) determined by DSC , *Polymer,* **19** (1978), p.1142-1144.

21) Q. Yuan, S. Awate, R.D.K. Misra. Nonisothermal crystallization behavior of polypropylene–clay nanocomposites. *European Polymer Journal*, **42** (2006), p.1994–2003.

22) . T. Liu, Z. Mo, S. Wang, and H. Zhang, Nonisothermal Melt and Cold Crystallization Kinetics of Poly(Aryl Ether Ether Ketone Ketone)', *Polymer Engineering and Science*, **37** (1997), p.568-575.

23) S. Nandi, A.K. Ghosh. Crystallization kinetics of impact modified polypropylene *Journal of Polymer Research*, **14** (2007), p.387-396.

24) J. Qian, P. He, K .Nie. Nonisothermal crystallization of PP/nano-SiO2 composites *Journal of Applied Polymer Science*. **91** (2004), p. 1013-1019.

25) J.D. He, M.K. Cheung, M.S. Yang, Z. Qi. Thermal stability and crystallization kinetics of isotactic polypropylene/organomontmorillonite nanocomposites**.** *Journal of Applied Polymer Science*, **89** (2003), p. 3404-3415.

26) A. Dobreva, I. Gutzow, Activity of substrates in the catalyzed nucleation of glass-forming melts .2. experimental-evidence. *Journal of Non Crystalline Solids*, **162** (1993), p.13-25.

27) M. Alonso, J.I. Velasco, J.A. de Saja, Constrained crystallization and activity of filler in surface modified talc polypropylene composites, *European Polymer Journal*, **33** (1997), p.255-262.

28) J.I. Velasco, C. Morhain, A.B. Martínez, M.A. Rodríguez-Pérez, J.A. de Saja, Anisotropy and microstructure heterogeneity of injection-moulded discs of poly(propylene) filled with platy magnesium hydroxide, *Macromolecular Materials Engineering*. **286** (2001), p.719-730, 25.

29) J.I. Velasco, J.A. de Saja and A.B. Martínez, Crystallization behavior of polypropylene filled with surface-modified talc. *Journal of Applied Polymer Science*, **61** (1996), p.125–132.

30) D. Arencón, J.I. Velasco, M.A. Rodríguez-Pérez, J.A. de Saja, Poly(propylene)/poly(ethylene terephthalate-co-isophthalate) blends and glass bead filled composites: Microstructure and thermomechanical properties *Journal of Applied Polymer Science,*. **94** (2004), p.1841-1852.

31) G.Z. Papageorgiu, D.S. Achilias, D.N. Bikiaris, G.P. Karayannidis, Crystallization kinetics and nucleation activity of filler in polypropylene/surface-treated SiO2 nanocomposites. *Thermochimica Acta* , **427** (2005), p. 117-128.

32) S. Vyazovkin, Is the Kissinger equation applicable to the processes that occur on cooling? *Macromolecular Rapid Communications*, **23(**2002), p.771-775.

33) R.L.Takhor. Advances in Nucleation and Crystallization of Glasses, Columbus, OH: Americal Chemical Society, 1971. p.166.

34) H.E. Kissinger. Variation of peak temperature with heating rate in differential thermal analysis;. *Journal of Research of the National Bureau of Standards Section A-Physics and Chemistry*. **57** (1956), p. 217-221.

35) S. Vyazovkin, Is the Kissinger equation applicable to the processes that occur on cooling? *Macromolecular Rapid Communications*, **23 (**2002), p.771-775.

36) S. Vyazovkin, N. Sbirrazzuoli. Isoconversional analysis of calorimetric data on nonisothermal crystallization of a polymer melt *Journal of Physical Chemistry B*, **107** (2003), p.882-888.

37) H. Friedman. Kinetics of thermal degradation of char-forming plastics from thermogravimetry. Application to a phenolic plastic. *Journal of Polymer Science*, *Part C*. **6** (1964), p.183–195.

38) J.H. Flynn, L.A. Wall. General treatment of thermogravimetry of polymers. *Journal of Research of the National Bureau of Standards Section A-Physics and Chemistry*, **A 70** (1966), p.487.

39) S. Vyazovkin, Modification of the integral isoconversional method to account for variation in the activation energy, *Journal of Computational Chemistry*, **22 (**2001), p.178-183.

40) S. Vyazovkin, N. Sbirrazzuoli.Isoconversional approach to evaluating the Hoffman-Lauritzen parameters (U* and K-g) from the overall rates of nonisothermal crystallization. *Macromolecular Rapid Communications*, **25** (2004), p.733-738.

41) M. Run, C.Yao, Y.Wang, J. Gao, kinetics and melting behaviors of nanocomposites of poly(trimethylene terephthalate) filled with nano-CaCO3. *Journal of Applied Polymer Science*. **106** (2007), p. 1557-1567.

42) J.L .Lauritzen, J.D. Hoffman. Extension of theory of growth of chain-folded polymer crystals to large undercoolings. *Journal of Applied Physics*, **44** (1973), p. 4340-4352.

43) J.D. Hoffman, R.L. Miller. Kinetics of crystallization from the melt and chain folding in polyethylene fractions revisited: Theory and experiment. *Polymer*, **38** (1997), p. 3151-3212.

44) Advance Thermal Analysis System (ATHAS Databank). Available at http://web.utk.edu/athas/edu.

45) J.N. Xu, S. Srinivas, H. Marand, P. Agarwal. Equilibrium melting temperature and undercooling dependence of the spherulitic growth rate of isotactic polypropylene. *Macromolecules,* **31** (1998), p.8230-8242.

46) E.J. Clark, J.D. Hoffman. Regime-III crystallization in polypropylene, *Macromolecules*, **17** (1984), p. 878-885.

47) H.S. Bu, S.Z.D. Cheng, B.Wunderlich. Addendum to the thermal-properties of polypropylene *Makromolekulare Chemie-Rapid Communications,* **9** (1988), p.75-77.

48) X.F. Lu, J.N. Hay. Isothermal crystallization kinetics and melting behaviour of poly(ethylene terephthalate). *Polymer,* **42** (2001), p. 9423-9431.

49) M. Mucha, Z. Krolikowski. Application of DSC to study crystallization kinetics of polypropylene containing fillers .*Journal of Thermal Analysis and Calorimetry,* **74 (**2003), p. 549-557.

50) S. Bruckner, S. V. Meille, V. Petraccone, B. Pirozzi, Polymorphism in isotactic polypropylene. *Progress in Polymer Science* **16** (1991), p. 361-404.

51) R.A. Philips, M.D. Wolkowicz, In E. P. Moore (Ed.), Polypropylene handbook, Hanser, Munich, 1996, pp.113-122.

52) J. Wang, Q. Dou. Crystallization Behaviors and Optical Properties of Isotactic Polypropylene: Comparative Study of a Trisamide and a Rosin-type nucleating agent, *Colloid Polymer Science*. **286** (2008), p. 699–705.

53) T. Liu, Z. Mo, S.Wang, H. Zhang, Isothermal melt and cold crystallization kinetics of poly(aryl ether ether ketone ketone) (PEEKK), *European Polymer Journal*, **33** (1997), p.1405-1414.

54) X. F. Lu, J.N. Hay, Isothermal crystallization kinetics and melting behaviour of poly(ethylene terephthalate), *Polymer*, **42** (2001), p. 9423-9431.

55) K. Levenberg, A method for the solution of certain problems in least squares, *Quart. Appl. Math.*, **2** (1944), p. 164–168.

56) D. Marquardt, An algorithm for least-squares estimation of nonlinear parameters, *SIAM Journal of Applied Mathematics*, **11** (1963), p.431–441.

Chapter 7

PHOTO-OXIDATION BEHAVIOR AND PHOTOSTABILIZATION STUDIES

"We know very little, and yet it is astonishing that we know so much, and still more astonishing that so little knowledge can give us so much power"

~Bertrand Russell

Sunil P. Lonkar, S. Therias, N. Cappera, F. Lereoux J-L. Gardette, *"Photooxidation of Polypropylene/Layered Double Hydroxide Nanocomposites: Influence of Interlamellar Cations*, ***European Polymer Journal (Accepted for Publication).***

7.1 Introduction

Under the action of sun light, polymer materials undergo a series of oxidative reactions that lead to chemical degradation, with consequence of brittleness, loss of brightness, color change, opacity and formation of surface cracks. Besides the reduction in molecular weight, a number of changes take place in the molecules during photodegradation with the formation of chemical groups like carbonyl, carboxylic acids and other than hydroperoxides [1-2] (**Figure 7.1**). A natural weathering that has great effect is produced by oxygen and light radiation, referred to technically as photo-oxidation. The photooxidative degradation of polymers is extremely important from scientific and industrial point of views. Oxidative degradation reactions are the main limitation in the active life of synthetic polymers. This undesirable degradation may be accelerated by exposure to UV radiation.

Polypropylene is one of the extensively used plastics in outdoor applications. Its outdoor durability in modern days is very important because of large scale production. Hence, the resistance to UV-light is a key factor for most outdoor applications of polymeric materials. Recently, the study of photo-oxidation processes of polypropylene materials has attracted the attention of researchers, even though some questions

concerning the oxidation mechanism remained unanswered [3-4]. However, recent developments in synthesis, properties and future applications of polymer nanocomposites has revived an interest in observing the matrix behavior of this new type of composite material when subjected to the photo-oxidation process [5-6]. In the last few years, the impact of light on polymer/clay nanocomposites has been extensively studied [7-13]. It has been shown that nanocomposites prepared with montmorillonite as a nanoclay and polypropylene, as a polymer display similar behaviors under exposure to UV-light. The nanocomposites degrade faster than the pristine polymers, as a consequence of a significant reduction of the oxidation induction time (OIT) is observed. There is not only academic, but also commercial interest in fully understanding the properties of this material, because polymer/clay nanocomposites display generally a variety of desirable properties, compared to both conventional composites and unfilled bulk polymers. These special properties include mechanical strength, flame retardancy and dimensional stability. Some of such characteristic improvements have already been found in PP/ clay nanocomposites as summarized in Chapter 2 and still new positive results about the behavior of this kind of nanocomposites are expected. However, the usefulness of these materials depends on their durability in a particular environment in which they are used or their interaction with environmental factors. Thus, the study of degradation and stabilization of polymer nanocomposites is an extremely important area from the scientific and industrial point of view and a better understanding of the degradation mechanism of these materials will help to ensure a longer endurance of the product. Not enough attention has been paid to study of the durability of polymer nanocomposites. Since polymer–clay hybrids are now expanding to numerous outdoor applications, their exposure to ultraviolet (UV) light of the solar spectrum and other environmental deterrents is unavoidable. That is why as a potential new material, PP nanocomposites, necessitate investigation from the standpoint of photoaging behavior and requires a careful study of their photo-oxidation behavior. As previously reported in the literature survey, montmorillonite type organo-clay filled films show faster photo-oxidation rate with respect to the unfilled polymer matrix. Such adverse effect on durability of polymeric materials under UV-light is not due to the faster photo-oxidation kinetics but rather to a reduction of the oxidation induction time. In order to explain this faster photo-

oxidation behavior, several hypotheses have been put forward: degradation of the organo-modifier at the high melt polymer processing temperature, catalytic effect of the iron ions on the intermediate macroalkyl-hydroperoxides decomposition, and adsorption of the adopted stabilization systems onto the clay layers. Recently, Bocchini *et al.* [14] have reported the influence of nanodispersed hydrotalcites on the photo-oxidation behaviour of polypropylene. It is observed that the presence of hydrotalcite was shown to change the global rate of photooxidation of polypropylene by reducing the oxidation induction time and increasing the oxidation rate. The differences of the oxidation induction time disappeared after solvent extraction of the antioxidant. They were attributed to a quenching of the antioxidant activity resulting from a migration onto the filler surface induced by the preferential interaction with the polar hydrotalcite. Extracting the antioxidant did not change the oxidation rate at the permanent regime. The increase of the oxidation rate was attributed to transition metal ions, present as impurities in hydrotalcite, which can accelerate the oxidation of the polymer by various mechanisms including a catalyzed decomposition of hydroperoxides. Also, in a previous reports concerning the photooxidation of montmorillonite/polypropylene [7, 9] and nanoboehmite/ polypropylene nanocomposites [11], one has proposed several hypotheses to explain the oxidative degradation of these materials. The reduction of the OIT could result of the adsorption of antioxidants onto the nanofiller, of a catalytic effect of transition metal impurities of nanofillers, and also of additional initiation routes due to the oxidation of the organic modifiers in the nanofillers. The most probable hypothesis was the interactions between the nanofillers and the stabilizers: the antioxidant can be adsorbed on the nanofillers thus preventing their antioxidant action [9, 15]. The photochemical behavior of nanocomposites PS/LDH with synthetic hybrid LDH where M = Zn and Al has also been studied [12] and in this case it was shown that the nanocomposites did not degrade faster than the PS pristine polymer.

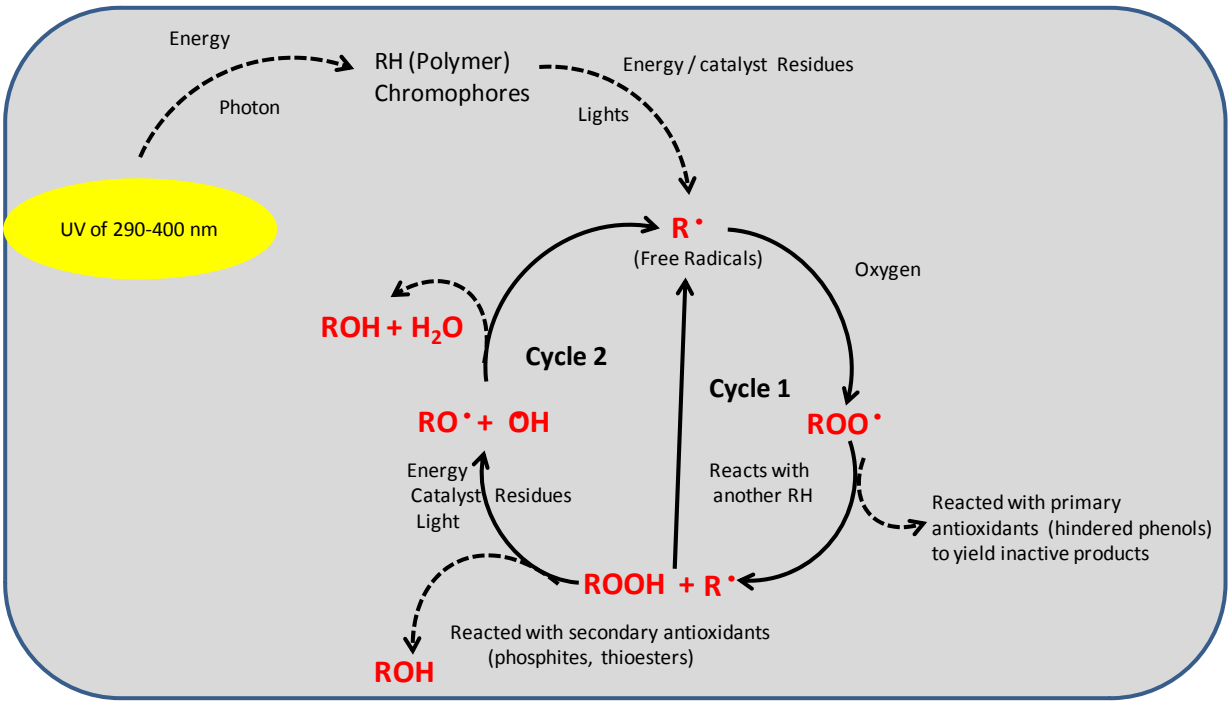

Figure 7.1 : Photo-oxidation and stabilization of polymers

Hence, it would be very interesting to investigate the effect of LDH type nanofiller towards photo-oxidative degradation of polypropylene. Thus, far the photo-oxidation of PP/LDH nanocomposites has not received particular attention. In the present study, we have focused our attention on the photo-aging behavior of polypropylene / LDH nanocomposites in presence of PP-g-MAH as a compatibilizing agent. The effect of interlamellar cations of LDH on photo-oxidation behavior of PP was also assessed. Hence, the aim of the present work is to study this peculiar point which has considerable consequences in terms of both fundamental aspects of the photooxidation of nanocomposites and durability of these materials. Furthermore, present study also aims to investigate the interactions between LDH comprising different metal cations and stabilizing additive *i.e* antioxidants. Special attention has to be given to the influence of each component on the rate of oxidation of the polymeric matrix. Two kinds of stabilizers were tested: a phenolic antioxidant generally used to process polypropylene and a redox antioxidant of the hindered amine light stabilizer (HALS) class, which is used as long-term stabilizer for polypropylene.

The photo-oxidation of all the samples was followed by FT-IR spectroscopy. The surface morphology after photoageing is studied by scanning electron microscopy (SEM). The knowledge obtained from this investigation will be useful in the design of PP nanocomposites less prone to UV light for potential outdoor applications.

7.2 Photo-oxidation of PP/LDH Nanocomposites

7.2.1 Infrared Analysis

The photo-oxidation of polypropylene is known to result in the formation of hydroxyl and carbonyl groups that can be easily detectable and monitored by infrared spectroscopy in the regions of 3200-3600 cm^{-1} and 1600-1800 cm^{-1} respectively [4]. The shape of the IR spectra recorded after exposure of the various samples to UV light in the presence of atmospheric oxygen reveals notable changes of the chemical structure of the materials as shown in **Figure 7.2**. The general evolution of the FT-IR spectra of films of nanocomposites PP/LDH and PP/OMMt upon irradiation in the presence of oxygen is comparable to that of pristine compatibilized polypropylene and is mainly characterized by an increase of absorbance in the carbonyl and hydroxyl region mainly hydroperoxides, alcohols, ketones, esters and acids. Because of strong initial hydroxyl absorption of LDH in the starting composites, it is very difficult to distinguish and monitor the hydroxyl photoproducts developed during the course of PP/LDH photo-oxidation. Hence, the nature of the main oxidation products can be considered in the carbonyl domain. The photochemical oxidation of PP leads to the formation of a broad band with several maxima peaking at 1713, 1735 and 1780 cm^{-1}. The photoproducts corresponding to these absorption maxima have been identified formerly [8] and it is agreed that the main absorption at 1713 cm^{-1} is attributed to carbonyl group of carboxylic acid in the dimer form. In present case, as shown in **Figure 7.2** (PPLA, B, and C), an increase of absorbance was observed in spectral domains in the FT-IR spectra of the PP/LDH nanocomposites, corresponding to the carbonyl stretching vibrations domains. Moreover, in the PP samples containing LDH, the shape of the oxidation bands in the carbonyl domain is different than those observed in case of PP or PP/OMMt as shown in **Figure 7.2** (fPP and PPM5). Upon irradiation, the IR spectra of PP/LDH develop two broad

absorption bands in the carbonyl region. One band has a maximum at 1715 cm^{-1} and two shoulders at 1735 cm^{-1} and 1770 cm^{-1}, which are also observed with pristine PP or the PP/OMMt nanocomposite. The shoulder on the carbonyl band at 1770 cm^{-1} results from the formation of γ-lactones. The absorption maximum at 1735 cm^{-1} is postulated to result either from the carbonyl groups of esters or from the carbonyl vibrations of carboxylic acids associated to hydroxyl groups. In the case of LDH, another FT-IR band appears at 1595 cm^{-1}, and is shifted to1610 cm^{-1} for longer irradiation times which could be attributed to carboxylate ions as photoproduct, indicating that the PP/LDH nanocomposites develop different photoproducts compared to pristine PP. This peculiar behaviour was not observed in the case of PP/OMMt nanocomposites [8-9]. Hence, overall results indicate that the presence of LDH can modify the mechanism of polymer oxidation or the final oxidation products in the material.

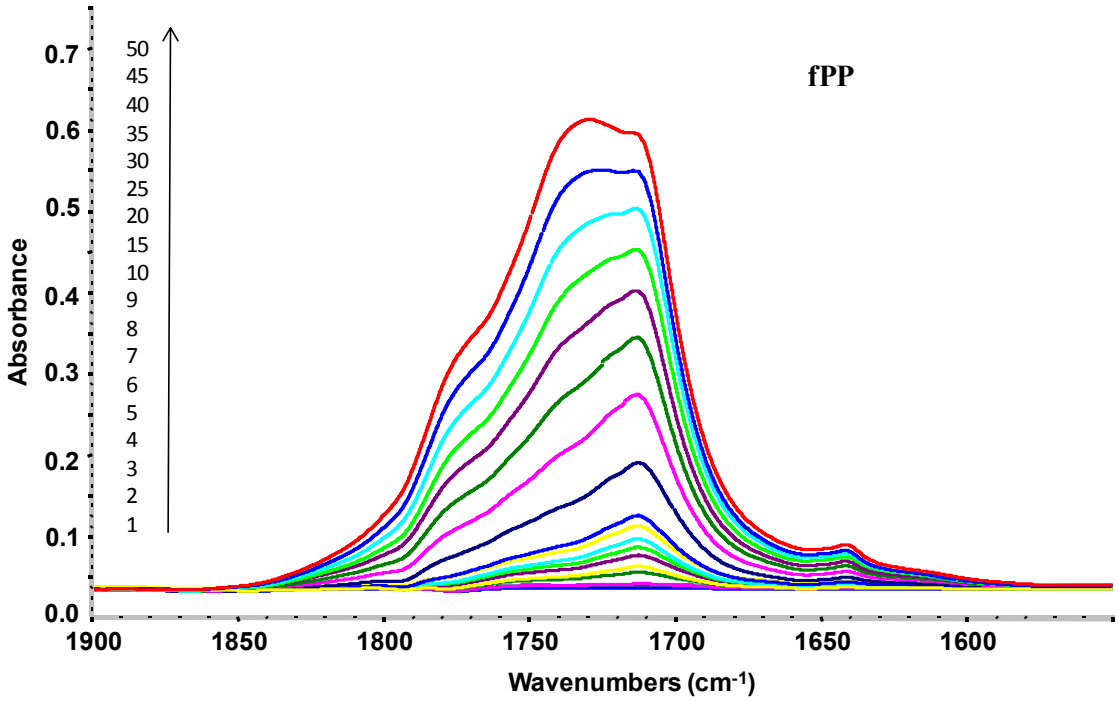

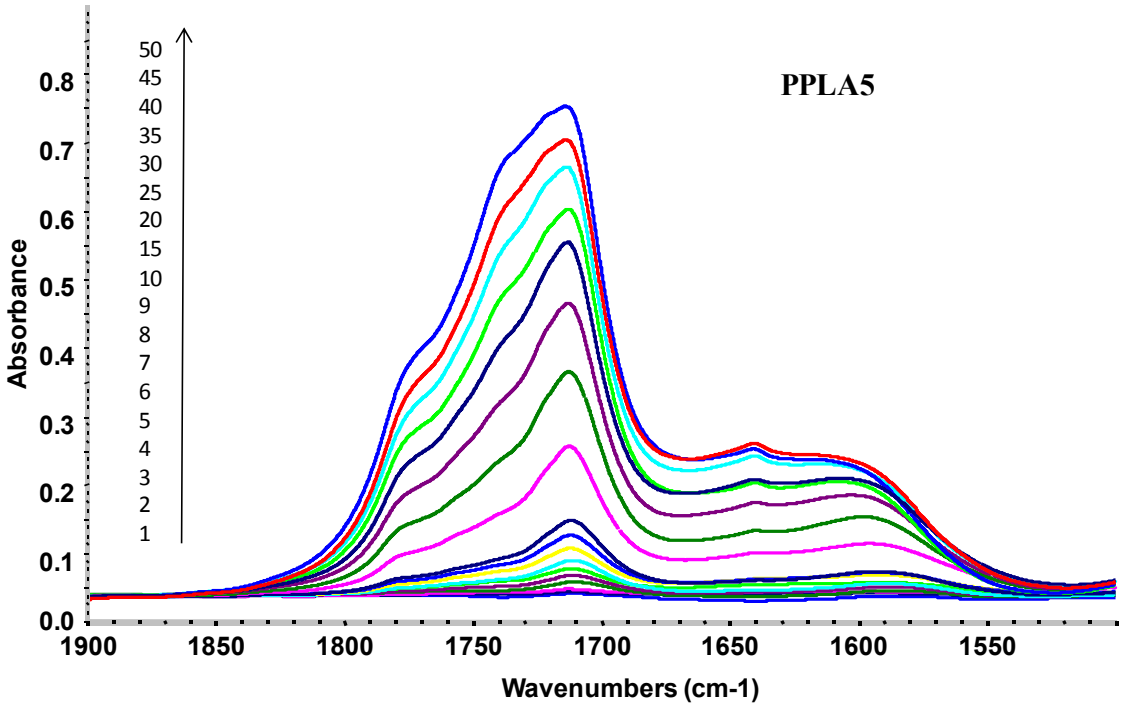
PPLA5
Absorbance
0.0
0.1
0.2
0.3
0.4
0.5
0.6
0.7
0.8
50
45
40
35
30
25
20
15
10
9
8
7
6
5
4
3
2
1
1900
1850
1800
1750
1700
1650
1600
1550
Wavenumbers (cm-1)

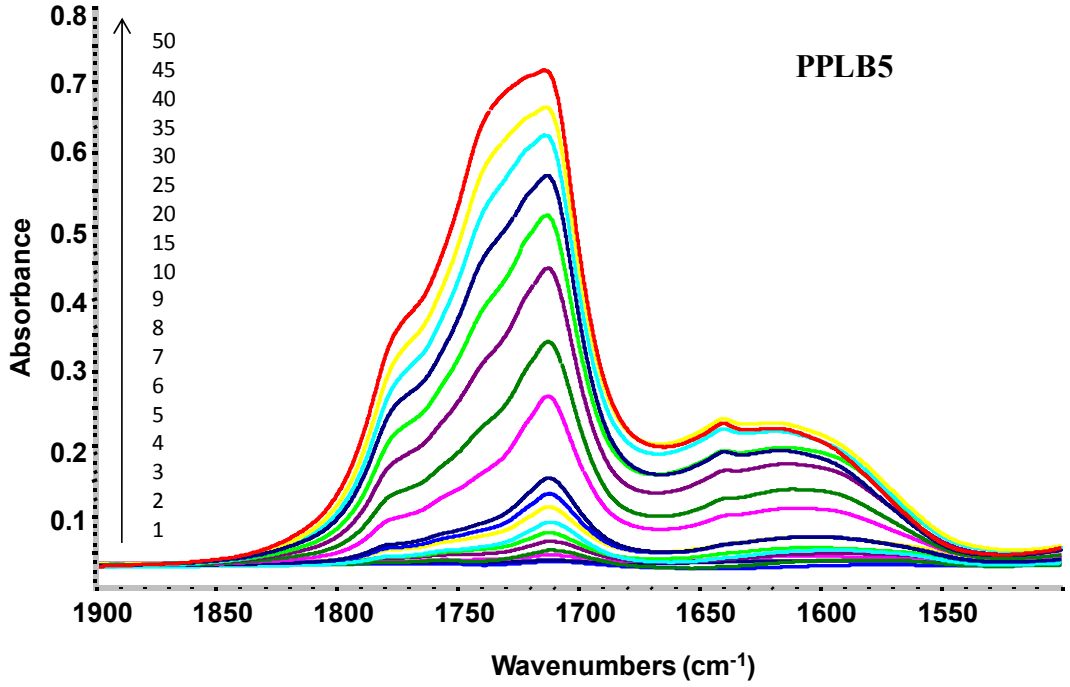
PPLB5
Absorbance
0.1
0.2
0.3
0.4
0.5
0.6
0.7
0.8
50
45
40
35
30
25
20
15
10
9
8
7
6
5
4
3
2
1
1900
1850
1800
1750
1700
1650
1600
1550
Wavenumbers (cm-1)

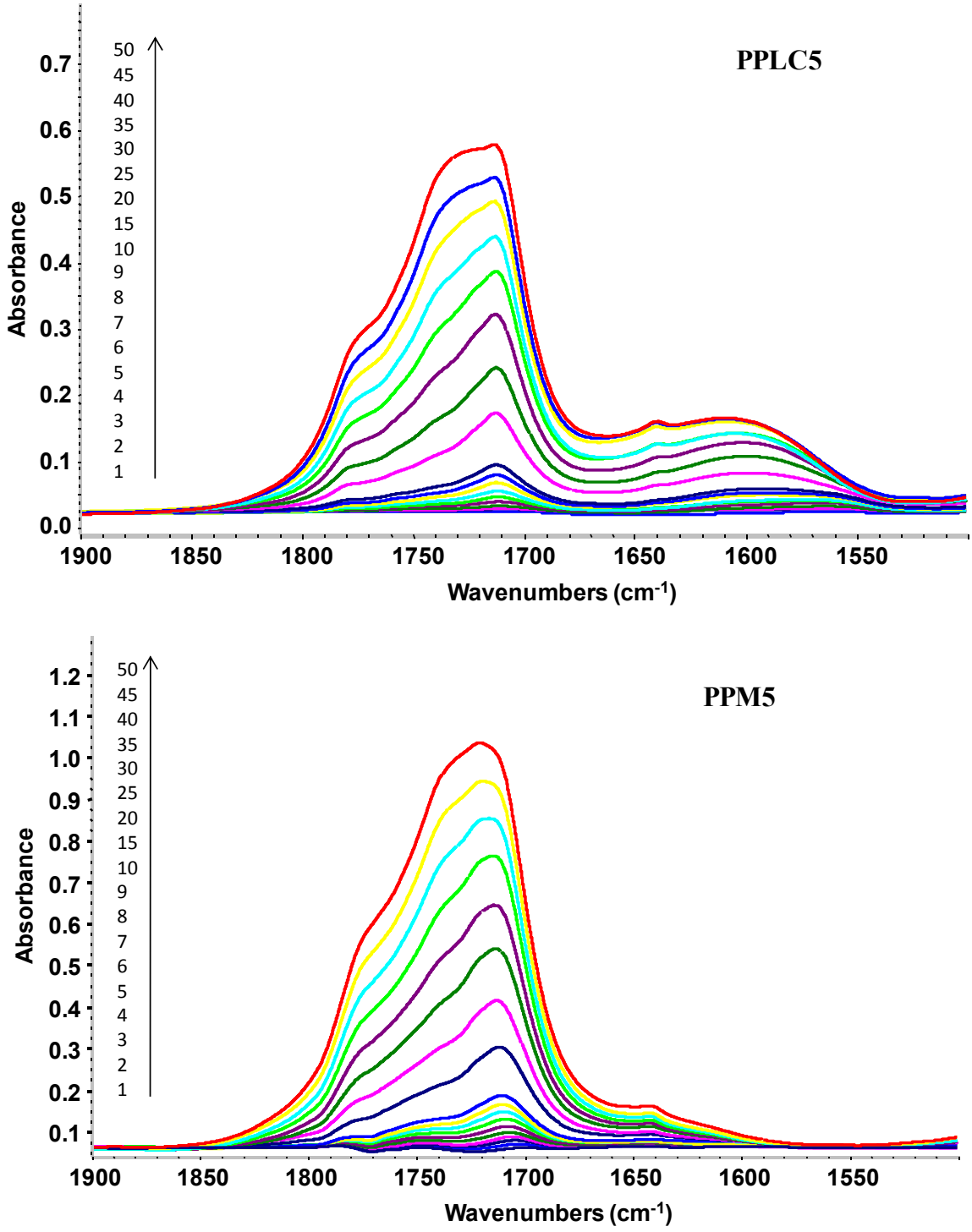

Figure 7.2 : FTIR spectra of a) fPP, b) PPLA5, c) PPLB5, d)PPLC and e) PPM5 nanocomposite photo-oxidized at $\lambda > 300$mn, 60°C in the domain of 1900-1500 cm^{-1}.

7.2.2 Mechanism of Photoxoidation

The photo-oxodation mechanism of polypropylene can be summarised as follows in **Figure 7.3**. The first step of the reaction is the formation of hydroperoxides which can decompose to produce alkoxy radicals, which abstract a hydrogen on the polymeric backbone or undergo a β-scission. Alcohol and ketone are formed with a macro-radical. The macro-radical is further oxidized to form carboxylic acids with scission of the macromolecular backbone, and some other carbonylated products. Because the carboxylic acids are final stable products, the increase of their concentration can be quantify the rate of photooxidation.

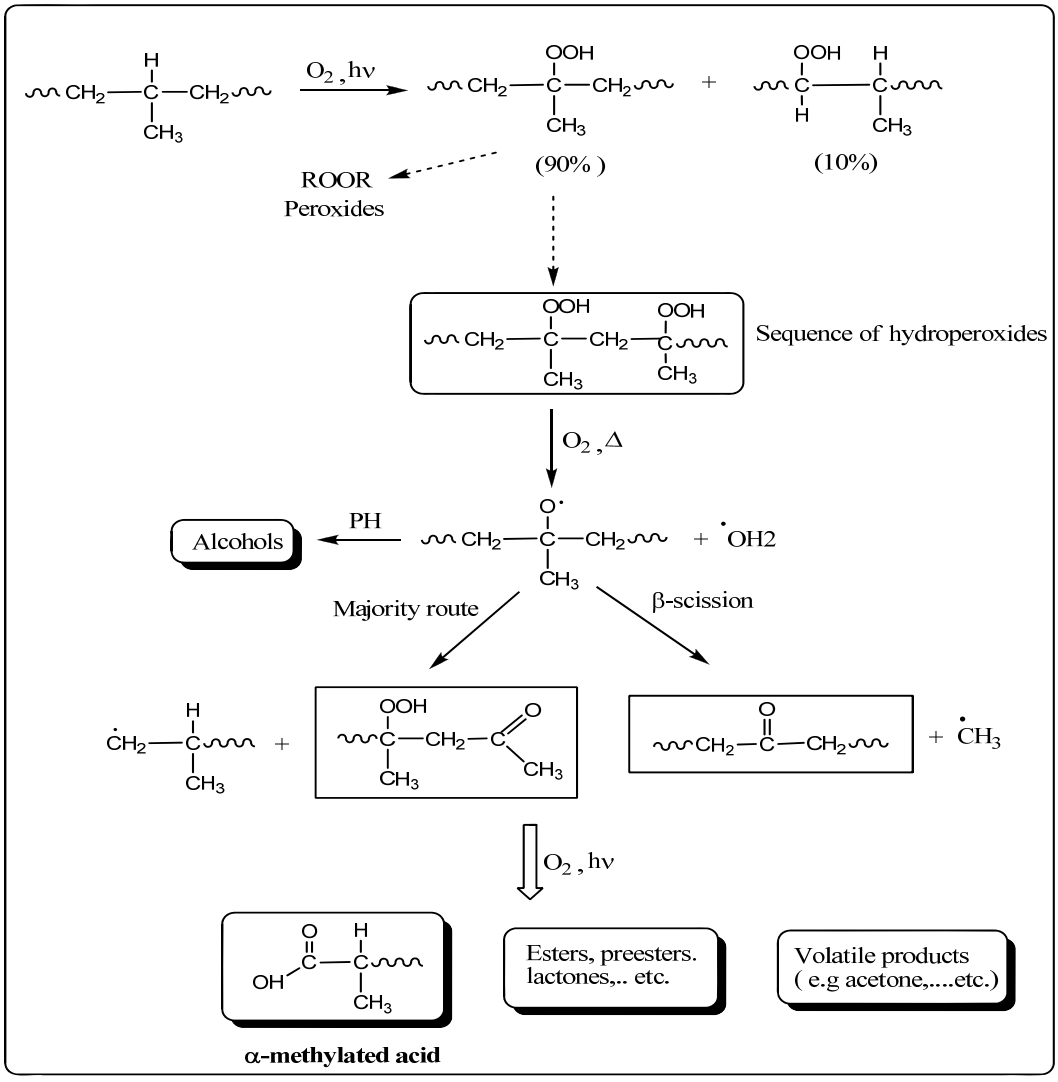

Figure 7.3: Schematic Photo-oxidation mechanism of polypropylene [4]

7.2.3 Rate of Photo-oxidation

The rates of photo-oxidation of the various nanocomposites (PP/LDH and PP/OMMt) were compared by measuring the increase of absorbance at 1713 cm^{-1} with irradiation time. Because all of the formulations contained maleic anhydride (even fPP), an absorption band was initially present at the same frequency in the spectrum of the samples before irradiation. The increase in absorbance at 1713 cm^{-1} was plotted as the difference from the absorbance before irradiation as a function of irradiation time. The samples had slightly different thicknesses, therefore, the absorbance values had to be normalised. A correction factor was applied to adjust the characteristic absorption band at 2722 cm^{-1} of PP to the same value. **Figures 7.4a** and **7.4b** show the variation of absorbance at 1713 cm^{-1} as a function of irradiation time for fPP, PP/MMt and PP/LDH, respectively, loaded at 5% and 10% (w/w) in the nanofiller.

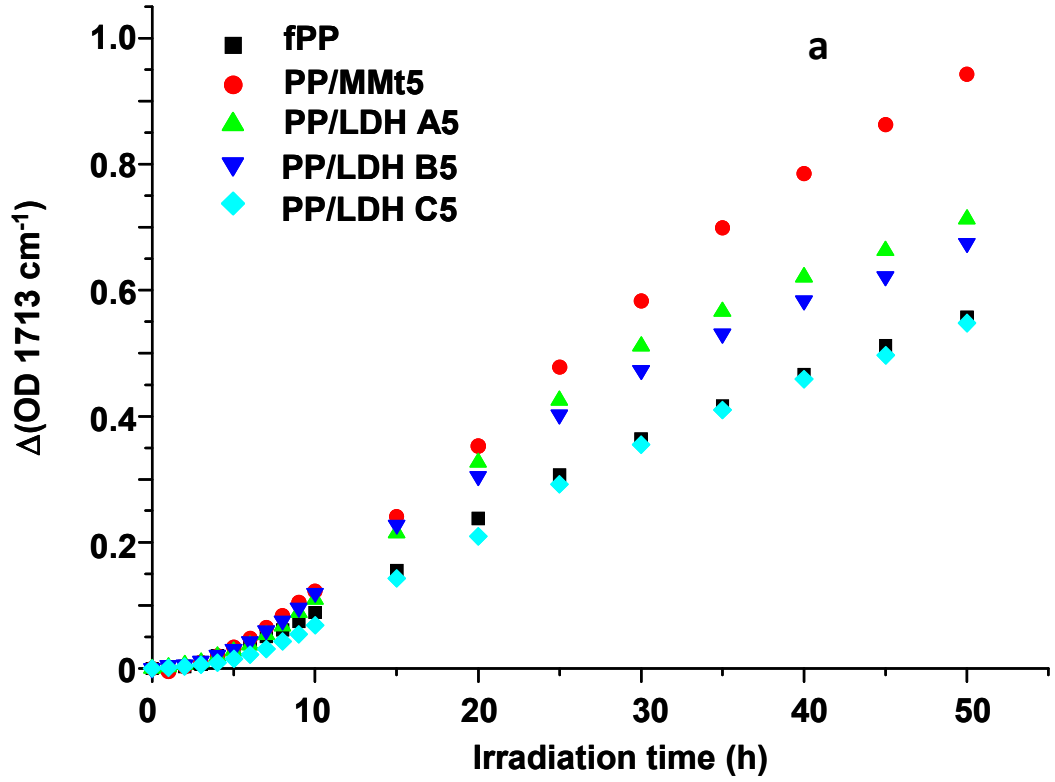

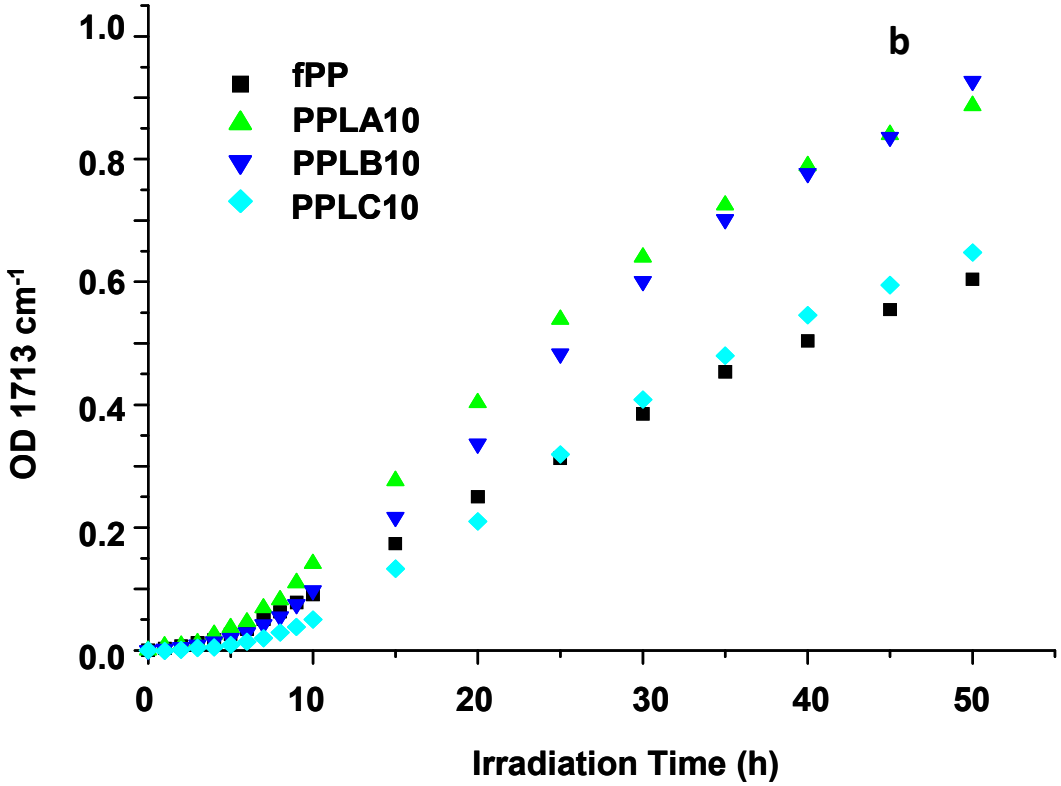

Figure 7.4: Rates of photooxidation of PP/LDH nanocomposites a) at 5% loading b) at 10% loading**.**

In the case of the fPP film (**Figure 7.4a**), a short induction period of 5 hours was observed before the oxidation of PP. This delay is always observed in PP photooxidation, and reflects the activity of the remaining antioxidant, which is consumed as a sacrificial additive. Once the active form of the antioxidant is consumed, oxidation starts and the photoproducts accumulate in the polymeric matrix. **Figure 7.4a** compares the nanocomposites with 5% clay. The PP/OMMt film degrades much more rapidly than fPP; after 20 hours of exposure to UV light, the normalised absorbance is 0.37, but is only 0.22 with fPP. The three LDH nanocomposites are less degraded than the nanocomposites with OMMt. The oxidation rate of the polymeric matrix in PP/LDH depends on the divalent cations present in the LDH. The LDH phases containing Mg degrade faster than those with Zn as the divalent cation. However, the Zn-containing LDH phases have a rate of photooxidation almost similar to that of fPP. The influence of LDH on polypropylene oxidation appears to depend on the divalent cations; the presence of the LDH has no influence on the durability of the nanocomposite material, such as

with the Zn_2-Al-DS LDH. Increasing the loading of the LDH to 10% gives similar effects as the 5% loading, and the kinetic curves shown in **Figure 7.4b** reveal the same behaviour as observed in **Figure 7.4a**. The nanocomposites with LDH phases containing Mg^{2+} (Mg_2-Al-DS and ZnMg-Al-DS) degrade faster than those with Zn_2-Al-DS.

7.2.4 Morphological Aspects

The SEM is a reliable tool to monitor the surface changes during degradation of polymeric materials. The morphologies of irradiated samples were studied by using scanning electron microscopic analysis. **Figure 7.5** displays the surface morphology of nanocomposite films that were irradiated for 50 h in air. After irradiation for 50 hours, large amounts of irregular cracks appeared on the surface of the composite films, which revealed its degradation, while only a small cavities and mass of stripes appeared on the surface of pure fPP film. It also can be seen that the cracking intensity is modernly low in case of PPLC5 in comparison of PPLA5 and PPLB5. This is in clear agreement with conclusion derived from FT-IR analysis that the Zn_2Al-LDH based PP nanocomposites are is less prone towards photo-oxidation.

Apparently, the structure of PP/OMMt nanocomposites exhibits a severe damage through surface erosion as a result of photo-oxidative degradation; this fact again supported the conclusion that the presence of OMMt clay increases degradation PP in comparison to the LDH type nanofillers. Overall findings indicate that OMMt nanoparticles greatly enhanced the photocatalytic degradation of the PP materials in compare to LDHs. Whereas, in LDH containing different metal cations the surface erosion follows the order of Mg_2Al LDH $\geq$ ZnMgAl-LDH > Zn_2Al-LDH. SEM observations agree well with the result of FT-IR analysis.

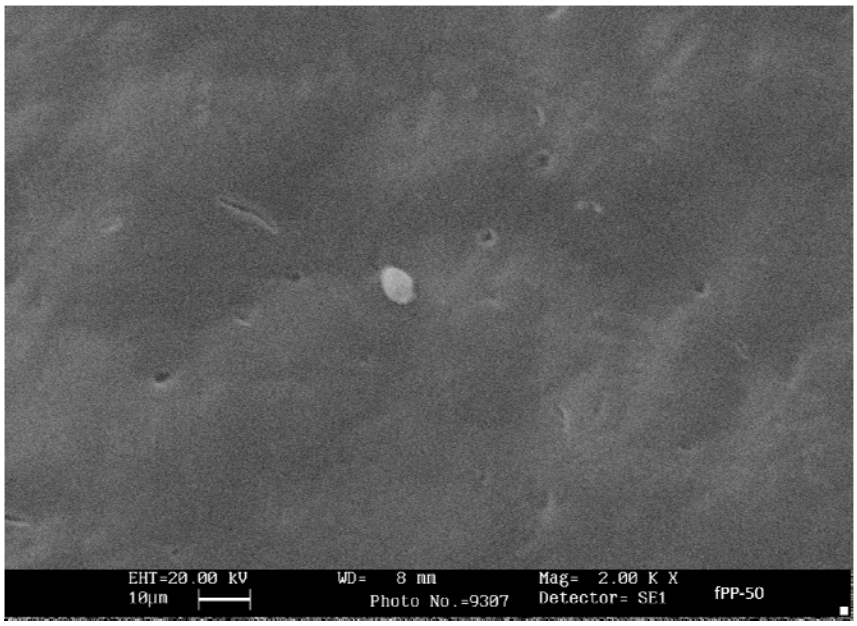
EHT=20.00 kV
WD= 8 mm
Mag= 2.00 K X
10µm
Photo No.=9307
Detector= SE1
fPP-50

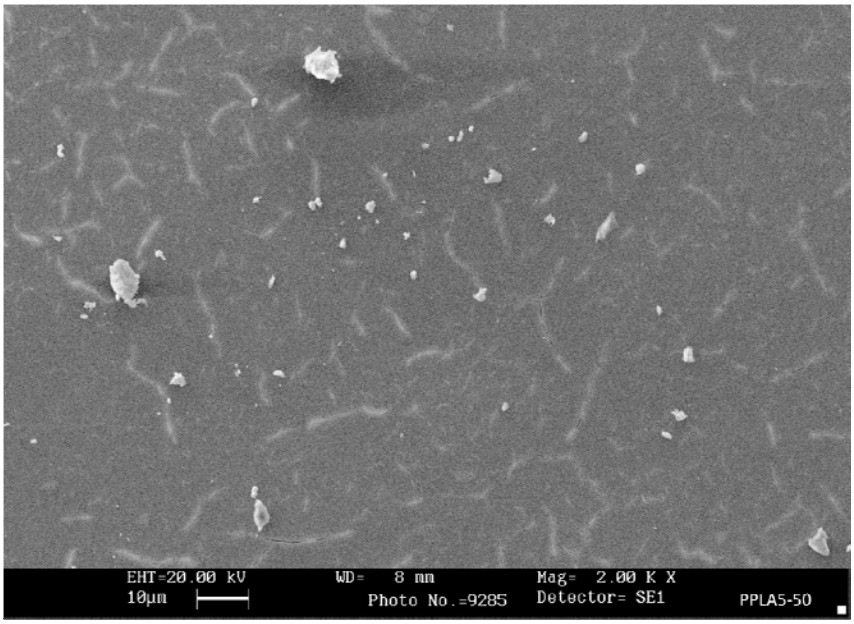
EHT=20.00 kV
WD= 8 mm
Mag= 2.00 K X
10µm
Photo No.=9285
Detector= SE1
PPLA5-50

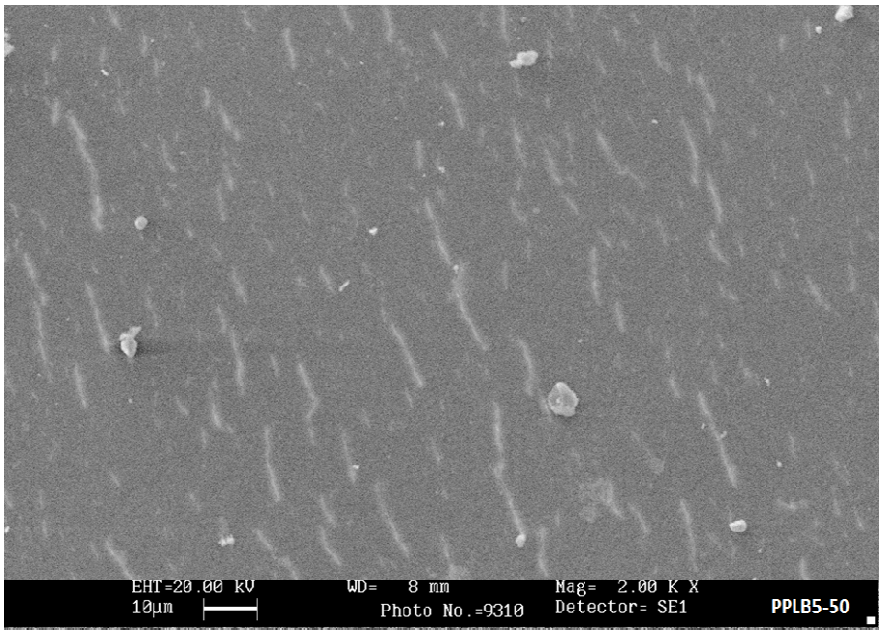
EHT=20.00 kV
10µm
WD= 8 mm
Photo No.=9310
Mag= 2.00 K X
Detector= SE1
PPLB5-50

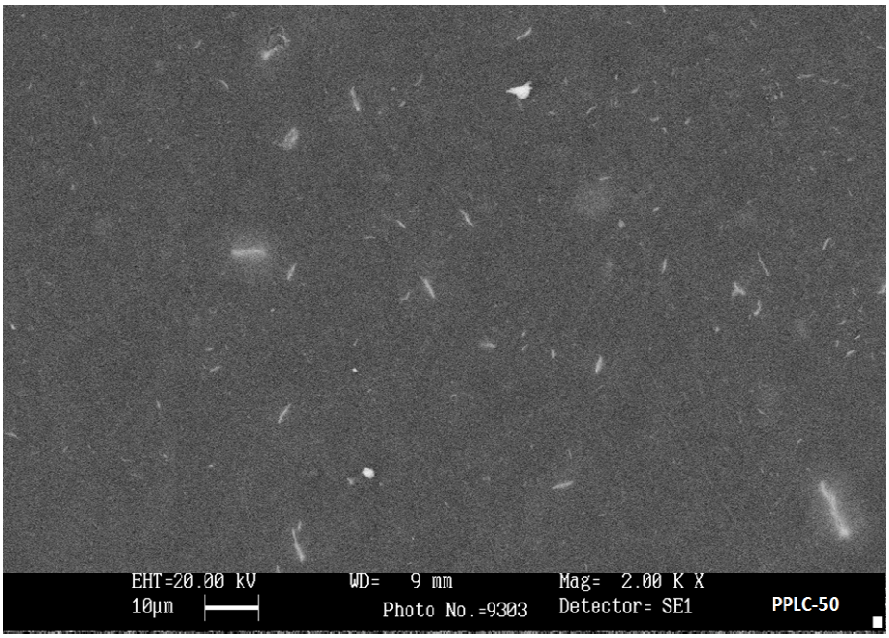
EHT=20.00 kV
10µm
WD= 9 mm
Photo No.=9303
Mag= 2.00 K X
Detector= SE1
PPLC-50

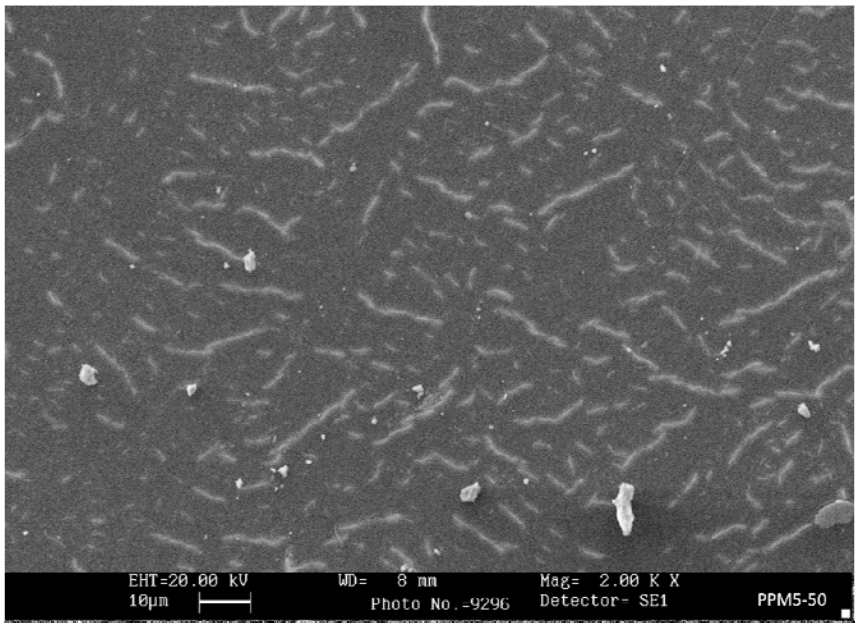

Figure 7.5: Surface erosion of PP, PP/LDH and PP/OMMt nanocomposites after 50h of UV irradiation

7.3 Photostabilization Studies of PP/LDH Nanocomposites

7.3.1 Effect of Phenolic Antioxidants

The influence of LDH nanofiller in presence of phenolic antioxidants were studied under photo-oxidative conditions as mentioned in above section. From **Figure 7.6**, it can be seen that the induction time (i.e. time required to start the degradation) is considerable varied for unfilled PP, PP/LDH and PP/OMMt nanocomposites. The induction time for PP/OMMt is observed to be 5h which is 20 h earlier than PP/PP-g-MAH and 15 h than PP/LDH nanocomposites. This results clearly reveals two facts, firstly, the PP/OMMt nanocomposites have very short induction time i.e degradation starts faster in comparison to PP/LDH nanocomposites (20h). Secondly, OMMt decrease the efficiency of phenolic antioxidants, whereas, nanocomposites with LDH the phenolic antioxidants retains its stabilizing effect on PP.

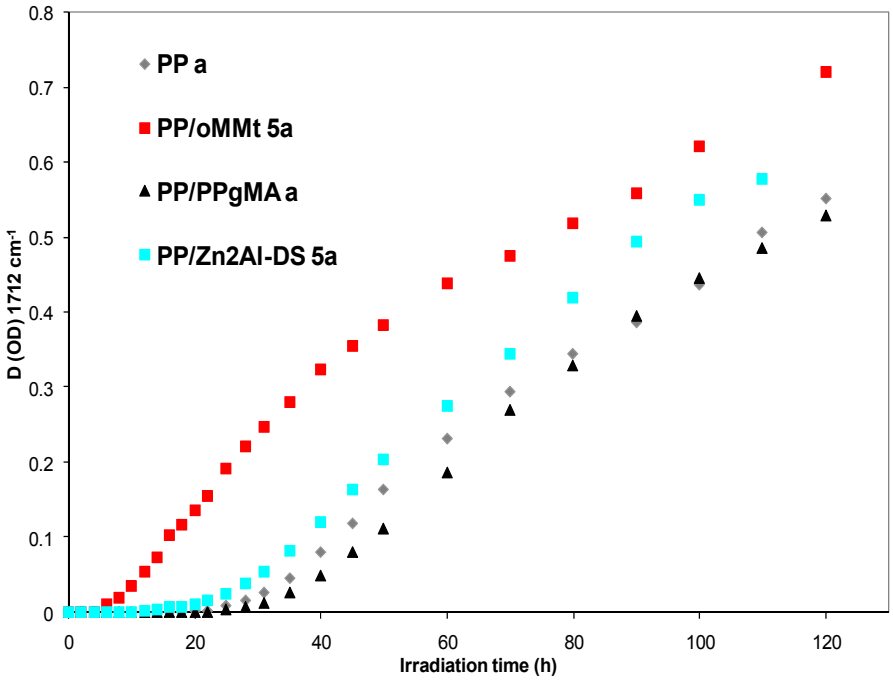

Figure 7.6: Influence of phenolic antioxidant (0.1 % Irganox 1010)

In **Figure 7.7**, the effect of interlamellar LDH metal cations on efficiency of phenolic antioxidant was assessed. It is observed that by increasing the amount of phenolic antioxidant from 0.1 % to 0.6 % the induction time is slightly increased. The rate of photo-oxidation is found to be higher in case of PPA5b i.e. Mg_2Al-LDH reinforced PP. Similarly, in PPLB5b also moderate increase in photo-oxidation is observed. Interestingly, in case of PPLC5b (Zn_2Al-LDH) this behavior is considerably lowered. This observations supports that the Zn_2Al-LDH is the best LDH nanofiller in presence of phenolic antioxidants for polypropylene photostabilization.

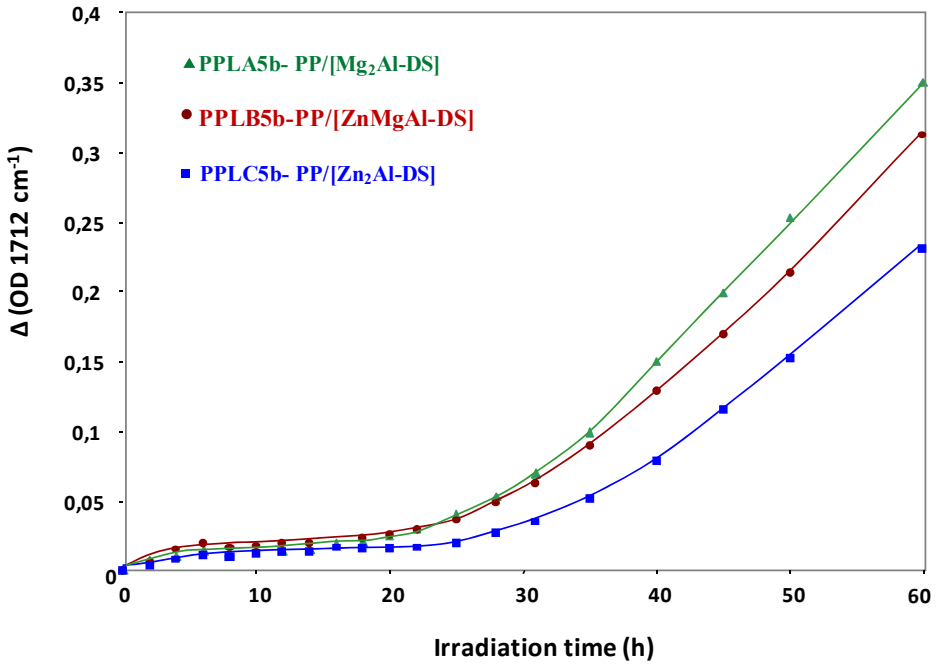

Figure 7.7: Influence LDH cations in presence of phenolic antioxidants (0.6% Irganox 1010).

7.3.1 Effect of redox antioxidants

The efficiency of redox antioxidant (HALS: Tinuvin-770) in presence of LDH containing different metal cations have been assessed and shown in **Figure 7.8.** The HALS used here was chosen because it has a tertiary methylated amine group, which is supposed to have less interaction with acidic species and also less hydrogen interaction with the clay platelets compared to the non-methylated amine group [16]. The rates of photo-oxidation of this series of samples are reported in **Figure 7.8** and compared with those of the samples with the phenolic antioxidant. It can be seen that the induction time is considerably increased in presence of redox antioxidants. These results give evidence that interactions between the nanoclay and the light stabilizer reduce its efficiency towards PP photostabilization. Compared LDH type nanoclays the OMMt clay drastically decrease the efficiency of stabilizers. The antagonism between redox antioxidants and OMMt type clay described in earlier reports [5] and it is because of presence in iron impurities that has photocatalytic activity; it can absorb these additives and reduces their efficiency.

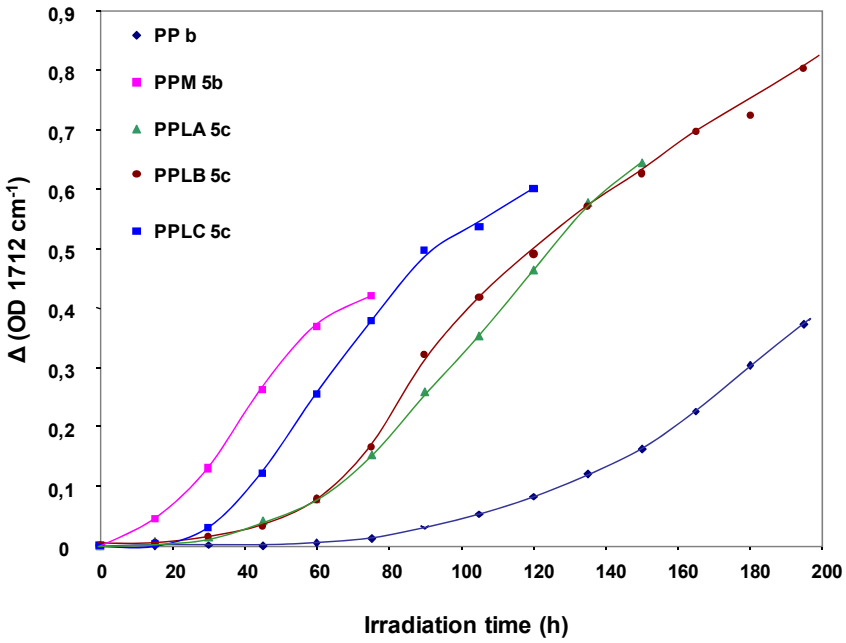

Figure 7.8: Effect of redox antioxidant of photooxidation behavior of PP, PP/LDH and PP/OMMt nanocomposites. ((0.1% Irganox 1010 + 0.1% Tinivin-770)

Also, the decomposition of organic modifier can also contribute to such behavior. In presence of LDH, the adsorption of such stabilizing additives is not as prominent as in case of OMMt.

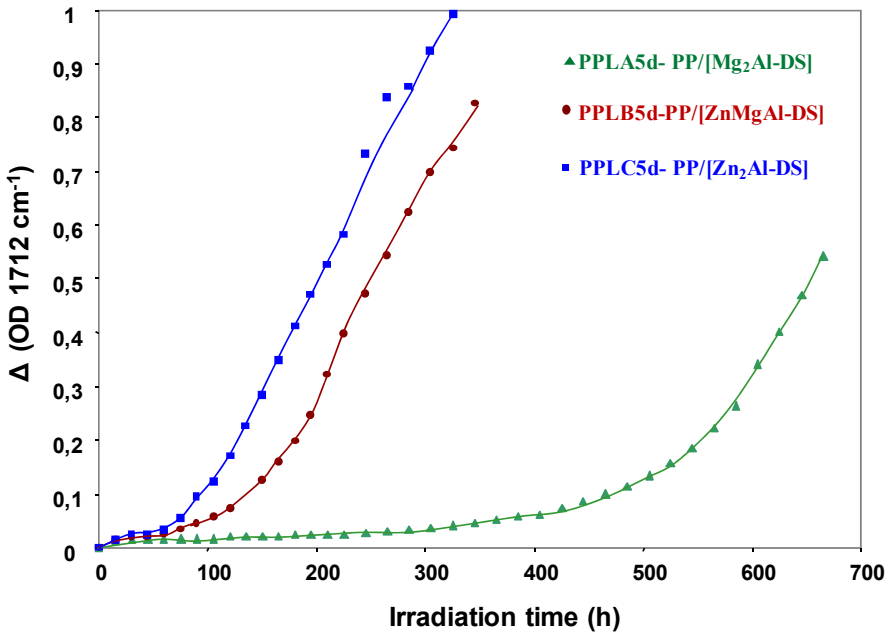

Figure 7.9: Influence LDH cations in presence of redox antioxidants (0.6% Irganox 1010 + 0.6% Tinivin-770).

However, in case of different LDHs the efficiency of stabilizing additives is significantly altered as shown in **Figure 7.9**. An opposite behavior is observed between phenolic and redox antioxidants in photostabilization of PP/LDH nanocomposites. The redox antioxidant showed higher efficiency for PP photostabilization in presence of Mg_2Al-LDH in contrast to the Zn_2Al and ZnMgAl-LDH, respectively. Such behavior can be ascribed due to the possible photocatalytic effect of metal cations or decomposition of organomodifiers. The effect of phenolic and redox antioxidants in different composition on photostabilization of PP/LDH nanocomposites is shown in **Figure 7.10**. It is observed that the higher concentrations (PPLA 5d-0.6% Irganox 1010 + 0.6% Tinivin-770) have better photostabilizing ability over rest of the compositions. Small quantity of redox antioxidant (PPLA 5c) shows better performance as compared to higher phenolic antioxidants. This could be because of the sacrificial loss of phenolic antioxidant during the processing.

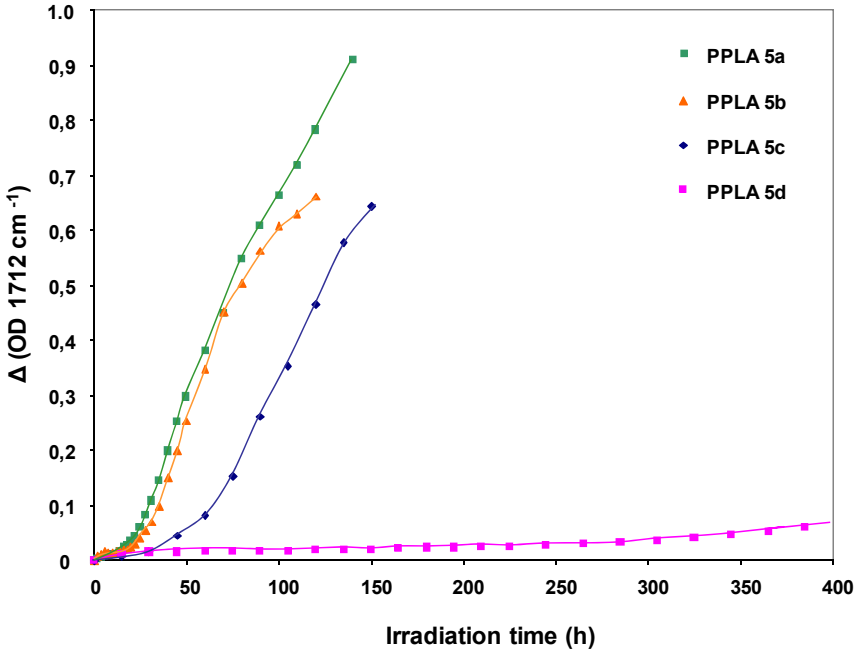

Figure 7.10: Effect of different antioxidant composition on PP/LDH photostabilization

7.4 Conclusions

The effect of accelerated photo-oxidation on the structure and morphology of PP/LDH nanocomposites has been studied as a function of LDH comprising different metal cations using FT-IR spectroscopy and SEM, respectively. The results obtained were compared with PP/OMMt nanocomposites under similar photo-oxidative conditions. The study reveals that the presence of LDH can modify the chemical structure of the photoproducts accumulating in the matrix. The rates of oxidation are influenced by the nanofiller, depending on the divalent cations of the LDH layers. The LDH phases containing Mg^{2+} have a prodegradant effect on the nanocomposite material, whereas LDH with only Zn^{2+} has no influence on the rate of oxidation of the polymer matrix. From this study it is also concluded that, certainly, the PP/LDH nanocomposites are more durable in comparison with PP/OMMt nanocomposites under accelerated weathering conditions.

The photostabilization results show clearly that OMMt hinders antioxidants in stabilizing polypropylene, which results in a dramatic decrease of the photochemical stability of the PP. Whereas, nanocomposites with LDH the phenolic antioxidants retains its stabilizing activity towards PP photostabilization. The effect of interlamellar LDH metal cations on efficiency of phenolic antioxidant shows that the Zn_2Al-LDH is the better LDH nanofiller in presence of phenolic antioxidants for polypropylene photostabilization. An opposite behavior is observed when compared the antioxidant efficiency in presence on redox antioxidant in photostabilization of PP/LDH nanocomposites. The redox antioxidant showed higher efficiency for PP photostabilization in presence of Mg_2Al-LDH in contrast to the Zn_2Al and ZnMgAl-LDH.

References

1. G. J. M. Fechine and N. R. Demarquette, "Cracking Formation on the Surface of Extruded Photodegraded Polypropylene Plates", *Polymer Engineering and Science*, **48** (2008),p. 365- 372
2. S. Bocchini, S. M-Therias, J. L. Gardette and G. Camino, "Influence of nanodispersedhydrotalcite on polypropylene photooxidation", *European Polymer Journal*, **44** (2008), p. 3473- 3481.
3. A.Tidjani, Photooxidation of polypropylene under natural and accelerated weathering conditions. *Journal of Applied Polymer Science*, **64** (1997), p.2497–2503.
4. J.L Philippart, Ch. Sinturel, R. Arnaud and J-L Gardette Influence of the exposure parameters on the mechanism of photooxidation of polypropylene. *Polymer Degradation and Stability*, **64** (1999), p.213–225.
5. S. Morlat, B. Mailhot, D. Gonzalez, J-L. Gardette Photooxidation of Polypropylene/Montmorillonite Nanocomposites. 2. Interactions with Antioxidants. *Chemistry of Materials,* **17** (2005), p.1072–1078.
6. S. Bocchini, S.Morlat-Therias, J-L. Gardette, G. Camino, Influence of nanodispersed hydrotalcite on polypropylene photooxidation *European Polymer Journal,* **44** (2008), p.3473–3481.
7. B. Mailhot, S. Morlat, J-L Gardette, Boucard S, Duchet J, Gerard JF. Photodegradation of polypropylene nanocomposites. *Polymer Degradation Stability,* **82** (2003), p.163–167.
8. S. Morlat-Therias, B. Mailhot, D. Gonzalez, J-L Gardette. Photo-oxidation of polypropylene/ montmorillonite nanocomposites. 1. Influence of nanoclay and compatibilizing agent. *Chemistry of Materials,* **16** (2004), p.377–383.
9. S. Morlat-Therias, B. Mailhot, D. Gonzalez, J-L Gardette. Photooxidation of polypropylene/ montmorillonite nanocomposites. 2. Interactions with antioxidants. *Chemistry of Materials*, **17** (2005), p.1072–1078.
10. S. Morlat-Therias, B. Mailhot, J-L Gardette, C. Da Silva, B. Haidar, A. Vidal. Photooxidation of ethylene-propylene-diene/montmorillonite nanocomposites. *Polymer Degradation Stability,* **90** (2005), p.78–85.

11. S. Bocchini, S. Morlat Therias, J.L Gardette, G. Camino. Influence of nanodispersed boehmite on polypropylene photooxidation. *Polymer Degradation Stability,* **92** (2007), p.1847–1856.
12. F. Leroux, L. Meddar, B. Mailhot, S. Morlat-Therias, J-L Gardette. Characterization and photooxidative behaviour of nanocomposites formed with polystyrene and LDHs organo-modified by monomer surfactant, *Polymer,* **46** (2005), p.3571–3578.
13. J.L. Philippart, C. Sinturel, J-L Gardette. Influence of light intensity on the photooxidation of polypropylene, *Polymer Degradation Stability*, **58** (1997), p.261–268.
14. S. Bocchini, S.Morlat-Therias, J-L. Gardette, G. Camino. Influence of nanodispersed hydrotalcite on polypropylene photooxidation, *European Polymer Journal,* **44** (2008), p.3473–3481.
15. S.P. Lonkar, A.P. Kumar, R.P Singh, Photo-stabilization of EPDM-clay nanocomposites: Effect of antioxidant on the preparation and durability. *Polymers for Advanced Technologies,* **18** (2007), p.891-900.
16. C. Sinturel, J. Lemaire, J-L. Gardette, Photooxidation of fire retarded polypropylene. III. Mechanism of HAS inactivation. *Euopean Polymer Journal,* **36** (2000), p.1431-1343.

Chapter 8

CONCLUSIONS AND FUTURE PERSPECTIVES

"I am always willing to learn, however I do not always like to be taught"

~ Winston Churchill

8.1 Summary and Conclusions

The principal objective of this work has been to investigate the feasibility of layered double hydroxide (LDH) type anionic clays as reinforcement to the polypropylene (PP). The potential of these nanofiller was assessed in terms of the structure-property improvement e.g. mechanical properties, flame resistance, thermal stability and gas barrier properties of the resulting hybrid composites, crystallization behavior and durability under accelerated photoaging. It is also found that the LDH type anionic clays can be a potential alternative to montmorillonite (MMT) type cationic clays, especially in terms of photoageing behavior of these hybrid materials. The chapter wise silent points of conclusions are summarized as follows:

Chapter 1 portrays the brief background of polymer/clay nanocomposites, main motivation and research objective for this study. **Chapter 2** reviews the literature background and A thorough literature survey was carried out on PP based nano structured materials, methods of synthesis, material processing methods and their property evaluations. **Chapter 3** describes the experimental methods and characterization techniques used in the preparation and characterization of PP-LDH nanocomposites. In **Chapter 4,** the successful synthesis and characterization of different phases of organomodified LDH is described. The intercalation of surfactant, certainly make LDH more organophilic and facilitating the intercalation and dispersion of polymer chains. The characterization means well revealed the crystalline structure, organomodification and thermal behavior of different LDHs. Also, the successful preparation of PP/LDH hybrid nanocomposites by melt intercalation using PP-g-MAH

as a compatibilizing agent is summarized. The spectral analysis reveals the possible interactions between LDHs and PP-g-MAH. The characterization techniques give direct evidence for the formation of intercalated/exfoliated PP/LDH nanocomposites structures. In **Chapter 5** discusses the influence of nano LDH reinforcement on different characteristic properties of polypropylene. Incorporation of the LDH which is in a platelet form resulted in a significant improvement in the thermal stability of PP. The addition of LDH can contribute to the reinforcement effect by increasing the elastic modulus. The mechanical response of these hybrid materials is also found to be remarkable. A strong influence of LDH particles on the flow behavior of the PP/LDH melt is observed. At higher LDH content, system develops more and more solid-like behavior with increasing resistance against relaxation. The incorporation of well dispersed LDH platelets into PP shows improved oxygen barrier properties. Moreover, the PP/LDH nanocomposites exhibits fairly better barrier performance than PP/ OMMt nanocomposites. The flammability studies also showed improved flame retardancy in PP/LDH nanocomposites. The crystallization studies discussed in **Chapter 6** reveal enhanced crystallization rates for non-isothermal as well as isothermal crystallization for nanocomposites with LDH as nanofillers. Also, LDH at nanometer level found to act as effective nucleating agent. The Avrami exponent n varies from 1.9 to 2.9 for suggesting spherulitic crystal growth with heterogeneous nucleation at the low cooling rates. The melting behavior of PP is also slightly altered by addition of LDH. The addition of LDH does not change the overall crystalline structure of PP matrix. The crystallization studies can lead to the development of a fine grain micron-sized structure for the PP/LDH composites. **Chapter 7** concludes that the PP/LDH nanocomposites are more durable in comparison with PP/OMMt nanocomposites under accelerated weathering conditions. The rates of oxidation are influenced by the divalent cations of the LDH layers. The LDH phases containing Mg^{2+} have a prodegradant effect on the nanocomposite material, whereas LDH with only Zn^{2+} has no influence on the rate of oxidation of the polymer matrix. The influence of stabilizing additives on the photooxidation of PP/LDH nanocomposites exposed to UV light shows that additive retains their activity in presence of LDH in contrast to the OMMt type nanoclay. The Zn_2Al-DDS is found to be better LDH nanofiller for stabilization in presence in phenolic antioxidants.

Finally, we envision that this new hybrid material, which combines the advantages various physico-mechanical properties and better performance towards weathering, could play a significant role in the development of new nanocomposites for automotive, construction and packaging applications.

8.2 Recommendations for Future Work

This work contributes to achieve the comprehensive investigations of PP/LDH nanocomposites with a remarkable property enhancement through the material formulation, melt processing and experimental characterization. It is recommended that future research work should be carried out as follows:

- Since PP-g-MAH as the compatibilizer plays a crucial role in the formulations of PP/LDH nanocomposites by the melt compounding method, it is worthwhile to use different types of PP-g-MAH with various molecular weights and grafting contents in order to greatly improve the interactions and miscibility between LDH particles and the PP matrix.
- The cationic nature of the metal hydroxide layers in LDH makes the choice of organic species more flexible. Organic species containing functional groups -OH, -COOH, $-SO_3H$ etc. shows favorable interaction with LDH clays. Therefore, LDH can be modified with wide range of organic species. Such flexibility in selecting modifying anionic species makes LDH a suitable candidate for designing multifunctional nanohybrids filler for polymers. For example, LDH can be modified by organic species having specific properties, like UV absorption, photo stabilization, antimicrobial effect, fluorescent effect etc. All these nanohybrids can be potential functionalized fillers for polymers to develop novel composite materials.
- It also would be interesting to use other divalent cations like Ca^{2+}, Ni^{2+}, Co^{2+} and Mn^{2+} or Cu^{2+} and trivalent cation Cr^{3+}, Co^{3+}, Mn^{3+}, Fe^{3+} and V^{3+} in developing the different LDH phases. These fillers can be explored to study the improvement in structure-property, crystallization, mechanical properties and flame resistance of polypropylene.

- Due to the complex morphological structures of nanocomposites with partially intercalated/exfoliated LDH platelets and tactoids, effect of such nanofiller in PP nanocomposites with respect to the actual morphology through numerical modeling and simulations will be interesting to study.

❖ List of Publications

❖ *Journal Publications*

1) **Sunil P. Lonkar,** S. Morlat-Therias, F. Leroux, J.L. Gardette, R.P.Singh, "*Preparation and Nonisothermal Crystallization Behavior of Polypropylene/Layered Double Hydroxide Nanocomposites*", ***Polymer,*** 50 (2009), p. 1505-1515.

2) **Sunil P. Lonkar** and R.P. Singh, "*Isothermal Crystallization and Melting Behavior of Polypropylene/Layered Double Hydroxide Nanocomposites*", ***Thermochimica Acta,*** 491 (2009), p. 63-70.

3) **Sunil P. Lonkar**, S. Therias, N. Cappera, F. Leroux, J.L. Gardette, "*Photooxidation of Polypropylene/Layered Double Hydroxide Nanocomposites: Influence of Interlamellar Cations*, ***European Polymer Journal (Accepted for Publication).***

4) **Sunil P. Lonkar,** S. Morlat-Therias, F. Leroux, J.L. Gardette, R.P.Singh, "*Thermal, Mechanical and Rheological Characterization of Polypropylene/ Layered Double Hydroxide Nanocomposites*", Submitted to ***Composites Science and Technologies.***

5) **Sunil P. Lonkar**, A.P. Kumar, R.P Singh, "*Photo-stabilization of EPDM-clay Nanocomposites: Effect of Antioxidant on the Preparation and Durability*" ***Polymers for Advanced Technologies,*** 18 (2007), p.891-900.

6) **Sunil P. Lonkar**, S. Therias, M. Gardette, F. Leroux, J.L. Gardette, R.P.Singh "*Photooxidation of Polypropylene/Layered Double Hydroxide Nanocomposites: Interactions with Antioxidants*", in preparation for ***Polymer Degradation and Stability.***

7) **Sunil P. Lonkar,** S. Morlat-Therias, F. Leroux, J.L. Gardette, R.P.Singh, "*Influence of Reactive Compatibilization on the Structure and Properties of Polypropylene/Layered Double Hydroxide Nanocomposites*", in preparation for ***European Polymer Journal.***

❖ *Oral Presentations*

1. **Sunil P. Lonkar** and R. P. Singh, "*Structure and Properties of Nanocomposites Based on Polypropylene / Layered Double Hydroxide*", 2nd International Conference on Polymer Processing and Characterization (ICPPC-2010), Kottayam, India, 15-17 January, 2010.

2. **Sunil P. Lonkar** and R. P. Singh, "*Influence of reactive compatibilization on the structure and properties of PP/LDH nanocomposites*", New Delhi, India, 17-20 December, 2009.

3. **Sunil P. Lonkar** and R. P. Singh "*Preparation and Properties of Polypropylene / Layered Double Hydroxide Nanocomposites*" 2nd Conference on Recent Advances in Polymer Technologies (RAPT), North Maharashtra University, Jalgoan, India, 28-29 December, 2009.

4. **Sunil P. Lonkar** and R. P. Singh, "*Nanocomposites based on Polypropylene and Layered Double Hydroxide - Synthesis and Characterization*" North Maharashtra University, Jalgoan, India, 15 February, 2009.

5. S. Thérias, **S.P. Lonkar**, M. Gardette, F. Leroux, J.L. Gardette, "*Influence of LDH Cations on the Photostabilization of PP/LDH nanocomposites***"** International Conference on Polymers (POLYMERFEST), University of Palermo, Italy, 2 September, 2009.

6. **Sunil P. Lonkar** and R.P. Singh, "*Effect of UV Irradiation on Durability of PP / LDH Nanocomposites*" 2nd International Conference on Advanced Materials and Polymers for Aerospace and Defense Applications (SAMPADA-2008), Pune, India, 8-12 December, 2008.

❖ *Poster Presentations*

1. **S. P. Lonkar**, V. K. Rana, S. Kumari and R.P. Singh, "*Preparation and Crystallization Behavior of PP/LDH Nanocomposites*", MACRO-2009, Chennai, India.

2. **S. P. Lonkar**, S. Morlat-Therias, F. Leroux, J.L. Gardette, "*Photooxidation of Polypropylene/Layered Double Hydroxide (PP/LDH) nanocomposites*", MoDeSt-2008, Leigh, Belgium.

3. **S.P. Lonkar**, A.P. Kumar, R.P Singh, "*Photo-stabilization of EPDM-clay Nanocomposites: Effect of Antioxidant on the Preparation and Durability*" International conference 'Polymer 2006' at IACS, 10–12 February 2006, Kolkata, India.

4. **S.P. Lonkar**, R. P. Singh, N.Singh, P.K.Khanna, "*Synthesis and characterization of CdS/polyaniline nano-composites: Effect of organic acid dopants*", International Conference on nano Materials for Electronics (ICNME), 27-29 November, 2006, Pune, India.

5. **S.P. Lonkar**, M. Chrysanthos, R. P. Singh, "*Synthesis and Characterization of New Polymerizable Hindered Amine Light Stabilizer*", MACRO-2006, Pune, India.

6. **S.P.Lonkar** and R.P.Singh, "*Synthesis and performance evaluation of polymeric HALS in EPDM*" MACRO-2004, 14-17 Dec. 2004, Trivendrum, Kerala, India.